Chemical Retention and Diffusional Uptake of Secondary Organic Aerosol Precursors in Hydrometeors

Dissertation

For the award of the degree

'Doctor rerum naturalium (Dr. rer. nat)' through the departments of:

08 - Physics, Mathematics, and Informatics

09 - Chemistry, Pharmacy, and Earth Sciences

At the Max Planck Graduate Center of the Johannes Gutenberg University Mainz

JOHANNES GUTENBERG UNIVERSITÄT MAINZ

Max Planck Graduate Center mit der Johannes Gutenberg-Universität

Jackson Cotten Seymore

Born 26.01.1998 in North Carolina, United States

Mainz, 2025

The present work was performed from August 2022 to June 2025 in the Mainz Wind Tunnel Laboratory of the Johannes Gutenberg University Institute for Atmospheric Physics.

"I hereby declare that I wrote the dissertation submitted without any unauthorized external assistance and used only sources acknowledged in the work. All textual passages which are appropriated verbatim or paraphrased from published and unpublished texts as well as all information obtained from oral sources are duly indicated and listed in accordance with bibliographical rules. In carrying out this research, I complied with the rules of standard scientific practice as formulated in the statutes of Johannes Gutenberg University Mainz to ensure standard scientific practice."

Name of Supervisor:	Prof. Dr. Thorsten Hoffmann	MPIC JGU-IIAC
Name of Co-Supervisor:	PD Dr. Miklós Szakáll	JGU-IPA

Date of the oral examination: July 9, 2025

Special thanks to my colleagues and contributors from the Mainz Wind Tunnel Laboratory of the Johannes Gutenberg University Institute for Atmospheric Physics: Martanda Gautam, Laura Werner, Florian Ungeheuer, Sudha Yadav, Jan Wallner, Moritz Hey, Laura Gömmer, Andreas Arndt, PD. Dr. Miklós Szakáll, Dr. Alexander Theis, Dr. Subir Kumar Mitra; the Johannes Gutenberg University Department of Chemistry: Christine Borchers, Stefanie Hildmann, Yannik Müller, Isabell Erdmann, Prof. Dr. Thorsten Hoffmann; the Goethe University Frankfurt Institute for Atmospheric and Environmental Sciences: Anna Breuninger, Jianling Ma, Markus Thoma, Konstantin Dörholt, Prof. Dr. Alexander L. Vogel; and Prof. Dr. Stephan Borrmann.

Additional thanks to Mahesh Yadav, the Institute of Molecular Biology, and the Historical Society of the Mainz Wind Tunnel Archaeological Site for the coffee, continued support, and productive conversation

For Hannah

And where that you have vow'd to study, Lords,
In that each of you have forsworn his Book,
Can you still dream and pore and thereon look?
For when would you, my Lord, or you, or you,
Have found the ground of study's excellence,
Without the beauty of a woman's face?
From women's eyes this doctrine I derive,
They are the Ground, the Books, the Academes,
From whence doth spring the true Promethean fire.

LLL: IV.3

Table of Contents

Abstract

The phase changes of hydrometeors can cause chemical exchange that may lead to transport of certain water-soluble organic compounds (WSOC) between the lower troposphere and the upper troposphere lower stratosphere (UTLS). Specifically, during droplet freezing WSOC dissolved in the supercooled cloud droplets can be released into the gas phase. Alternately, many volatile organic compounds can be removed from the UTLS via ice phase deposition scavenging. These microphysical and multiphase chemical processes may lead to the vertical redistribution of substances that become available for atmospheric processes in the upper troposphere. Motivations for understanding the processes of chemical retention and diffusional ice uptake as well as descriptions of them are detailed in this dissertation as justification for their investigation through several publications. These publications detail the measurement of retention coefficients and ice-gas partitioning coefficients through the use of wind tunnel studies, acoustic levitator experiments, and flowtube experiments. These measurements complicate the current understanding of the relationship between chemical retention and Henry's law solubilities as well as reveal previously unknown entropy-enthalpy compensation behavior resulting from diffusional ice uptake.

Zusammenfassung

Die Phasenänderungen von Hydrometeoren können einen chemischen Austausch bewirken, der zum Transport bestimmter wasserlöslicher organischer Verbindungen (WSOC) zwischen der unteren Troposphäre und der oberen Troposphäre und unteren Stratosphäre (UTLS) führen kann. Insbesondere können beim Gefrieren der Tröpfchen die in den unterkühlten Wolkentröpfchen gelösten WSOC in die Gasphase freigesetzt werden. Alternativ dazu können viele flüchtige organische Verbindungen durch Eisphasenabscheidung aus der UTLS entfernt werden. Diese mikrophysikalischen und mehrphasigen chemischen Prozesse können zu einer vertikalen Umverteilung von Substanzen führen, die für atmosphärische Prozesse in der oberen Troposphäre verfügbar werden. Die Beweggründe für das Verständnis der Prozesse der chemischen Retention und der diffusiven Eisaufnahme sowie deren Beschreibungen werden in dieser Dissertation detailliert dargelegt, um ihre Untersuchung durch mehrere Veröffentlichungen zu rechtfertigen. In diesen Veröffentlichungen wird die Messung von Retentionskoeffizienten und Eis-Gas-Verteilungskoeffizienten anhand von Windkanalstudien, akustischen Levitatorexperimenten und Flowtube-Experimenten beschrieben. Diese Messungen verkomplizieren das derzeitige Verständnis der Beziehung zwischen chemischer Retention und Löslichkeiten nach dem Henry'schen Gesetz und offenbaren ein bisher unbekanntes Entropie-Enthalpie-Kompensationsverhalten, das aus der diffusiven Eisaufnahme resultiert.

Summary of Dissertation *"Chemical Retention and Diffusive Deposition of Secondary Organic Aerosol Precursors in Hydrometeors"*

This dissertation is a collection of the following publications that I have authored or co-authored:

2025, Seymore J., Szakáll, M., Theis, A., Mitra, S.K., Borchers, C., Hoffmann, T. Gas-Ice Partitioning Coefficients of Carbonyls during Diffusional Ice Crystal Growth. **Accepted** for Publication after revision with *Atmospheric Chemistry and Physics* https://doi.org/10.5194/egusphere-2025-1425

2025, Seymore, J., Gautam, M., Szakáll, M., Theis, A., Hoffmann, T., Ma, J., Zhou, L., and Vogel, A. Retention During Freezing of Raindrops, Part II: Investigation of Ambient Organics from Beijing Urban Aerosol Samples**. Accepted** for Publication with *Atmospheric Chemistry and Physics* https://doi.org/10.5194/egusphere-2024-3940

2025, Gautam, M., Theis A., **Seymore, J.**, Hey, M., Borrmann, S., Diehl, K., Mitra, S.K., and Szakáll, M. Retention During Freezing of Raindrops, Part I: Investigation of Single and Binary Mixtures**, Accepted** for Publication with *Atmospheric Chemistry and Physics* https://doi.org/10.5194/egusphere-2024-3917

2024, Borchers, C., **Seymore, J.**, Gautam, M., Dörholt, K., Müller, Y., Arndt, A., Gömmer, L., Ungeheuer, F., Szakáll, M., Borrmann, S., Theis, A., Vogel, A.L., and Hoffmann, T., Retention of α-pinene oxidation products and nitro-aromatic compounds during riming. **Published** with *Atmospheric Chemistry and Physics*. Atmos. Chem. Phys., 24, 13961–13974, https://doi.org/10.5194/acp-24-13961-2024

These publications concern the transport of organic compounds into the troposphere and lower stratosphere through the possible pathways of chemical retention during deep convective transport and associated cirrus formation. Chemical redistribution between the liquid and gas phase during freezing as well as between the gas and ice phase during diffusional ice crystal growth is not fully understood, particularly for the wide variety of atmospheric organics. This is despite its relevance to the vertical redistribution of organics across the planetary boundary layer and its support of new particle formation in convective

outflows. Thereby, it plays an essential role in cloud condensation nucleation and the radiation budget of the atmosphere, which has direct implications for climate processes.

The experiments presented in these publications were performed at the Mainz Wind Tunnel Laboratory where I was either the main contributor or a significant contributor. These experiments demonstrate (1) the measurement of retention coefficients through the use of the Mainz Wind Tunnel or an acoustic levitation apparatus; (2) the measurement of gas-ice partitioning coefficients through the use of a self-designed Flowtube apparatus; (3) and the significance of these measurements for atmospheric processing and the associated transport of the implicated organic species.

Zusammenfassung der Dissertation *„Chemische Retention und diffusive Deposition von sekundären organischen Aerosolvorläufergasen in Hydrometeoren“*

Diese kumulative Dissertation basiert auf den folgenden Veröffentlichungen, die ich verfasst oder mitverfaßt habe:

2025, Seymore J., Szakáll, M., Theis, A., Mitra, S.K., Borchers, C., Hoffmann, T. Gas-Ice Partitioning Coefficients of Carbonyls during Diffusional Ice Crystal Growth. **Angenommen** zur Veröffentlichung nach Überarbeitung bei *Atmospheric Chemistry and Physics* https://doi.org/10.5194/egusphere-2025-1425

2025, Seymore, J., Gautam, M., Szakáll, M., Theis, A., Hoffmann, T., Ma, J., Zhou, L., and Vogel, A. Retention During Freezing of Raindrops, Part II: Investigation of Ambient Organics from Beijing Urban Aerosol Samples. **Angenommen** zur Veröffentlichung mit *Atmospheric Chemistry and Physics* https://doi.org/10.5194/egusphere-2024-3940

2025, Gautam, M., Theis A., **Seymore, J.,** Hey, M., Borrmann, S., Diehl, K., Mitra, S.K., und Szakáll, M. Retention During Freezing of Raindrops, Part I: Investigation of Single and Binary Mixtures, **Angenommen** zur Veröffentlichung bei *Atmospheric Chemistry and Physics* https://doi.org/10.5194/egusphere-2024-3917

2024, Borchers, C., **Seymore, J.,** Gautam, M., Dörholt, K., Müller, Y., Arndt, A., Gömmer, L., Ungeheuer, F., Szakáll, M., Borrmann, S., Theis, A., Vogel, A.L., and Hoffmann, T., Retention of α-pinene oxidation products and nitro-aromatic compounds during riming. **Veröffentlicht** bei *Atmospheric Chemistry and Physics*. Atmos. Chem. Phys., 24, 13961-13974, https://doi.org/10.5194/acp-24-13961-2024

Die oben genannten Veröffentlichungen befassen sich mit dem Transport organischer Verbindungen in die Troposphäre und die untere Stratosphäre. Insbesondere wurde die chemische Retention beim Transport in hochreichenden konvektiven Wolken und der damit verbundenen Zirrusbildung untersucht. Die chemische Partitionierung zwischen der Flüssig- und der Gasphase während des Gefrierens sowie zwischen der Gas- und der Eisphase während des diffusiven Eiskristallwachstums ist noch nicht vollständig verstanden. Dies gilt insbesondere für die Vielfalt der organischen Stoffe in der Atmosphäre. Die Kenntnis der chemischen Partitionierung ist von besonderer Bedeutung um die vertikale Umverteilung von

organischen Stoffen von der planetaren Grenzschicht in die obere Troposphäre und ihrer damit einhergehenden Rolle bei der Bildung neuer Partikel in der Ausströmungsregion von hochreichenden konvektiven Wolken bestimmen zu können. Dadurch spielt sie eine wesentliche Rolle bei der Bildung von Wolkenkondensationskeimen und dem Strahlungshaushalt der Atmosphäre, was direkte Auswirkungen auf klimarelevante Prozesse hat.

Die in diesen Veröffentlichungen vorgestellten Experimente wurden im Mainzer Windkanal-Laboratorium durchgeführt, zu denen ich entweder den Hauptbeitrag oder einen wesentlichen Beitrag geleistet habe. Diese Experimente beinhalten (1) die Messung von Retentionskoeffizienten durch den Einsatz des Mainzer Windkanals oder einer akustischen Falle; (2) die Messung von Gas-Eis-Verteilungskoeffizienten durch den Einsatz einer selbst entworfenen Flowtube-Apparatur; (3) und die Bedeutung dieser Messungen für die atmosphärische Prozessierung und den damit verbundenen Transport der untersuchten organischen Spezies.

1. Introduction

1.1 Atmospheric Organics

Atmospheric organic matter is a critical constituent of the chemical composition of Earth's atmosphere. It has a vital role in many processes that moderate climate systems as well as influence air quality and thereby public health. One of the most important and yet unresolved issues in cloud chemistry and global models is understanding the transport of atmospheric organic matter. Specifically, how does ice phase processing in tropical deep convective clouds and in extratropical warm conveyor belts (WCBs) contribute to the redistribution of atmospheric trace organic substances from the boundary layer to the upper troposphere and lower stratosphere (UTLS)? To address this question, the understanding and proper representation of the underlying microphysical, multiphase chemical aspects, and macrophysical transport processes must be explored. Investigating these areas of interest is especially important to furthering the understanding of the formation and the atmospheric life cycle of organic aerosols (OA), and in particular secondary organic aerosol (SOA) particles.

Aerosols have a net cooling effect on the global climate and their reduction from certain systems has been associated with climate warming (Wang et al., 2023). Of the many processes that moderate climate systems, OA participates in direct and indirect influences on Earth's radiation budget through radiation forcing and altering cloud albedo by cloud condensation nucleation (Kanakidou et al., 2005; Liu et al., 2018; Mahowald, 1952, 2011). For radiative forcing, the optical properties of OA are its most relevant properties. This direct influence on climate moderation concerns the light absorption (Andreae and Gelencsér, 2006) and scattering of solar radiation by an OA (Chylek et al., 2019). These optical properties are determined by the chemical composition of the organics comprising the OA as well as the aerosol hygroscopicity (Cerully et al., 2015; Chan et al., 2005). Specifically, different molecular compositions will influence the aerosol size distribution, particle shape, water solubility, hygroscopicity, and refractive index (Lesins et al., 2002).

Organic compounds have been recognized for decades as active cloud condensation and ice formation nuclei (Sun and Ariya, 2006). Cloud condensation nuclei (CCN) are known contributors to cloud brightening in the natural environment via the Twomey effect (Mace et al., 2023) and support cloud lifetime through the Albrecht effect (Albrecht, 1989; Lindsey and Fromm, 2008). This effect results from the increased production of hydrometeors from additionally available CCN, which creates smaller and more numerous cloud droplets. This

increases the amount of radiation that clouds can reflect. As such, by acting as CCN atmospheric organics can have an indirect cooling effect on climate. However, the exact understanding of which organics participate as CCN, how they participate, and what properties they possess influence their abilities as CCN is complex. Factors such as surface tension, impurities, volatility, morphology, contact angle, deliquescence, and oxidation are considered in the theoretical prediction of an organic compound's ability as a CCN (Sun and Ariya, 2006). These factors however are not static and may be altered as OA undergo secondary processing (Petters et al., 2016).

Secondary processing of atmospheric organics proceeds in a variety of pathways. Some of the more general pathways tend to functionalize or oxidatively degrade large nonpolar species into more water-soluble, less volatile species (John H. Seinfeld and Spyros N. Pandis, 2019). Specifically, aqueous phase droplet chemistry is known to facilitate condensed phase SOA formation from highly volatile species (McNeill, 2015). In contrast, many freshly aged terpene oxidation products increase in volatility or see only small decreases in vapor pressure with oxidation for their early generation products (Bilde and Pandis, 2001; Kurtén et al., 2018; Wu et al., 2021). Additionally, oligomerization reactions that produce high molecular weight, humic-like compounds are known to occur in the presence of ozone via OA ozonolysis (Reynolds et al., 2006). These products are particularly of interest as they may dominate the organic mass and hence aerosol chemical and optical properties (Rudich et al., 2007).

While atmospheric organics influence many natural systems, their role in air quality and public health is often the most publicly visible. In the form of particulate matter (PM) and volatile organic compounds (VOCs)—the dominant forms of atmospheric organic matter—it is an environmental factor that is associated with increased respiratory morbidity and mortality (Heft-Neal et al., 2018a; Lelieveld et al., 2018; Rager et al., 2011). PM is responsible for 3.7-4.8 million premature deaths worldwide (Cohen et al., 2017). Of these deaths, 92% occur in low and middle income countries (Heft-Neal et al., 2018b; Landrigan et al., 2018; Lelieveld et al., 2018) and 2.8 million of these deaths are due to biomass burning for wood cookstoves (Gordon et al., 2014). VOCs have complex risk factors, supporting ozone production (Carter and L Carter, 1994) and posing individual toxic and carcinogenic risks (Barrefors and Petersson, 1995). High mass concentrations of PM and VOCs are common indications of poor air quality and smog events (Chang et al., 2019; Kumar et al., 2019).

The currently understood driving forces of PM toxicity are size fraction, mass concentration, and composition/oxidative potential (Reiss et al., 2007; Steenhof et al., 2011; Twigg and Phillips, n.d.). While government agencies like the EPA regulate PM based on mass concentration (EPA, 2023), recent studies using *in vitro* exposure techniques now suggest that PM mass concentration is not the only causal factor in health risks and that overall PM toxicity differs from the toxicity of its individual components (Valberg, 2004). *In vitro* exposure techniques in tandem with chemical and biological characterization have begun to identify specific constituents of PM most relevant to overall toxicity (Lichtveld et al., 2012a; Sotty et al., 2019; Steenhof et al., 2011). Current research has demonstrated that secondary processing of aerosols, namely photochemical changes, result in differential *in vitro* genomic responses, suggesting an increase in overall toxicity (de Bruijne et al., 2009; Lichtveld et al., 2012b; Rager et al., 2011; Vizuete et al., 2015). For example, SOA from isoprene photooxidation are demonstrated to significantly increase known inflammatory biomarkers IL-8 and COX-2 mRNA levels in human bronchial epithelial cells (BEAS-2B)(Arashiro et al., 2016).

1.2 Transport of Atmospheric Organics

With the many complex roles that atmospheric organics play in climate and public health, it is then critical to quantify its transport through the atmosphere so that its availability for these processes is better understood. However, recent studies raise the concern that under certain conditions, such as in convective systems and WCBs, current models underestimate available organic matter at high altitudes and are thus not accounting for certain transport processes (Bardakov et al., 2021; Williamson et al., 2019). Specifically, nucleation-mode particles—with sizes in the lower tens of nm—have consistently been observed in concentrations of up to 10^4 cm^{-3} from aircraft in the upper troposphere (Andreae et al., 2018; Andrés Casquero-Vera et al., 2020; Clarke et al., 1999; Heitto et al., 2024; Weigel et al., 2011; Williamson et al., 2019). These measurements significantly exceed the corresponding concentrations in the planetary boundary layer and indicate that the main source of such ultra-fine particles in the upper troposphere is in situ NPF rather than their direct transport from the boundary layer (Bardakov et al., 2021).

The traditional explanation for this phenomenon has been that the reduction of existing aerosol particles in deep convective clouds eliminates removal processes for small particles and condensable vapors, supporting NPF (Clarke et al., 1998). However, Williamson et al. (2019) also showed that even without these conditions, such as in tropical convection,

these newly formed particles can still be found. They then argue that most models underestimate available organic matter at high altitudes and as a result predict less NPF in these regions. If this NPF is the result of an overlooked mechanism of organic matter transport, it is then critical to elucidate this mechanism that transports NPF precursors so to constrain uncertainty around the influence of high altitude NPF from convective outflows (Bardakov et al., 2021).

1.3 Chemical Retention and Ice Uptake of Organics

A potential mechanism for this organic matter transport is chemical retention during droplet freezing. More specifically, organic compounds that are exchanged between the gas and aqueous phase in cloud droplets can either be trapped in the ice phase during freezing—washing them out by precipitation—or return to the gas phase by volatilization. This revolatilization caused by the freezing process leads to a vertical redistribution and has the potential to explain the occurrence of organic matter at high altitudes in regions with deep convection. However, while theoretical models that try to describe this process exist in the literature (Audiffren et al., 1999; Mari et al., 2000; Stuart and Jacobson, 2003, 2004) as well as some basis of experimental data concerning inorganics (Von Blohn et al., 2011b, a; Snider et al., 1992; Snider and Huang, 1998), the experimental data for organics and their associated retention is limited (Borchers et al., 2024a; Jost et al., 2017a).

While revolatization caused by hydrometeor freezing may provide a transport source of organics to the UTLS, the removal processes and sinks are just as critical to understand. One such understudied process is the uptake of organics on ice particles, specifically its adsorption to static ice and its codeposition with water vapor on growing ice particles. This uptake of a compound on an ice particle that is growing from vapor-to-ice is known as diffusional uptake. While there are many studies that investigate the diffusional uptake for inorganic species (e.g. H_2O_2, HCl, HNO_3, etc.) (Bartels-Rausch et al., 2014; Conklin et al., 1993; Diehl et al., 1995; Dominé and Thibert, 1996; Mitra et al., 1990; Santachiara et al., 1998), there are only a few for organic compounds (Fries et al., 2007; Huffman and Snider , 2004).

Previous investigations into how organics are transported in the atmosphere have largely been hindered by the analytical instrumentation available. For instance, rainwater dissolved organic matter (DOM) is a complex heterogeneous mixture of organic compounds, the composition of which is considered less than 50% chemically characterized (Altieri et al.,

2009; Willey et al., 2000). Identifying the composition of organic species in atmospheric waters has been held back largely by the difficulty of analyzing species present in very low abundances in a complex matrix of thousands of unique compounds. Significant progress has been made to identify the composition of complex DOM in organic aerosols and rainwater DOM using Fourier transform ion cyclotron resonance mass spectrometry (FT-ICR MS) (Altieri et al., 2012; Mead et al., 2013, 2015; Willoughby et al., 2016), however these methods have a low throughput and the resultant studies are limited in sample size (the highest being seven samples (Altieri et al., 2012)). These methods also involve preconcentration usually through solid-phase extraction (SPE), which contribute to analyte loss particularly for higher oxygen content and more polar species (Li et al., 2019; Reemtsma et al., 2008; Sleighter and Hatcher, 2008). Alternative high resolution mass analyzers in the Fourier transform family such as the Orbitrap have started to become part of routine analysis in numerous areas of research (Eliuk and Makarov, 2015; Martins et al., 2016). Orbitrap mass spectrometry has now been used to characterize rainwater and riverine DOM as well as ambient aerosols (Laskin et al., 2009; Nguyen et al., 2011; Remucal et al., 2012; Seymore et al., 2023) and its high resolution, mass accuracy, and ability to be used in combination with other mass selection technologies make it an ideal candidate for complex analysis and has begun to garner global attention for its application in studying environmental systems.

2. Theoretical Background

2.1 Chemical Retention

Ice growth in the atmosphere proceeds via a few distinct processes: (1) the collection of supercooled cloud droplets by ice (riming), (2) direct liquid freezing, and (3) vapor-to-ice growth by diffusion. While still in the liquid phase, water droplets in the atmosphere can exchange their dissolved chemical components with their surroundings. This proceeds to an equilibrium of the trace chemical substances present between the gas and aqueous phase in cloud droplets. When these hydrometeors are uplifted such as in convective updraft, they undergo freezing through riming or direct liquid freezing. The dissolved trace chemical substances are then thought to either become trapped in the ice phase or return to the gas phase by volatilization. By becoming trapped in the ice phase, these chemical constituents remain in the hydrometeor and are then washed out of the atmosphere by precipitation. If these chemical substances are instead revolatized to the gas phase, they are now available as gas phase components at whatever altitude freezing occurred. This potentially results in a net vertical transport of these chemical components where exchange happens at low altitudes and freezing expulsion occurs at higher altitudes.

To understand this macrophysical transport process, the underlying microphysics and multiphase chemistry need to be explored. On the theoretical basis, whether a substance is retained in the ice phase or not can be thought of as a comparison of the freezing time and the total time required for expulsion, which is estimated as a sum of the time required for a chemical component to diffuse through the aqueous phase, exchange across the interfacial boundary, and then proceed as a gas. Comparing freezing time and expulsion time produces a value called a Retention Indicator (RI). This RI is used by theorists to model and estimate what proportion of a substance will remain in the ice phase after freezing. Experimentally, retention is described by a retention coefficient R which indicates the proportion of a substance that remains in the ice during this phase change as a percentage of the trapped substance with a value between 0 and 1 (Bela et al., 2018; Iribarne and Pyshnov, 1990; Snider et al., 1992; Stuart and Jacobson, 2004).

Current experimental studies to determine retention coefficients for atmospheric constituents and relevant SOA precursors have focused on inorganic species, small organics, or single component mixtures with significantly higher than natural concentrations (Von Blohn et al., 2011b, a; Snider et al., 1992; Snider and Huang, 1998). The few studies that look

at complex mixtures are limited to compounds of similar families and only a handful of species (Borchers et al., 2024b; Jost et al., 2017a). These studies have revealed that a species' retention is influenced by its chemical properties, such as its dimensionless effective Henry's law solubility constant (H^*), as well as the physical properties of the droplet and its environment such as temperature, liquid water content, droplet size, and ventilation. One of the most applicable findings across several studies is that substances with a small H^* are more likely to return to the gas phase during riming, which results in a lower retention coefficient. Additionally, the external and physical conditions of the droplet disproportionally influence the retention for these small H^* substances (Jost et al., 2017b; Stuart and Jacobson, 2003, 2004).

H^* is a unitless value derived from a temperature and pressure defined Henry's law solubility constant (H_s^{cp}). This value is defined as the ratio of the aqueous-phase concentration of a chemical to its equilibrium partial pressure in the gas phase (at infinite dilution). While Henry's law coefficients are available to describe the interactions with most organic gases with liquid water (Sander, 2023), less is known about its relationship with ice phase processes. Because of the findings of the experimental studies, the current models that describe chemical retention use H^* as one of the most important chemical parameters. Thus, the most relevant and discussed model is the semi-empirical model of Stuart and Jacobson (Stuart and Jacobson, 2003, 2004) which assimilated the most relevant factors on retention to calculate RI. These factors include chemical properties such as H^*, mass accommodation, aqueous diffusivity, and gas diffusivity as well as physical factors such as temperature, droplet size, and ventilation. This model and its further details are also explained in Jost et al., (2017a) and Stuart and Jacobson, (2003, 2004).

2.2 Semi-Empirical Modeling of Retention

This model primarily attempts to explain the retention of chemicals under dry growth riming conditions, which is the mode of freezing where supercooled cloud droplets have little time in the liquid phase when undergoing accretion with the rime collector (Brownscombe and Hallett, 1967). To explain this semi-empirical model more thoroughly, the RI is calculated by the ratio of the expulsion timescale (τ_{exp}) of a species from the liquid phase to the freezing time (τ_{frz}) of the droplets.

$$\mathrm{RI} = \frac{\tau_{exp}}{\tau_{frz}} \tag{1}$$

The calculations for the individual timescales are less trivial and are comprised of several terms that assimilate the chemical and physical factors. τ_{exp} is calculated as the sum of all the relevant timescales that characterize an individual substance's path to leave the droplet and enter the gas phase (Schwartz, 1986). This term accounts for all the expected chemical influences that might impede expulsion. This is calculated formally as:

$$\tau_{\text{exp}} = \underbrace{\frac{h^2 H^*}{3 D_g \bar{f}}}_{\tau_g} + \underbrace{\frac{4 h H^*}{3 \bar{v} \alpha_m}}_{\tau_i} + \underbrace{\frac{h^2}{D_{\text{aq}}}}_{\tau_{aq}} + \tau_r \tag{2}$$

where $h = 4a/3S^2$ is the spread droplet height, a the droplet radius, S the spreading factor, H^* the effective Henry's law coefficient, $\bar{f}$ the mean gas-phase ventilation coefficient (related to the collector's fall speed), D_g the diffusivity of the chemical in air, $\bar{v}$ the thermal velocity of the chemical in air, α the mass accommodation coefficient, and D_{aq} the diffusivity of the chemical in water. The first term on the right-hand side of Eq. (2) describes gas-phase mass transport (τ_g), the second term the interfacial mass transport (τi) and the third term the aqueous-phase mass transport (τ_{aq}). Here, a fourth term (τ_r) which describes the kinetics of aqueous-phase reactions (i.e., association, John H. Seinfeld and Spyros N. Pandis, 2019 or reaction with NH_4 or CO_2, Jost et al., 2017a) is also included in the expulsion timescale. This reaction timescale is often neglected (Stuart and Jacobson, 2003, 2004) because acid/base reactions are generally fast compared to the other processes involved.

To estimate τ_{frz}, (Stuart and Jacobson, 2003, 2004) use an iterative thermophysical model that balances the total latent heat released due to drop freezing (q_{frz}) with the heat loss during the freezing time to both air (q_{out}) and the rime collector (q_{in}). This iterative model is used because there is no closed solution for freezing time that accounts for both heat loss to air and heat loss to the rime collector. This takes after an earlier model by Baker et al. (1987). To briefly summarize this calculation, the energy balance of the heat transfer is calculated as:

$$q_{frz} - q_{out} - q_{in} = \varepsilon \tag{3}$$

where ε is the convergence tolerance of the energy balance. The individual heat transfers (q) are then estimated first with the assumption that either heat loss to the rime collector or heat loss to the air is negligible (q_{in} or $q_{out} = 0$). If either of these assumptions cannot account for the energy balance such that $\varepsilon < 1\%$ of q_{frz}, the model repeats the estimations of the individual heat transfers with a new guess for the freezing time through a

series of multistep calculations until the heat balance converges with ε < 1% of q_{frz}. The new guess for freezing time is set by the equation:

$$t = \frac{q_{frz} - q_{in}}{\dot{q}_{out}} \tag{4}$$

where $\dot{q}_{out}$ is the rate of heat loss to air such that when multiplied with time (t), it produces the total heat loss to air (q_{out}). The individual estimations for the heat transfer terms are described in more detail in Stuart and Jacobson (2003, 2004), but the core idea is that they use expressions for linear heat flow, latent heat of freezing, heat absorption capacity, and the droplet geometry as a basis for these calculations. With the relevant timescales for τ_{exp} and τ_{frz} determined, RI can be calculated from Eq. (1). However, RI spans a wide domain space (1×10^{-n} and 1×10^{n}, where n is a large number) such that it's not directly applicable with the 0 to 1 range of the retention fraction (R, which is equivalent to the experimentally determined retention coefficient). Thus to relate the theoretical value RI to the experimental R, Stuart and Jacobson (2003, 2004) map RI to R with the expression:

$$\mathrm{R} = 1 - \exp\left(-K * \mathrm{RI}\right) \tag{5}$$

where K is a constant that produces the best fit value that relates the theoretical calculations for RI with the available experimental data for R. Jost et al. (2017) however suggests a smoother transition between high and low values of R and represents this R and RI relationship by the equation:

$$\mathrm{R_{RI}} = \left(1 + \left(\frac{a}{\mathrm{RI}}\right)^{b}\right)^{-1} \tag{6}$$

where a and b are the fit paraments of the relationship that best minimize the average absolute error between R and $\mathrm{R_{RI}}$. Since this relationship minimized the error between the available experimental results and the associated estimations for RI, the fit function in Eq. (6) has been used in the experimental studies that followed Jost et al. (2017) (these being the publications within this dissertation). Considering the experimentally revealed dependency of R on H^*, Jost et al. (2017) takes this further into account by directly describing the relationship between R_{H^*} and H^* with the same parameterization of $\mathrm{R_{RI}}$:

$$\mathrm{R}_{H^*} = \left(1 + \left(\frac{a}{H^*}\right)^{b}\right)^{-1} \tag{7}$$

where a and b are the fit paraments of the relationship that best minimize the average absolute error between R and R_{H^*}. The application of the R_{H^*} parameterization from Eq. (7) is

often more accurate than the parameterization for R_{RI} from Eq. (6) and so is frequently used in experimental studies exploring the relationship between R and H^*. While the R_{H^*} parameterization is rather accurate for a first order approximation, it only accounts for the characteristics that H^* describes, which are aqueous solubility and dissociation. The R_{RI} parameterization also accounts for ventilation, temperature, droplet size, and liquid water content. This parameterization for R_{H^*} is believed to be accurate for measurements within similar physical conditions because the temperature and ventilation effects are small for most investigated substances. That is to say, R likely depends the most on changes in the expulsion time (τ_{exp}) resulting from solubility and dissociation described by H^* than it does on changes in freezing time (τ_{frz}), temperature dependent diffusivity, or mass transfer enhancement from ventilation.

These mathematical descriptions provide a framework for the understanding of the microphysics and multiphase chemistry of retention. The implications then to the macrophysical transport are clearer. The vertical transport of these chemical components resulting from the aqueous phase exchange at low altitudes and freezing expulsion at higher altitudes primarily affects the transport of chemical species with sufficiently low H*. More particularly, the main formation pathway of precipitation-size ice particles in convective clouds is riming. Thus, riming retention is an important process for the vertical redistribution of water-soluble organic compounds (WSOC). Convective clouds with warm bases favor the formation of mm-sized drops by collision-coalescence (Lamb and Verlinde, 2011), which subsequently can be uplifted in the updraft to regions with temperatures below 0°C. Once beyond the freezing level they can freeze and thereby release dissolved matter into the gas phase. This identifies freezing retention of mm-sized drops as a potential contributor to the vertical redistribution of WSOCs. In the literature, most current studies have only examined retention for droplets in the size range found in natural clouds rather than raindrop sizes. This highlights the differing physical conditions resulting from the freezing mode of riming and direct liquid freezing as notable contributors to chemical transport.

Alternatively, earlier publications by Pruppacher and Klett (2010) and Snider and Huang (1998) have suggested that complete sublimation of ice particles can also transport ‘retained’ compounds trapped in the ice phase and release them at high altitudes. This demonstrates that the sublimation and depositional phase changes of hydrometeors are possible transport pathways for chemical substances in the atmosphere. The release of chemical components from complete sublimation of an ice particle is thought to equitably

transport the retained compounds out of the ice phase. Afterall, a substance cannot remain in the ice phase if the ice particle is completely sublimated. However, the deposition of a volatile compound, particularly a VOC, to the ice phase can differ between compounds that may have different potentials for ice uptake.

2.3 Diffusional Ice Uptake

The growth of ice via water vapor-to-ice deposition is often interchangeably referred to as depositional growth or diffusional growth. To keep the meteorological use of 'deposition' and 'precipitation' distinct from their chemical usage, 'deposition' will hereafter strictly refer to the process by which particles fall from the atmosphere to the ground either directly or with rainfall or snowfall; 'precipitation' will strictly refer to water of any form that falls from the atmosphere to the ground. The chemical usage of 'deposition' and 'precipitation' will be serviced by the terms 'uptake' and 'phase change' respectively. The mode of freezing referenced above will be hereafter referred to as 'diffusional growth' or 'diffusional freezing'. This mode of ice production is highly relevant as diffusional growth ice is the responsible mechanism for all cloud formations in the upper troposphere (Heymsfield et al., 2020; Mülmenstädt et al., 2015). Further, most precipitation in the midlatitudes as well as all cloud formation in the upper troposphere is formed via ice and subsequently indicates that diffusional growth ice is a significant contributor to the wet deposition of trace atmospheric constituents (Franz and Eisenreich, 2000; Heymsfield et al., 2020; Mülmenstädt et al., 2015). This process of diffusional ice crystal growth is considered rather similar to the condensational growth of liquid cloud droplets as they are governed by the same laws of vapor saturation.

Water vapor exists in equilibrium with respect to its other phases as defined by the chemical properties of water as well as the temperature and pressure of the system it inhabits. Water vapor saturation is met when a parcel of air contains the maximum density of water vapor that can be held, i.e. any further addition of water vapor will result in the phase change of some portion of the vapor in the system. This saturation is typically described by a saturation vapor pressure which is the partial pressure of the vapor at which saturation is achieved. For water, the saturation pressure can either be defined with respect to liquid water or ice. Concerning a system that is below the temperature at which liquid water proceeds to ice (< 0 ºC at 1 atm), the saturation pressure is normally defined with respect to ice. Thus, if water vapor at these temperatures has a partial pressure above the saturation pressure (wrt ice), it will proceed in a phase change from vapor-to-ice. There are several equations that

exist to calculate the pressure of water vapor over a surface of liquid water or ice, such as the WMO, Hardy, Buck, Hyland and Wexler, or Sonntag parameterizations ((WMO), 2011). One of the most commonly used equations to describe the saturation pressure of water vapor over ice is the Sonntag parameterization (Sonntag, 1994).

Sonntag (1994) presents a few of the several iterations to thermodynamically calculate saturation vapor pressures before it presents the set of equations developed by D. Sonntag (1990) that was then incorporated into the World Meteorological Organization's No.8 "Guide to Meteorological Instruments and Methods of Observation" 6th ed. This parameterization is still in wide use and the most relevant here being the parameterization over the given temperature range of –100.0 to + 0.01°C. This is given as:

$$\begin{aligned}\log e_i \;=\; & -6024.5282 \,/\, T \\ & + 24.721994 \\ & + 1.0613868 \times 10^{-2} \cdot T \\ & - 1.3198825 \times 10^{-5} \cdot T^2 \\ & - 0.49382577 \cdot \log T\end{aligned} \tag{8}$$

This equation calculates the saturation pressure of water vapor over ice (e_i) in units of hPa as a function of air temperature (T) in units of K. Comparing the saturation pressure (wrt ice) with the actual vapor pressure as a ratio then produces the saturation ratio of water vapor with respect to ice (S_{ice}). This ratio is usually expressed as a percentage concerning the relative humidity (RH_i) and is a common descriptor of the available vapor and its capacity for ice phase transition. Many cirrus clouds have RH_i in the ranges of 60-140%, but many higher altitude clouds are in the range of 80-180% (Dekoutsidis et al., 2023).

On the microscale, the rate at which an ice crystal grows is equivalent to the diffusive flux of water vapor to the crystal surface. This can then be calculated using a Fick diffusion expression:

$$J = D_T \frac{C_0 - C_f}{l_m} \tag{9}$$

where l_m is the thickness of the diffusion layer, D_T is the diffusion coefficient of water vapor (2.2×10^{-5} m^2 s^{-1}) and C_0 and C_f are the initial and final water vapor concentrations across the vapor gradient. The value of l_m is calculated by the Einstein equation:

$$l_m = \sqrt{2D_T t_k} \quad (10)$$

where t_k is the condensation time. With the saturation and growth rate established, the uptake for an individual volatile compound can be addressed. The experiments in the literature that describe ice uptake often describe either "growing ice" or "static ice" which then have investigated the effects of volume uptake and surface processes respectively. Static ice uptake is typically a reversible adsorption process (Fries et al., 2006; Von Hessberg et al., 2008). Volume uptake by growing ice however is a more significant process (Fries et al., 2007; Huffman and Snider, 2004).

2.4 Ice-Gas Partitioning Coefficients

Treating the uptake of a compound by ice crystals growing through diffusion as an equilibrium allows for the calculation of ice-gas partitioning coefficients, referred interchangeably as uptake coefficients. These coefficients ($K_{g,ss}$) describe the ratio of the gas phase concentration of the analyte vapor to its concentration in the ice phase. More specifically, with the possibility for a liquid solution phase that coexists with ice, this relationship is described as:

$$K_{g,ss} = K_{g,l} K_{l,ss} \quad (11)$$

where the equilibrium constants $K_{g,ss}$ and $K_{g,l}$ relate the analyte concentrations in the ice solid solution (*ss*) and liquid water (*l*) phases to the analyte partial pressure in the gas phase (*g*). The last equilibrium constant ($K_{l,ss}$) relates the concentrations in the liquid water (*l*) and solid solution (*ss*) phases. Most studies report direct measurements of $K_{g,ss}$ for their compounds and neglect thorough investigation of gas to liquid or liquid to ice equilibrium. This partitioning to and from the liquid layer is complicated to study directly and there is much discussion on whether these terms accurately describe any sort of liquid phase or quasi-liquid layer behavior. What is more relevant is that quasi-liquid layers are routinely observed experimentally despite disagreements over what their properties may be (Shi et al., 2022). Regardless, most experimental investigations of diffusional growth ice uptake focus on measuring $K_{g,ss}$. Hereafter, $K_{g,ss}$ will be referred to simply as K and is specifically considered a volume uptake coefficient.

To determine a partitioning coefficient, the concentrations of an analyte in two different phases are measured at equilibrium. To determine an ice-gas partitioning coefficient,

the gas phase concentration of the analyte vapor and its concentration in the ice phase are measured and compared in a ratio such as in the equation:

$$K = \frac{\rho_{ice} C_{ice}}{m_{ice} C_{gas}} \quad (12)$$

where C_{ice} is the absolute mass of the analyte in ice (ng), ρ_{ice} is the density of ice at the freezing temperature (g cm^{-3}), C_{gas} is the concentration of the analyte in the gas phase (ng m^{-3}), and m_{ice} is the total mass of ice (g). For proper unit conversion, a factor of 10^6 is applied for the conversion of m^3 to cm^{-3}. Practically speaking, K is also used as a sorption coefficient or a dimensionless uptake coefficient with respect to the removal of trace gases in the upper atmosphere. A larger value for K indicates more uptake into the ice phase.

2.5 Thermodynamics of Ice Uptake

Strictly speaking, chemical uptake on growing ice crystals is a stationary state and not an equilibrium. However, diffusional crystal growth is slow relative to other modes of freezing (day vs. ms timescales) and so the system can be approximated as an equilibrium state (Dominé and Thibert, 1996; Fries et al., 2007; Huffman and Snider, 2004). Then as a thermodynamic equilibrium, K can also be used to calculate the Gibbs energy (ΔG) of the uptake process at each temperature. This is a direct calculation using the equation:

$$\Delta G = -RTln(K) \quad (13)$$

where T is temperature (K) and R is the ideal gas-constant (8.31447 J K^{-1} mol^{-1}). These values describe the energy available for the uptake process. Positive values of ΔG indicate the analyte favors the gas phase while negative values of ΔG indicate the analyte favors the ice phase. Even lower, more negative values of ΔG would indicate more efficient uptake of the analyte into the ice phase.

Continuing the thermodynamic analysis, the theoretical temperature dependence of the sorption coefficient K can be determined with the van't Hoff equation, which when substituting with the Gibbs-Helmholtz equation produces the following:

$$\ln(K) = -\frac{\Delta H - T\Delta S}{RT} = -\frac{\Delta H}{R}\frac{1}{T} + \frac{\Delta S}{R} \quad (14)$$

where ΔH and ΔS are the heat of sorption and the sorption entropy respectively. Here the heat of uptake and uptake entropy are used instead. Performing a linear regression of $\ln(K)$ against $1/T$ using the van't Hoff equation provides a slope of $-\Delta H/R$ and an intercept of

$\Delta S/R$. Multiplying each of these values by –R and R respectively produces the values of ΔH and ΔS. Increasing values of the uptake enthalpy ΔH and the uptake entropy ΔS along with decreasing compound vapor pressure—i.e. the volatility of the pure analyte—can indicate that the uptake of the analyte is dependent on the physical parameters of the compounds and ice surface. Specifically, these are the parameters that determine thermodynamic sorption such as temperature, molecular mass, ice surface coverage, surface morphology and porosity, surface crystallographic phases, quasi-liquid layer behavior, and crystal imperfections (Behr et al., 2006; Fries et al., 2006; Orem and Adamson, 1969; Sokolov and Abbatt, 2002). However, lower values of ΔH and poor linear regression can be a sign that the uptake process cannot be exclusively described by thermodynamic sorption.

While there are many studies that investigate the diffusional uptake for inorganic species (e.g. H_2O_2, HCl, HNO_3, etc.) (Bartels-Rausch et al., 2014; Conklin et al., 1993; Diehl et al., 1995; Dominé and Thibert, 1996; Mitra et al., 1990; Santachiara et al., 1998), there are only a few for organic compounds (Fries et al., 2007; Huffman and Snider , 2004). The publications by Fries et al. (2007) and Huffman and Snider (2004) concern the ice uptake of aromatic hydrocarbons and oxyhydrocarbons. These are the first studies to describe the interactions between diffusion-growing ice and the uptake of organic vapors.

3. Summaries of Experimental Results

The publications herein concern experimental studies exploring the chemical retention and diffusional uptake of various chemical substances, primarily diverse organics and SOA precursors, on hydrometeors involved in an ice phase transition. The experiments presented in these publications were performed at the Mainz Wind Tunnel Laboratory. These experiments demonstrate the measurement of retention coefficients through the use of the Mainz Wind Tunnel or an acoustic levitation apparatus; the measurement of gas-ice partitioning coefficients through the use of a self-designed Flowtube apparatus; and the significance of these measurements for atmospheric processing and the associated transport of the implicated organic species.

3.1 Summary of *Gas-Ice Partitioning Coefficients of Carbonyls during Diffusional Ice Crystal Growth*

2025, Seymore J., Szakáll, M., Theis, A., Mitra, S.K., Borchers, C., Hoffmann, T. Gas-Ice Partitioning Coefficients of Carbonyls during Diffusional Ice Crystal Growth. **Accepted** for Publication after revision with *Atmospheric Chemistry and Physics*
https://doi.org/10.5194/egusphere-2025-1425

This study addresses the underrepresented topic of chemical uptake via diffusional ice growth. Chemical redistribution between the gas and ice phase during diffusional freezing is not fully understood, particularly for the wide variety of atmospheric organics and more specifically atmospherically relevant carbonyls. This is despite its relevance as a removal process of organics from the atmosphere and thereby its role in secondary organic aerosol production, atmospheric oxidative capacity, and tropospheric photochemistry.

We conducted laboratory studies on the partitioning of gas-phase carbonyls to the ice phase during the diffusional growth of ice crystals using a flowtube type experimental apparatus. In a series of experiments, precise mixtures of water vapor and gas-phase carbonyls were passed through a flowtube in order to grow ice crystals from diffusion. Inside the flowtube, the ice crystals were grown under conditions that mimic naturally occurring temperatures and humidities in cirrus clouds. During the experiment, influent and effluent gas samples were passed through reagent coated gas denuders to collect integral samples of the carbonyl gas concentrations. At the conclusion of the experiment, the deposited ice was

collected along with extracts from the gas denuders and then analyzed using ultra-high performance liquid chromatography with ultra-high resolution mass spectrometry. From the result-ant analyte concentrations in the gas and ice phases, along with the ice mass yields, the partitioning coefficients for each of the 14 carbonyls studied were determined at –20, –30, and –40 ºC. Using van't Hoff analysis, the entropy and enthalpy of uptake were determined. An inverse relationship between partitioning coefficients and temperature was observed for all species except methyl vinyl ketone. A linear correlation between ΔS and ΔH arose which was statistically validated and determined with 99% confidence to not be a statistical artifact. This compensation behavior could be an indication of a surface liquid layer or quasi-liquid layer behavior involved in the uptake process and could also indicate a single dominant influence on a compound's uptake. The most significant physicochemical properties correlated with uptake were identified to be vapor pressure and molar mass, which indicate that smaller compounds with higher vapor pressures are more readily taken into the ice phase.

I was the main contributor to this publication. Specifically, I along with MS, AT, SM designed the experiments; I along with AT, SM constructed the experimental apparatus; I prepared the solutions for experiments, performed the experiments, and collected the samples; I along with CB conducted the analytical measurements; I analyzed the data and wrote the manuscript draft; I along with MS, AT, CB, TH reviewed and edited the manuscript.

3.2 Summary of *Retention During Freezing of Raindrops, Part II: Investigation of Ambient Organics from Beijing Urban Aerosol Samples*

2025, Seymore, J., Gautam, M., Szakáll, M., Theis, A., Hoffmann, T., Ma, J., Zhou, L., and Vogel, A. Retention During Freezing of Raindrops, Part II: Investigation of Ambient Organics from Beijing Urban Aerosol Samples**. Accepted** for Publication with *Atmospheric Chemistry and Physics* https://doi.org/10.5194/egusphere-2024-3940

This study addresses the underrepresented topic of chemical retention during drop freezing processes. Chemical redistribution between the liquid and gas phase during freezing is not fully understood, particularly for the wide variety of atmospheric organics. This is despite its relevance to the vertical redistribution of organics along the UTLS and its support of new particle formation in convective outflows, thereby its subsequent role in radiation scattering and cloud condensation nucleation.

We conducted laboratory studies on the chemical retention of water-soluble compounds sampled from ambient Beijing aerosols during drop freezing experiments in an acoustic levitator setup. An aqueous extract of filter samples collected from PM2.5 Beijing aerosols was introduced via syringe into an acoustic levitator housed inside a cold chamber held at -15ºC. The contact-free single-drop was allowed to freeze without the introduction of artificial freezing nucleator and then collected for comparative analysis with the native extract. The samples were then chemically analyzed with ultra-high resolution mass spectrometry and the retention coefficients determined. Our results show that the retention of WSOC forms a real, nonnormal distribution up to 1 and that raindrop freezing does not have a sigmoidal relation with effective Henry's Law solubilities. This contrasts with the behavior currently described in the literature specifically for cloud droplets. Our data also shows that different classes of organics may have different distributions of retention coefficients. For example, nitro and sulphate substituted species—often the products of anthropogenically related NOx and SOx chemistry—are highly retained. This suggests that NOx and SOx chemistry may enhance the retention of these SOA species and reduce their likelihood of reaching the upper atmosphere. This contrasts with the wide distribution for CHO groups like sugars, organic acids, and terpenoids with highly variable retentions.

I was the main contributor to this publication. Specifically, I along with MG, MS, AT designed the experiments; I along with JM prepared the samples for experiments; I along with JM, AV conducted the analytical measurements; I analyzed the data and wrote the manuscript draft; I along with MG, MS, AT, JM, AV, TH reviewed and edited the manuscript.

3.3 Summary of *Retention During Freezing of Raindrops, Part I: Investigation of Single and Binary Mixtures*

2025, Gautam, M., Theis A., **Seymore, J.**, Hey, M., Borrmann, S., Diehl, K., Mitra, S.K., and Szakáll, M. Retention During Freezing of Raindrops, Part I: Investigation of Single and Binary Mixtures**, Accepted** for Publication with *Atmospheric Chemistry and Physics* https://doi.org/10.5194/egusphere-2024-3917

This study addresses the underrepresented topic of chemical retention during drop freezing processes. Chemical redistribution between the liquid and gas phase during freezing is not fully understood, particularly for the wide variety of atmospheric organics. This is despite its relevance to the vertical redistribution of organics along the UTLS and its support

of new particle formation in convective outflows, thereby its subsequent role in radiation scattering and cloud condensation nucleation.

We investigated the retention of specific chemical species and their binary mixtures during freezing of raindrops via acoustic levitation. Prepared solutions of analyte samples were introduced via syringe into an acoustic levitator housed inside a cold chamber held at –15ºC. The contact-free single-drop was allowed to freeze without the introduction of artificial freezing nucleator and then collected for comparative analysis with the native solution. Our results reveal high retention with nearly all substances being fully retained during freezing. This could be attributed to faster freezing time compared to slower mass expulsion time, along with ice-shell formation during freezing. This result helps improve our understanding of interaction between ice microphysical processes and chemistry in deep convective clouds.

I was a significant contributor to this publication. Specifically, I along with MG, MZ, AT, SM designed the experiments; I along with MG, MH, conducted analytical measurements, I along with AT, MH, SB, KD, MZ reviewed and edited the manuscript.

3.4 Summary of *Retention of α-pinene oxidation products and nitro-aromatic compounds during riming*

2024, Borchers, C., **Seymore, J.**, Gautam, M., Dörholt, K., Müller, Y., Arndt, A., Gömmer, L., Ungeheuer, F., Szakáll, M., Borrmann, S., Theis, A., Vogel, A.L., and Hoffmann, T., Retention of *α*-pinene oxidation products and nitro-aromatic compounds during riming. **Published** with *Atmospheric Chemistry and Physics*. Atmos. Chem. Phys., 24, 13961–13974, https://doi.org/10.5194/acp-24-13961-2024

This study addresses the underrepresented topic of chemical retention during rime freezing processes. Riming is an important growth process of graupel and hailstones in mixed-phase zones of clouds, during which supercooled liquid droplets freeze on the surface of ice particles by contact. Compounds dissolved in the supercooled cloud droplets can remain in the ice or be released to the gas phase during freezing, which might play an important role in the vertical redistribution of these compounds in the atmosphere by convective cloud processes. This is important for estimating the availability of these compounds in the upper troposphere, where organic matter can promote new particle formation and growth. The amount of a chemical species remaining in the ice phase can be described by the retention coefficient. At the time of publication, only inorganic, and small

organic molecules have been investigated regarding their retention during the freezing process. We performed experiments in the Mainz vertical wind tunnel under dry and wet growth conditions as well as different pH values to obtain the retention coefficients of cis-pinic acid, cis-pinonic acid and (-)-pinanediol, 4-nitrophenol, 4-nitrocatechol, 2-nitrobenzoic acid and 2-nitrophenol. Our results are in accordance with previous studies which showed a dependence between the dimensionless effective Henry's law constant H^* and the retention coefficient for inorganic and small organic molecules. Our results reveal that this correlation can also be applied to more complex organic molecules.

I was a significant contributor to this publication. Specifically, I along with CB, MG, KD, YM, AA, LG, AT, AV, and TH designed and performed the wind tunnel experiments; I along with MG, MS, AT, AV, and TH reviewed and edited the paper.

4. Publications

4.1 *Gas-Ice Partitioning Coefficients of Carbonyls during Diffusional Ice Crystal Growth*

The following manuscript addresses the underrepresented topic of chemical uptake via diffusional ice growth. Chemical redistribution between the gas and ice phase during diffusional freezing is not fully understood, particularly for the wide variety of atmospheric organics and more specifically atmospherically relevant carbonyls. This is despite its relevance as a removal process of organics from the atmosphere and thereby its role in secondary organic aerosol production, atmospheric oxidative capacity, and tropospheric photochemistry.

We conducted laboratory studies on the partitioning of gas-phase carbonyls to the ice phase during the diffusional growth of ice crystals using a flowtube type experimental apparatus. In a series of experiments, precise mixtures of water vapor and gas-phase carbonyls were passed through a flowtube in order to grow ice crystals from diffusion. Inside the flowtube, the ice crystals were grown under conditions that mimic naturally occurring temperatures and humidities in cirrus clouds. During the experiment, influent and effluent gas samples were passed through reagent coated gas denuders to collect integral samples of the carbonyl gas concentrations. At the conclusion of the experiment, the deposited ice was collected along with extracts from the gas denuders and then analyzed using ultra-high performance liquid chromatography with ultra-high resolution mass spectrometry. From the resultant analyte concentrations in the gas and ice phases, along with the ice mass yields, the partitioning coefficients for each of the 14 carbonyls studied were determined at –20, –30, and –40 ºC. Using van't Hoff analysis, the entropy and enthalpy of uptake were determined.

An inverse relationship between partitioning coefficients and temperature was observed for all species except methyl vinyl ketone. A linear correlation between ΔS and ΔH arose which was statistically validated and determined with 99% confidence to not be a statistical artifact. This compensation behavior could be an indication of a surface liquid layer or quasi-liquid layer behavior involved in the uptake process and could also indicate a single dominant influence on a compound's uptake. The most significant physicochemical properties correlated with uptake were identified to be vapor pressure and molar mass, which

indicate that smaller compounds with higher vapor pressures are more readily taken into the ice phase.

I was the main contributor to this publication. Specifically, I along with MS, AT, SM designed the experiments; I along with AT, SM constructed the experimental apparatus; I prepared the solutions for experiments, performed the experiments, and collected the samples; I along with CB conducted the analytical measurements; I analyzed the data and wrote the manuscript draft; I along with MS, AT, CB, TH reviewed and edited the manuscript.

Supplementary material supporting this manuscript can be found in Section 8.

https://doi.org/10.5194/egusphere-2025-1425
Preprint. Discussion started: 3 April 2025

Gas-Ice Partitioning Coefficients of Carbonyls during Diffusional Ice Crystal Growth

Jackson Seymore*[1], Miklós Szakáll[1], Alexander Theis[3], Subir K. Mitra[3], Christine Borchers[2], Thorsten Hoffmann[2]

[1] Institute for Atmospheric Physics, Johannes Gutenberg University, Mainz, Germany
[2] Department of Chemistry, Johannes Gutenberg–University, Mainz, Germany
[3] Particle Chemistry Department, Max Planck Institute for Chemistry, Mainz, Germany

*Corresponding author: Jackson Seymore seymorej@uni-mainz.de

Keywords: gas-ice partitioning, diffusional crystal growth, Orbitrap MS, secondary organic aerosol, SOA, convective clouds, entropy-enthalpy compensation, EEC

Abstract

Carbonyls are highly relevant atmospheric constituents that influence tropospheric photochemistry and oxidative capacity. They can be removed from the upper troposphere via ice phase deposition scavenging. The gas-ice partitioning coefficients for 14 different carbonyl compounds were determined using a flowtube apparatus. Ice crystals were grown from vapor deposition in the presence of gas phase carbonyls at –20, –30, and –40 ºC. Using van't Hoff analysis, the entropy and enthalpy of uptake were determined. An inverse relationship between partitioning coefficients and temperature was observed for all species except methyl vinyl ketone. A linear correlation between ΔS and ΔH arose which was statistically validated and determined with 99% confidence to not be a statistical artifact. This compensation behavior could be an indication of a surface liquid layer or quasi-liquid layer behavior involved in the uptake process and could also indicate a single dominant influence on a compound's uptake. The most significant physicochemical properties correlated with uptake were identified to be vapor pressure and molar mass, which indicate that smaller compounds with higher vapor pressures are more readily taken into the ice phase. The gas-ice partitioning coefficients observed here are below the 10 mol m^{-3} Pa^{-1} threshold given by Crutzen and Lawrence (2000) to be considered a substantial atmospheric removal process.

1 Introduction

Scavenging of organic gases by hydrometeors—such as rain, snow, graupel, and cloud droplets—has a cleaning effect on the atmosphere. While Henry's law coefficients are available to describe the interactions with

https://doi.org/10.5194/egusphere-2025-1425
Preprint. Discussion started: 3 April 2025

most organic gases with liquid water (Sander, 2023), less is known about its interactions with ice phase deposition. Most precipitation in the midlatitudes as well as all cloud formation in the upper troposphere is formed via ice and subsequently indicates that ice is a significant contributor to the wet deposition of trace atmospheric constituents (Franz and Eisenreich, 2000; Heymsfield et al., 2020; Mülmenstädt et al., 2015). Ice growth in the atmosphere operates under a few distinct processes: (1) the collection of supercooled cloud droplets by ice (riming), (2) direct liquid freezing, and (3) vapor-to-ice growth by diffusion. The latter process—often referred to as depositional growth—is hereafter referred to as diffusional growth and is the responsible mechanism for all cloud formations in the upper troposphere (Heymsfield et al., 2020; Mülmenstädt et al., 2015). There has been significant research in recent years on the redistribution and revolatization of organics during riming or liquid freezing (Borchers et al., 2024; Jost et al., 2017; Gautam et al., 2025; Seymore et al., 2025), but very little for diffusional growth.

Carbonyls as a class of trace atmospheric constituents are highly relevant secondary organic aerosol precursors and intermediates (Ervens and Kreidenweis, 2007; Galeazzo et al., 2024; Srivastava et al., 2022; Yu et al., 2014). Specifically, they are ubiquitous and play vital roles in tropospheric photochemistry and oxidative capacity, which affects radical cycling and ozone formation (Xu et al., 2023). Despite this, there are limited studies describing their removal from the atmosphere via deposition scavenging and only then describe their resultant wet deposition (Mu and Xu, 2009). Huffman and Snider (2004) attempted to measure uptake of acetone as a representative for ketones as hydrogen bond acceptors, however background contamination prevented thorough characterization. They did, however, publish a volume uptake coefficient for acetone and concluded that it had a significantly lower uptake than the alkanols studied.

The publications by Fries et al. (2007) and Huffman and Snider (2004) concern the ice uptake of aromatic hydrocarbons and oxyhydrocarbons. These are the first studies to describe the interactions between diffusion-growing ice and depositing organic vapors. Outside of these, the only measurements for diffusional uptake are for select inorganic species (e.g. H_2O_2, HCl, HNO_3, etc.) (Bartels-Rausch et al., 2014; Conklin et al., 1993; Diehl et al., 1995; Dominé and Thibert, 1996; Mitra et al., 1990; Santachiara et al., 1998) or adsorption on nongrowing ice (Abbatt et al., 2008; Von Hessberg et al., 2008). These experiments to evaluate gas interactions with ice describe either “growing ice” or “static ice” which have investigated the effects of volume uptake and surface processes respectively. From this distinction, these publications reveal that many uptake processes are predominately volume

https://doi.org/10.5194/egusphere-2025-1425
Preprint. Discussion started: 3 April 2025

uptake with secondary contributions from certain surface processes, notably (1) bonding to the air-ice interface or (2) uptake into a liquid solution phase coexisting with ice (Conklin et al., 1993; Goss, 1993). Further, they show that equilibrium treatments of both surface and volume uptake can correctly predict the resulting concentrations in snow (Dominé and Thibert, 1996).

Treating the uptake of organic compounds by ice crystals growing through diffusion as an equilibrium allows for the calculation of ice-gas partitioning coefficients, referred interchangeably as uptake coefficients. These coefficients ($K_{g,ss}$) describe the ratio of the gas phase concentration of the analyte vapor to its concentration in the ice phase. More specifically, with the possibility for a liquid solution phase that coexists with ice, this relationship is described as:

$$K_{g,ss} = K_{g,l}K_{l,ss} \quad (1)$$

where the equilibrium constants $K_{g,ss}$ and $K_{g,l}$ relate the analyte concentrations in the ice solid solution (ss) and liquid water (l) phases to the analyte partial pressure in the gas phase (g). The last equilibrium constant ($K_{l,ss}$) relates the concentrations in the liquid water (l) and solid solution (ss) phases. The present study reports direct measurements of $K_{g,ss}$ for carbonyl compounds and neglects thorough investigation of gas to liquid or liquid to ice equilibrium. Hereafter, $K_{g,ss}$ will be referred to simply as K and is specifically considered a volume uptake coefficient.

In the present study, laboratory experiments explore the uptake of 14 different carbonyl species by ice crystals during vapor deposition growth. Ice crystals were grown from vapor deposition under controlled humidity conditions in the presence of gaseous carbonyl species. The blended gas mixture was targeted to produce roughly 10 ppbv of each gaseous analyte to maintain analytical reliability, approximately one order of magnitude larger than the partial pressures of these compounds in the unpolluted troposphere. Water vapor saturation was controlled to 50% supersaturation (wrt ice) to achieve realistic growth conditions in natural cirrus clouds. Gas phase concentrations were determined using an integrative denuder technique and subsequent derivation to aid detection for both gas and ice phase concentrations. Ultra-high performance liquid chromatography with ultra-high resolution mass spectrometry (UHPLC-UHRMS) was then used to analyze the samples and determine their ice-gas partitioning coefficients.

https://doi.org/10.5194/egusphere-2025-1425
Preprint. Discussion started: 3 April 2025

2 Methods

2.1 Experimental Setup

The experimental design in this paper is a variation on the experiment presented by Fries et al. (2007) with gas measurement techniques developed by Kahnt et al. (2011).

Three uptake experiments were performed with three replicates at atmospheric pressure with the experimental apparatus shown in Figure 1. The setup had three main sections: an ambient temperature gas-mixing stage, a chilled crystal growth flowtube, and outflowing gas measurement. In the first stage (Stage 1. Gas Mixing), pressurized dry nitrogen gas was passed through a bubbler with known concentrations of the analytes in aqueous solution. This stream of gas then reached saturation at ambient temperature (maintained at 23 ºC and confirmed by measurment) and passed through a glass frit and a droplet catching chamber to ensure no liquid droplets remained in the gas stream. The saturated gas stream was then diluted with dry nitrogen to reach the desired humidity and vapor concentration. The specific saturation and vapor concentration mix was maintained using a Mass Flow Controller (Brooks Instrument B.V. 5850TR/FA1B201). The resulting mixed gas was allowed to homogenize inside a 0.5 L mixing chamber and then was introduced into the insulated chamber with the crystal growth tube. Another Mass Flow Controller was used to ensure a constant volumetric flowrate was maintained through the flowtube and through a branching line for input gas measurement.

https://doi.org/10.5194/egusphere-2025-1425
Preprint. Discussion started: 3 April 2025

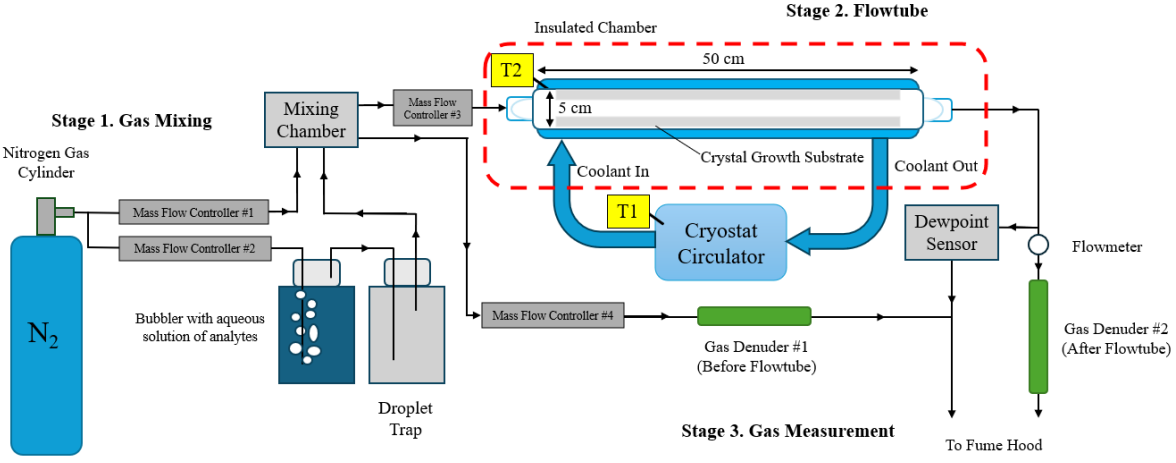

Figure 1. Experimental Apparatus Design

The second stage of the apparatus is the flowtube portion of the setup (Stage 2. Flowtube). The flowtube is a quartz-glass tube of 50 cm length and 5 cm diameter with an approximate interior volume of 1 L where ice crystals were grown from diffusional vapor deposition. It is capped at both ends with a uniform flow PTFE nozzle with double silicon VMQ O-rings to ensure proper sealing of the gas stream at low temperatures. The flowtube is inserted into a copper thermal exchange coil with a PT100 temperature sensor (T2) mounted between the coil and the tube. The flowtube and coil are housed inside an insulated chamber while ethanol coolant is circulated through the coil from a cryostat circulator (Julabo F81) outside the chamber. Using the coolant bath temperature (T1) and T2, the temperature of the flowtube glass substrate can be maintained within 0.1 C of the target temperature using PID control. Prior to each experiment, the flowtube substrate is ethanol cleaned, dried with nitrogen gas, and brought to the target temperature under the flow of dry nitrogen. This prevents ice nucleating contaminants and ambient humidity from depositing on the substrate prior to exposure to the test gas. The flowtube is allowed to cool for 1 hour prior to exposure to ensure temperature stability. This setup was also thermally characterized using a PT100 sensor mounted on a probe inserted along the center of the tube. The quantitated temperature error was determined using this method and the resulting temperature profiles can be found in Figure S1 of the Supplemental Materials.

After the flowtube is the third stage of the setup where the effluent gas is analyzed (Stage 3. Gas Measurement). Continuous dewpoint measurements along with an integrative measurement of vapor analytes were taken on the before and after flowtube gas streams using a dewpoint hydrometer (Michell Instruments S8000) and a

https://doi.org/10.5194/egusphere-2025-1425
Preprint. Discussion started: 3 April 2025

pair of reagent-coated gas denuders. Ice samples were collected from the flowtube, massed, and analyzed for their analyte concentration. This data is then able to be used to calculate the uptake coefficient. PTFE tubing was used for all the tubing connections and the flow conditions in these experiments remained laminar with a Reynolds number of approximately 160, which is well below the critical value of 2300 for pipe flow (Warhaft, 1998). Experiments were performed 24 hours at –20 and –30 ºC, 48 hours for –40 ºC to allow for adequate crystal growth and saturation of any vapor wall losses.

2.2 Crystal Growth Conditions

Ice crystals were grown from vapor deposition under controlled humidity conditions in the presence of gaseous carbonyl species. For the experimental temperatures of –20, –30, and –40 ºC, ice was grown at 50% supersaturation (wrt ice) with 10 ppbv of analyte vapor (a 140 ppbv total organics gas concentration). To achieve these target conditions, different dilutions of dry nitrogen with the saturated gas stream were mixed using different bubbler solutions with the required aqueous concentrations of analytes to reach the target gas concentration. The saturation pressure of water vapor over ice (e_i) was calculated using the Sonntag parameterization (Sonntag, 1994) so that the saturation ratio of water vapor with respect to ice (S_{ice}) was maintained at 1.50 at experimental temperatures of –20, –30, –40 ºC. This S_{ice} was chosen as it is a high but realistic saturation for the growth conditions in natural cirrus clouds (Comstock et al., 2004; Dekoutsidis et al., 2023; Hoareau et al., 2016; Zhao and Shi, 2023) with a similarly realistic temperature range that still allows for high enough water vapor pressures and crystal growth rates to be experimentally viable. Specifically, the Sonntag parameterization is shown in Eq. 2 as:

$$\begin{aligned}\log e_i \;=\; & -6024.5282 \,/\, T \\ & + 24.721994 \\ & + 1.0613868\,10^{-2} \cdot T \\ & - 1.3198825\,10^{-5} \cdot T^2 \\ & - 0.49382577 \cdot \log T\end{aligned} \tag{2}$$

https://doi.org/10.5194/egusphere-2025-1425
Preprint. Discussion started: 3 April 2025

where the air temperature (T) is in units of K and e_i is in units of hPa. For each experimental temperature, this calculation was performed, and an experimental water vapor pressure was chosen to produce the desired S_{ice}. For the gas stream mixing, this was first theoretically calculated as a dilution of saturated bubbler water vapor (19.42 g m^{-3} at 23 ºC) with dry gas (< 0.03 g m^{-3}) to within 10% error. This was also then empirically determined by measuring the mixed gas dewpoint using the hygrometer, calculating the water vapor pressure using Eq. 2 and adjusting the flowrates accordingly.

The crystal growth rate (J), which is equivalent to the diffusive flux, was calculated using a Fick diffusion term:

$$J = D_T \frac{C_0 - C_f}{l_m} \quad (3)$$

where l_m is the thickness of the diffusion layer, D_T is the diffusion coefficient of water vapor (2.2×10^{-5} m^2 s^{-1}) and C_0 and C_f are the input and output water vapor concentrations. The value of l_m is calculated by the Einstein equation:

$$l_m = \sqrt{2 D_T t_k} \quad (4)$$

where t_k is the condensation time, i.e. residence time within the flowtube. l_m was estimated to be 0.025 m, which is roughly the interior radius of the flowtube. J is then multiplied by the interior surface area of the flowtube substrate (approximately 785 cm^2) to produce the total ice growth rate in the flowtube. While the crystal growth rate was theoretically calculated for all experiments, it was also empirically determined by dividing the collected ice mass by the total experiment time.

With the experimental humidity determined and the flowrates fixed, the gas dilution factor of the bubbler gas is then also fixed. From this, the aqueous concentrations of all the analytes in the bubbler that produce the desired vapor concentrations in the flowtube can be determined. Using Henry's law and the compiled Henry's law constants and calculations from Sander (2023), (provided in Table S1 in the Supplemental Materials), the necessary aqueous concentrations to produce 10 ppbv of analyte vapor in the flowtube were determined. 10 ppbv was selected as the analyte vapor mixing ratio as it was a low mixing ratio that could still maintain signal in the ice samples. The Henry's law constant was first adjusted to ambient conditions using the equation:

https://doi.org/10.5194/egusphere-2025-1425
Preprint. Discussion started: 3 April 2025

$$H_T = H^\theta \cdot \exp\left(\frac{-\Delta_{sol}H}{R}\left(\frac{1}{T} - \frac{1}{T^\theta}\right)\right) \quad (5)$$

Here, Henry solubility (H^θ) at the reference temperature (T^θ) and the molar enthalpy of dissolution ($\Delta_{sol}H$) are used along with the gas constant (R) and ambient temperature (T) to correct to the Henry solubility (H_T). With the concentration/pressure defined H_T adjusted to ambient conditions, the aqueous concentration of the analyte in the bubbler can be calculated using the equation:

$$[x]_{aq} = H_T^{cp} \cdot p_x^{FT} \cdot d \quad (6)$$

where the dilution factor (d) corrects the partial pressure of x analyte in the flowtube (p_x^{FT}) to the partial pressure required in the bubbler due to the gas mixing dilution to provide the aqueous concentration ($[x]_{aq}$). These concentrations are stable in the bubbler, assuming that the mass fraction in the aqueous phase is much larger than the mass fraction in the vapor phase. The actual aqueous concentrations and Henry solubilities used can be found in Table S1 the Supplementary Materials. While these calculations were performed to reach a target gas concentration of 10 ppbv, the actual gas concentration in the flowtube was determined by dividing the mass of analyte collected on the reagent-coated gas denuders and dividing by the total volume passed through the denuders. Corrections for mass error due to the breakthrough potential of a species through the denuder were made following the same method as (Kahnt et al., 2011). The average breakthrough potential for all species under these conditions was determined to be less than 4%. While Kahnt et al. (2011) observed much higher breakthrough potentials at lower relative humidities, the absolute humidity in these experiments is lower by 5 orders of magnitude. Since water can both encourage and inhibit the DNPH derivation, any changes in humidity conditions may alter the breakthrough potential of any of the analytes.

2.3 Chemicals and Materials

The derivation reagent 2,4-dinitrophenylhydrazine (DNPH) was purchased from Sigma-Aldrich (~0.2 M, ~4% Phosphoric acid solution, Darmstadt, Germany). The denuder coating solution was prepared with 10 mM DNPH in acetonitrile (ACN). The following carbonyl compounds were obtained from Sigma-Aldrich (St. Louis, MO, USA): benzaldehyde (≥99%), methacrolein (95%), norcamphor (98%), (1R)-(+)-nopinone (98%), and methyl vinyl ketone (MVK, with 0.5% hydroquinone and 0.1% acetic acid). Formaldehyde (30%, methanol-free) and

https://doi.org/10.5194/egusphere-2025-1425
Preprint. Discussion started: 3 April 2025

acetaldehyde (≥99%) were obtained from Roth (Karlsruhe, Germany). Hydroxyacetone (95%) and propionaldehyde (97%) were obtained from Thermo Scientific (Darmstadt, Germany). Glyoxal (39% in water) and diacetyl (>98%) were purchased from TCI (Toshima, Tokyo, Japan). Methylglyoxal (40% in water) was purchased from MP Biomedicals (Irvine, CA, USA). d/l-camphor (97.5%) was obtained from WHI pharma services (Frankfurt, Germany). These compounds were used without further purification. For the aqueous bubbler solution, 98 % LC/MS grade water (Thermo Fisher Scientific) was used for the solvent and >99.8% technical grade nitrogen was used for the carrier gas.

Supelco carbonyl-DNPH mix 13, a commercially available hydrazone standard solution, was purchased from Sigma-Aldrich and used for the analysis of benzaldehyde, MVK, methacrolein, acetaldehyde, formaldehyde, acetone, and propionaldehyde. Hydrazone crystals were prepared for benzaldehyde, nonpinone, norcamphor, camphor, diacetyl, glyoxal, hydroxyacetone, and methylglyoxal. Benzaldehyde-DNPH was purified by recrystallization from ethanol and then prepared in ACN. All other synthesized carbonyl-DNPHs were purified using a solid phase extraction (SPE) method (Chromabond® C_{18}, 6 mL, 1000 mg bedweight) and then referenced to the prepared benzaldehyde-DNPH standard with UHPLC-HRMS. This was then referenced to the Supelco standard. The difference in the signal was about 23% (n = 6) between commercial and synthesized benzaldehyde-DNPHs confirming the concentration of the benzaldehyde-DNPH. Since the ice-gas partitioning coefficients are unitless and the sample matrices are the same, true quantitation is not necessary for the calculation. However, since these standards are referenced to the Supelco standard, true quantitation was performed for benzaldehyde, MVK, methacrolein, acetaldehyde, formaldehyde, acetone, and propionaldehyde and pseudo-quantitation (estimating concentration by referencing signal intensity to an internal standard) was performed for nonpinone, norcamphor, camphor, diacetyl, glyoxal, hydroxyacetone, and methylglyoxal.

2.4 Sample Collection and Preparation

Three samples were collected from each experiment: input gas denuder extract, output gas denuder extract, and ice. The gas denuders were prepared in the method described by Kahnt et al., (2011). Two 5-channel annular denuders with 750 mm length and 1 mm annular spacing (URG 4531, URG Corporation, Chapel Hill, NC, USA) were coated with XAD–4 resin following the method presented by Kahnt et al. (2011) and then coated with DNPH

https://doi.org/10.5194/egusphere-2025-1425
Preprint. Discussion started: 3 April 2025

before immediate use. The resin coating was renewed after five experiments. At the conclusion of the experiment, the denuder samples were directly extracted three times with 50 mL of ACN by capping and inverting twenty times while rotating along its axis. These samples were then left overnight to ensure complete derivatization.

Ice samples were collected by methanol extraction of the flowtube. At the conclusion of the experiment, the flowtube and thermal exchange coil were sealed, disconnected from the setup, and taken into a walk-in cold chamber kept at –5 ºC. The caps were removed from the flowtube and the interior was rinsed with 14 mL of anhydrous methanol. The flowtube extract was massed and then the water content was determined by measuring the refractive index using an Abbe refractometer. Knowing the percent water content (w/w%) of the extract and the total mass of the extract (g), the ice yield could be determined (g). This extract was then spiked with 0.1 mL of the DNPH solution and left overnight to ensure complete derivatization. This method prevents deposition by ambient humidity onto the flowtube substrate and is a more efficient recovery method than physical scraping, which was not a viable method due to the low ice masses deposited.

The samples were then all concentrated by rotary evaporation (25 ºC at 150 mbar) and were reconstituted in 1 mL of methanol to be purified by SPE (Chromabond® C_{18}, 6 mL, 1000 mg bedweight). The cartridges were first flushed with 6 mL ACN, conditioned with 3 mL methanol and 6 mL of ultra-pure water. The denuder extract was loaded on the SPE cartridge and washed with 3 mL of methanol/water solution (5/95%, v/v%) to remove any phosphoric acid. The carbonyl-DNPHs were eluted using 10 mL ACN and stored out of light at –25 ºC in a deep freezer. For analysis, 0.25 mL of the output gas denuder extract, 0.5 mL of the input gas denuder extract, and 1 mL of the ice sample were taken and evaporated to dry in a nitrogen evaporator at 18 ºC. These were reconstituted to 0.5 mL ACN/H2O (50/50, v/v%) for ultra-high-performance liquid chromatography coupled with high resolution mass spectrometry (UHPLC-HRMS). The dilution/concentration for these respective samples were performed to bring the expected concentration into quantitation range.

2.5 UHPLC-HRMS Analysis

Analysis was performed in triplicate using a Dionex UltiMate 3000 ultra-high-performance liquid chromatography (UHPLC) system coupled to a heated electrospray ionization source (HESI) and a high-resolution Q-Exactive Orbitrap mass spectrometer (HRMS) (all Thermo Fisher Scientific). A Hypersil Gold, C18, 50 x 2.0 mm

https://doi.org/10.5194/egusphere-2025-1425
Preprint. Discussion started: 3 April 2025

column with 1.9 µm particle size (Thermo Fisher Scientific) was used for the chromatography. Eluent A consisted of 98 % LC/MS grade water (Thermo Fisher Scientific) with 0.04 % formic acid and ACN (VWR Chemicals), eluent B consisted of 98 % ACN and water, and the injection volume was 10 µL. Column temperature was held at 40 ºC. The HESI source was used in negative mode, resulting in the formation of deprotonated molecular ions. Sheath gas and auxiliary gas pressure was 40 and 20 a. u. (arbitrary unit) respectively. The temperature of the auxiliary gas heater was 150 °C and the capillary temperature was 350 °C. The sprayer voltage was set to –4.00 kV. To further enhance ionization, a post-column flow of 50 mmol L^{-1} NH_4OH in MeOH was added after 1 min at a flow rate of 0.1 mL min^{-1}. The following H_2O/ACN chromatography gradient was used: Starting with 30% B isocratically for 1 min, increasing to 80% at 10 min, then to 100% at 11 min, and back to 30% B at 11.5 min allowed to equilibrate to initial conditions for 1 min. The first minute of eluent was ejected to waste to reduce excess unreacted DNPH being fed into the HRMS. The mass traces used to identify the species in this experiment can be found in Table S2 in the Supplementary Materials.

2.6 Calculations

The partitioning coefficient between the gas and ice phase K was calculated by the equation:

$$K = \frac{\rho_{ice} C_{ice}}{m_{ice} C_{gas}} \quad (7)$$

where C_{ice} is the absolute mass of the analyte in ice (ng), ρ_{ice} is the density of ice at the experimental temperature (0.9194, 0.9200, 0.9208 g cm^{-3}), C_{gas} is the concentration of the analyte in the gas phase (ng m^{-3}), and m_{ice} is the total mass of ice (g). For proper unit conversion, a factor of 10^6 is applied for the conversion of m^3 to cm^{-3}. Practically speaking, K is also used as a sorption coefficient or a dimensionless uptake coefficient with respect to the removal of trace gases in the upper atmosphere. A larger value for K indicates more uptake into the ice phase.

Strictly speaking, chemical uptake on growing ice crystals is a stationary state and not an equilibrium. However, diffusional crystal growth is slow relative to other modes of freezing (day vs. ms timescales) and so the system can be approximated as an equilibrium state (Dominé and Thibert, 1996; Fries et al., 2007; Huffman and Snider, 2004). Then as a thermodynamic equilibrium, K can also be used to calculate the Gibbs energy (ΔG) of the uptake process at each temperature. This is a direct calculation using the equation:

$$\Delta G = -RTln(K) \quad (8)$$

https://doi.org/10.5194/egusphere-2025-1425
Preprint. Discussion started: 3 April 2025

where T is temperature (K) and R is the ideal gas-constant (8.31447 J K^{-1} mol^{-1}). These values describe the energy available for the uptake process. Positive values of ΔG indicate the analyte favors the gas phase while negative values of ΔG indicate the analyte favors the ice phase. Even lower, more negative values of ΔG would indicate more efficient uptake of the analyte into the ice phase.

Continuing the thermodynamic analysis, the theoretical temperature dependence of the sorption coefficient K can be determined with the van't Hoff equation, which when substituting with the Gibbs-Helmholtz equation produces the following:

$$\ln(K) = -\frac{\Delta H - T\Delta S}{RT} = -\frac{\Delta H}{R}\frac{1}{T} + \frac{\Delta S}{R} \quad (9)$$

where ΔH and ΔS are the heat of sorption and the sorption entropy respectively. Here the heat of uptake and uptake entropy are used instead. Performing a linear regression of $\ln(K)$ against $1/T$ using the van't Hoff equation provides a slope of $-\Delta H/R$ and an intercept of $\Delta S/R$. Multiplying each of these values by –R and R respectively produces the values of ΔH and ΔS. Increasing values of the uptake enthalpy ΔH and the uptake entropy ΔS along with decreasing compound vapor pressure—i.e. the volatility of the pure analyte—can indicate that the uptake of the analyte is dependent on the physical parameters of the compounds and ice surface. Specifically, these are the parameters that determine thermodynamic sorption such as temperature, molecular mass, ice surface coverage, surface morphology and porosity, surface crystallographic phases, quasi-liquid layer behavior, and crystal imperfections (Behr et al., 2006; Fries et al., 2006; Orem and Adamson, 1969; Sokolov and Abbatt, 2002). However, lower values of ΔH and poor linear regression can be a sign that the uptake process cannot be exclusively described by thermodynamic sorption.

3 Results and Discussion

3.1 Ice Crystal Growth

Nine ice samples were grown in the presence of vapor phase carbonyl compounds. While the target gas concentration for each species was 10 ppbv, the actual (excluding glyoxal) concentrations as referenced against denuder #1 was 11.5 ± 2.5 ppbv on average. The actual gas concentrations for each species can be found in the Supplemental Materials. The typical ice yield at –20 ºC was calculated to be roughly 3.07 g while the actual yield

https://doi.org/10.5194/egusphere-2025-1425
Preprint. Discussion started: 3 April 2025

was measured to be 5.77 ± 0.45 g on average. The corresponding theoretical and actual crystal growth rates were 128.1 mg hr $^{-1}$ and 237.8 mg hr $^{-1}$ at 1.55 ± 0.14 hPa water vapor pressure (49.9 ± 13.8 % S wrt ice). For –20 ºC, the actual ice yield measurement is strictly an overestimate as the refractive index measurement was closest to the parabolic vertex of the water-MeOH mixture where small deviations in the refractive index produce large differences in the estimated water content. At –30 ºC, the calculated ice yield was 1.13 g while the average actual yield was 1.07 ± 0.52 g. The corresponding theoretical and actual crystal growth rates were 47.1 mg hr $^{-1}$ and 44.6 mg hr $^{-1}$ at 0.57 ± 0.05 hPa water vapor pressure (49.6 ± 14.1 % S wrt ice). For –40 ºC, the calculated ice yield was 0.79 g while the actual was 0.57 ± 0.11 g. The corresponding theoretical and actual crystal growth rates were 16.4 mg hr $^{-1}$ and 11.8 mg hr $^{-1}$ at 0.20 ± 0.01 hPa water vapor pressure (54.9 ± 5.9 % S wrt ice).

The lower actual ice yield than calculated is most likely due to deposition losses on non-extractible surfaces of the apparatus such as the caps of the flowtube or excess tubing inside the insulated chamber. Deposition of ambient humidity during sample extraction appears to be much lower than the losses present in the experimental setup. On average, the vapor deposition efficiency—that is the percent difference between the input and exhaust water vapor concentration, presumed to be the percentage of water deposited as ice—was 46%. This value never deviated more than 8% over the course of all experiments. This is potentially a geometric constraint of the flowtube apparatus as this value did not appear to change with temperature, flow rate, nor experiment time.

The size of any individual crystal was too small to reliably determine crystal morphology with nondestructive methods as the entire crystal yield was thinly coated over the entire interior surface of the flowtube (approximately 785 cm^2). This produced an ice coating that was typically less than 1 mg cm^{-2} and often not evenly distributed across the surface of the flowtube. While true morphology could not rigorously be determined, nucleation sites where crystal growth was quicker along with areas with needle-like structures were observed.

3.2 Ice-Gas Partitioning Coefficients

To establish background signal during uptake experiments, ice crystals were grown from pure LC/MS grade water in three separate experiments at –20 ºC without organic gases. The signals in the ice blanks and clean

https://doi.org/10.5194/egusphere-2025-1425
Preprint. Discussion started: 3 April 2025

denuder extract were in the same range as analytical blanks, which were all below detection limits. This demonstrates that no measurable contamination occurred during crystal growth or sample extraction.

At –20 ºC (3.949×10^{-3} K^{-1}), all compounds showed a $K < 1$. At lower temperatures, the K for all compounds increased except for MVK. This matches the expected behavior for exothermic deposition processes. Table 1 shows the calculated values for K at each temperature while Figure 2 plots these values against each other as a van't Hoff plot. Values of $K > 1$ or $\ln(K) > 0$ indicate net uptake of the compound into the ice phase. Conversely, values of $K < 1$ or $\ln(K) < 0$ indicate negligible uptake and that the compound favors remaining in the gas phase. At –30 ºC (4.112×10^{-3} K^{-1}), formaldehyde is favorable to deposit to the ice phase while acetaldehyde reaches conditions where K is close to 1 and the amount deposited to the ice phase and that remaining in the vapor phase are roughly equal. While formaldehyde is still mainly present in the gas phase at –20°C (3.949×10^{-3} K^{-1}), deposition of formaldehyde in the ice phase is favored from about –30°C (4.112×10^{-3} K^{-1}), while at this temperature acetaldehyde reaches conditions where K is close to 1 and thus the amount deposited in the ice phase and the amount remaining in the gas phase are approximately equal. At –40 ºC (4.288×10^{-3} K^{-1}), glyoxal and diacetyl also approach the point where K is approximately equal to 1, while formaldehyde, acetaldehyde, acetone, and propionaldehyde preferentially deposit in the ice phase. Formaldehyde is the only species, however, that strongly favors the ice phase with a K value in the order of 10^2, while the other values are still around 10^0 or far below. Formaldehyde is thought to be the main source of OH radicals in the upper troposphere (Cooke et al., 2010; Fried et al., 2016). It then is likely that this ice uptake could be a significant influence on OH radical formation in the upper troposphere.

Table 1. Average Ice-gas partitioning coefficients from uptake experiments at different temperatures

	***K* at –20 ºC**	***K* at –30 ºC**	***K* at –40 ºC**
MVK	$(2.21 \pm 1.23) \times 10^{-2}$	$(2.05 \pm 2.08) \times 10^{-3}$	$(9.01 \pm 8.26) \times 10^{-3}$
Acetaldehyde	$(1.27 \pm 0.35) \times 10^{-1}$	0.98 ± 1.37	3.10 ± 1.62
Acetone	$(1.87 \pm 0.54) \times 10^{-1}$	$(2.92 \pm 3.84) \times 10^{-1}$	2.14 ± 2.36
Benzaldehyde	$(7.68 \pm 2.86) \times 10^{-5}$	$(6.64 \pm 4.98) \times 10^{-4}$	$(1.43 \pm 1.14) \times 10^{-2}$
Camphor	$(5.08 \pm 0.70) \times 10^{-4}$	$(6.99 \pm 7.67) \times 10^{-3}$	$(5.97 \pm 4.25) \times 10^{-2}$
Diacetyl	$(3.69 \pm 1.13) \times 10^{-3}$	$(3.17 \pm 2.94) \times 10^{-2}$	1.33 ± 1.10
Formaldehyde	$(2.10 \pm 0.62) \times 10^{-1}$	$(1.38 \pm 1.98) \times 10^{1}$	$(1.03 \pm 0.63) \times 10^{2}$
Glyoxal	$(9.01 \pm 1.22) \times 10^{-3}$	$(6.78 \pm 2.45) \times 10^{-2}$	1.05 ± 1.54
Hydroxyacetone	$(1.64 \pm 0.23) \times 10^{-3}$	$(2.34 \pm 3.12) \times 10^{-2}$	$(3.55 \pm 4.63) \times 10^{-1}$
Methacrolein	$(3.94 \pm 1.89) \times 10^{-3}$	$(1.15 \pm 1.43) \times 10^{-2}$	$(2.10 \pm 3.06) \times 10^{-1}$
Methylglyoxal	$(7.29 \pm 2.99) \times 10^{-3}$	$(5.61 \pm 3.65) \times 10^{-2}$	$(3.95 \pm 3.40) \times 10^{-1}$

https://doi.org/10.5194/egusphere-2025-1425
Preprint. Discussion started: 3 April 2025

Nopinone	$(9.28 \pm 2.39) \times 10^{-6}$	$(1.10 \pm 0.67) \times 10^{-4}$	$(1.65 \pm 2.44) \times 10^{-3}$
Norcamphor	$(4.32 \pm 2.07) \times 10^{-5}$	$(9.05 \pm 2.72) \times 10^{-5}$	$(6.15 \pm 7.59) \times 10^{-3}$
Propionaldehyde	$(1.38 \pm 1.25) \times 10^{-1}$	$(2.11 \pm 2.30) \times 10^{-1}$	2.93 ± 3.23

Every measured species except for MVK displays a strong correlation of ln(K) with inverse temperature and can likely be exclusively described by thermodynamic sorption. Furthermore, the uptake of these species can almost exclusively to attributed to codeposition during crystal growth as sorption on nongrowing crystals has been demonstrated to be insignificant or completely reversible for almost all chemical species studied. This specifically includes acetone, acetaldehyde, formaldehyde, and benzaldehyde (Fries et al., 2006; Hudson et al., 2002; Roth et al., 2004; Winkler et al., 2002). MVK however shows a weak negative trend with inverse temperature with a nonsignificant correlation.

This observation of strong correlations with inverse temperature could indicate that K is controlled by transport, specifically if analyte transport is limited by accommodation at the ice-air interface (Davidovits et al., 2006; Jayne et al., 1991). The absence of this correlation for MVK complicates this view. However, this could be explained by kinetic control resulting from transport phenomena occurring in either the gas or solid phases, i.e. processes that change the rates of transport of MVK relative to water rather than a K that is controlled by an equilibria established between MVK and water. However, without sufficient evidence for a mechanism of kinetically controlled transport, the measurements of K here will be interpreted using equilibrium thermodynamics.

https://doi.org/10.5194/egusphere-2025-1425
Preprint. Discussion started: 3 April 2025

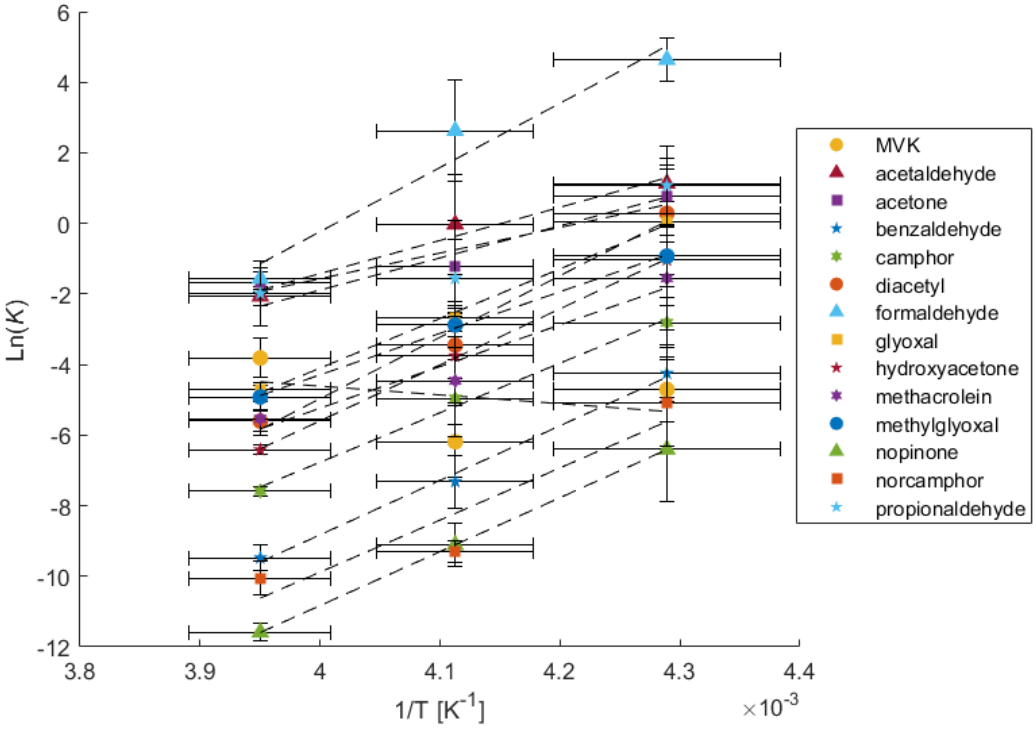

Figure 2. Van't Hoff plot of inverse temperature (K^{-1}) against the natural log of the calculated partitioning coefficient *K* (unitless)

3.3 Thermodynamic Results

Tables 2 and 3 apply the thermodynamic analysis from Eqs. 7 and 8 to the data given in Table 1 and the linear regressions seen in Figure 1. Table 3 contains the slopes, intercepts, and regression coefficients (r^2) for the linear regressions in Figure 1 as well as the calculated uptake enthalpy (ΔH) and uptake entropy (ΔS) produced by Eq. 8. Table 2 provides the ΔG values produced by applying Eq. 7 to the partitioning coefficients given in Table 1. In Table 2, a $\Delta G > 0$ indicates unfavorable uptake of the species into the ice phase while $\Delta G < 0$ indicates favorable uptake into the ice phase. At –20 ºC, it is not favorable for uptake into the ice phase to occur for any species. At –30 ºC, it is thermodynamically favorable for formaldehyde to be taken into the ice phase. At –40 ºC, glyoxal, diacetyl, formaldehyde, acetaldehyde, acetone, and propionaldehyde are thermodynamically favorable to be taken into the ice

https://doi.org/10.5194/egusphere-2025-1425
Preprint. Discussion started: 3 April 2025

phase. Interpolating for these species, it becomes favorable to deposit acetaldehyde, acetone, and propionaldehyde into the ice phase between –32 ºC and –35 ºC while formaldehyde begins to deposit at –24.3 ºC. Both glyoxal and diacetyl deposit at approximately –40 ºC. Since cirrus clouds often can occur at temperatures such as –60 ºC and lower, this data implies that uptake at those temperatures could significantly affect the availability of these species. With these carbonyls being the typical source of atmospheric OH radicals, this would significantly reduce the availability of OH radicals within cirrus clouds.

The other species—MVK, benzaldehyde, camphor, hydroxyacetone, methacrolein, methlyglyocal, nopinone, and norcamphor—were unfavorable to deposit into the ice phase under any of the conditions studied here. Extrapolating based on the linear regression in Table 3, the estimated temperature below which it is favorable to deposit the species (excepting MVK) is presented in Table 2. For these species, they would presumably become favorable to deposit into the ice phase within the range of –43 to –61 ºC, which is within the natural range for cirrus clouds. With MVK having both a poor regression ($r^2 = 0.1235$) and nonexothermic behavior, the temperature at which $\Delta G = 0$ cannot be meaningfully extrapolated.

Table 2. Calculated Δ*G* of uptake at different temperatures.

	ΔG (kJ mol^{-1})			Calculated T where $\Delta G = 0$
Temperature (°C)	–20	–30	–40	(°C)
MVK	8.0	12.5	9.1	–
Acetaldehyde	4.3	0.1	–2.2	–32.2
Acetone	3.5	2.5	–1.5	–35.4
Benzaldehyde	19.9	14.8	8.2	–54.3
Camphor	16.0	10.0	5.5	–49.9
Diacetyl	11.8	7.0	–0.6	–39.6
Formaldehyde	3.3	–5.3	–9.0	–24.3
Glyoxal	9.9	5.4	–0.1	–40.1
Hydroxyacetone	13.5	7.6	2.0	–43.4
Methacrolein	11.7	9.0	3.0	–47.3
Methylglyoxal	10.4	5.8	1.8	–43.9

https://doi.org/10.5194/egusphere-2025-1425
Preprint. Discussion started: 3 April 2025

Nopinone	24.4	18.4	12.4	–60.7
Norcamphor	21.2	18.8	9.9	–56.5
Propionaldehyde	4.2	3.1	–2.1	–34.8

Table 3. Slopes ($\Delta H/R$), intercepts ($\Delta S/R$), and regression coefficients (r^2) of regression lines from Figure 1, calculated uptake enthalpy (ΔH), and uptake entropy (ΔS).

	$-\Delta H/R$ (K)	$\Delta S/R$	r^2	ΔH (kJ mol^{-1})	ΔS (J mol^{-1} K^{-1})
MVK	–2486.8	5.33	0.1235	20.68	44.4
Acetaldehyde	9392.4	–38.99	0.9672	–78.09	–324.2
Acetone	7256.3	–30.59	0.8972	–60.33	–254.4
Benzaldehyde	15452.5	–70.64	0.9941	–128.48	–587.3
Camphor	14040.3	–62.93	0.9934	–116.74	–523.2
Diacetyl	17426.7	–74.67	0.9830	–144.89	–620.9
Formaldehyde	18197.2	–73.02	0.9508	–151.30	–607.1
Glyoxal	14049.0	–60.30	0.9960	–116.81	–501.3
Hydroxyacetone	15872.3	–69.09	0.9997	–131.97	–574.4
Methacrolein	11804.2	–52.45	0.9450	–98.15	–436.1
Methylglyoxal	11766.5	–51.36	0.9987	–97.83	–427.0
Nopinone	15285.4	–71.97	1.0000	–127.09	–598.4
Norcamphor	14765.6	–68.95	0.8752	–122.77	–573.2
Propionaldehyde	9111.8	–38.34	0.8690	–75.76	–318.7

All linear regressions calculated in Table 3 except for MVK have r^2 greater than 0.86 which indicate good linearity. The weakest regressions include norcamphor, propionaldehyde, and acetone which are between 0.869 and 0.897 while all the other regressions are above 0.945; those above 0.993 are benzaldehyde, camphor, glyoxal, hydroxyacetone, methylglyoxal, and nopinone. It can then be concluded that the ice-gas partitioning of all the species studied here except for MVK can be explained by the thermodynamic parameters of bulk uptake. The

https://doi.org/10.5194/egusphere-2025-1425
Preprint. Discussion started: 3 April 2025

calculated ΔH and ΔS are then accurate descriptions of the thermodynamic process for these species' uptake in the ice phase. ΔH and ΔS are negative for all species except MVK and are within the ranges of –60 to –151 kJ mol^{-1} and –254 to –621 J mol^{-1} K^{-1} respectively. These values indicate that at increasingly colder temperatures the uptake of all these species becomes more efficient and uptake decreases at warmer temperatures.

For MVK, since the linearity of the regression is poor, thermodynamic discussion of its measured partitioning coefficients is limited. Taking the calculated ΔH and ΔS at face value suggests that MVK behaves endothermically, and that uptake decreases at colder temperatures. This positive correlation with temperature has also been seen in the uptake of C_1–C_4-alkanols (Huffman and Snider, 2004), which is contributed to weakened water-water bonding when incorporated into ice due to supposed hydrogen bonding. MVK as a ketone is a hydrogen bond acceptor, as are the other ketones and aldehydes in this study, so this weak correlation is unlikely related to hydrogen bonding effects. More importantly, MVK is demonstrated to efficiently undergo functionalization and oligomerization in the aqueous phase through photooxidation (Renard et al., 2014). It is then a possibility that this photodegradation process is the main cause of the weak correlation that MVK has with inverse temperature. However, other similar compounds such as glyoxal and methacrolein also have demonstrated efficient functionalization and oligomerization through photooxidation but they do not exhibit the same poor regression as MVK.

3.4 Entropy-Enthalpy Compensation

Plotting the calculated ΔH and ΔS, as seen in Figure 3, demonstrates an apparent entropy-enthalpy compensation (EEC) effect, where ΔH scales proportionately with ΔS. This relationship appears to also extend to the calculated ΔH and ΔS for MVK. This form of linear correlation between ΔS and ΔH, where it arises for a series of homologous compounds employed in a process, is referred to as the strong form of EEC (Sharp, 2001). This compensation effect appears to have good linearity with an r^2 of 0.9809 with no noticeable outliers with a compensation temperature (i.e. slope; $Tc = d\Delta H/d\Delta S$) of 235.5 K. EEC however has been known to arise artifactually with high r^2 and is often controversial (Grunwald and Steel, 1995; Krug et al., 1976; Leffler, 1955; Leung et al., 2008; Liu and Guo, 2001; Moulik et al., 2019; Pan et al., 2015; Sharp, 2001). This is because methods such as van't Hoff analysis are indirect and do not measure ΔH and ΔS independently. Thus, for measurements on a

https://doi.org/10.5194/egusphere-2025-1425
Preprint. Discussion started: 3 April 2025

limited temperature range, true observation of ΔH and ΔS can be obscured by trivial correlation arising from larger errors in determining ΔH than ΔG rather than some extra-thermodynamic mechanism of EEC (Sharp, 2001). Additionally, the assumption in van't Hoff analysis that $\Delta H°$ is constant (i.e., the heat capacity change is negligible) may be invalid (Leung et al., 2008). Therefore, it is critical to evaluate EEC occurrence through statistical methods. For brevity, many of the specifics of this analysis has been moved to the Supplementary Materials under Section S1. The most relevant aspects and conclusions are presented here.

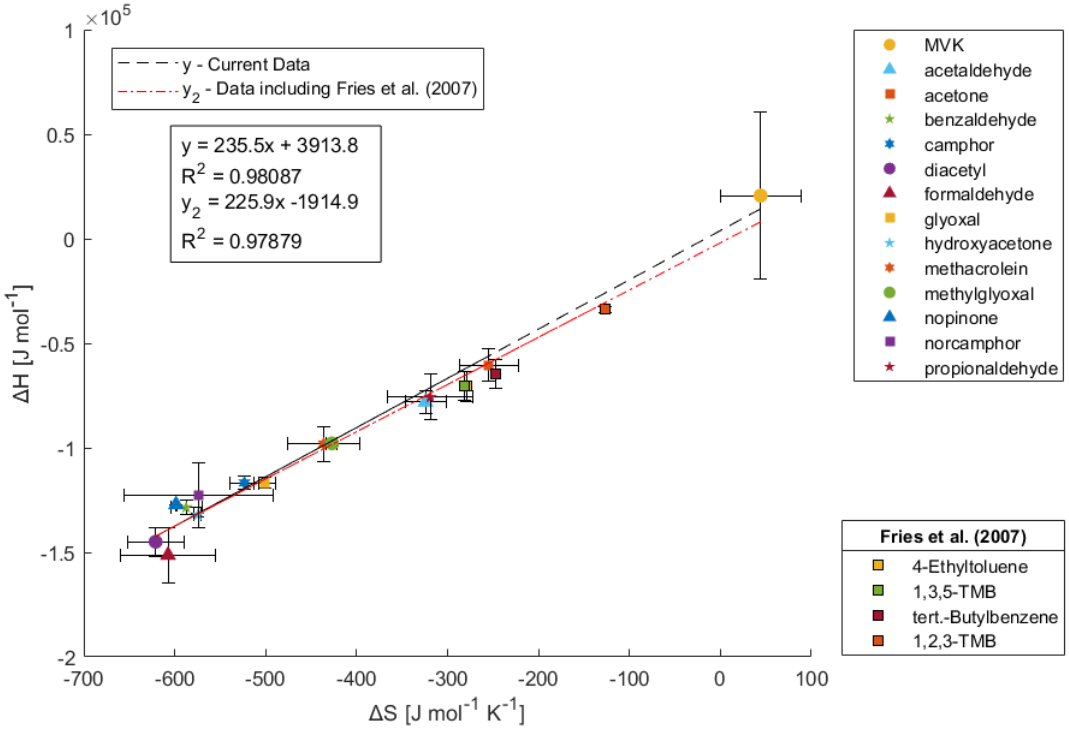

Figure 3. Enthalpy versus entropy plot using the ΔH and ΔS determined from the Van 't Hoff plots in Figure 2

To rigorously investigate EEC, the simple statistical verification of EEC provided by Griessen and Dam (2021) is applied to this data. The calculated dimensionless coalescence location parameter and Compensation

https://doi.org/10.5194/egusphere-2025-1425
Preprint. Discussion started: 3 April 2025

Quality Factor pair (k, CQF) for this data is (–0.278, 0.062); which when plotted on Griessen and Dam's confidence contours, lies outside the 99% confidence contour for n = 12 (This dataset is n = 14). This indicates that there is 99% confidence that the EEC seen here is not of statistical origin. For good measure, if the data from Fries et al. (2007) is included in the (k, CQF) calculation, the calculated (k, CQF) pair is (–1.264, 0.205) and lies even further from the 99% confidence contour for n = 12 (This dataset is n = 18). From this statistical analysis, it can then be rigorously stated that the EEC seen in ice-gas partitioning is not artifactual in origin and likely has an extra-thermodynamic mechanism.

While an initial explanation of this mechanism might stem from a discussion on specific functional group-driven interactions, the appearance of this EEC effect includes aromatic hydrocarbons in addition to the ketones and aldehydes studied here. This could indicate that instead there may be weak, nonspecific supramolecular interactions. A few such explanations for EEC that are applicable to ice-gas equilibrium have been discussed in literature. Firstly, EEC due to solvation effects (i.e. solvent reorganization) are commonly discussed (Dragan et al., 2017; Leung et al., 2008; Lumry and Rajender, 1970; Pan et al., 2015). These discussions often center around the concept that any process that changes the free volume of nearby liquid water is inherently compensatory due to "structure making" and "structure breaking" of hydration shells. This explanation of EEC for ice-gas partitioning during depositional ice growth implies a surface liquid layer or quasi-liquid layer behavior. Indeed, there is already evidence for this as Huffman and Snider (2004) observe that at temperatures colder than approximately –20ºC there is overlap with models describing uptake into a surface liquid layer.

Regardless of the specific mechanism of the EEC in this system, its presence does support (but does not necessarily prove) that there is a single source of additivity for the series of compounds studied (Lumry, 1995). Contrarily, there are also those who believe that EEC is not explainable and that it is an arbitrary phenomenon that arises from narrow free energy ranges (Moulik et al., 2019).

3.5 Partitioning Coefficients versus Heat of Vaporization and Molar Mass

The values for K and ln$K$ at –20 ºC were regressed with several physiochemical properties, specifically molar mass (MM), HPLC retention time (RT), vapor pressure (P_{vap} at 25ºC), heat of vaporization (ΔH^{o}_{vap}) (Chickos et al.,

https://doi.org/10.5194/egusphere-2025-1425
Preprint. Discussion started: 3 April 2025

1995), van der Waals volume (Zhao et al., 2003), and Henry solubility (Sander, 2023). These regressions were also made for K and ln$K$ at –30 and –40 ºC, however all the notable trends are the same. Further, regressions were made with uptake ΔH and ΔG, however the only significant correlations were from ln$K$ against lnP_{vap}, MM, ΔH^o_{vap}, and van der Waals volume (n = 14, r^2 = 0.749, 0.737, 0.711, 0.702 respectively). lnP_{vap} positively correlates while the rest of these properties all correlate negatively with ln$K$, indicating a relationship where larger compounds have lower uptake into ice and higher vapor pressures indicate more uptake. These correlations for MM and ΔH^o_{vap} at –20 ºC are displayed in Figure 4 while the same for –30 and –40 ºC are provided in the Supplemental Material as Figures S3 and S4. The higher r^2 for the regression against MM suggests that molecular size is the main contributor for uptake of carbonyls as opposed to solubility or hydrogen bonding potential. The ability for ketones and aldehydes to hydrogen bond is limited as they are only capable of being bond acceptors. If hydrogen bonding between analyte and water played a significant role in the uptake process, then it would be expected that Henry solubilities would be more relevant contributors. Since carbonyls are unable to form hydrogen bonds between themselves, it's likely that the correlation from ΔH^o_{vap} is driven mostly from molecular size, as ΔH^o_{vap} is a property describing a pure substance. In this case, MM and ΔH^o_{vap} positively correlate with an r^2 of 0.746 so their similar regressions are proxies of each other. Further, the residuals of the regressions for both properties are very similar. Almost all compounds stay on the same side of both regressions, i.e. few compounds change between positive and negative residuals. The exceptions to this are MVK, methylglyoxal, and hydroxyacetone. MM and van der Waals volume also positively correlate with an r^2 of 0.987, so van der Waals volume is considered a proxy for MM. lnP_{vap} however negatively correlates with MM with an r^2 of 0.778, so lnP_{vap} can also be considered a collinear factor to MM.

The negative relationship of uptake with molecular size and positive relationship with vapor pressure is a unique finding that may seem counterintuitive if not considering inclusion into the ice lattice structure. One might expect that compounds with a higher affinity for the gas phase will remain in the gas phase and therefore have lower uptake coefficients. However, the reverse is observed. Compounds with higher vapor pressures and lower masses are more readily taken into the ice phase. If in order to be taken into the ice phase, a compound must be incorporated into the ice crystal lattice structure, then this trend becomes more reasonable. Smaller compounds may induce less deviation in lattice structure relative to the preferred ice crystal structure. It may then be energetically less favorable for a larger compound to fit into the ice crystal as it forces a larger crystallographic defect. This trend might not be expected if analytes are phase separated from the ice crystal in grain boundaries. This trend has been similarly

https://doi.org/10.5194/egusphere-2025-1425
Preprint. Discussion started: 3 April 2025

hypothesized by Jost et al. (2017) for rime growth ice, but recent studies have not found this trend in rime growth ice nor bulk phase liquid freezing (Borchers et al., 2024; Gautam et a., 2024; Seymore et al., 2024). Huffman and Snider (2004) did not observe any specific dependence of uptake on compound saturation partial pressure nor molecular mass for acetone, touluene, or the C_1–C_3 alkanols, but they observed a similar negative correlation with ΔH^o_{vap} as also seen here. Fries et al. (2007) did not observe any trends between the physical properties of aromatic hydrocarbons and their uptake.

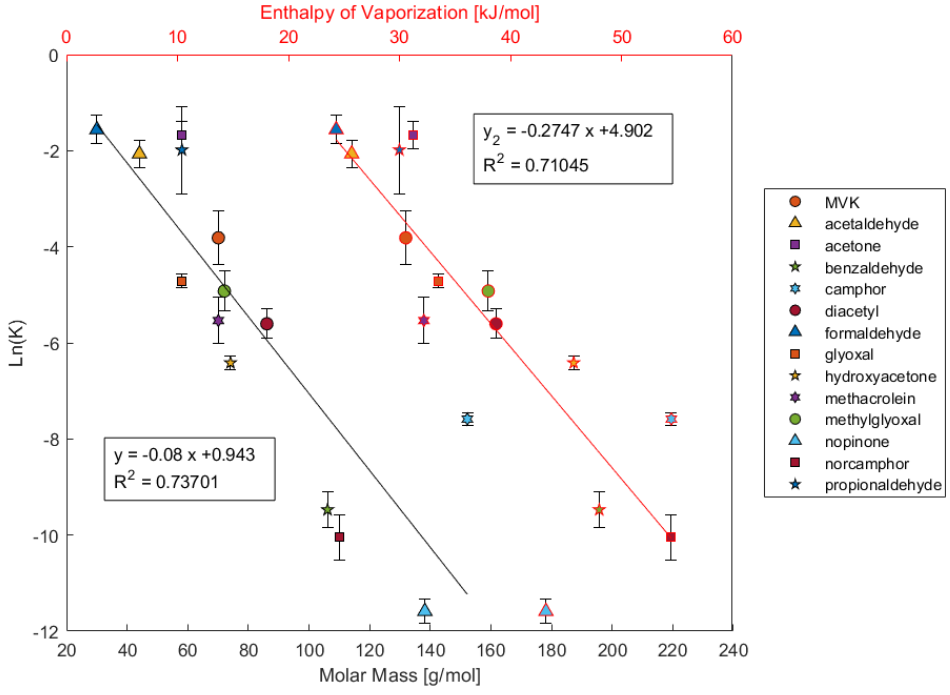

Figure 4. Scatterplot of ln(*K*) at –20 ºC versus the heat of vaporization (red line) and molar mass (black line).

4 Conclusions

The uptake of carbonyls by ice crystals grown by deposition was studied at temperatures between –20 ºC and –40 ºC. Ice was grown from the vapor phase in the presence of gas phase carbonyls using a flowtube apparatus where ice saturation was controlled for a realistic saturation prevalent in in natural cirrus clouds. Uptake of the

https://doi.org/10.5194/egusphere-2025-1425
Preprint. Discussion started: 3 April 2025

carbonyl compounds from the gas phase during crystal growth was observed. Performing this experiment at different temperatures allowed for the entropy and enthalpy of uptake to be determined. A linear correlation between ΔS and ΔH arose which was statistically validated and determined with 99% confidence that the EEC seen is not a statistical artifact. This compensation behavior could be an indication of a surface liquid layer or quasi-liquid layer behavior involved in this process; or it could also indicate a single dominant influence on a compound's uptake. The most significant chemical properties correlated with uptake were identified to be molecular size and vapor pressure. Their relationship to uptake is indicative of incorporation into the ice crystal structure, as smaller compounds have higher observed uptakes.

In agreement with previous studies, these results indicate that deposition into the ice phase is a possible uptake process for organic compounds in cirrus clouds. Since ice growth in the troposphere at low temperatures is a major contributor to precipitation, in-cloud scavenging is a plausible explanation for the occurrence of organics in fresh snow (Roth et al., 2004; Su et al., 2021). Therefore, interactions of ice and organic compounds can influence atmospheric transport and removal of those compounds from the atmosphere by deposition. The partitioning coefficients observed here are however below,—by at least 3 orders of magnitude—the 10 mol m^{-3} Pa^{-1} threshold from Crutzen and Lawrence (2000) to be considered a substantial atmospheric removal process. For reference, the partitioning coefficients reported here can be converted from dimensionless coefficients to mol m^{-3} Pa^{-1} by dividing by RT. Further, the uptake coefficients for carbonyls are on average smaller than those for aromatic hydrocarbons studied by (Fries et al., 2007), which have already been estimated to be removed primarily by photochemical processes rather than ice phase scavenging. While this removal process cannot be considered substantial in terms of mass transport, it may be relevant as an influence on vertical tracer transport.

These measurements are exclusively a description of the gas to ice solid solution equilibrium and neglect investigation of gas to liquid or liquid to ice equilibrium. These partitioning coefficients do not directly describe whether a compound is actually incorporated into the ice crystal lattice or if it phase separates into crystal grain boundaries, but only its uptake into the bulk phase. However, the negative correlation of molecular size and uptake may suggest incorporation into the ice crystal lattice or void space. It is also difficult to say if this data describes uptake into a liquid solution phase that coexists with ice, but the observed compensation effect may insinuate its

https://doi.org/10.5194/egusphere-2025-1425
Preprint. Discussion started: 3 April 2025

presence. While the measurements here are for multicomponent mixtures of compounds, single component uptake is likely the same, which is also supported by Huffman and Snider (2004).

Further investigation to determine the contribution of liquid layer influence should focus on measuring on ice-specific surface area and the volume of solution associated with the liquid layer. Additionally, similar experiments with other families of compounds are required to better understand the root of the compensation effect seen here. Crystallographic analysis of this data may also yield more information about the ice uptake process. With more investigation to reveal the main contributors of additivity, it seems possible that the EEC seen here could be used to help model the uptake process with a significant degree of accuracy.

Acknowledgements

This work was funded by the Deutsche Forschungsgemeinschaft (DFG, German Research Foundation) – TRR 301 – Project-ID 428312742.

This work was supported by the Max Planck Graduate Center with the Johannes Gutenberg University of Mainz (MPGC) as well as by internal funding from the Max Planck Institute for Chemistry (MPIC). We would also like to acknowledge the mechanical workshop of the Johannes Gutenberg University Institute of Atmospheric Physics (JGU-IPA) and the glass workshop of the Max Planck Institute for Polymer Research (MPIP) for their technical expertise and contributions.

Special thanks to Jan Wallner for his contributions testing the experimental setup.

Author Contributions

JS, MS, AT, SM participated in designing the experiments; JS, AT, SM participated in constructing the experimental apparatus; JS prepared the solutions for experiments, performed the experiments, and collected the samples; JS, CB conducted the analytical measurements; JS analyzed the data and wrote the manuscript draft; JS, MS, AT, CB, TH reviewed and edited the manuscript.

Competing Interests

The contact author has declared that none of the authors has any competing interests

https://doi.org/10.5194/egusphere-2025-1425
Preprint. Discussion started: 3 April 2025

References

Abbatt, J. P. D., Bartels-Rausch, T., Ullerstam, M., and Ye, T. J.: Uptake of acetone, ethanol and benzene to snow and ice: effects of surface area andtemperature, Environmental Research Letters, 3, 045008, https://doi.org/10.1088/1748-9326/3/4/045008, 2008.

Bartels-Rausch, T., Jacobi, H. W., Kahan, T. F., Thomas, J. L., Thomson, E. S., Abbatt, J. P. D., Ammann, M., Blackford, J. R., Bluhm, H., Boxe, C., Domine, F., Frey, M. M., Gladich, I., Guzmán, M. I., Heger, D., Huthwelker, T., Klán, P., Kuhs, W. F., Kuo, M. H., Maus, S., Moussa, S. G., McNeill, V. F., Newberg, J. T., Pettersson, J. B. C., Roeselová, M., and Sodeau, J. R.: A review of air-ice chemical and physical interactions (AICI): Liquids, quasi-liquids, and solids in snow, Atmos Chem Phys, 14, 1587–1633, https://doi.org/10.5194/ACP-14-1587-2014, 2014.

Behr, P., Terziyski, A., and Zellner, R.: Acetone adsorption on ice surfaces in the temperature range T = 190-220 K: Evidence for aging effects due to crystallographic changes of the adsorption sites, Journal of Physical Chemistry A, 110, 8098–8107, https://doi.org/10.1021/JP0563742/ASSET/IMAGES/LARGE/JP0563742F00011.JPEG, 2006.

Borchers, C., Seymore, J., Gautam, M., Dörholt, K., Müller, Y., Arndt, A., Gömmer, L., Ungeheuer, F., Szakáll, M., Borrmann, S., Theis, A., Vogel, A. L., and Hoffmann, T.: Retention of α -pinene oxidation products and nitro-aromatic compounds during riming, Atmos Chem Phys, 24, 13961–13974, https://doi.org/10.5194/ACP-24-13961-2024, 2024a.

Borchers, C., Seymore, J., Gautam, M., Dörholt, K., Müller, Y., Arndt, A., Gömmer, L., Ungeheuer, F., Szakáll, M., Borrmann, S., Theis, A., Vogel, A. L., and Hoffmann, T.: Retention of α-pinene oxidation products and nitro-aromatic compounds during riming, https://doi.org/10.5194/egusphere-2024-1443, 2024b.

Chickos, J. S., Hosseini, S., and Hesse, D. G.: Determination of vaporization enthalpies of simple organic molecules by correlations of changes in gas chromatographic net retention times, Thermochim Acta, 249, 41–62, https://doi.org/10.1016/0040-6031(95)90670-3, 1995.

Comstock, J. M., Ackerman, T. P., Turner, D. D., Comstock, J. M., Ackerman, T. P., and Turner, D. D.: Evidence of high ice supersaturation in cirrus clouds using ARM Raman lidar measurements, Geophys Res Lett, 31, 11106, https://doi.org/10.1029/2004GL019705, 2004.

Conklin, M. H., Sommerfeld, R. A., Kay Laird, S., and Villinski, J. E.: Sulfur dioxide reactions on ice surfaces: implications for dry deposition to snow, Atmospheric Environment. Part A. General Topics, 27, 159–166, https://doi.org/10.1016/0960-1686(93)90346-Z, 1993.

Cooke, M. C., Utembe, S. R., Gorrotxategi Carbajo, P., Archibald, A. T., Orr-Ewing, A. J., Jenkin, M. E., Derwent, R. G., Lary, D. J., and Shallcross, D. E.: Impacts of formaldehyde photolysis rates on tropospheric chemistry, Atmospheric Science Letters, 11, 33–38, https://doi.org/10.1002/ASL.251, 2010.

Crutzen, P. J. and Lawrence, M. G.: The Impact of Precipitation Scavenging on the Transport of Trace Gases: A 3-Dimensional Model Sensitivity Study, Journal of Atmospheric Chemistry, 81–112 pp., 2000.

Davidovits, P., Kolb, C. E., Williams, L. R., Jayne, J. T., and Worsnop, D. R.: Mass Accommodation and Chemical Reactions at Gas−Liquid Interfaces, https://doi.org/10.1021/cr040366k, 2006.

Dekoutsidis, G., Groß, S., Wirth, M., Krämer, M., and Rolf, C.: Characteristics of supersaturation in midlatitude cirrus clouds and their adjacent cloud-free air, Atmos Chem Phys, 23, 3103–3117, https://doi.org/10.5194/ACP-23-3103-2023, 2023.

Diehl, K., Mitra, S. K., and Pruppacher, H. R.: A laboratory study of the uptake ofHNO3 and HCl vapor by snow crystals and ice spheres at temperatures between 0 and -40 C, Atmos Environ, 29, 975–981, 1995.

https://doi.org/10.5194/egusphere-2025-1425
Preprint. Discussion started: 3 April 2025

Dominé, F. and Thibert, E.: Mechanism of incorporation of trace gases in ice grown from the gas phase, Geophys Res Lett, 23, 3627–3630, https://doi.org/10.1029/96GL03290, 1996.

Dragan, A. I., Read, C. M., and Crane-Robinson, C.: Enthalpy–entropy compensation: the role of solvation, https://doi.org/10.1007/s00249-016-1182-6, 1 May 2017.

Ervens, B. and Kreidenweis, S. M.: SOA formation by biogenic and carbonyl compounds: Data evaluation and application, Environ Sci Technol, 41, 3904–3910, https://doi.org/10.1021/ES061946X/SUPPL_FILE/ES061946XSI20061123_082532.PDF, 2007.

Franz, T. P. and Eisenreich, S. J.: Accumulation of polychlorinated biphenyls and polycyclic aromatic hydrocarbons in the snowpack of Minnesota and Lake Superior, J Great Lakes Res, 26, 220–234, https://doi.org/10.1016/S0380-1330(00)70688-5, 2000.

Fried, A., Barth, M. C., Bela, M., Weibring, P., Richter, D., Walega, J., Li, Y., Pickering, K., Apel, E., Hornbrook, R., Hills, A., Riemer, D. D., Blake, N., Blake, D. R., Schroeder, J. R., Luo, Z. J., Crawford, J. H., Olson, J., Rutledge, S., Betten, D., Biggerstaff, M. I., Diskin, G. S., Sachse, G., Campos, T., Flocke, F., Weinheimer, A., Cantrel, C., Pollack, I., Peischl, J., Froyd, K., Wisthaler, A., Mikoviny, T., and Woods, S.: Convective transport of formaldehyde to the upper troposphere and lower stratosphere and associated scavenging in thunderstorms over the central United States during the 2012 DC3 study, Journal of Geophysical Research: Atmospheres, 121, 7430–7460, https://doi.org/10.1002/2015JD024477, 2016.

Fries, E., Haunold, W., Jaeschke, W., Hoog, I., Mitra, S. K., and Borrmann, S.: Uptake of gaseous aromatic hydrocarbons by non-growing ice crystals, Atmos Environ, 40, 5476–5485, https://doi.org/10.1016/J.ATMOSENV.2006.03.055, 2006.

Fries, E., Starokozhev, E., Haunold, W., Jaeschke, W., Mitra, S. K., Borrmann, S., and Schmidt, M. U.: Laboratory studies on the uptake of aromatic hydrocarbons by ice crystals during vapor depositional crystal growth, Atmos Environ, 41, 6156–6166, https://doi.org/10.1016/j.atmosenv.2007.04.028, 2007.

Galeazzo, T., Aumont, B., Camredon, M., Valorso, R., Lim, Y. B., Ziemann, P. J., and Shiraiwa, M.: Secondary organic aerosols derived from intermediate-volatility n-alkanes adopt low-viscous phase state, Atmos Chem Phys, 24, 5549–5565, https://doi.org/10.5194/ACP-24-5549-2024, 2024.

Goss, K. U.: Adsorption of Organic Vapors on Ice and Quartz Sand at Temperatures Below 0 °C, Environ Sci Technol, 27, 2826–2830, https://doi.org/10.1021/ES00049A024/ASSET/ES00049A024.FP.PNG_V03, 1993.

Griessen, R. and Dam, B.: Simple Accurate Verification of Enthalpy-Entropy Compensation and Isoequilibrium Relationship, ChemPhysChem, 22, 1774–1784, https://doi.org/10.1002/CPHC.202100431, 2021.

Grunwald, E. and Steel, C.: Solvent Reorganization and Thermodynamic Enthalpy-Entropy Compensation, J. Am. Chem. Soc, 5687–5692 pp., 1995.

Von Hessberg, P., Pouvesle, N., Winkler, A. K., Schuster, G., and Crowley, J. N.: Interaction of formic and acetic acid with ice surfaces between 187 and 227 K. Investigation of single species- and competitive adsorption, Physical Chemistry Chemical Physics, 10, 2345–2355, https://doi.org/10.1039/B800831K, 2008.

Heymsfield, A. J., Schmitt, C., Chen, C. C. J., Bansemer, A., Gettelman, A., Field, P. R., and Liu, C.: Contributions of the Liquid and Ice Phases to Global Surface Precipitation: Observations and Global Climate Modeling, J Atmos Sci, 77, 2629–2648, https://doi.org/10.1175/JAS-D-19-0352.1, 2020.

Hoareau, C., Noel, V., Chepfer, H., Vidot, J., Chiriaco, M., Bastin, S., Reverdy, M., and Cesana, G.: Remote sensing ice supersaturation inside and near cirrus clouds: a case study in the subtropics, Atmospheric Science Letters, 17, 639–645, https://doi.org/10.1002/ASL.714, 2016.

https://doi.org/10.5194/egusphere-2025-1425
Preprint. Discussion started: 3 April 2025

Hudson, P. K., Zondlo, M. A., and Tolbert, M. A.: The interaction of methanol, acetone, and acetaldehyde with ice and nitric acid-doped ice: Implications for cirrus clouds, Journal of Physical Chemistry A, 106, 2882–2888, https://doi.org/10.1021/jp012718m, 2002.

Huffman, W. A. and Snider, J. R.: Ice-oxyhydrocarbon interactions in the troposphere, Journal of Geophysical Research: Atmospheres, 109, https://doi.org/10.1029/2003jd003778, 2004.

Jayne, J. T., Duan, S. X., Davidovits, P., Worsnop, D. R., Zahniser, M. S., and Kolb, C. E.: Uptake of gas-phase alcohol and organic acid molecules by water surfaces, Journal of Physical Chemistry, 95, 6329–6336, https://doi.org/10.1021/J100169A047/ASSET/J100169A047.FP.PNG_V03, 1991.

Jost, A., Szakáll, M., DIehl, K., Mitra, S. K., and Borrmann, S.: Chemistry of riming: The retention of organic and inorganic atmospheric trace constituents, Atmos Chem Phys, 17, 9717–9732, https://doi.org/10.5194/ACP-17-9717-2017, 2017.

Kahnt, A., Iinuma, Y., Böge, O., Mutzel, A., and Herrmann, H.: Denuder sampling techniques for the determination of gas-phase carbonyl compounds: A comparison and characterisation of in situ and ex situ derivatisation methods, J Chromatogr B Analyt Technol Biomed Life Sci, 879, 1402–1411, https://doi.org/10.1016/j.jchromb.2011.02.028, 2011.

Krug, R. R., Hunter, W. G., and Grieger, R. A.: Statistical interpretation of enthalpy–entropy compensation, Nature 1976 261:5561, 261, 566–567, https://doi.org/10.1038/261566a0, 1976.

Leffler, J. E.: The enthalpy-entropy relationship and its implications for organic chemistry, J. org. Chem., 20, 1202–1231, https://doi.org/10.1021/jo01126a009, 1955.

Leung, D. H., Bergman, R. G., and Raymond, K. N.: Enthalpy-entropy compensation reveals solvent reorganization as a driving force for supramolecular encapsulation in water, J Am Chem Soc, 130, 2798–2805, https://doi.org/10.1021/ja075975z, 2008.

Liu, L. and Guo, Q. X.: Isokinetic relationship, isoequilibrium relationship, and enthalpy-entropy compensation, https://doi.org/10.1021/cr990416z, March 2001.

Lumry, R.: [29] On the interpretation of data from isothermal processes, in: Methods in Enzymology, vol. 259, Academic Press, 628–720, https://doi.org/10.1016/0076-6879(95)59065-X, 1995.

Lumry, R. and Rajender, S.: Enthalpy–entropy compensation phenomena in water solutions of proteins and small molecules: A ubiquitous properly of water, Biopolymers, 9, 1125–1227, https://doi.org/10.1002/bip.1970.360091002, 1970.

Mitra, S. K., Barth, S., and Pruppacher, H. R.: A laboratory study on the scavenging of SO2 by snow crystals, Atmospheric Environment. Part A. General Topics, 24, 2307–2312, https://doi.org/10.1016/0960-1686(90)90324-G, 1990.

Moulik, S. P., Naskar, B., and Rakshit, A. K.: Current Status of Enthalpy–Entropy Compensation Phenomenon, Curr Sci, 117, 1286, https://doi.org/10.18520/cs/v117/i8/1286-1291, 2019.

Mu, Y. and Xu, Z.: Scavenging of carbonyl sulfide precursor in the atmosphere by precipitation, Journal of Geophysical Research: Atmospheres, 114, https://doi.org/10.1029/2008JD010622, 2009.

Mülmenstädt, J., Sourdeval, O., Delanoë, J., and Quaas, J.: Frequency of occurrence of rain from liquid-, mixed-, and ice-phase clouds derived from A-Train satellite retrievals, Geophys Res Lett, 42, 6502–6509, https://doi.org/10.1002/2015GL064604, 2015.

Orem, M. W. and Adamson, A. W.: Physical adsorption of vapor on ice: II. n-alkanes, J Colloid Interface Sci, 31, 278–286, https://doi.org/10.1016/0021-9797(69)90337-3, 1969.

https://doi.org/10.5194/egusphere-2025-1425
Preprint. Discussion started: 3 April 2025

Pan, A., Biswas, T., Rakshit, A. K., and Moulik, S. P.: Enthalpy-Entropy Compensation (EEC) Effect: A Revisit, Journal of Physical Chemistry B, 119, 15876–15884, https://doi.org/10.1021/acs.jpcb.5b09925, 2015.

Renard, P., Siekmann, F., Salque, G., Smaani, A., Demelas, C., Coulomb, B., Vassalo, L., Ravier, S., Temime-Roussel, B., Voisin, D., and Monod, A.: Aqueous phase oligomerization of methyl vinyl ketone through photooxidation – Part 1: Aging processes of oligomers, https://doi.org/10.5194/acpd-14-15283-2014, 12 June 2014.

Roth, C. M., Goss, K. U., and Schwarzenbach, R. P.: Sorption of diverse organic vapors to snow, Environ Sci Technol, 38, 4078–4084, https://doi.org/10.1021/ES0350684, 2004.

Sander, R.: Compilation of Henry's law constants (version 5.0.0) for water as solvent, Atmos Chem Phys, 23, 10901–12440, https://doi.org/10.5194/ACP-23-10901-2023, 2023.

Santachiara, G., Prodi, F., Udisti, R., and Prodi, A.: Scavenging of SO2 and NH3 during growth of ice, Atmos Res, 47–48, 209–217, https://doi.org/10.1016/S0169-8095(97)00087-2, 1998.

Sharp, K.: Entropy—enthalpy compensation: Fact or artifact?, Protein Science, 10, 661–667, https://doi.org/10.1110/ps.37801, 2001.

Sokolov, O. and Abbatt, J. P. D.: Adsorption to ice of n-alcohols (ethanol to 1-hexanol), acetic acid, and hexanal, Journal of Physical Chemistry A, 106, 775–782, https://doi.org/10.1021/JP013291M/ASSET/IMAGES/MEDIUM/JP013291ME00004.GIF, 2002.

Sonntag, D.: Fortschritte in der Hygrometrie, Meteorologische Zeitschrift, 3, 51–66, https://doi.org/10.1127/metz/3/1994/51, 1994.

Srivastava, D., Vu, T. V., Tong, S., Shi, Z., and Harrison, R. M.: Formation of secondary organic aerosols from anthropogenic precursors in laboratory studies, npj Climate and Atmospheric Science 2022 5:1, 5, 1–30, https://doi.org/10.1038/s41612-022-00238-6, 2022.

Su, S., Xie, Q., Lang, Y., Cao, D., Xu, Y., Chen, J., Chen, S., Hu, W., Qi, Y., Pan, X., Sun, Y., Wang, Z., Liu, C.-Q., Jiang, G., and Fu, P.: High Molecular Diversity of Organic Nitrogen in Urban Snow in North China, Environ Sci Technol, https://doi.org/10.1021/acs.est.0c06851, 2021.

Warhaft, Zellman.: An introduction to thermal-fluid engineering : the engine and the atmosphere, Cambridge University Press, 266 pp., 1998.

Winkler, A. K., Holmes, N. S., and Crowley, J. N.: Interaction of methanol, acetone and formaldehyde with ice surfaces between 198 and 223 K, Physical Chemistry Chemical Physics, 4, 5270–5275, https://doi.org/10.1039/b206258e, 2002.

Xu, Y., Feng, X., Chen, Y., Zheng, P., Hui, L., Chen, Y., Yu, J. Z., and Wang, Z.: Development of an enhanced method for atmospheric carbonyls and characterizing their roles in photochemistry in subtropical Hong Kong, Science of The Total Environment, 896, 165135, https://doi.org/10.1016/J.SCITOTENV.2023.165135, 2023.

Yu, L., Smith, J., Laskin, A., Anastasio, C., Laskin, J., and Zhang, Q.: Chemical characterization of SOA formed from aqueous-phase reactions of phenols with the triplet excited state of carbonyl and hydroxyl radical, Atmos Chem Phys, 14, 13801–13816, https://doi.org/10.5194/ACP-14-13801-2014, 2014.

Zhao, M. and Shi, X.: A Study on the Wide Range of Relative Humidity in Cirrus Clouds Using Large-Ensemble Parcel Model Simulations, Atmosphere 2023, Vol. 14, Page 583, 14, 583, https://doi.org/10.3390/ATMOS14030583, 2023.

Zhao, Y. H., Abraham, M. H., and Zissimos, A. M.: Fast calculation of van der Waals volume as a sum of atomic and bond contributions and its application to drug compounds, Journal of Organic Chemistry, 68, 7368–7373, https://doi.org/10.1021/jo034808o, 2003.

4.2 *Retention During Freezing of Raindrops, Part II: Investigation of Ambient Organics from Beijing Urban Aerosol Samples*

The following publication addresses the underrepresented topic of chemical retention during drop freezing processes. Chemical redistribution between the liquid and gas phase during freezing is not fully understood, particularly for the wide variety of atmospheric organics. This is despite its relevance to the vertical redistribution of organics along the UTLS and its support of new particle formation in convective outflows, thereby its subsequent role in radiation scattering and cloud condensation nucleation.

We conducted laboratory studies on the chemical retention of water-soluble compounds sampled from ambient Beijing aerosols during drop freezing experiments in an acoustic levitator setup. An aqueous extract of filter samples collected from PM2.5 Beijing aerosols was introduced via syringe into an acoustic levitator housed inside a cold chamber held at –15ºC. The contact-free single-drop was allowed to freeze without the introduction of artificial freezing nucleator and then collected for comparative analysis with the native extract. The samples were then chemically analyzed with ultra-high resolution mass spectrometry and the retention coefficients determined. Our results show that the retention of WSOC forms a real, nonnormal distribution up to 1 and that raindrop freezing does not have a sigmoidal relation with effective Henry's Law solubilities. This contrasts with the behavior currently described in the literature specifically for cloud droplets. Our data also shows that different classes of organics may have different distributions of retention coefficients. For example, nitro and sulphate substituted species—often the products of anthropogenically related NOx and SOx chemistry—are highly retained. This suggests that NOx and SOx chemistry may enhance the retention of these SOA species and reduce their likelihood of reaching the upper atmosphere. This contrasts with the wide distribution for CHO groups like sugars, organic acids, and terpenoids with highly variable retentions.

I was the main contributor to this publication. Specifically, I along with MG, MS, AT designed the experiments; I along with JM prepared the samples for experiments; I along with JM, AV conducted the analytical measurements; I analyzed the data and wrote the manuscript draft; I along with MG, MS, AT, JM, AV, TH reviewed and edited the manuscript.

Supplementary material supporting this manuscript can be found in Section 8.

https://doi.org/10.5194/egusphere-2024-3940
Preprint. Discussion started: 20 December 2024

Retention During Freezing of Raindrops, Part II: Investigation of Ambient Organics from Beijing Urban Aerosol Samples

Jackson Seymore*[1], Martanda Gautam[1], Miklós Szakáll[1], Alexander Theis[2], Thorsten Hoffmann[2], Jialiang Ma[3], Lingli Zhou[4], Alexander L. Vogel[3]

[1] Institute for Atmospheric Physics, Johannes Gutenberg University, Mainz, Germany
[2] Particle Chemistry Department, Max Planck Institute for Chemistry, Mainz, Germany
[3] Institute for Atmospheric and Environmental Sciences, Goethe University Frankfurt, Germany
[4] South China Institute of Environmental Sciences, Ministry of Ecology and Environment, Guangzhou, P.R. China
*Corresponding author: seymorej@uni-mainz.de

Keywords: retention, dissolved organic matter, DOM, Orbitrap MS, secondary organic aerosol, SOA, convective clouds, acoustic levitator

Abstract

The freezing of hydrometeors incurs certain water-soluble organic compounds dissolved in the supercooled cloud droplets to be released into the gas phase. This may lead to the vertical redistribution of substances that become available for new particle formation in the upper troposphere. Drop freezing experiments were performed on the Mainz Acoustic Levitator (M-AL) using aqueous extracts of ambient samples of Beijing urban aerosol. The retention coefficients of over 450 compounds were determined. Most nitroaromatics and organosulfates were fully retained along with the aliphatic amines (AA) and higher-order amines and amides while sulfides, lipids, aromatic hydrocarbons, and long chain compounds are among the most unretained and incidentally the fewest species observed. The findings here also indicate that NO_x and SO_x chemistry, particularly anthropogenically related, enhances the retention of the resulting secondary organic aerosols (SOA). A positive correlation between polarity and freezing retention along with a negative correlation with vapor pressure and freezing retention was observed. No sigmoidal relationship with effective Henry's law constant was observed which differs with the parameterizations of riming retention presented in current literature, which is justified by the lower surface-to-volume ratio of the large drop size investigated.

https://doi.org/10.5194/egusphere-2024-3940
Preprint. Discussion started: 20 December 2024

1 Introduction

Atmospheric organic matter (OM) plays a critical role in climate regulation directly through radiation scattering and indirectly through cloud condensation nucleation which impacts Earth's energy balance through radiative forcing (Fofie et al., 2018; Liu et al., 2018). These effects are controlled by factors such as their optical properties, size, and the hygroscopicity (Dusek et al., 2006; Sun et al., 2021), which can change based on the proportions of primary organic aerosols (POA)—directly emitted aerosols—and secondary organic aerosols (SOA)—aerosols formed from the oxidation products of volatile organic compounds (VOC) as part of new particle formation (NPF) (Hallquist et al., 2009; Liu et al., 2021; Riva et al., 2019). Convective systems have been suggested to support NPF in the outflow region by reducing existing particle concentrations, facilitating cold temperatures, and transporting reactive gases into regions with high actinic fluxes (Clarke et al., 1998; Zheng et al., 2021)

Nucleation-mode particles—with sizes in the lower tens of nm—have consistently been observed in concentrations of up to 10^4 cm^{-3} from aircraft in the upper troposphere (Andreae et al., 2018; Andrés Casquero-Vera et al., 2020; Clarke et al., 1999; Heitto et al., 2024; Weigel et al., 2011; Williamson et al., 2019). These measurements significantly exceed the corresponding concentrations in the planetary boundary layer and indicate that the main source of such ultra-fine particles in the upper troposphere is in situ NPF rather than their direct transport from the boundary layer (Bardakov et al., 2021). The traditional explanation for this phenomenon has been that the reduction of existing aerosol particles in deep convective clouds eliminates removal processes for small particles and condensable vapors, supporting NPF (Clarke et al., 1998). However, Williamson et al. (2019) also showed that even without these conditions, such as in tropical convection, these newly formed particles can still be found. They then argue that most models underestimate available organic matter at high altitudes and as a result predict less NPF in these regions. If this NPF is the result of an overlooked mechanism of organic matter transport, it is then critical to elucidate this mechanism so to constrain uncertainty around the influence of high altitude NPF from convective outflows (Bardakov et al., 2021).

https://doi.org/10.5194/egusphere-2024-3940
Preprint. Discussion started: 20 December 2024

Publications by Borchers et al. (2024) and Jost et al., (2017) have demonstrated a potential mechanism for organic matter transport in mixed-phase clouds. They describe how organic compounds that are exchanged between the gas and aqueous phase in cloud droplets can either be trapped in the ice phase during freezing—washing them out by precipitation—or return to the gas phase by volatilization. This revolatilization incurred by the freezing process leads to a vertical redistribution and has the potential to explain the occurrence of organic matter at high altitudes in regions with deep convection. Alternatively, earlier publications by Pruppacher and Klett (2010) and Snider and Huang (1998) have suggested that complete sublimation of ice particles can also transport 'retained' compounds trapped in the ice phase and release them at high altitudes.

In convective clouds the main formation pathway of precipitation-size ice particles is riming, i.e. the freezing of supercooled µm-sized cloud droplets on the surface of a mm-sized ice particle. Thus, riming retention is an important process for the vertical redistribution of water-soluble organic compounds (WSOC). Convective clouds with warm bases favor the formation of mm-sized drops by collision-coalescence (Lamb and Verlinde, 2011), which subsequently can be uplifted in the updraft to regions with temperatures below 0°C. Once beyond the freezing level they can freeze and thereby release dissolved matter into the gas phase. This identifies freezing retention of mm-sized drops as a potential contributor to the vertical redistribution of WSOCs and was experimentally investigated in the present study.

The proportion of a substance that remains in the ice during this phase change is described by the retention coefficient R, which indicates the percentage of the trapped substance with a value between 0 and 1 (Bela et al., 2018; Iribarne and Pyshnov, 1990; Snider et al., 1992; Stuart and Jacobson, 2004). A species' retention is influenced by its chemical properties, such as its dimensionless effective Henry's law solubility constant (H*), as well as the physical properties of the droplet such as temperature, liquid water content, droplet size, and ventilation. Substances with a small H* are more likely to return to the gas phase during riming, which results in a lower retention coefficient. Additionally, these external and

https://doi.org/10.5194/egusphere-2024-3940
Preprint. Discussion started: 20 December 2024

physical conditions of the droplet disproportionally influence the retention for these small H* substances (Jost et al., 2017; Stuart and Jacobson, 2003, 2004)

Current experimental studies to determine retention coefficients for atmospheric constituents and relevant SOA precursors have focused on inorganic species, small organics, or single component mixtures with significantly higher than natural concentrations. Additionally, current studies have only examined retention in droplets within natural cloud size range rather than raindrop sizes. The few studies that look at complex mixtures are limited to compounds of similar families and only a handful of species (Borchers et al., 2024). Naturally occurring atmospheric constituents that are observed in rainwater are present as complex mixtures of potentially thousands of species (Seymore et al., 2023). To get closer to observing the retention of compounds in their natural conditions, this study presents measurements of retention coefficients for a real, complex mixture of WSOC extracted from filter samples taken in an urban environment.

2 Methods

2.1 Sampling Location and Method

A high-volume sampler (HiVol) was run with quartz fiber TSP filters over three nights between March 3 and 5, 2022 in Beijing, China (40.0426° N, 116.4197° E) for an approximate sample volume of 550 m^3 between the hours of 21:00 to 9:00. These filters were sealed in aluminum foil and stored at -20ºC until analysis. Aqueous extracts of these filters were prepared by taking 1/4 of each filter, combining them (in total 3/4 of a 203 x 254 mm filter area) in 30 ml Milli-Q water, and then extracting with an orbital shaker for 15 min. The same was performed for a blank sample; a total 3/4 of unsampled filter area was extracted in 30 ml Milli-Q water for 15 min. These extracts were filtered through a 0.2 µm PTFE filter. 10 ml of the prepared extract was reserved for Ultra-High Performance Liquid Chromatography High-

https://doi.org/10.5194/egusphere-2024-3940
Preprint. Discussion started: 20 December 2024

Resolution Orbitrap Mass Spectrometry (UHPLC-HRMS) analysis and stored at 3 ºC while the remaining 20 ml was sent to Institute for Atmospheric Physics at the Johannes Gutenberg University of Mainz, Germany for freezing experiments.

2.2 Mainz Acoustic Levitator (M-AL)

Freezing experiments were performed in an acoustic levitator (APOS BA 10, tec5 GmbH). This allows contact-free single-drop levitation maintained by a standing ultrasonic wave. This setup and its relevant physical influences are described in detail by Diehl et al., (2014), Szakáll et al., (2021), and in part 1 of this publication series by Gautam et al. (2024). For the freezing experiment, the M-AL is placed inside a walk-in cold room where the ambient temperature was set to -15ºC. The M-AL is surrounded by a protective acrylic housing to prevent any disturbance from air motion which may cause unsteady temperature conditions, unstable levitation, or carry unwanted ice-nucleating particles onto the drop surface. Air temperature in the M-AL was measured by a PT100 sensor and an infrared thermometer (KT 19.82 II, Heitronics) was used to monitor drop surface temperature.

The aqueous filter extract was injected with a syringe into the M-AL node to form a single free-floating drop with a diameter of 2 ± 0.1 mm. The drop was allowed to freeze without the introduction of artificial freezing nucleator. Freezing time was approximately 90 seconds on average but not longer than 3 min. Once the drop was fully frozen, it was removed from the M-AL and stored in a polytetrafluoroethylene (PTFE) vial at –20ºC until analysis. Enough drop to reach the minimum viable sample volume for analysis, 50 µl, were collected to produce a single sample (approximately 12 drops). Two full samples were collected for UHPLC-HRMS analysis. The blank filter extract was also used in the freezing experiment to produce two more travel blank samples for comparative analysis and background subtraction.

https://doi.org/10.5194/egusphere-2024-3940
Preprint. Discussion started: 20 December 2024

2.3 UHPLC-HRMS analysis

In addition to the M-AL frozen extract and the travel blanks, 100 µl of the reserved extract and Milli-Q solvent was analyzed by UHPLC-HRMS. Chromatographic separation was performed (Vanquish Flex, Thermo Fisher Scientific Inc.) on a reversed phase column (Cortecs Solid Core T3, 2.7 µm, 150 × 3 mm, with the corresponding VanGuard Cartridge, Waters Corp.). Samples were ionized in negative and positive mode using a heated electrospray ionization source (HESI-II Probe, Thermo Fisher Scientific Inc.) and then detected with a high-resolution hybrid quadrupole-Orbitrap mass spectrometer (Q Exactive Focus, Thermo Fisher Scientific Inc.). The chromatographic settings and gradient are as follows: LC solvent A: ultrapure water with 0.1% formic acid; LC solvent B: methanol with 0.1% formic acid; Flow rate 400 µl min^{-1}; pre-column heater and post-column cooler 40 °C; Gradient: 0 min 1% B; 1 min 1% B; 15 min 99% B; 16.5 min 99% B; 17.5 min 1% B; 20 min 1% B. The MS settings were at fullMS scan (*m/z* 50-750; resolution 70k) along with data-dependent MS2 in discovery mode (resolution at 17.5k) for acquiring fragmentation spectra of the largest peaks.

2.4 Non-targeted Analysis and Property Estimation

Compound identification confidence is communicated here using the convention described in Schymanski et al., (2014). The raw UHPLC-HRMS files were processed on Compound Discoverer 3.3 (Thermo Fisher Scientific). This software aligned chromatographic peaks of interest with a maximum shift of 0.1 min in retention time and a mass tolerance of ±2 ppm. Mass traces with retention times less than 1.8 min were excluded as they are not considered to be chromatographically separated. Ions were detected if the peak intensity was at least 5×10^5 counts for $[M-H]^-$ for negative mode or $[M+H]^+$ and $[M+Na]^+$ for positive mode. In addition to the mass-to-charge ratio of the detected ion, at least one corresponding isotopologue had to be measured. The tolerance between the measured and calculated intensity of the isotopologue was less than 30 %. These unknown compounds were then grouped with a

https://doi.org/10.5194/egusphere-2024-3940
Preprint. Discussion started: 20 December 2024

retention time tolerance of 0.1 min to produce a merged MS feature and those of them with a sample-to-blank ratio smaller than 5 were marked as background and removed from the dataset. Any compounds that did not appear in the reserved sample of filter extract were also removed from the dataset. A peak quality score was given on a scale of 0 to 10—with 10 being a perfect chromatographic peak—for each mass trace based on its peak shape qualities, e.g. peak jaggedness, modality. For all mass traces with a peak quality higher than 6 in all samples, a predicted composition for each mass trace was calculated within ±2 ppm with the allowed elements of carbon (C), hydrogen (H), nitrogen (N), oxygen (O), and sulfur (S). Compounds were grouped together as CHO, CHNO, CHOS, and CHNOS. It is important to note that phosphorus (P) containing species were not considered for this study. All level 5 (L5) or higher compounds including any mass traces that did not fit a predicted composition within ±2 ppm were used for calculating retention coefficients using their integrated MS signals. Level 4 (L4) or higher compounds with determined compositions were used for Van Krevelen and Kroll analysis to highlight the validity of the dataset as a real, complex mixture of urban-influenced WSOC. To aid the visualization of MS data, a Van Krevelen diagram cross-plots the H:C ratio as a function of the O:C ratio while a Kroll diagram cross-plots the estimated average carbon oxidation state as a function of the number of carbon atoms. An estimated vapor pressure at 298 K was then calculated for the elemental composition based on the parameterization by Li et al. (2016).

The predicted compound list was then matched against the mzCloud database (HighChem LLC, 2013-2021) for comparing MS^2 spectra. If a compound had at least one positive match with the predicted compound in either database as well as a peak quality score above 8 in the reserved extract, this level 3 (L3) or higher tentative candidate was selected to be used for calculating its effective Henry's law constant (K_H, mol Pa^{-1} m^{-3}). These properties were predicted using the HENRYWIN™ model as part of the EPI Suite™ package which provides the values at 298 K (US EPA, n.d.). If the EPI Suite™ was able to find an experimental value based on a CAS lookup match, those values were used over the model

https://doi.org/10.5194/egusphere-2024-3940
Preprint. Discussion started: 20 December 2024

prediction. This is only applicable to the minority of identified species. The effective Henry's law solubility was converted to a dimensionless effective Henry's law constant (H*) using the equation:

$$H^* = K_H * \bar{R}T \quad (1)$$

Where $\bar{R}$ is the ideal gas constant (8.3144626 m^3 Pa K^{-1} mol^{-1}) and T is temperature (K). This conversion allows for a dimensionless comparison and considers dissociation and hydration effects. This calculation, however, requires structural information about a compound. As a result, performing this calculation on a L3 tentative structural candidate can be specious or misleading. Regardless, H* for structural isomers using HENRYWIN™ typically differs less than 3 orders of magnitude with an overall average of approximately 1.5. This accuracy is sufficient for this analysis (Isaacman-Vanwertz and Aumont, 2021).

2.3 Retention Calculation and Tracer Corrections

The signals of species that also appeared in the travel blanks were first subtracted from the M-AL samples to remove their ambient signal but remained in the dataset as they exceeded the sample-to-blank ratio of 5 and could not be considered background. A naturally occurring tracer was selected from the dataset for both positive and negative mode to correct for any dilution, evaporation, and desorption that may occur. To be an ideal tracer, the compound should be fully retained during freezing and have an adequate MS signal. For this work, the peak quality was required to be higher than 8 in the reserved extract and for there to be a positive database match for the predicted composition. For negative mode, this tracer was 4-Nitrophenol ($C_6H_5NO_3$, 139.0269 *m/z*, 9.7 min, L3). This was chosen as previous experiments by Borchers et al., (2024) have identified this compound to have a retention coefficient of 1.01 ± 0.07 during riming experiments, where desorption and evaporation effects are likely to be more influential than in the present experiment due to enhanced ventilation and much smaller droplet size. For positive mode, xylitol ($C_5H_{12}O_5$, 152.0685 *m/z*, 1.6 min, L3) was selected as the tracer as its H* has been determined to be higher than 10^8 (Compernolle and Müller, 2014), which according to Borchers et al.,

https://doi.org/10.5194/egusphere-2024-3940
Preprint. Discussion started: 20 December 2024

(2024) and Jost et al., (2017) indicate its retention coefficient can be safely assumed to be 1, even under the higher exchange conditions of wind tunnel experiments. Regardless of the accuracy of the L3-assigned structure, these tracers represent species with retentions very close to 1 that allow for a reference to that value to compare between samples and make corrections for non-freezing mass exchange.

The equation for calculating the retention coefficient is adopted from Borchers et al., (2024) and Jost et al., (2017) and used here as

$$R = \frac{S^{\text{sample}}_{\text{substance}} / S^{\text{RES}}_{\text{substance}}}{S^{\text{sample}}_{\text{tracer}} / S^{\text{RES}}_{\text{tracer}}} \quad (2)$$

where the numerator describes the ratio between the peak area of the substance of interest in the ice sample ($S^{\text{sample}}_{\text{substance}}$) and in the reserved extract sample ($S^{\text{RES}}_{\text{substance}}$). The denominator describes the same ratio but for the tracer ($S^{\text{sample}}_{\text{tracer}} / S^{\text{RES}}_{\text{tracer}}$). Since no dilution effects are involved in the measurement and all samples are measured in the same aqueous matrix, signal ratios can be compared directly without a calibration curve, provided that detector response is linear within the given range of measurement. Given that ions below the threshold intensity of linearity were excluded from measurement, dynamic mass calibration of the HRMS was performed prior to measurement, and that HRMS instruments of this generation show linear dynamic ranges of at least five orders of magnitude (Kaufmann and Walker, 2017), it is reasonable to assume linearity over the measurement range. As ventilation and evaporation effects are quite low in the M-AL (Szakáll et al., 2021), their effects are compensated for by the tracer. Compensating for desorption effects is more complex. As desorption is thought to be driven mainly by linear diffusion and thus enhanced by increased ventilation, species with higher than ambient concentrations as well as species with higher vapor pressures are thought to be disproportionally influenced. However, since the M-AL has little ventilation to enhance desorption, HiVol filter sampling already bias against high vapor pressure species (Bidleman et al., 2020), and ambient filter sampling is closer to ambient concentrations relative to previously simulated single component mixtures, desorption

https://doi.org/10.5194/egusphere-2024-3940
Preprint. Discussion started: 20 December 2024

effects are only compensated for by the tracer and nonuniform desorption effects are considered negligible.

Further data analysis was performed with MATLAB ver. R2023a. Distribution modeling was performed using the Distribution Fitter from the Statistics and Machine Learning Toolbox 12.5, based on the Stable Distribution and t Location Scale Distribution models provided in *Univariate Stable Distributions* (2020) and *Univariate Continuous Distributions* (2015) (Nolan, 2020; Yee, 2015).

3 Results and Discussion

3.1 Dataset Description

In the negative mode, from over 2800 MS features measured, 548 significant, non-background detected compounds were found. 208 met the peak quality constraints and were then used for analysis. 196 compounds (94%) had successfully assigned compositions and 77 were then selected for additional property calculations.

In the positive mode, 342 significant, non-background detected compounds were found from over 1800 features. 250 met the peak quality constraints and were then used for analysis. 218 of those compounds (87%) had successfully assigned compositions. 84 were then selected for additional property calculations. Comparatively fewer compounds were assigned compositions in the positive mode as phosphorous containing species were not considered. These can represent almost a third of positively ionizable species in rainwater WSOC (Seymore et al., 2023) so it likely makes up a significant portion of species variety that is not considered.

https://doi.org/10.5194/egusphere-2024-3940
Preprint. Discussion started: 20 December 2024

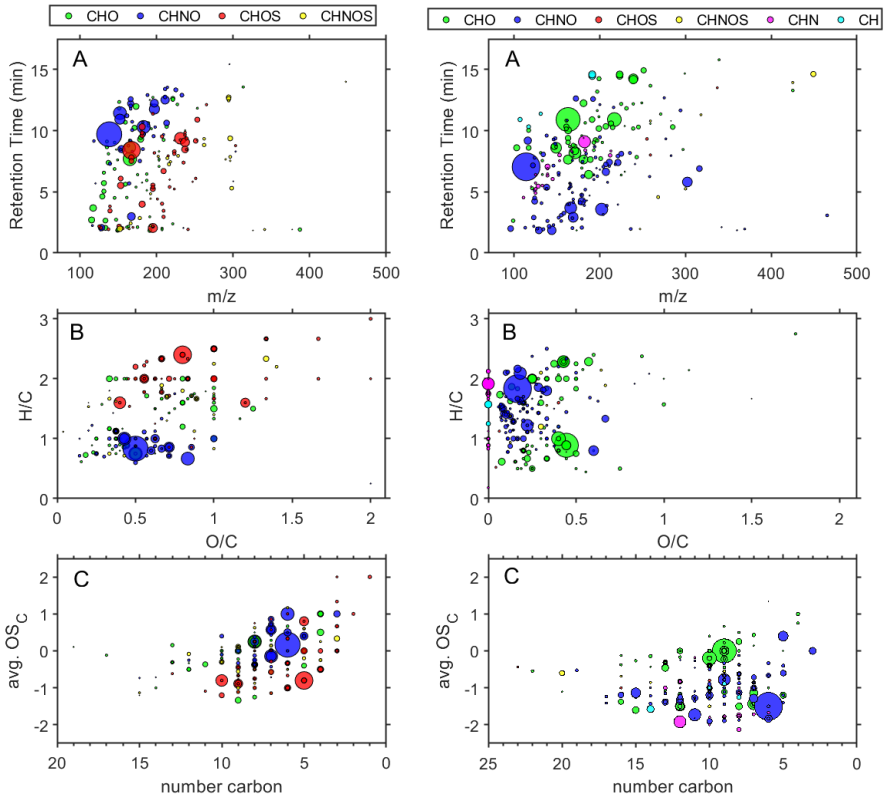

Figure 1. (A) Scatter plot of HPLC Retention time (min) vs *m/z* ratio; (B) van Krevelen diagram of O/C ratio vs H/C ratio; (C) Kroll diagram of number of C atoms against the average oxidation state of C; Left panels are for negative ionization mode (−)HESI, right panels are positive ionization mode (+)HESI. Area of the marker indicates relative intensity in the reserved extract while color denotes compositional class of the assigned compound: Green for CHO, blue for CHNO, red for CHOS, yellow for CHNOS, magenta for CHN, cyan for CH.

Figure 1 illustrates that the dataset is indicative of a typical urban influenced WSOC profile of a dilute sample. In the negative mode, the most significant signals are several nitrophenols and nitroaromatics; notably $C_6H_5NO_3$ (139 *m/z*, 9.7 min, L3) and $C_6H_4N_2O_5$ (184 *m/z*, 10.3 min, L3) are

https://doi.org/10.5194/egusphere-2024-3940
Preprint. Discussion started: 20 December 2024

tentatively identified as 4-nitrophenol and 2,4-dinitrophenol respectively. These nitrophenols ionize efficiently in (−)HESI which explains in part their prominence in Figure 1.B where they cluster around 0.6-0.9 H/C and are indications of biomass and fossil fuel burning emissions (Taneda et al., 2004). The prominent CHOS compounds in the negative mode are alkylorganosulfates, notably $C_5H_{12}O_4S$ (168 *m/z*, 8.4 min, L3) and $C_8H_{18}O_4S$ (210 *m/z*, 12.9 min, L3), which are typical markers of secondary processed automobile and shipping traffic OM.(Blair et al., 2017; Qi et al., 2021) These can most easily be seen in Figure 1.B above 2 H/C. Some of the other notable CHOS compounds below 2 H/C are terpene-derived organosulfates such as camphorsulfonic acid ($C_{10}H_{16}O_4S$, 232 *m/z*, 9.4 min, L2), which also demonstrate secondary processing under urban conditions (Iinuma et al., 2007; Surratt et al., 2007).

The most significant positive mode signals in Figure 1 come from caprolactam ($C_6H_{11}NO$, 114 *m/z*, 7.0 min, L2) and several coumarin derivatives ($C_9H_6O_2$, 146 *m/z* 7.4 min, L2; $C_9H_8O_4$, 162 *m/z*, 10.9 min, L3; $C_9H_8O_3$, 164 *m/z*, 8.7 min, L3; $C_{10}H_8O_4$, 192 *m/z*, 9.0 min, L3). Caprolactam is a cyclic amide and indicative of industrial emission influence as it is primarily used for manufacturing synthetic fibers but also used in numerous other manufacturing activities. Caprolactam is a monitored compound on the hazardous air pollutants list by the United States Environmental Protection Agency (U. S. Environmental Protection Agency, n.d.). Coumarin species are known brown carbon components and have biomass burning sources as well as potential secondary pathways (Xing et al., 2023).

The several other prominent CHNO compounds are mostly amines, e.g. $C_{11}H_{23}NO_2$ (201 *m/z*, 3.6 min, L3), $C_9H_{11}NO_2$ (165 *m/z*, 3.7 min, L3), DL-Stachydrine ($C_7H_{13}NO_2$, 143 *m/z*, 1.8 min, L2), etc. This is consistent with known amine-nitrate aerosol formation during winter months where there are sources of amine salts and semi-volatile organic amine compounds, particularly in areas with high agricultural and combustion emissions (Price et al., 2016). The other prominent CHNO compounds are tentatively identified as amides such as $C_{12}H_{18}N_2O$ (206 *m/z*, 6.6 min, L3), $C_{10}H_{14}N_2O$ (178 *m/z*, 4.2 min, L4), $C_3H_4N_4O_2$ (128 *m/z*, 1.8 min, L3), etc; which can either be further secondary products of AA (Price et al., 2014) or the result of anthropogenic emissions (Li et al., 2022; Schollée et al., 2017). These amine and

https://doi.org/10.5194/egusphere-2024-3940
Preprint. Discussion started: 20 December 2024

amides tend to have lower retention times and can been seen in the lower cluster in Figure 1.A. The CHO species present are generally either aromatics or aliphatic acids and separate out as so in the van Krevelen diagram in Figure 1.B, with aromatics below 1.5 H/C and acids above such as $C_{12}H_{24}O_3$ (216 *m/z*, 14.2 min, L3) and $C_9H_{10}O_3$ (166 *m/z*, 9.1 min, L3). Very few biogenic CHO species are present as there are very few CHO species within 1.5-1.8 H/C that would indicate humics, ligins, or other raw biomass markers (Qian et al., 2013). This is consistent with the winter season sampling. Further characterization of the nonaromatic CHO is difficult to generalize, as there are a variety of sugars, ethers, alcohols, and acids that represent various possible biogenic species, terpenoids, and terpene derivatives. For example, xylitol (possibly arabitol) ($C_5H_{12}O_5$, 152 *m/z*, 1.6 min, L3), hexitol ($C_6H_{14}O_6$, 182 *m/z*, 1.6 min, L3), cinnamic acid ($C_9H_8O_2$, 148 *m/z*, 8.7 min, L3), phthalates such as dimethyl phthalate ($C_{10}H_{10}O_4$, 194 *m/z*, 10.9 min, L2) and phthalic acid ($C_8H_6O_4$, 166 *m/z*, 7.6 min, L3), as well as succinic acid ($C_4H_2O_3$, 98 *m/z*, 2.6 min, L3), levoglucosan ($C_6H_{10}O_5$, 162 *m/z* , 4.5 min, L2) and farnesol ($C_{15}H_{26}O$, 222 *m/z*, 14.6 min, L3) are all species potentially identified in the dataset.

A few CH and CHN compounds were found only in the positive mode, primarily AA and a couple of aromatic hydrocarbons. Combined, these represent less than 11% of the positive mode compounds. Only one CHS species was identified ($C_{18}H_{12}S$, 260 *m/z*, 10.0 min, L4) but was not used for analysis as it was below peak quality requirements. No CH, CHN, or CHS species were found in the negative mode.

3.2 Retention Coefficients

Table 1. Mean and Median Retention Coefficients by Compound Class and Heteroatom Group

	(−)HESI					(+)HESI				
	Mean	**σ**	**Median**	**n**	**n%**	**Mean**	**σ**	**Median**	**n**	**n%**
Total	0.95	0.21	0.96	208	100	0.95	0.53	0.93	250	100
CHO	0.90	0.25	0.91	68	32.7	1.01	0.82	0.90	73	29.2
CHN	-	-	-	-	-	1.07	0.21	1.04	22	8.8
CHNO	0.96	0.08	0.95	46	22.1	0.94	0.21	0.93	108	43.2

https://doi.org/10.5194/egusphere-2024-3940
Preprint. Discussion started: 20 December 2024

CHNOS	0.97	0.23	0.98	26	12.5	1.11	0.34	0.99	7	2.8
CHOS	0.99	0.23	0.98	56	26.9	0.67	0.59	0.99	3	1.2
CH	-	-	-	-	-	0.66	0.55	0.78	5	2.0
O Containing	0.95	0.21	0.96	196	94.2	0.97	0.54	0.92	191	76.4
N Containing	0.96	0.15	0.96	73	35.1	0.97	0.22	0.95	137	54.8
S Containing	0.99	0.23	0.98	83	39.9	0.98	0.44	0.99	10	4.0

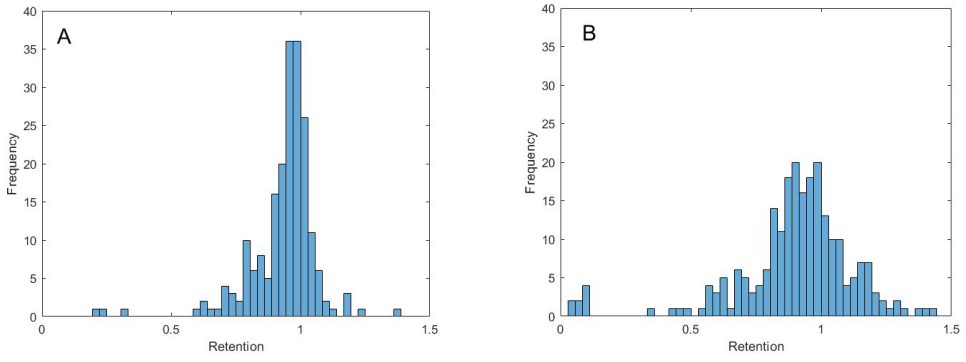

Figure 2. Histograms of Retention Coefficients for all measured L5 and above compounds that met peak quality constraints; (A) (−)HESI, (B) (+)HESI

https://doi.org/10.5194/egusphere-2024-3940
Preprint. Discussion started: 20 December 2024

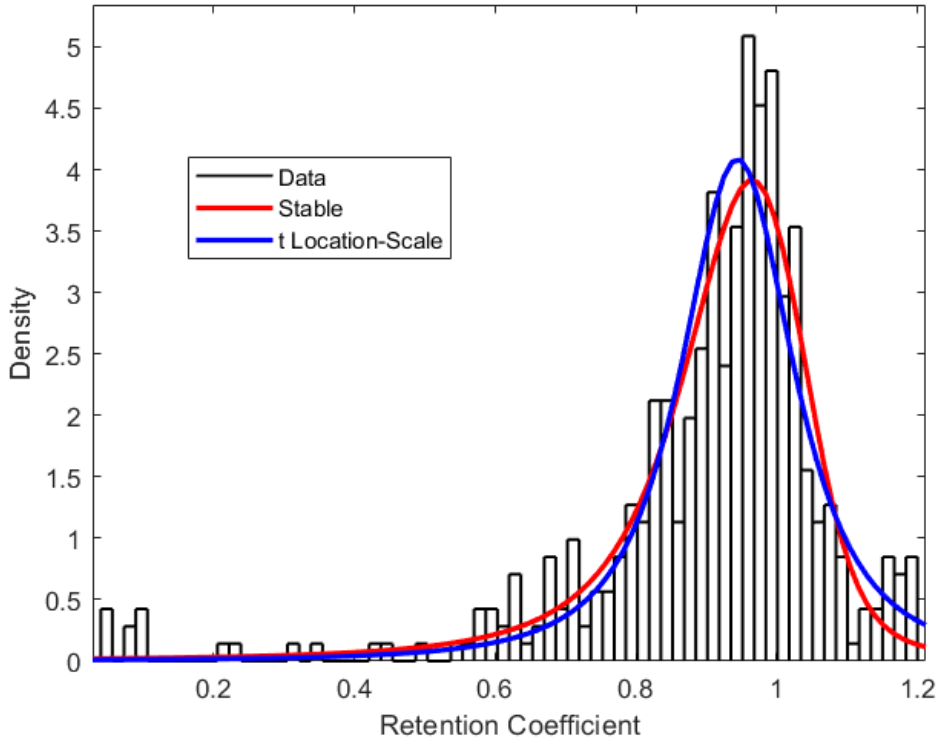

Figure 3. Merged Histogram for (−)HESI and (+)HESI of all Retention Coefficients measured fit with Stable and t Location-Scale distribution parameterizations of statistical density.

Table 2. Parameters for Stable Distribution Fit presented in Figure 3

Mean	0.8894	
Log Likelihood	224.657	
Parameter	**Value**	**Std. Error**
Alpha (α)	1.38642	0.06988
Beta (β)	-0.61652	0.10241
Gamma (γ)	0.07289	0.00383
Delta (δ)	0.95409	0.00608

305

Table 3. Parameters for t Location-Scale Distribution Fit presented in Figure 3

Mean	0.9442	
Log Likelihood	210.775	
Parameter	**Value**	**Std. Error**
Mu (μ)	0.94415	0.00566
Sigma (σ)	0.08665	0.00630
Nu (ν)	2.02867	0.26969

https://doi.org/10.5194/egusphere-2024-3940
Preprint. Discussion started: 20 December 2024

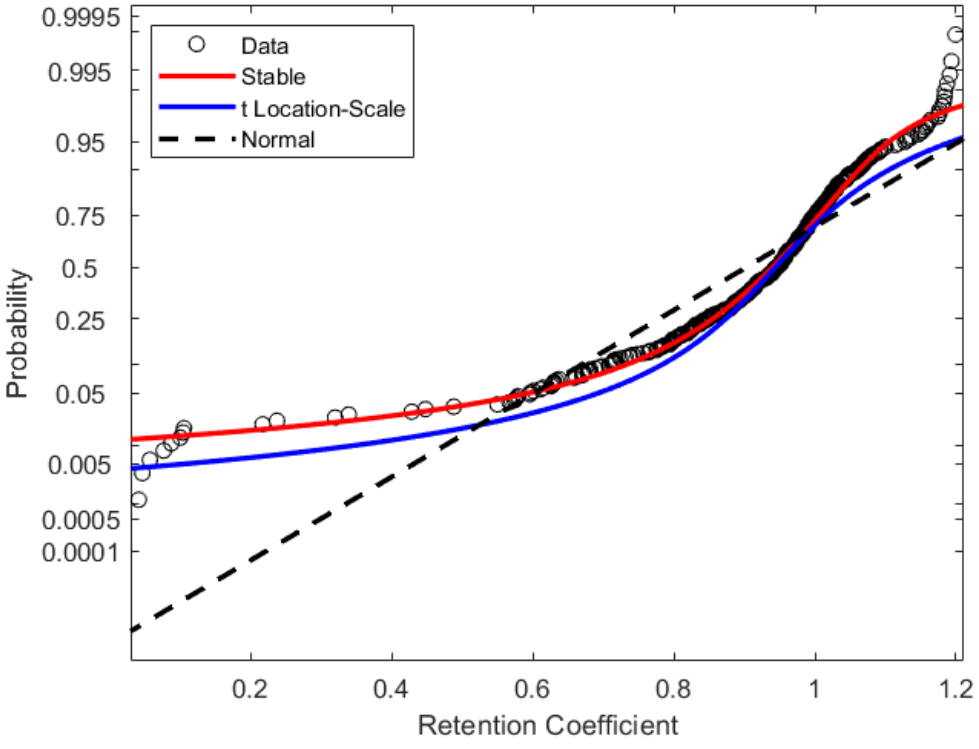

Figure 4. Probability plot of Retention Coefficients with the Stable and t Location-Scale distribution parameterizations and a Normal distribution

The histograms presented in Figure 2 and Figure 3 illustrate the distribution of retention coefficients determined for this dataset. Each histogram shows a peak at 0.96, 0.93, and 0.94 for (−)HESI, (+)HESI, and the full dataset respectively with average retentions all at 0.95 with standard deviations of 0.21 and 0.53 respectively. These values and the values for each compound class are presented in Table 1. Visually the distributions in Figure 2 appear nonnormal, suggesting a true distribution is being measured. Additionally, Figure 4 shows the data deviates strongly from a normal distribution. Both Shapiro-Wilk and Shapiro-Francia tests indicate nonnormality (p-values: 0.4052, 0.3940 (−)HESI; 0.5698, 0.5611 (+)HESI respectively).

https://doi.org/10.5194/egusphere-2024-3940
Preprint. Discussion started: 20 December 2024

320 Combining these distributions and filtering out outliers, the dataset is fitted with two distributions to model the dataset: Stable and t Location-Scale. The parameters for these fits can be found in Tables 2 and 3. These distributions are functional estimations of the statistical density of retention coefficients based on the empirical measurements in this experiment. The Stable distribution appears to model the data most accurately as the parameter errors are lower than the t Location-Scale and the data points in
325 Figure 4 lie closer to the Stable distribution curve.

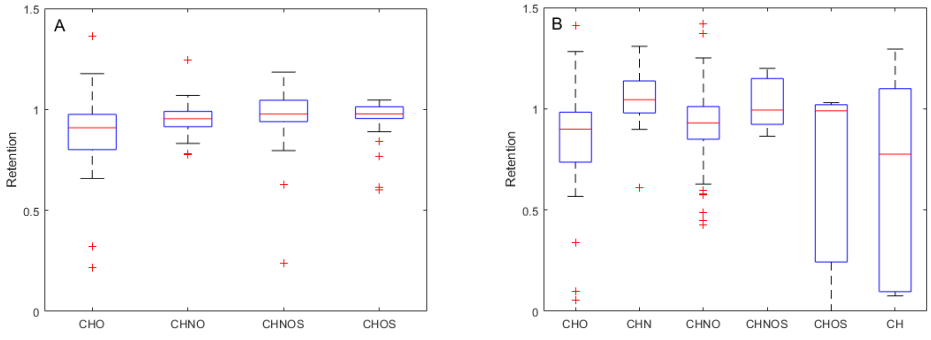

Figure 5. Boxplot of Retention Coefficients by Composition Class; (A) (−)HESI, (B) (+)HESI

330 The means of the composition classes in (−)HESI vary little, generally less than 5% from each other. In contrast, the means of the composition classes in (+)HESI vary more, up to 40%. The deviations and ranges of values are also wider in (+)HESI, from 0.21 to 0.82 as seen in Table 1. Visually this can be seen in Figure 5. For both ionizations, CHNOS tends to be the highest retained along with CHN in (+)HESI. CHNOS represents more of the heaviest species in the sample set while CHN is entirely AA. In
335 (+)HESI, CHNOS, CHOS, and CH represent the smallest portion of the dataset—less than 6%—and some of the most variably retained species. For CH, this follows with the variability in hydrocarbon aqueous solubility, however this variability is more likely explained for CHNOS, CHOS as well with the

https://doi.org/10.5194/egusphere-2024-3940
Preprint. Discussion started: 20 December 2024

smaller sample set bias. Notably, CHO has lower retention with a wider distribution than CHNO in both ionizations. In (−)HESI, CHNO is mostly nitroaromatics while in (+)HESI, CHNO is mostly amines and amides. CHO represents a more similar distribution of organic acids and terpenoids in both positive and negative mode, with more nonpolar species represented in (+)HESI. The lower retention among CHO may then be based on its distribution of organic acids versus terpenoids. This data suggests that nitrate species and amines/amides have similar retentions. It is known that NO_x removal is enhanced by aqueous phase reactions (Daito et al., 2000) and that organic nitrogen represents an important fraction of WSOC (Saxena and Hildemann, 1996; Zhang et al., 2002), but this data may also indicate that nitrogen chemistry on CHO species enhances their retention in hydrometeors. Other UHRMS studies of rainwater have suggested similar explanations for nitrogen uptake in hydrometeors and rainwater organic nitrogen's high bioavailability (Seymore et al., 2023).

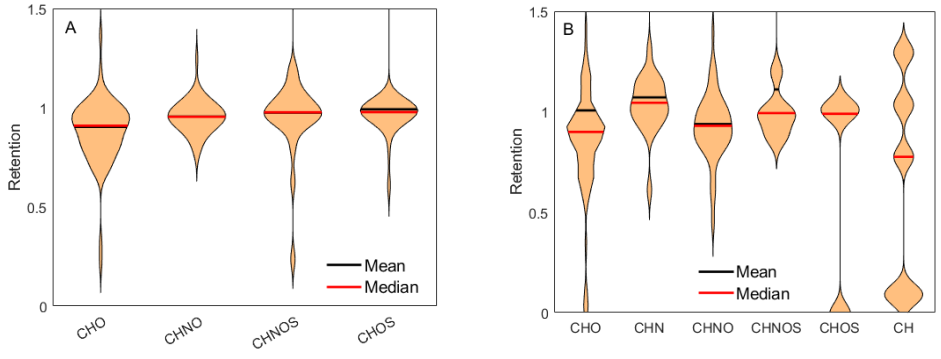

Figure 6. Violin plots of Retention Coefficients by Composition Class; (A) (−)HESI, (B) (+)HESI

The distributions of CHNO and CHOS in (−)HESI seen in Figure 6 show a coincidence of the mean and median along with strong symmetry around the mean. This indicates visually that they appear to be normally distributed, suggesting that the true retentions for the whole of these compound classes may be close to 1. Both Shapiro-Wilk and Shapiro-Francia tests indicate normality (p-values: 0.1920,

https://doi.org/10.5194/egusphere-2024-3940
Preprint. Discussion started: 20 December 2024

0.1922) for CHNO but not for CHOS (7.7595×10^{-9}). It therefore would be reasonable to assume a normal distribution for CHNO, but CHOS cannot be rigorously stated as normally distributed. CHO and CHNOS show unique distributions with a significant number of values within -σ and below, indicating there are certain CHO species that are not retained during freezing.

For (+)HESI, the samples sizes for CHNOS, CHOS, and CH are too small to make meaningful descriptions of their distributions. For CHO, CHN, CHNO, the distributions are visually nonnormal and also do not pass any statistical test for normality. The distributions also appear less smooth than their negative mode counterparts, likely a result of previously discussed ionization variability in (+)HESI. Notably, (+)HESI shows a few species with very low retention specifically within the CHO, CHOS, and CH groups. Specifically, these are $C_{14}H_{22}$ (190 *m/z*, 14.5 min, L3), $C_{15}H_{26}O$ (222 *m/z*, 14.6 min, L3), and what appears to be a phenyl-sulfide species ($C_{16}H_{18}OS$, 258 *m/z*, 8.0 min, L4). This is the only identified organosulfide within the dataset. It would be speculative to say that its low retention may indicate that organosulfides as a class are unretained and thus unlikely to appear in the dataset. Its low retention likely has more to do with its low polarity. $C_{14}H_{22}$ and $C_{15}H_{26}O$ as long chain, nonpolar species demonstrate that species with lower aqueous solubilities are also likely to have low retentions.

Concerning heteroatoms, the distributions and ranges of retentions are quite similar among all groups. Oxygen-containing species appear to have a slightly wider distribution which is mostly weighted by the CHO class. Nitrogen-containing species have a smaller standard deviation than the O or S containing species, indicating fewer species with variable retentions and more fully retained compounds. This further suggests that nitrogen inclusion enhances retention (see also Figure S1).

3.3 Correlation of Retention Coefficients with Chemical Properties

https://doi.org/10.5194/egusphere-2024-3940
Preprint. Discussion started: 20 December 2024

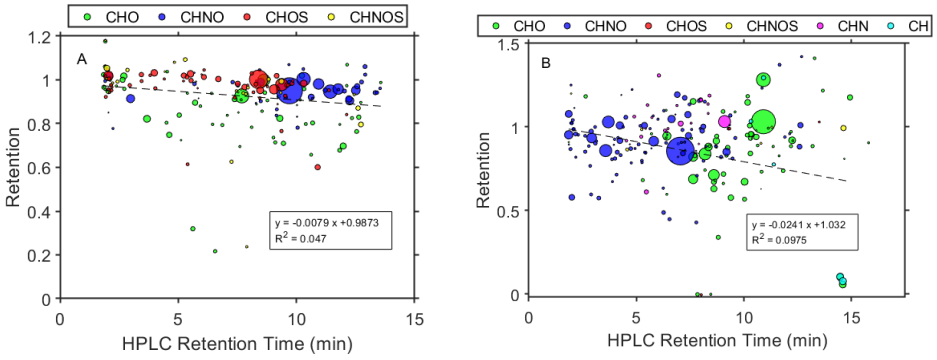

Figure 7. Retention Coefficient as a function of HPLC Retention time; (A) (−)HESI, (B) (+)HESI; Color denotes compositional class of the assigned compound, as used in Fig. 1: Green for CHO, blue for CHNO, red for CHOS, yellow for CHNOS, magenta for CHN, cyan for CH. Dashed line shows linear fit.

The determined molecular weight (MW) shows little correlation linearly with retention (as seen in Figure S2). In (−)HESI, there is a weak positive correlation, suggesting larger compounds are more likely to be retained. This is likely related to lower vapor pressures associated with larger MW species in the negative mode. An F-test against the constant value model indicates that this correlation is not significant (p-value: 0.0857). However in (+)HESI, there's a very weak negative correlation for MW which suggests the opposite. An F-test against the constant value model indicates that this correlation with MW is also not significant (p-value: 0.1440). This trend in the positive mode is likely driven more by polarity, as Figure 1.A also demonstrates that larger species in (+)HESI tend to have higher HPLC retention times and are therefore more nonpolar. The plot in Figure 8 further demonstrates this with a stronger negative correlation between the HPLC retention time and the retention.

Figures 7 shows correlations for retention coefficients with HPLC retention time. With reverse-phase HPLC, retention time is a direct proxy for molecular polarity, i.e. shorter retention times indicate higher polarity and longer retention times indicate more nonpolar species. Both (−)HESI and (+)HESI show significant negative correlation between retention and retention time and therefore polarity; an F-

https://doi.org/10.5194/egusphere-2024-3940
Preprint. Discussion started: 20 December 2024

test against the constant value model shows p-values of 0.00193 for (−)HESI and 1.44×10^{-6} for (+)HESI. This indicates that nonpolar species are likely to be unretained and this appears to be especially true for the previously discussed long chain species, such as $C_{14}H_{22}$ (190 *m/z*, 14.5 min, L3) and $C_{15}H_{26}O$ (222 *m/z*, 14.6 min, L3) compounds. In Figure 7, a few compound classes separate distinctly by polarity, particularly the CHOS and CHNO in (−)HESI as well as CHO and CHNO in (+)HESI. These polarity differences in these classes may be the driving force in the difference of the retention between CHOS and CHNO in (−)HESI, but unlikely for CHO and CHNO in (+)HESI as CHO spans a much wider range of retentions that cannot be explained solely by polarity.

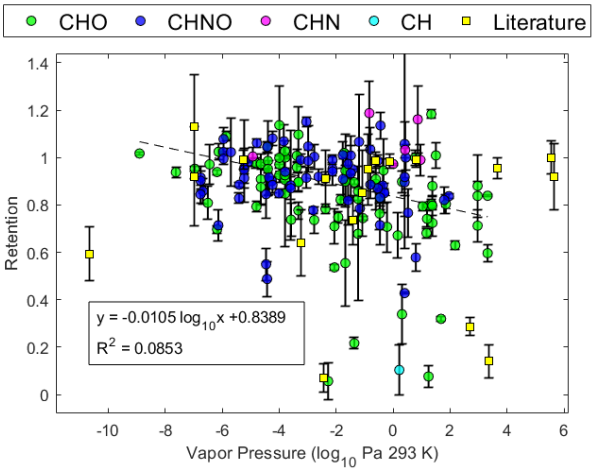

Figure 8. Retention Coefficient as a function of Estimated Vapor Pressure; Color denotes compositional class of the assigned compound: Green for CHO, blue for CHNO, magenta for CHN, cyan for CH, yellow squares for values taken from literature. Dashed line shows linear fit.

Further chemical property correlations with retention could be made for the species with estimated chemical properties. The first plot, Figure 8, uses the measured retention coefficient to plot against calculated vapor pressure (VP). It demonstrates a significant negative correlation with VP; an F-

https://doi.org/10.5194/egusphere-2024-3940
Preprint. Discussion started: 20 December 2024

415 test against the constant value model gives a p-value of 1.42×10^{-4}. It is relevant to note that the majority of species measured are considered semi-volatile (vapor pressure: 10^{-9} to 10 Pa; SVOC) with few low volatility (LVOC) and intermediate volatility organic compounds (IVOC) (Weschler and Nazaroff, 2008). LVOC and IVOC are bias against in the sampling method as many LVOCs are highly oxygenated compounds which may be less sensitive compared to other compounds in UHPLC-Orbitrap MS (Wang et
420 al., 2024) and most IVOCs are revolatilized during sampling (Bidleman et al., 2020). VP is also the property most associated with desorption effects, likely contributing to some of the negative trend seen in Figure 8. However, it is mostly associated with IVOC and less with SVOC so desorption alone is not likely to fully explain this correlation.

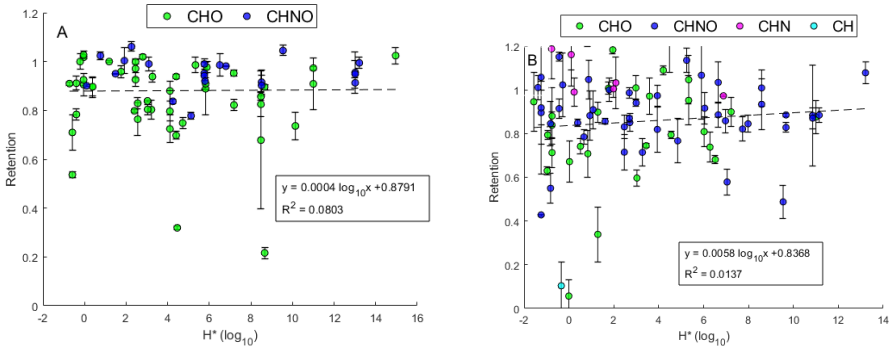

425

Figure 9. Effective Henry's Law Constant H* versus Retention Coefficient; (A) (−)HESI, (B) (+)HESI; Color denotes compositional class of the assigned compound: Green for CHO, blue for CHNO, magenta for CHN, cyan for CH. Dashed line shows linear fit.

430 Demonstrated in Figure 9, retention shows little or no dependency on H* under the present experimental conditions. The linear correlations are not significant for neither (−)HESI or (+)HESI; with p-values of 0.9270 and 0.3530 respectively for the F-test against the constant value model. The very slight

https://doi.org/10.5194/egusphere-2024-3940
Preprint. Discussion started: 20 December 2024

positive correlation shows agreement with Stuart and Jacobson's (2003, 2004) observation that high H* species are more likely to be 100% retained but does not show sigmoidal behavior as modeled by Jost et al., 2017 (plotted for reference in Figure 10). This could be the result of differing physical experimental parameters, such as larger droplet size (2 mm versus 20 micron). However, directly comparing the known literature values for retention coefficients with the observations made here does not immediately indicate the systems are incompatible or exclude the comparison.

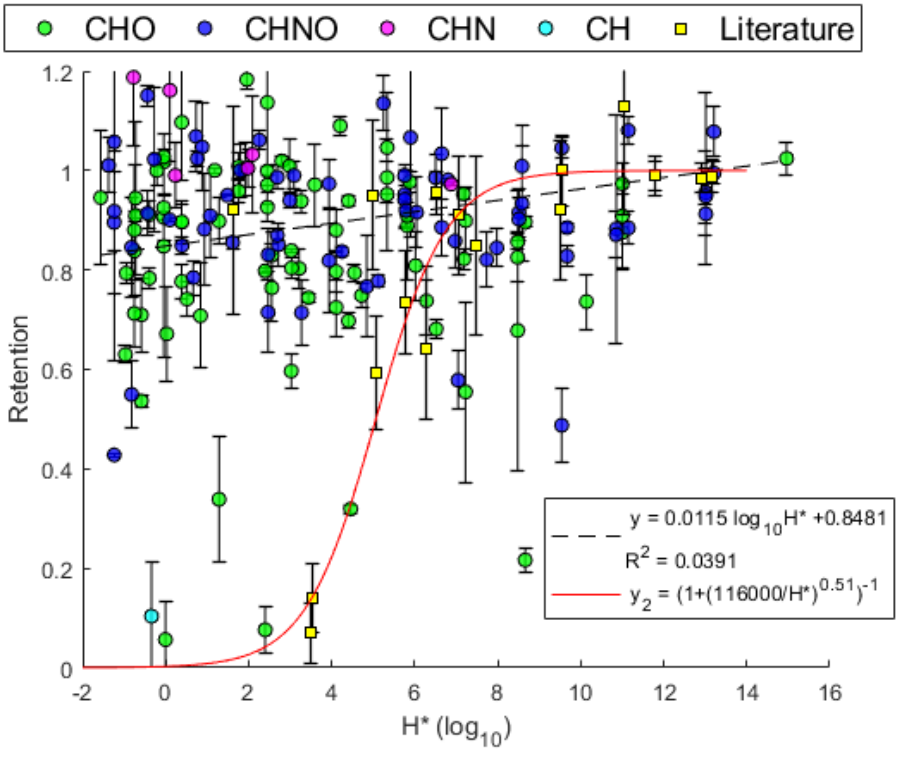

Figure 10. Effective Henry's Law Constant H* versus Retention Coefficient; Color denotes compositional class of the assigned compound: Green for CHO, blue for CHNO, magenta for CHN, cyan for CH; Yellow squares denote values taken from Borchers et al., (2024), Jost et al., (2017), and Von Blohn et al., (2011, 2013). Dashed line shows linear fit. Solid red line gives the parameterization by Jost et al., (2017).

https://doi.org/10.5194/egusphere-2024-3940
Preprint. Discussion started: 20 December 2024

Figure 10 compares the data presented in Figure 9 against the literature values presented by Borchers et al., (2024), Jost et al., 2017, and Von Blohn et al., (2011, 2013). This comparison does not appear incongruous, i.e. no discernible difference can be seen between wind tunnel experiments and these observations. While the measurements presented by Borchers et al., (2024), Jost et al., (2017), and Von Blohn et al., (2011, 2013) are physically dissimilar experiments to this study—i.e. wind tunnel experiments, small droplets of micrometer size, high ventilation conditions—their observations are congruent with this experiment. The literature values include only three species with $H^* < 10^4$ and the lowest H* of them, pinandiol, is excluded from the parameterization presented by Borchers et al., (2024) as it was perceived as an outlier. Without more measurements of compounds with $H^* < 10^4$ under wind tunnel conditions, it is difficult to determine if the nonsigmoidal behavior seen in this experiment is the result of different physical parameters—specifically the lower surface-to-volume ratio—or if the sigmoidal behavior described by Borchers et al., (2024) and Jost et al., (2017) is an overfit of a limited dataset. Evidence presented by Gautam et al., (2024) in part 1 of this publication series makes a compelling case for the dominance of physical parameters at these drop sizes. Critical to these experiments, Gautam et al., (2024) observed the formation of an ice shell, which inhibited any further expulsion of dissolved substances during freezing.

4 Conclusions

This study presents the measurement of the retention coefficients for real, complex WSOCs from urban particulate matter for direct drop freezing under raindrop size conditions. The overall distribution of the retention of WSOCs forms a real, nonnormal distribution up to 1. Looking at the individual compound classes of organics, the data shows that they may have different distributions of retention coefficients. Most negatively ionizable CHNO and CHOS compounds appear to be fully retained, indicating that nitroaromatics and organosulphates are favorable to be retained. Slight positive

https://doi.org/10.5194/egusphere-2024-3940
Preprint. Discussion started: 20 December 2024

correlations between MW, polarity, and H* are seen with retention along with a negative correlation with VP. No sigmoidal relationship with H* was observed. This is likely the result of the lower surface-to-area ratio for this drop size and the ice shell formation observed by Gautam et al., (2024) in part 1 of this publication series. However without further measurements of single component solutions for compounds with $H^* < 10^4$ under wind tunnel conditions, specifically for small cloud droplet sizes, it is difficult to determine if the nonsigmoidal behavior seen in this experiment is solely the result of physical parameters or if the sigmoidal behavior described by other studies is an overfit of a limited dataset.

Sulfides, lipids, aromatic hydrocarbons, and long chain compounds are among the most unretained and incidentally the fewest species observed. These are also among the most nonpolar species observed, which is presumably the dominant factor in that regard. CHO species show the highest variability for their measured retentions, most likely related to the distributions of polarity and VPs among the sugars, organic acids, and terpenoids seen here.

AA don't follow the trends associated with polarity and VP but are among the most highly retained species. The explanation for this is possibly in its structural properties, which cannot be easily determined using this analytical method. AA solubility in water is largely determined by the dimension and structure of the alkyl substituents, such that AA with longer chains are less soluble than AA with shorter chains and AA with branched substituents are less soluble than AA with linear groups with the same number of carbons (Badocco et al., 2015). Polarity and hydrogen bonding are also known contributors to AA solubility but this is not unique to AA. Hydrogen bonding potential may enhance retention along oxygen functionalities such as among nitro and sulphate species. Hydrogen bonding alone, however, is unlikely to fully explain the high retentions among nitro and sulphate species. Specifically, nitro species have weak hydrogen bonding potential (Shugrue et al., 2016) and as a result is likely influenced mostly by the increased polarity imparted by the nitro substituent or its dissociation.

The data suggests that nitrogen and sulfur inclusion generally increase a species' ability to be retained. Overall, this insulates that the products of NO_x and SO_x reactions from anthropogenic emissions

https://doi.org/10.5194/egusphere-2024-3940
Preprint. Discussion started: 20 December 2024

enhances the retention of these SOA species, reducing the likelihood of reaching the upper atmosphere. Further on this, other studies have demonstrated that NO_x removal is enhanced by aqueous phase reactions (Daito et al., 2000). These findings may also indicate that this NO_x chemistry on CHO species enhances their retention in hydrometeors, potentially by increasing its polarity or solubility. Other UHRMS studies of rainwater have suggested similar explanations for nitrogen uptake in hydrometeors and rainwater organic nitrogen's high bioavailability (Seymore et al., 2023). Additionally, correlations with VP and polarity show that lower VP species and more polar species tend to be retained. Atmospheric chemical processing generally tends to oxidatively degrade large nonpolar species into more water-soluble, less volatile species (Iavorivska et al., 2016). Specifically, aqueous phase droplet chemistry is known to facilitate condensed phase SOA formation from highly volatile species (McNeill, 2015). However, many freshly aged terpene products increase in volatility or see only small decreases in VP with oxidation for their early generation products (Bilde and Pandis, 2001; Kurtén et al., 2018; Wu et al., 2021). This insulates that many freshly oxidized SOA precursors may have a lower potential to be retained than aged organics and may generally suggest that freshly oxidized SOA precursors are more likely to reach the upper atmosphere than primary organics or aged SOA.

The use of UHPLC-HRMS has allowed for the study of ambient WSOC retention rather than single component or limited mixture experiments from previous studies. The experiment in this paper demonstrates the viability of UHPLC-HRMS analysis for ambient WSOC and shows the need for further complex mixture study regarding retention. Future study on retention within hydrometeors should include complex mixture analysis under the physical conditions most similar to the atmosphere, i.e. wind tunnel experiments, smaller droplets, increased ventilation. These studies would also be improved with more distinguishable tracers with known retentions and more sophisticated corrections for desorption. Further studies on single component solutions of species with $H^* < 10^4$ under atmospherically similar physical conditions would also allow for stronger conclusions from the comparison of the retentions measured in this study with other experiments performed under wind tunnel conditions.

https://doi.org/10.5194/egusphere-2024-3940
Preprint. Discussion started: 20 December 2024

The experiment presented here also cannot distinguish between species incorporated within ice crystal structure and those phase-separated but physically constrained to the hydrometeor, potentially between crystal grain boundaries or on the particle surface. That distinction is also not atmospherically relevant regarding the net transport of organics into the upper troposphere. While this method aims to demonstrate the retention for real WSOC, this method is still sample method biased against higher volatility species and likely features other sampling bias typical for HiVol filter based measurements such as filter extraction bias and solvation effects. These measurements also present the distribution of retention coefficients for the variety of species present and not necessarily the mass distribution of species potentially present in the atmosphere. Corrections for species abundancy must first be made in order to apply this data to organic transport models.

Acknowledgements

Special thanks to Konstantin Dörholt for his initial work and experimentation in the Mainz Wind Tunnel with these samples.

This work was funded by the Deutsche Forschungsgemeinschaft (DFG, German Research Foundation) – TRR 301 – Project-ID 428312742.

This work was supported by the Max Planck Graduate Center with the Johannes Gutenberg University of Mainz (MPGC).

Author Contributions

JS, MG, MS, AT participated in designing the experiments; LZ provided the samples; JS, JM prepared the samples for experiments; MG performed the experiments; JS, JM, AV conducted the analytical

https://doi.org/10.5194/egusphere-2024-3940
Preprint. Discussion started: 20 December 2024

measurements; JS analyzed the data and wrote the manuscript draft; MG, MS, AT, JM, AV, TH reviewed and edited the manuscript.

Competing Interests

The contact author has declared that none of the authors has any competing interests.

References

Andreae, M. O., Afchine, A., Albrecht, R., Holanda, B. A., Artaxo, P., Barbosa, H. M. J., Borrmann, S., Cecchini, M. A., Costa, A., Dollner, M., Fütterer, D., Järvinen, E., Jurkat, T., Klimach, T., Konemann, T., Knote, C., Krämer, M., Krisna, T., Machado, L. A. T., Mertes, S., Minikin, A., Pöhlker, C., Pöhlker, M. L., Pöschl, U., Rosenfeld, D., Sauer, D., Schlager, H., Schnaiter, M., Schneider, J., Schulz, C., Spanu, A., Sperling, V. B., Voigt, C., Walser, A., Wang, J., Weinzierl, B., Wendisch, M., and Ziereis, H.: Aerosol characteristics and particle production in the upper troposphere over the Amazon Basin, Atmos. Chem. Phys, 18, 921–961, https://doi.org/10.5194/acp-18-921-2018, 2018.

Andrés Casquero-Vera, J., Lyamani, H., Dada, L., Hakala, S., Paasonen, P., Román, R., Fraile, R., Petäjä, T., Olmo-Reyes, F. J., Alados-Arboledas, L., Andrés, J., and Vera, C.: New particle formation at urban and high-altitude remote sites in the south-eastern Iberian Peninsula, Atmos. Chem. Phys, 20, 14253–14271, https://doi.org/10.5194/acp-20-14253-2020, 2020.

Badocco, D., Di Marco, V., Mondin, A., and Pastore, P.: Cyclic voltammetry as a new approach for the determination of solubility of aliphatic amines in water, J Chem Eng Data, 60, 895–901, https://doi.org/10.1021/je5009735, 2015.

Bardakov, R., Thornton, J. A., Riipinen, I., Krejci, R., and Ekman, A. M. L.: Transport and chemistry of isoprene and its oxidation products in deep convective clouds, Tellus B Chem Phys Meteorol, 73, 1–21, https://doi.org/10.1080/16000889.2021.1979856, 2021.

Bela, M. M., Barth, M. C., Toon, O. B., Fried, A., Ziegler, C., Cummings, K. A., Li, Y., Pickering, K. E., Homeyer, C. R., Morrison, H., Yang, Q., Mecikalski, R. M., Carey, L., Biggerstaff, M. I., Betten, D. P., and Alford, A. A.: Effects of Scavenging, Entrainment, and Aqueous Chemistry on Peroxides and Formaldehyde in Deep Convective Outflow Over the Central and Southeast United States, Journal of Geophysical Research: Atmospheres, 123, 7594–7614, https://doi.org/10.1029/2018JD028271, 2018.

Bidleman, T. F., Falconer, R. L., and Harner, T.: Particle/Gas Distribution of Semivolatile Organic Compounds: Field and Laboratory Experiments with Filtration Samplers, Gas and Particle Phase Measurements of Atmospheric Organic Compounds, 39–71, https://doi.org/10.1201/9781003078340-4, 2020.

Bilde, M. and Pandis, S. N.: Evaporation rates and vapor pressures of individual aerosol species formed in the atmospheric oxidation of α- and β- pinene, Environ Sci Technol, 35, 3344–3349, https://doi.org/10.1021/es001946b, 2001.

https://doi.org/10.5194/egusphere-2024-3940
Preprint. Discussion started: 20 December 2024

Blair, S. L., MacMillan, A. C., Drozd, G. T., Goldstein, A. H., Chu, R. K., Paša-Tolić, L., Shaw, J. B., Tolić, N., Lin, P., Laskin, J., Laskin, A., and Nizkorodov, S. A.: Molecular Characterization of Organosulfur Compounds in Biodiesel and Diesel Fuel Secondary Organic Aerosol, Environ Sci Technol, 51, 119–127, https://doi.org/10.1021/ACS.EST.6B03304/SUPPL_FILE/ES6B03304_SI_002.XLSX, 2017.

Von Blohn, N., Diehl, K., Mitra, S. K., and Borrmann, S.: The retention of nitric acid, hydrochloric acid, and hydrogen peroxide Wind tunnel experiments on the retention of trace gases during riming: nitric acid, hydrochloric acid, and hydrogen peroxide The retention of nitric acid, hydrochloric acid, and hydrogen peroxide, Atmos. Chem. Phys. Discuss, 11, 17447–17472, https://doi.org/10.5194/acpd-11-17447-2011, 2011a.

Von Blohn, N., Diehl, K., Mitra, S. K., and Borrmann, S.: Wind tunnel experiments on the retention of trace gases during riming: Nitric acid, hydrochloric acid, and hydrogen peroxide, Atmos Chem Phys, 11, 11569–11579, https://doi.org/10.5194/ACP-11-11569-2011, 2011b.

Borchers, C., Seymore, J., Gautam, M., Dörholt, K., Müller, Y., Arndt, A., Gömmer, L., Ungeheuer, F., Szakáll, M., Borrmann, S., Theis, A., Vogel, A. L., and Hoffmann, T.: Retention of α-pinene oxidation products and nitro-aromatic compounds during riming, https://doi.org/10.5194/egusphere-2024-1443, 2024.

Clarke, A. D., Varner, J. L., Eisele, F., Mauldin, R. L., Tanner, D., and Litchy, M.: Particle production in the remote marine atmosphere: Cloud outflow and subsidence during ACE 1, Journal of Geophysical Research Atmospheres, 103, 16397–16409, https://doi.org/10.1029/97JD02987, 1998.

Clarke, A. D., Eisele, F., Kapustin, V. N., Moore, K., Tanner, D., Mauldin, L., Litchy, M., Lienert, B., Carroll, M. A., and Albercook, G.: Nucleation in the equatorial free troposphere: Favorable environments during PEM-Tropics, Journal of Geophysical Research Atmospheres, 104, 5735–5744, https://doi.org/10.1029/98JD02303, 1999.

Compernolle, S. and Müller, J. F.: Henry's law constants of polyols, Atmos Chem Phys, 14, 12815–12837, https://doi.org/10.5194/acp-14-12815-2014, 2014.

Daito, S., Tochikubo, F., and Watanabe, T.: Improvement of NOx removal efficiency assisted by aqueous-phase reaction in corona discharge, Japanese Journal of Applied Physics, Part 1: Regular Papers and Short Notes and Review Papers, 39, 4914–4919, https://doi.org/10.1143/JJAP.39.4914/XML, 2000.

Diehl, K., Debertshäuser, M., Eppers, O., Schmithüsen, H., Mitra, S. K., and Borrmann, S.: Particle surface area dependence of mineral dust in immersion freezing mode: Investigations with freely suspended drops in an acoustic levitator and a vertical wind tunnel, Atmos Chem Phys, 14, 12343–12355, https://doi.org/10.5194/ACP-14-12343-2014, 2014.

Dusek, U., Frank, G. P., Hildebrandt, L., Curtius, J., Schneider, J., Walter, S., Chand, D., Drewnick, F., Hings, S., Jung, D., Borrmann, S., and Andreae, M. O.: Size matters more than chemistry for cloud-nucleating ability of aerosol particles, Science (1979), 312, 1375–1378, https://doi.org/10.1126/SCIENCE.1125261/SUPPL_FILE/DUSEK.SOM.PDF, 2006.

Fofie, E. A., Donahue, N. M., and Asa-Awuku, A.: Cloud condensation nuclei activity and droplet formation of primary and secondary organic aerosol mixtures, Aerosol Science and Technology, 52, 242–251, https://doi.org/10.1080/02786826.2017.1392480/SUPPL_FILE/UAST_A_1392480_SM6542.PDF, 2018.

https://doi.org/10.5194/egusphere-2024-3940
Preprint. Discussion started: 20 December 2024

Hallquist, M., Wenger, J. C., Baltensperger, U., Rudich, Y., Simpson, D., Claeys, M., Dommen, J., Donahue, N. M., George, C., Goldstein, A. H., Hamilton, J. F., Herrmann, H., Hoffmann, T., Iinuma, Y., Jang, M., Jenkin, M. E., Jimenez, J. L., Kiendler-Scharr, A., Maenhaut, W., McFiggans, G., Mentel, T. F., Monod, A., Prévôt, A. S. H., Seinfeld, J. H., Surratt, J. D., Szmigielski, R., and Wildt, J.: The formation, properties and impact of secondary organic aerosol: Current and emerging issues, Atmos Chem Phys, 9, 5155–5236, https://doi.org/10.5194/acp-9-5155-2009, 2009.

Heitto, A., Wu, C., Aliaga, D., Blacutt, L., Chen, X., Gramlich, Y., Heikkinen, L., Huang, W., Krejci, R., Laj, P., Moreno, I., Sellegri, K., Velarde, F., Weinhold, K., Wiedensohler, A., Zha, Q., Bianchi, F., Andrade, M., Lehtinen, K. E. J., Mohr, C., and Yli-Juuti, T.: Analysis of atmospheric particle growth based on vapor concentrations measured at the high-altitude GAW station Chacaltaya in the Bolivian Andes, Atmos. Chem. Phys, 24, 1315–1328, https://doi.org/10.5194/acp-24-1315-2024, 2024.

Iavorivska, L., Boyer, E. W., and DeWalle, D. R.: Atmospheric deposition of organic carbon via precipitation, Atmos Environ, 146, 153–163, https://doi.org/10.1016/j.atmosenv.2016.06.006, 2016.

Iinuma, Y., Müller, C., Berndt, T., Böge, O., Claeys, M., and Herrmann, H.: Evidence for the existence of organosulfates from β-pinene ozonolysis in ambient secondary organic aerosol, Environ Sci Technol, 41, 6678–6683, https://doi.org/10.1021/ES070938T/SUPPL_FILE/ES070938TSI20070723_080104.PDF, 2007.

Iribarne, J. V. and Pyshnov, T.: The effect of freezing on the composition of supercooled droplets—I. Retention of HCl, HNO3, NH3 and H2O2, Atmospheric Environment. Part A. General Topics, 24, 383–387, https://doi.org/10.1016/0960-1686(90)90118-7, 1990.

Isaacman-Vanwertz, G. and Aumont, B.: Impact of organic molecular structure on the estimation of atmospherically relevant physicochemical parameters, Atmos. Chem. Phys, 21, 6541–6563, https://doi.org/10.5194/acp-21-6541-2021, 2021.

Jost, A., Szakáll, M., DIehl, K., Mitra, S. K., and Borrmann, S.: Chemistry of riming: The retention of organic and inorganic atmospheric trace constituents, Atmos Chem Phys, 17, 9717–9732, https://doi.org/10.5194/ACP-17-9717-2017, 2017.

Kaufmann, A. and Walker, S.: Comparison of linear intrascan and interscan dynamic ranges of Orbitrap and ion-mobility time-of-flight mass spectrometers, Rapid Communications in Mass Spectrometry, 31, 1915–1926, https://doi.org/10.1002/RCM.7981, 2017.

Kurtén, T., Hyttinen, N., Louise D'Ambro, E., Thornton, J., and Prisle, N. L.: Estimating the saturation vapor pressures of isoprene oxidation products C5H12O6 and C5H10O6 using COSMO-RS, Atmos Chem Phys, 18, 17589–17600, https://doi.org/10.5194/acp-18-17589-2018, 2018.

Lamb, D. and Verlinde, J.: Physics and Chemistry of Clouds, Cambridge University Press, 275–414 pp., https://doi.org/10.1017/CBO9780511976377, 2011.

Li, J., Gao, X., He, Y., Wang, L., Wang, Y., and Zeng, L.: Elevated emissions of melamine and its derivatives in the indoor environments of typical e-waste recycling facilities and adjacent communities and implications for human exposure, J Hazard Mater, 432, https://doi.org/10.1016/J.JHAZMAT.2022.128652, 2022.

Li, Y., Pöschl, U., and Shiraiwa, M.: Molecular corridors and parameterizations of volatility in the chemical evolution of organic aerosols, Atmos Chem Phys, 16, 3327–3344, https://doi.org/10.5194/ACP-16-3327-2016, 2016.

https://doi.org/10.5194/egusphere-2024-3940
Preprint. Discussion started: 20 December 2024

Liu, J., Zhang, F., Xu, W., Sun, Y., Chen, L., Li, S., Ren, J., Hu, B., Wu, H., and Zhang, R.: Hygroscopicity of Organic Aerosols Linked to Formation Mechanisms, Geophys Res Lett, 48, https://doi.org/10.1029/2020GL091683, 2021.

Liu, Z., Yim, S. H. L., Wang, C., and Lau, N. C.: The Impact of the Aerosol Direct Radiative Forcing on Deep Convection and Air Quality in the Pearl River Delta Region, Geophys Res Lett, 45, 4410–4418, https://doi.org/10.1029/2018GL077517, 2018.

McNeill, V. F.: Aqueous organic chemistry in the atmosphere: Sources and chemical processing of organic aerosols, Environ Sci Technol, 49, 1237–1244, https://doi.org/10.1021/es5043707, 2015.

Nolan, J. P.: Univariate Stable Distributions, https://doi.org/10.1007/978-3-030-52915-4, 2020.

Price, D. J., Clark, C. H., Tang, X., Cocker, D. R., Purvis-Roberts, K. L., and Silva, P. J.: Proposed chemical mechanisms leading to secondary organic aerosol in the reactions of aliphatic amines with hydroxyl and nitrate radicals, Atmos Environ, 96, 135–144, https://doi.org/10.1016/J.ATMOSENV.2014.07.035, 2014.

Price, D. J., Kacarab, M., Cocker, D. R., Purvis-Roberts, K. L., and Silva, P. J.: Effects of temperature on the formation of secondary organic aerosol from amine precursors, Aerosol Science and Technology, 50, 1216–1226, https://doi.org/10.1080/02786826.2016.1236182, 2016.

Qi, L., Zhang, Z., Wang, X., Deng, F., Zhao, J., and Liu, H.: Molecular characterization of atmospheric particulate organosulfates in a port environment using ultrahigh resolution mass spectrometry: Identification of traffic emissions, J Hazard Mater, 419, 126431, https://doi.org/10.1016/J.JHAZMAT.2021.126431, 2021.

Qian, K., Kumar, A., Patil, K., Bellmer, D., Wang, D., Yuan, W., and Huhnke, R. L.: Effects of Biomass Feedstocks and Gasification Conditions on the Physiochemical Properties of Char, Energies 2013, Vol. 6, Pages 3972-3986, 6, 3972–3986, https://doi.org/10.3390/EN6083972, 2013.

Riva, M., Chen, Y., Zhang, Y., Lei, Z., Olson, N., Chelmo, H. B., Narayan, S., Yee, L., Green, H., Cui, T., Zhang, Z., Baumann, K., Fort, M., Edgerton, E., Budisulistiorini, S., Rose, C., Ribeiro, I., Oliveira, R. e, Santos, E. dos, Machado, C., Szopa, S., Zhao, Y., Alves, E., Sá, S. de, Hu, W., Knipping, E., Shaw, S., Junior, S. D., Souza, R. de, Palm, B., Jimenez, J., Glasius, M., Goldstein, A., Pye, H., Gold, A., Turpin, B., Vizuete, W., Martin, S., Thornton, J., Dutcher, C., Ault, A., and Surratt, J.: Rising Importance of Organosulfur Species for Aerosol Properties and Future Air Quality, https://doi.org/10.26434/CHEMRXIV.7597397.V1, 2019.

Saxena, P. and Hildemann, L. M.: Water-Soluble Organics in Atmospheric Particles: A Critical Review of the Literature and Application of Thermodynamics to Identify Candidate Compounds, J Atmos Chem, 24, 57–109, 1996.

Schollée, J. E., Schymanski, E. L., Stravs, M. A., Gulde, R., Thomaidis, N. S., and Hollender, J.: Similarity of High-Resolution Tandem Mass Spectrometry Spectra of Structurally Related Micropollutants and Transformation Products, J Am Soc Mass Spectrom, 28, 2692–2704, https://doi.org/10.1007/S13361-017-1797-6/ASSET/IMAGES/LARGE/JS8B05447_0005.JPEG, 2017.

Schymanski, E. L., Jeon, J., Gulde, R., Fenner, K., Ruff, M., Singer, H. P., and Hollender, J.: Identifying small molecules via high resolution mass spectrometry: Communicating confidence, Environ Sci Technol, 48, 2097–2098, https://doi.org/10.1021/ES5002105/ASSET/IMAGES/LARGE/ES-2014-002105_0001.JPEG, 2014.

https://doi.org/10.5194/egusphere-2024-3940
Preprint. Discussion started: 20 December 2024

Seymore, J., Felix, J. D., Abdulla, H., Bergmann, D., Campos, M. L. A. M., and Florêncio, J.: Pandemic-Related Anthropogenic Influences on the Dissolved Organic Matter Chemical Character in São Paulo State Wet Deposition by Ultrahigh-Resolution Mass Spectrometry, ACS Earth Space Chem, 7, 1929–1946, https://doi.org/10.1021/acsearthspacechem.3c00076, 2023.

Shugrue, C. R., Defrancisco, J. R., Metrano, A. J., Brink, B. D., Nomoto, R. S., and Linton, B. R.: Detection of weak hydrogen bonding to fluoro and nitro groups in solution using H/D exchange, Org Biomol Chem, 14, 2223–2227, https://doi.org/10.1039/C5OB02360B, 2016.

Snider, J. R., Montague, D. C., and Vali, G.: Hydrogen peroxide retention in rime ice, Journal of Geophysical Research: Atmospheres, 97, 7569–7578, https://doi.org/10.1029/92JD00237, 1992.

Stuart, A. L. and Jacobson, M. Z.: A timescale investigation of volatile chemical retention during hydrometeor freezing: Nonrime freezing and dry growth riming without spreading, Journal of Geophysical Research: Atmospheres, 108, https://doi.org/10.1029/2001JD001408, 2003.

Stuart, A. L. and Jacobson, M. Z.: Chemical retention during dry growth riming, Journal of Geophysical Research: Atmospheres, 109, https://doi.org/10.1029/2003JD004197, 2004.

Sun, H., Li, X., Zhu, C., Huo, Y., Zhu, Z., Wei, Y., Yao, L., Xiao, H., and Chen, J.: Molecular composition and optical property of humic-like substances (HULIS) in winter-time PM2.5 in the rural area of North China Plain, Atmos Environ, 252, 118316, https://doi.org/10.1016/j.atmosenv.2021.118316, 2021.

Surratt, J. D., Kroll, J. H., Kleindienst, T. E., Edney, E. O., Claeys, M., Sorooshian, A., Ng, N. L., Offenberg, J. H., Lewandowski, M., Jaoui, M., Flagan, R. C., and Seinfeld, J. H.: Evidence for organosulfates in secondary organic aerosol, Environ Sci Technol, 41, 517–527, https://doi.org/10.1021/ES062081Q/ASSET/IMAGES/LARGE/ES062081QF00006.JPEG, 2007.

Szakáll, M., Debertshäuser, M., Philipp Lackner, C., Mayer, A., Eppers, O., Diehl, K., Theis, A., Kumar Mitra, S., and Borrmann, S.: Comparative study on immersion freezing utilizing single-droplet levitation methods, Atmos Chem Phys, 21, 3289–3316, https://doi.org/10.5194/acp-21-3289-2021, 2021.

Taneda, S., Mori, Y., Kamata, K., Hayashi, H., Furuta, C., Li, C., Seki, K. I., Sakushima, A., Yoshino, S., Yamaki, K., Watanabe, G., Taya, K., and Suzuki, A. K.: Estrogenic and anti-androgenic activity of nitrophenols in diesel exhaust particles (DEP), Biol Pharm Bull, 27, 835–837, https://doi.org/10.1248/BPB.27.835, 2004.

U. S. Environmental Protection Agency: Caprolactam - EPA Health Effects Notebook for Hazardous Air Pollutants, n.d.

US EPA: EPI Suite™-Estimation Program Interface | US EPA, https://www.epa.gov/tsca-screening-tools/epi-suitetm-estimation-program-interface#citing.

Wang, K., Zhang, Y., Tong, H., Han, J., Fu, P., Huang, R. J., Zhang, H., and Hoffmann, T.: Molecular-Level Insights into the Relationship between Volatility of Organic Aerosol Constituents and PM2.5 Air Pollution Levels: A Study with Ultrahigh-Resolution Mass Spectrometry, Environ Sci Technol, 58, 7947–7957, https://doi.org/10.1021/acs.est.3c10662, 2024.

Weigel, R., Borrmann, S., Kazil, J., Minikin, A., Stohl, A., Wilson, J. C., Reeves, J. M., Kunkel, D., De Reus, M., Frey, W., Lovejoy, E. R., Volk, C. M., Viciani, S., D'amato, F., Schiller, C., Peter, T., Schlager, H., Cairo, F., Law, K. S., Shur, G. N., Belyaev, G. V, and Curtius, J.: Atmospheric Chemistry and Physics In situ observations of new particle formation in the tropical upper troposphere: the role of clouds and the

https://doi.org/10.5194/egusphere-2024-3940
Preprint. Discussion started: 20 December 2024

nucleation mechanism, Atmos. Chem. Phys, 11, 9983–10010, https://doi.org/10.5194/acp-11-9983-2011, 2011.

Weschler, C. J. and Nazaroff, W. W.: Semivolatile organic compounds in indoor environments, Atmos Environ, 42, 9018–9040, https://doi.org/10.1016/J.ATMOSENV.2008.09.052, 2008.

Williamson, C. J., Kupc, A., Axisa, D., Bilsback, K. R., Bui, T. P., Campuzano-Jost, P., Dollner, M., Froyd, K. D., Hodshire, A. L., Jimenez, J. L., Kodros, J. K., Luo, G., Murphy, D. M., Nault, B. A., Ray, E. A., Weinzierl, B., Wilson, J. C., Yu, F., Yu, P., Pierce, J. R., and Brock, C. A.: A large source of cloud condensation nuclei from new particle formation in the tropics, Nature 2019 574:7778, 574, 399–403, https://doi.org/10.1038/s41586-019-1638-9, 2019.

Wu, R., Vereecken, L., Tsiligiannis, E., Kang, S., Albrecht, S. R., Hantschke, L., Zhao, D., Novelli, A., Fuchs, H., Tillmann, R., Hohaus, T., Carlsson, P. T. M., Shenolikar, J., Bernard, F., Crowley, J. N., Fry, J. L., Brownwood, B., Thornton, J. A., Brown, S. S., Kiendler-Scharr, A., Wahner, A., Hallquist, M., and Mentel, T. F.: Molecular composition and volatility of multi-generation products formed from isoprene oxidation by nitrate radical, Atmos Chem Phys, 21, 10799–10824, https://doi.org/10.5194/acp-21-10799-2021, 2021.

Xing, C., Wan, Y., Wang, Q., Kong, S., Huang, X., Ge, X., Xie, M., and Yu, H.: Molecular Characterization of Brown Carbon Chromophores in Atmospherically Relevant Samples and Their Gas-Particle Distribution and Diurnal Variation in the Atmosphere, Journal of Geophysical Research: Atmospheres, 128, e2022JD038142, https://doi.org/10.1029/2022JD038142, 2023.

Yee, T. W.: Univariate Continuous Distributions, 343–370, https://doi.org/10.1007/978-1-4939-2818-7_12, 2015.

Zhang, Q., Anastasio, C., and Jimenez-Cruz, M.: Water-soluble organic nitrogen in atmospheric fine particles (PM2.5) from northern California, Journal of Geophysical Research: Atmospheres, 107, AAC 3-1, https://doi.org/10.1029/2001JD000870, 2002.

Zheng, G., Wang, Y., Wood, R., Jensen, M. P., Kuang, C., McCoy, I. L., Matthews, A., Mei, F., Tomlinson, J. M., Shilling, J. E., Zawadowicz, M. A., Crosbie, E., Moore, R., Ziemba, L., Andreae, M. O., and Wang, J.: New particle formation in the remote marine boundary layer, Nature Communications 2021 12:1, 12, 1–10, https://doi.org/10.1038/s41467-020-20773-1, 2021.

4.3 *Retention During Freezing of Raindrops, Part I: Investigation of Single and Binary Mixtures*

The following publication addresses the underrepresented topic of chemical retention during drop freezing processes. Chemical redistribution between the liquid and gas phase during freezing is not fully understood, particularly for the wide variety of atmospheric organics. This is despite its relevance to the vertical redistribution of organics along the UTLS and its support of new particle formation in convective outflows, thereby its subsequent role in radiation scattering and cloud condensation nucleation.

We investigated the retention of specific chemical species and their binary mixtures during freezing of raindrops via acoustic levitation. Prepared solutions of analyte samples were introduced via syringe into an acoustic levitator housed inside a cold chamber held at –15ºC. The contact-free single-drop was allowed to freeze without the introduction of artificial freezing nucleator and then collected for comparative analysis with the native solution. Our results reveal high retention with nearly all substances being fully retained during freezing. This could be attributed to faster freezing time compared to slower mass expulsion time, along with ice-shell formation during freezing. This result helps improve our understanding of interaction between ice microphysical processes and chemistry in deep convective clouds.

I was a significant contributor to this publication. Specifically, I along with MG, MZ, AT, SM designed the experiments; I along with MG, MH, conducted analytical measurements, I along with AT, MH, SB, KD, MZ reviewed and edited the manuscript.

https://doi.org/10.5194/egusphere-2024-3917
Preprint. Discussion started: 19 December 2024

Retention During Freezing of Raindrops, Part I: Investigation of Single and Binary Mixtures

Martanda Gautam[1], Alexander Theis[2], Jackson Seymore[1], Moritz Hey[1], Stephan Bormann[1,2], Karoline Diehl[1], Subir K. Mitra[2], and Miklós Szakáll[1]

[1]Institute for Atmospheric Physics, Johannes Gutenberg University, Mainz, Germany
[2]Particle Chemistry Department, Max Plank Institute for Chemistry, Mainz, Germany

Correspondence: Martanda Gautam (mgautam@uni-mainz.de) and Miklós Szakáll (szakall@uni-mainz.de)

Abstract. The interaction with freezing processes and vertical transport of trace gases into the upper atmosphere during deep convection is critical to understanding the distribution of aerosol precursors and their climate effects. We conducted experimental studies inside a walk-in cold room for freely levitating rain drops (D = 2 mm) using an acoustic levitator apparatus. We investigated the effect of freezing raindrops on the retention of organic species for the first time with silver iodide as the ice nucleating agent. Quantitative chemical analysis determined the retention coefficient, which is defined as the fraction of a chemical species remaining in the ice phase compared to their initial liquid phase concentrations. We measured the retention coefficients of nitric acid, formic acid, acetic acid, and 2-nitrophenol as single components. Furthermore, we determined the retention coefficients of these substances as binary mixtures. Our results show the dominance of physical properties over their chemical counterparts on overall retention for the investigated large drops. Thus, for rain sized drops almost everything is fully retained during the freezing process, even for species with low effective Henry's law constants. An ice shell is formed within 4.8 ms around the drops just after the freezing was initiated. This ice shell formation was found to be the controlling factor for the overall retention of the investigated species, which inhibited any further expulsion of dissolved substances from the drop.

1 Introduction

The Earth's atmosphere consists of a diverse range of chemical constituents, starting from ever present gases such as nitrogen, oxygen, carbon-dioxide, ozone, etc., to a wide range of chemicals in trace amounts as well. Biogenic and anthropogenic source contributors are known to be important for understanding the role that trace constituents have on the atmosphere over long timescales (Kolb et al., 2010; Andreae, 2019). However, vertical redistribution can be just as critical (Martini et al., 2011; Ervens, 2015; Wang et al., 2016). During convective transport, there is a rapid redistribution of trace gases and aerosols from boundary layer to the upper troposphere, which can alter the overall concentration of the chemical constituents (Warneck, 1999; Corti et al., 2008; Ervens, 2015).

Organic aerosol mass is usually underestimated in the boundary layer and beyond (Carlton et al., 2009; Hodzic et al., 2020). As a consequence, the potential impact of aerosols on the global radiation budget, radiative forcing, and overall climate can be misrepresented (Lohmann and Feichter, 2005; Tsigaridis et al., 2014; Shrivastava et al., 2017; Sporre et al., 2020). Williamson

https://doi.org/10.5194/egusphere-2024-3917
Preprint. Discussion started: 19 December 2024

et al. (2019) also reported that there is an under-representation of total organic mass due to low estimations for new particle formation, particularly in tropical convective regions.

During vertical transport in deep convective systems, there is an evident phase change of the water droplets as they undergo cooling and subsequent freezing at lower temperature regimes higher up in the atmosphere. Trace gases dissolved in these drops could be either retained, revolatized, or scavenged during the freezing process (Pruppacher and Klett, 2010). The fraction of chemical species remaining inside the frozen drop, compared to their initial concentration in liquid phase before freezing, results in the so-called retention coefficient. Substances that are completely retained after freezing will have a retention coefficient of 1. Modelling studies (Mari et al., 2000; Barth et al., 2001, 2007; Tost et al., 2010; Long et al., 2010; Bela et al., 2016; Cuchiara et al., 2020; Ryu and Min, 2022; Cuchiara et al., 2023) concerning convective transport and redistribution of trace gases have stressed on the importance of experimentally determined retention coefficients. However, such experimental databases are quite few in this regard.

Previous studies on experimentally determining retention coefficients in context of riming of supercooled droplets of single substances (Iribarne et al., 1983; Lamb and Blumenstein, 1987; Iribarne et al., 1990; Snider et al., 1992; Snider and Huang, 1998; von Blohn et al., 2011, 2013; Jost et al., 2017; Borchers et al., 2024) help bridge the uncertainty gap and provide a backbone for effective parameterization for modelling frameworks. The term "riming-retention" will be used to refer to these above mentioned studies collectively. The following substances were studied for retention during riming of supercooled droplets: SO_2, H_2O_2, O_2, HNO_3, HCl, NH_4, formic acid, acetic acid, malonic acid, oxalic acid, formaldehyde, α-pinene oxidation derivatives and nitro- aromatic compounds. These experimental studies revealed dependencies of the retention of trace gases on both chemical and physical properties. Additionally, there is established correlation with effective Henry's law coefficient (H^*) and a retention indicator (RI) parameter, which relates experimentally derived retention coefficients to model derived values (Stuart and Jacobson, 2003, 2004). H^* shows the dependence on the solubility and dissociative properties of trace gases, whereas RI provides a ratio of expulsion timescales to freezing timescales. A freezing time significantly lower than the solute expulsion time would result in a chemical substance being retained. These expulsion timescales are described in Schwartz (1986), that take into account the aqueous, interfacial, and gaseous mass transfer rates and the aqueous phase kinetics as explained in Jost et al. (2017). In addition to these chemical properties, physical properties such as drop size, ventilation around the drop, temperature, and liquid water content are the major contributing factors affecting retention (Jost et al., 2017; Jost, 2017). The above mentioned experimental studies concerning riming-retention were mostly related with cloud sized droplets (i.e. diameters in the µm size range), for which the chemical properties were determined to be the dominant factors. The present study focuses on large rain drops (diameters in the mm size range), which have not been experimentally investigated thus far. Freezing of raindrops are especially important for the case of convective clouds with warm bases where collision and coalescence can produce such large mm sized drops, which can be further transported into the upper troposphere during deep convection. Henceforth, the term "freezing-retention" will be used to refer to the present study, investigating retention during freezing of rain drops.

The motivation for this study was to investigate and understand the retention of chemical species dissolved in larger drops, and thereby augment experimental databases to further enhance modeling frameworks. To conceptualize our experimental

https://doi.org/10.5194/egusphere-2024-3917
Preprint. Discussion started: 19 December 2024

outlook, we selected four chemical substances with increasing H^* values, namely: 2-nitrophenol, acetic acid, formic acid, and nitric acid. These substances are commonly found in the atmosphere and their previously measured retention coefficient values for riming with cloud droplet sizes lie between 0 to 1 and scale with H^*. In addition to investigating these four substances as single components, we also studied their potential interactions as binary mixtures. Binary mixtures were studied to infer a more systematic understanding of the retention process as in how the differential incorporation or segregation of two substances during freezing might affect their overall retention.

2 Methods

2.1 Experimental Setup

In this study, we used the Mainz-Acoustic Levitator (M-AL) setup (Fig. 1), which was placed inside a walk-in cold room. M-AL employs an ultrasonic wave source (58 KHz) and a metal reflector to produce a standing wave. Water drops can be injected with a syringe and levitated contact-free at the intersection of the incident and reflected waves (i.e. at the nodes of the standing wave). The diameters of the levitated water drops used in this study were 2.0 ± 0.1 mm. The M-AL is enclosed inside a Plexiglas housing to minimize any external interference to the standing wave. More details about the M-AL can be found in Diehl et al. (2014) and Szakáll et al. (2021).

In addition to the ultrasonic source, an infrared thermometer (KT 19.82 II, Heitronics) was used to measure the surface temperature of the levitated drops, and a USB camera (USB-103H, Phytec GmbH, Germany) to record the drop size information. The top left section of the schematic (Fig. 1) shows the placement of the video camera, which had a wide video graphics array of 752 $\times$ 480 pixels and a minimum pixel size of 6 $\times$ 6 µm. The infrared thermometer can be seen at the bottom right section of the schematic. A small heating element was incorporated into the infrared thermometer to maintain its internal components when it was operated at temperatures lower than -15 °C. Both the video camera and the infrared thermometer were placed on adjustable stands, which allowed vertical and horizontal adjustments. In addition to the infrared thermometer, another temperature sensor (PT-100) was placed inside the Plexiglas housing to monitor the thermal stability of the setup during experiments.

The retention experiments were carried out inside the walk-in cold room of the laboratory at temperatures between -15 and -28 °C. Silver iodide (AgI; Sigma Aldrich-99%) was used as the ice nucleating particle (INP) to initiate the freezing process. We first characterized the INP at three different concentrations (0.2, 0.01, and 0.0003 g/L) at three different experimental temperatures (-15, -20, and -28 °C). This provided the freezing curves of silver iodide at various temperatures and concentrations (Fig. A2); more details can be found in Appendix A. These steps were a pre-requisite for retention experiments to infer the correct drop freezing temperature ranges during our measurements.

https://doi.org/10.5194/egusphere-2024-3917
Preprint. Discussion started: 19 December 2024

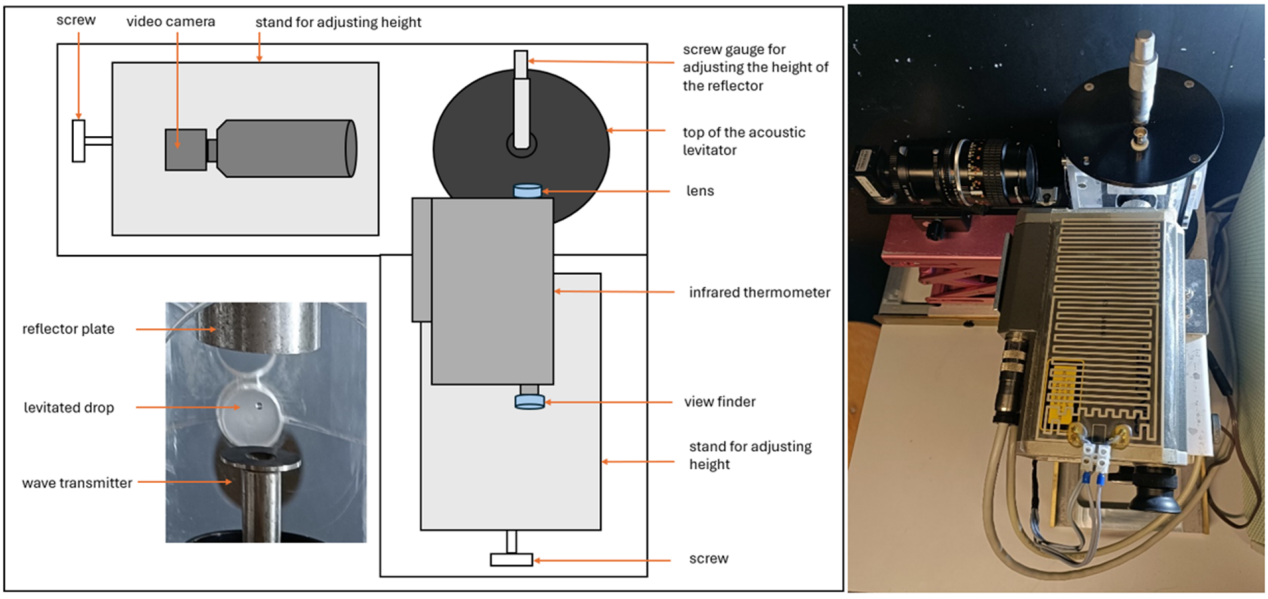

Figure 1. The Mainz Acoustic Levitator (M-AL) setup. Left: A schematic of the setup. Right: Setup in-situ.

.

2.2 Sampling procedure

In total, the retention of 4 single components and 3 binary mixtures were investigated. Nitric acid, formic acid, acetic acid, and 2-nitrophenol were measured as single components. Two sets of combinations were studied for the binary mixture of a strong and a weak acid, namely: nitric acid and acetic acid (mixture A1) as well as nitric acid and formic acid (mixture A2). Another set of binary mixtures was the combination of a small and a large molecule, due to their differences in molecular size and mobility. Here we investigated the mixture of formic acid and 2-nitrophenol (mixture B). The substances along with their purity labels are listed in Table 1.

Aqueous solutions of the investigated substances were prepared at an initial concentration of about 20 $\mathrm{mg/L}$. These solutions were transferred to a syringe for injecting a single drop inside the M-AL. For each experiment 11 measurement points were recorded. Each measurement point consisted of a total of 10 frozen drops collected in a vial. The volume of one frozen drop was approximately 4.2 µL which makes the total volume for one measurement point being about 42 µL. These frozen drops were diluted 10 times in order to increase the injection volume for chemical analysis and filtered with a 2 $\mu\mathrm{m}$ pore size filter (Carl Roth GmbH).

Subsequent quantitative analysis was done using a DIONEX-ICS 1000 anion Ion Chromatography unit (IonPac AS9-HC column, 9 $\mu\mathrm{m}$ particle size, 4 $\times$ 250 mm dimension, Thermo Fisher Scientific Inc.) for nitric, formic and acetic acid. 2-nitrophenol and 2-nitrobenzioc acid were analysed with a high precision liquid chromatography (HPLC) unit (Hypersil GOLD column, 9 $\mu\mathrm{m}$ particle size, 150 $\times$ 2.1 mm dimension, Vanquish-Thermo Fisher Scientific Inc.).

https://doi.org/10.5194/egusphere-2024-3917
Preprint. Discussion started: 19 December 2024

Table 1. Substances and mixtures investigated in this study.

Substance	Label/purity	Tracer	Concentration (mg/L)
Single components			
Nitric acid	Merck (65% w/w)	Sulphate^{+}	20
Acetic acid	Riedel-de Haen (100%)	Nitrate *	20
Formic acid	Emsure (98-100%)	Nitrate *	20
2-nitrophenol	Thermo Scientific (99%)	2-nitrobenzoic acid**	20
Binary mixtures			
A1. Nitric acid and Acetic acid	– –	Sulphate^{+}	20
A2. Nitric acid and Formic acid	– –	Sulphate^{+}	20
B. Formic acid and 2-nitrophenol	– –	Nitrate* and 2-nitrobenzoic acid**	20

Tracers: $^{+}$ Sulphate standard (SO_4): TraceCERT (99%), * Nitrate standard (NO_3): TraceCERT (99%), **2-nitrobenzoic acid: Thermo Scientific (95%)
Hydrochloric acid (HCl): Roth (37% w/w) and Sodium Hydroxide (NaOH): Merck (99%) were used to adjust the pH in the sensitivity studies.
The label/purity of the substances in binary mixtures are same as that of the single components.

For each of the investigated substances a concentration tracking tracer was added in order to track changes in mass concentration during the quantitative analyses. A tracer is a known chemical substance that is completely retained in ice, i.e. it has a retention coefficient of 1. The tracers used in this study were nitrate, sulphate, and 2-nitrobenzoic acid, which had a known retention of 1 from previous riming-retention studies (von Blohn et al., 2011; Borchers et al., 2024).

2.3 Calculation of retention coefficient

The retention during freezing was quantified by the retention coefficient R. It is the fraction of the chemical species that remains inside the frozen drops in the ice phase and the original solution in the liquid phase. The mathematical expression for calculating the initial retained fraction is given by

$$R_i = \frac{\frac{[substance]_{ice\ phase}}{[tracer]_{ice\ phase}}}{\frac{[substance]_{liquid\ phase}}{[tracer]_{liquid\ phase}}} \quad (1)$$

In Eq. 1, the square brackets indicate the concentration of the investigated chemical species and the tracers and R_i is the retention coefficient without any correction for desorption. The numerator is the ratio of ice phase concentration of the measured species with their specific tracer, whereas the denominator is the ratio of liquid phase concentrations.

2.3.1 Correction for desorption

The freezing of the levitated drops is not an instantaneous process when injected into the acoustic trap. The drop is initially at a temperature higher than 0 °C. It then undergoes gradual supercooling until the freezing is initiated (Fig. A1). During this stage, starting from injection of the drop into the acoustic field of the levitator and its subsequent progression to the supercooling

https://doi.org/10.5194/egusphere-2024-3917
Preprint. Discussion started: 19 December 2024

stage, the drop is exposed to external and internal forces until it is in equilibrium with its surroundings. Effects from the acoustic field potentially enhance ventilation while thermal stabilization can produce evaporation and desorption, leading to changes in aqueous concentration in the supercooled state. To account for all these effects, a correction parameter, called the desorption correction parameter D, was introduced:

$$D = \frac{\frac{[substance]_{supercooled\ phase}}{[tracer]_{supercooled\ phase}}}{\frac{[substance]_{liquid\ phase}}{[tracer]_{liquid\ phase}}} \tag{2}$$

To determine D, experiments were conducted under similar conditions as the retention experiments, with the exception of not adding any INP. In this case, the freezing process was not initiated and the liquid drop remained at a supercooled stage for a longer time. The drop was kept suspended for about 15 to 20 seconds, which is a typical time for the onset of freezing of the levitated drops under these experimental conditions (Fig. A1). Afterwards, the supercooled drops were instantly frozen inside a liquid nitrogen bath, which has a temperature of about -197 $^{\circ}$C (Scott, 1976; Jost et al., 2017). At such cold temperatures all substances inside the drops are retained during freezing. Quantitative analysis of these drops provided us with the concentration of the chemical substances in their supercooled stage and allowed the characterization of the desorption process.

The final retention coefficients R of the investigated chemical substances were calculated as:

$$R = \frac{R_i}{D} \tag{3}$$

Colder temperatures would essentially slow down the reaction kinetics for desorption to be effective (Mitra and Hannemann, 1993; Seinfeld and Pandis, 2016). For experimental temperatures below -15 $^{\circ}$C, desorption would play a negligible role. We applied the desorption corrections measured at -15 $^{\circ}$C for substances measured at lower temperatures as well.

2.4 Sensitivity studies

Retention experiments with the investigated substances were also carried out at different pHs and temperatures. pH sensitivity of the single components and the binary mixtures were studied at pH values of 3, 4, and 6/7. Hydrochloric acid (HCl) was used to lower the pH of the original solution and sodium hydroxide (NaOH) was used to increase the pH of the solution. The temperature sensitivity studies were performed at $-3.9 \pm 0.3^{\circ}$C and $-6.9 \pm 1.1^{\circ}$C drop freezing temperatures. These two different temperature ranges were evaluated from the INP freezing profiles (more details in Appendix A2). From the freezing profile obtained for experiments conducted at -15 $^{\circ}$C cold room temperatures and 0.2 g/L AgI, the 50% frozen fraction was found to be around $-3.9 \pm 0.3^{\circ}$C, which was taken as the average drop freezing temperature under these experimental conditions (Fig. A2). Similarly, retention experiments were conducted at -23 $^{\circ}$C cold room temperatures and AgI concentration of 0.008 ± 0.001g/L as the second experimental condition. The average drop freezing temperature for this second set of experimental conditions was obtained by extrapolating the freezing profile obtained at -20 $^{\circ}$C cold room temperature and 0.1 unitg/L AgI (Fig A2), as the drop surface temperature cooling rates at -20°C and -23°C were practically identical (0.4

https://doi.org/10.5194/egusphere-2024-3917
Preprint. Discussion started: 19 December 2024

Table 2. Retention coefficients of the investigated substances at $-3.9 \pm 0.3^{\circ}\mathrm{C}$ drop freezing temperature. The corresponding walk-in cold room temperatures (ambient temperature) was $-15 \pm 1^{\circ}\mathrm{C}$.

Substance	Retention coefficient (R)
Single components	
Nitric acid	1 ± 0.03
Acetic acid	0.88 ± 0.12
Formic acid	1.01 ± 0.08
2-nitrophenol	0.90 ± 0.05
Binary mixtures	
A. Mixture of a strong and a weak acid	
1. Nitric acid and Acetic acid	Nitric : 0.97 ± 0.06
	Acetic : 0.86 ± 0.15
2. Nitric acid and Formic acid	Nitric : 0.99 ± 0.05
	Formic : 0.99 ± 0.03
B. Mixture of a large and a small molecule	
Formic acid and 2-nitrophenol	Formic : 1 ± 0.07
	2-nitrophenol : 1.01 ± 0.09

$^{\circ}\mathrm{C/s}$). The 50% frozen fraction at -23°C was found to be $-6.9 \pm 1.1^{\circ}\mathrm{C}$. The two temperature ranges were selected to compare the temperature sensitivity in earlier experiments concerning retention coefficients for cloud sized droplets (von Blohn et al., 2011, 2013; Jost et al., 2017; Borchers et al., 2024). The average size of the droplets was $21.5 \pm 8.5\mu\mathrm{m}$ in the above mentioned studies involving riming-retention. In the present freezing-retention study with large levitated drops, the average drop sizes were $2.0 \pm 0.1\mathrm{mm}$.

3 Results and Discussions

3.1 Retention coefficient

The final retention coefficients for single components and binary mixtures are shown in Table 2. It can be seen that most of the substances measured as single components were completely retained in the ice phase. The exceptions were acetic acid and 2-nitrophenol, which were found to have retention coefficients of 0.88 and 0.90, respectively. However, for acetic acid as a single component, the standard deviation was much larger ($\pm$ 0.12) compared to the other single component substances. Thus, acetic acid could also be completely retained during freezing. The standard deviation of 2-nitrophenol was smaller compared to acetic acid and it was the least retained substance (0.85 to 0.95) of investigated single components.

Brand (2014) studied the retention of large drops (2.67 mm and 7.25 mm spherical equivalent diameter) by freezing them on a Teflon coated pallet and also reported high retention coefficients (close to 1). For example, for drop sizes of 2.67 mm (i.e.

https://doi.org/10.5194/egusphere-2024-3917
Preprint. Discussion started: 19 December 2024

10 µL drop volume), formic acid showed a retention coefficient of 0.94 ± 0.04. However, in our study contact-free immersion freezing (Diehl et al., 2014; Szakáll et al., 2021) was employed with which a more realistic scenario was realized to initiate freezing as in Brand (2014). Nevertheless, the measured retention coefficients in the present freezing-retention study and in Brand (2014) indicate near complete retention for the large rain sized drops.

Comparing our present results from freezing-retention experiments with previous riming-retention studies (von Blohn et al., 2011, 2013; Jost et al., 2017; Borchers et al., 2024), one can observe a deviation from their findings. Retention coefficients measured for cloud sized droplets during riming-retention experiments show a sigmoidal dependency on the solubility and dissociative properties of the individual substances (i.e. their effective Henry's law constant H^*). Our present experiments do not reveal these observed dependencies for the large rain sized drops. For instance, 2-nitrophenol (as single component in Table 2) having the least H^* among the investigated substances, was highly retained inside a freezing raindrop indicated by a retention coefficient of 0.9. However in the case of riming-retention, 2-nitrophenol showed a retention coefficient of 0.12 at pH 4 and 0.27 at pH 5.6 (Borchers et al., 2024). Further discussion comparing the results from riming-retention of cloud droplets and freezing-retention of raindrops from this study is provided in Section 3.4.

In the binary mixture experiments, in which we combined a strong and a weak acid (A1 and A2 in Table 2), nitric acid was the stronger acid with a pKa value of -1.3 (Haynes, 2016). Acetic acid and formic acid, having pKa values of 4.76 and 3.77 respectively, were the weaker acids compared to nitric acid. The results shown in Table 2 indicate that binary mixtures do not seem to alter the retention coefficients of their individual species for the combination of a strong and a weak acid.

Mixture B had the combination of a small and a large compound. There the average retention coefficient of 2-nitrophenol in a mixture with formic acid was observed to have increased slightly as compared to its retention as a single component. As a binary mixture component, both 2-nitrophenol and formic acid are completely retained during freezing.

3.2 pH Sensitivity

Retention coefficients of the single components were each measured at three different pH values. As a strong acid, nitric acid completely dissociates and is therefore assumed to be completely retained. Hence sensitivity studies for nitric acid were not done.

The original aqueous solutions at a concentration of 20 mg/L had pH values around 4.2 and 4.4 for each of the three substances shown in Fig. 2a. Acetic acid (green marker) and formic acid (blue marker) did not show any apparent dependency on pH. An argument could be made for acetic acid as its retention coefficient seems to increase with increasing pH, however, the standard deviation for each 11 sets of measurements at the three different pH values was quite large. The retention coefficients for acetic acid were 0.81, 0.88, and 1.05 for pH values of 3.1, 4.2, and 7.0, respectively, while their corresponding standard deviations were 0.18, 0.12, and 0.2. For 2-nitrophenol (red marker) an increase in retention (1.05) can be seen at pH 6. At lower pHs of 3.2 and 4.4, retention coefficients were about 0.90 for both cases. From Fig. 2a, one can infer a slight dependency on pH for 2-nitrophenol, and almost none for acetic acid and formic acid.

https://doi.org/10.5194/egusphere-2024-3917
Preprint. Discussion started: 19 December 2024

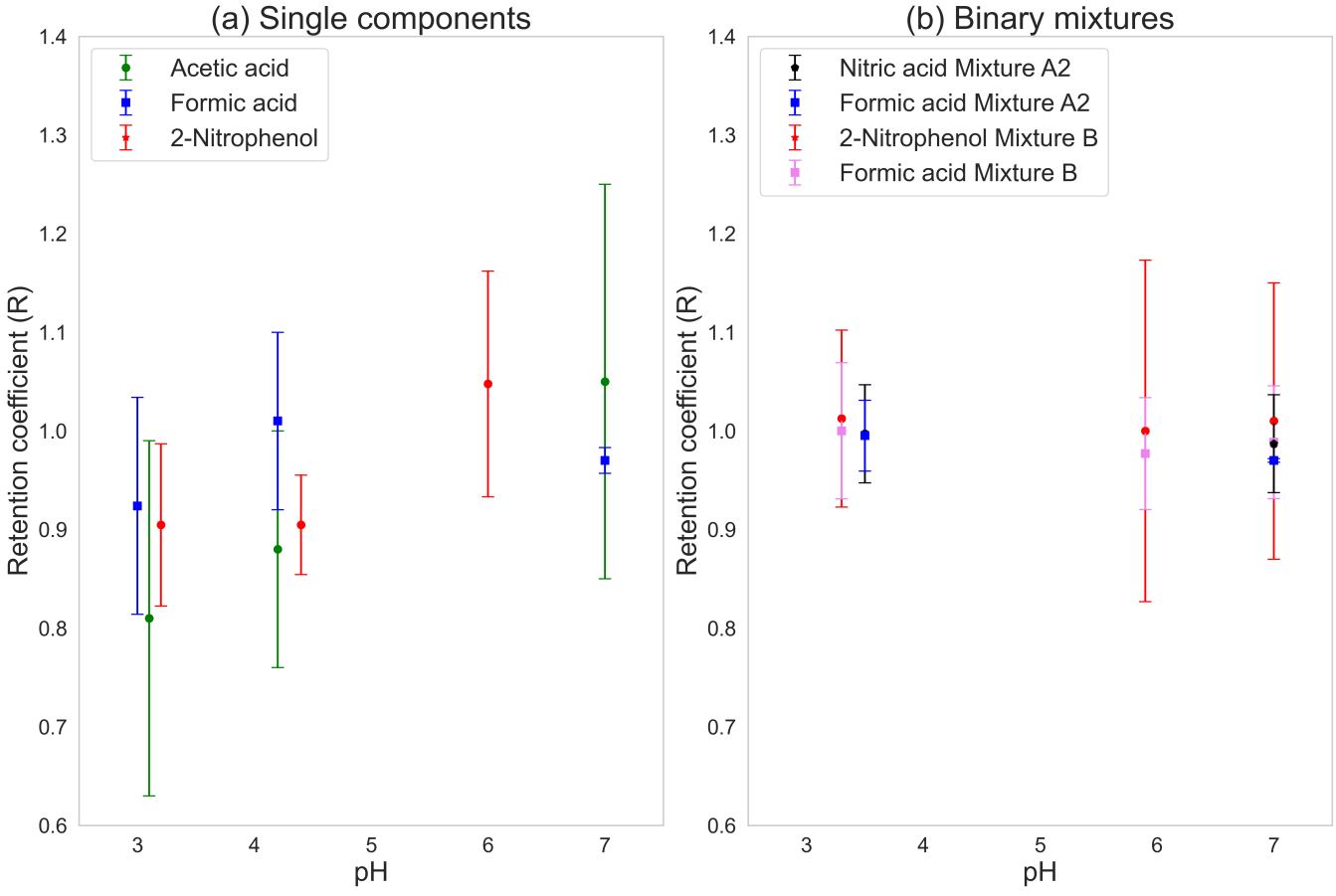

Figure 2. pH sensitivity of the retention coefficient of (a) single components, and (b) binary mixtures.

The pH sensitivities for the binary mixtures are shown in Fig. 2b. Mixture A1 was omitted due to the larger standard deviation for acetic acid compared to formic acid as a single component. In mixture A2, both substances were retained completely. The same was found for mixture B. As shown in Fig. 2b, none of mixtures show any sensitivity to changes in pH.

pH of the solutions were altered by adding HCl and NaOH, which could also interact with the investigated substances and dissociate them into their ionic form. In this case the overall concentration of the investigated substances could be lowered. A lower concentration of the substances, in turn, might not have enough partial pressure in the liquid phase (inside the levitated drops before freezing) for them to be expelled from the drop when it freezes. However, after the addition of HCl or NaOH, the initial concentration of 20 $\mathrm{mg/L}$ of the investigated substances did not change much. After addition, the lowest measured initial liquid phase concentration was 17.8 $\mathrm{mg/L}$ (11% decrease). The total number of moles of the dissolved substances had the same order of magnitude as their initial liquid phase concentration in the solution. Thus, any significant source of biases towards a higher retention coefficient due to addition of HCl or NaOH can be neglected in our measurements.

https://doi.org/10.5194/egusphere-2024-3917
Preprint. Discussion started: 19 December 2024

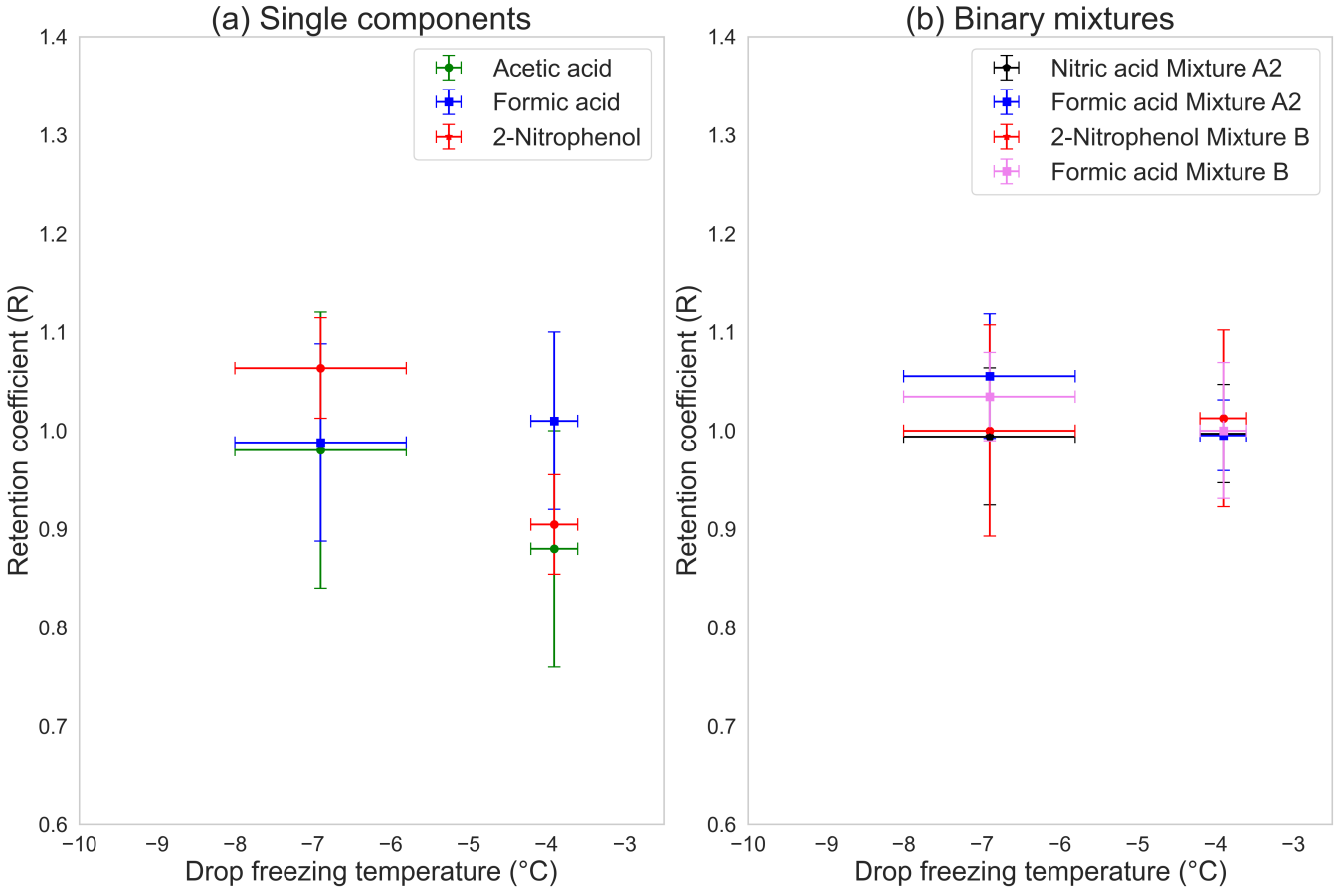

Figure 3. Temperature sensitivity of the retention coefficient of (a) single components, and (b) binary mixtures.

3.3 Temperature Sensitivity

The temperature sensitivities for the single components are shown in Fig. 3a. Acetic acid (green marker) showed a higher retention coefficient at the lower temperature with large standard deviations of the measurements at both temperatures. At -6.9°C the retention coefficient for acetic acid was 1.14±0.24 and at -3.9°C it was 0.88±0.12. Formic acid (blue marker) did not show any variation in retention coefficient with changes in the drop freezing temperatures and was completely retained at both temperatures. 2-nitrophenol (red marker) also had a higher retention coefficient at the colder temperature (1.06±0.05) as compared to the warmer temperature (0.90±0.08). The retention coefficients for both acetic acid and 2-nitrophenol appeared to have a weak dependency on temperature and were completely retained at (-6.9°C) along with formic acid, which had no dependency and was completely retained at both temperatures. In the atmosphere, freezing is initiated at lower temperatures than our experimental temperatures here, indicating towards complete retention of the investigated species.

https://doi.org/10.5194/egusphere-2024-3917
Preprint. Discussion started: 19 December 2024

Unlike the single components, the binary mixtures did not show any temperature dependency as seen in Fig. 3b. Both sets of binary mixtures were fully retained at $-3.9 \pm 0.3°\mathrm{C}$. At the colder temperature, the retention coefficients did not change and the mixtures were completely retained.

3.4 Relation with effective Henry's law coefficient

Retention coefficients of substances are strongly dependent on chemical properties such as aqueous diffusion, gaseous diffusion, interfacial mass transport, solubility and dissociation. Among them, solubility and dissociative effects characterized by effective Henry's law constant H^* were reported to be the dominant ones. Stuart and Jacobson (2003) and Jost et al. (2017) showed this relationship between the retention coefficient and H^*, where they stated that substances with H^* greater than 10^7 are completely retained. Substances with H^* lower than 10^4 are less likely to be retained or more likely expelled from the drop during riming-retention. Retention coefficients of all other substances with H^* values between these ranges followed a sigmoid shape (see Borchers et al., 2024, Figure 7).

The relation between effective Henry's law coefficient and retention coefficient for retention-riming was modeled by the following equation:

$$R_{H^*} = \left[1 + \left(\frac{a}{H^*}\right)^b\right]^{-1} \tag{4}$$

where the parameters $a = (2.41 \pm 1.06) \times 10^4$ and $b = 0.27 \pm 0.04$, respectively (Borchers et al., 2024).

Figure 4 shows the relation between H^* and R. The gray markers are from previous studies (von Blohn et al., 2011; Jost et al., 2017; Borchers et al., 2024) for riming-retention. The coloured markers are from the present study utilizing freezing-retention.

It is apparent from Fig. 4, that nitric acid with an H^* of 10^{11} was completely retained. Formic acid was completely retained, too, which is in contrast to previous measurements from riming-retention studies in which it showed a lower retention coefficient (0.76). No definitive conclusion regarding changes in its measured retention coefficient can be made for acetic acid (0.88 for single component), due to large standard deviation and the overlap between the single components and the binary mixture measurements. Conversely, the riming-retention of acetic acid was much lower (0.6). 2-nitrophenol showed a much higher retention coefficient for large drops (0.9 and above) compared to its retention for small µm sized droplets (0.27 at pH 5.6; Borchers et al. 2024). Considering its low H^* (10^3), one would expect the retention coefficient of 2-nitrophenol as a single component to be lower than 0.9, which was not the case here. In the mixture with formic acid, 2-nitrophenol was also completely retained. Specifically, Fig. 4 demonstrates that our results from freezing-retention deviate from the sigmoidal relationship between retention coefficients and H^* unlike the previous experimental studies involving riming-retention. This result is also seen in the conclusions of Part II of this publication series, where the retentions for ambient water soluble organic compounds of over 450 species were also investigated.

https://doi.org/10.5194/egusphere-2024-3917
Preprint. Discussion started: 19 December 2024

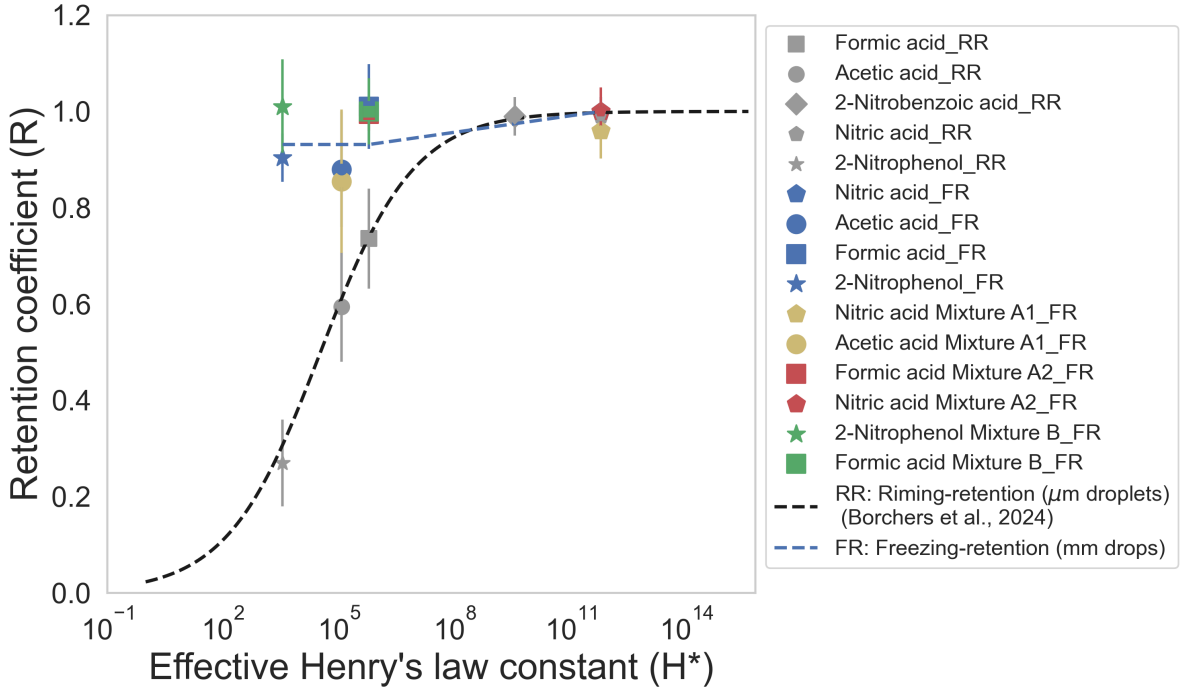

Figure 4. Retention coefficient (R) as a function of effective Henry's law coefficient (H^*). Grey markers: from riming-retention (RR) of small droplets (von Blohn et al., 2011; Jost et al., 2017; Borchers et al., 2024). Colored markers: from freezing-retention (FR, present study), with drop freezing temperature of -3.9 ± 0.3°C. Blue markers: single components. Yellow (mixture A1), red (mixture A2) and green (mixture B) markers: binary mixtures.

3.5 Retention indicator analysis

Another method to analyze retention is from the point of view of mass and heat transfer considerations, such as the mass expulsion and freezing timescales as suggested by Stuart and Jacobson (2003, 2004) and Jost et al. (2017). Retention indicator (RI) is introduced that is the ratio of total mass expulsion time (T_{exp}) to the freezing time (T_{frz}) as shown in Eq. (5). Table 3 shows the calculated timescales for the retention indicator of the single components investigated in this study.

$$RI = \frac{T_{exp}}{T_{frz}} \tag{5}$$

$$T_{exp} = T_g + T_{aq} + T_i \tag{6}$$

where, $T_g = \frac{a^2 H^*}{3 D_g f}$; $T_{aq} = \frac{a^2}{D_{aq}}$; $T_i = \frac{4aH^*}{3v\alpha}$

https://doi.org/10.5194/egusphere-2024-3917
Preprint. Discussion started: 19 December 2024

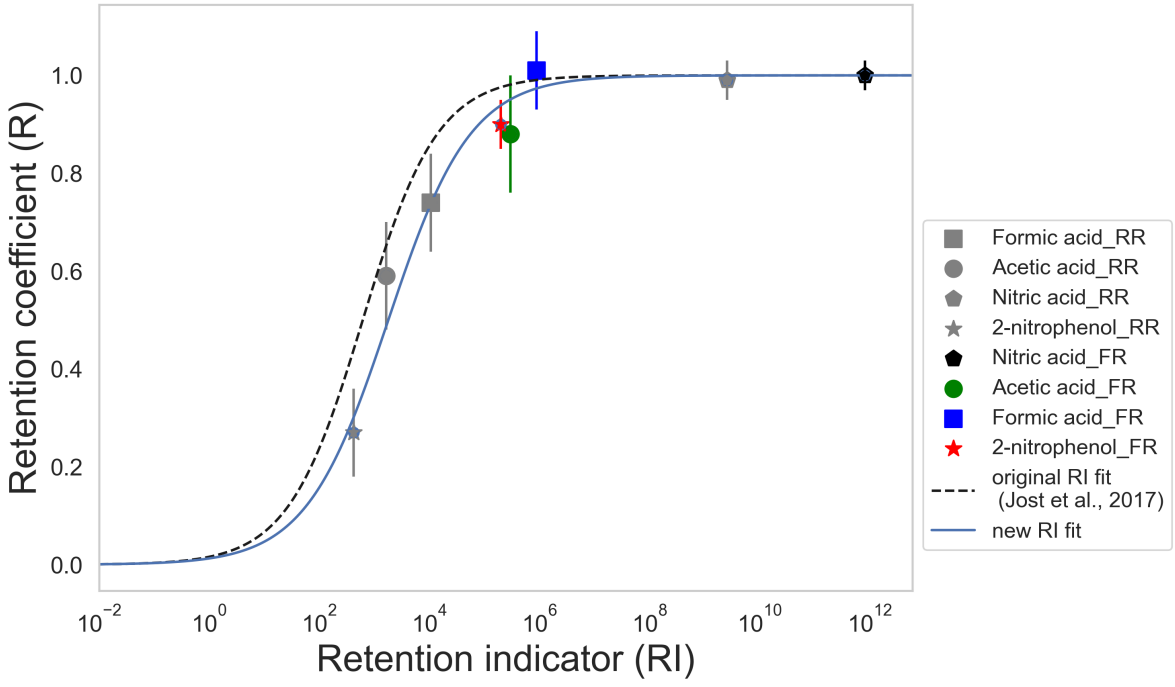

Figure 5. Retention coefficient of the substances investigated as single components as a function of the empirical retention indicator. Gray markers: from riming-retention (RR), coloured markers: from freezing-retention (FR). Dashed line: original retention indicator fit parameters from Jost et al. (2017), solid line: updated fit from current study.

The total solute mass expulsion time T_{exp} is the sum of aqueous phase mass expulsion time T_{aq}, gaseous phase mass expulsion time T_g, and interfacial mass transfer expulsion time T_i. In Eq. (6) T_g accounts for the gaseous diffusivity D_g, where a is the radius of the drop, H^* is the effective Henry's law coefficient and f is the ventilation coefficient (f= 5.6; Szakáll et al. 2021). T_{aq} accounts for the aqueous diffusivity D_{aq} of the substance. T_i takes into consideration for the mass accommodation coefficient α and the thermal velocity of the chemical in air, v .

A fourth timescale involving the aqueous phase kinetics was also introduced by Jost et al. (2017). This timescale is specifically important for substances such as ammonia and formaldehyde since they react with atmospheric carbon dioxide and are affected by dehydration of methanediol, respectively (Jost et al., 2017). For substances investigated in this study, the aqueous phase kinetics and reactions are negligible, so this timescale was not considered. The experimental temperatures, pH values, initial concentrations and H^* are also listed in Table 3 for reference. The freezing time T_{frz} was derived experimentally via high speed camera (Motion Pro Y3M; pixel size: 12 $\times$ 12 µm; resolution: 1024 $\times$ 1280 pixels) at 600 frames per second, as shown in Fig. B1. The time from the initiation of freezing to the complete formation of an ice shell around the levitated drop was approximately 4.8 ms. This value was taken as the freezing time for the retention indicator calculation. It is also clearly evident in Table 3 that T_{frz} is several orders of magnitude smaller compared to T_{exp}. Gas phase expulsion time T_g appears to

https://doi.org/10.5194/egusphere-2024-3917
Preprint. Discussion started: 19 December 2024

Table 3. List of parameters used for retention indicator calculation.

Parameters	Nitric acid	Acetic acid	Formic acid	2-nitrophenol	Comments
$^{1}D_{aq}$	2.25×10^{-5}	1.29×10^{-5}	1.63×10^{-5}	1.07×10^{-5}	Aqueous diffusivity (cm^2/s)
$^{1}D_{g}$	0.12	0.12	0.14	0.07	Gaseous diffusivity (cm^2/s)
pH	4.1	4.2	4.2	4.4	Experimental pH values
$^{2}H^*$	7.56×10^{11}	1.28×10^{5}	8.31×10^{5}	3.50×10^{3}	Effective Henry's law constant
$^{3}\alpha$	0.06	0.07	0.05	0.01	Mass accomodation coefficient
T	-3.9	-3.9	-3.9	-3.9	Temperature ($^\circ$C)
C	20	20	20	20	Concentration (mg/L)
T_g	3.88×10^{9}	6.37×10^{2}	3.55×10^{3}	2.81×10^{1}	Gas phase expulsion time (s)
T_i	2.11×10^{7}	7.78×10^{0}	6.36×10^{1}	2.19×10^{0}	Interfacial expulsion time (s)
T_{aq}	6.81×10^{2}	7.72×10^{2}	6.13×10^{2}	9.28×10^{2}	Aqueous phase expulsion time (s)
T_{exp}	3.90×10^{9}	1.42×10^{3}	4.23×10^{3}	9.59×10^{2}	Total expulsion time (s)
T_{frz}	4.80×10^{-3}	4.80×10^{-3}	4.80×10^{-3}	4.80×10^{-3}	Ice shell formation time (s)
RI	8.13×10^{11}	2.95×10^{5}	8.80×10^{5}	2.00×10^{5}	Retention indicator
R	1.00 ± 0.03	0.88 ± 0.12	1.01 ± 0.08	0.90 ± 0.05	Retention coefficient
Controlling parameter	T_g	T_{aq}	T_g	T_{aq}	–

[1]The diffusivities in water D_{aq} and in air D_g calculated at 273K (Thibodeaux and Mackay, 2010), [2]Effective Henry's law constant calculated at 273K and at their corresponding pH (Tremp et al., 1993; Johnson et al., 1996; Warneck and Williams, 2012), [3] The mass accommodation coefficient at 273K (Ervens et al., 2003; Davidovits et al., 2006).

be the controlling factor contributing to the total high T_{exp} for nitric and formic acid, and aqueous phase expulsion timescale T_{aq} for acetic acid and 2-nitrophenol. In Jost et al. (2017) the parameterization relating RI and retention coefficient is given as

$$R_{RI} = \left[1 + \left(\frac{c}{RI}\right)^{d}\right]^{-1} \tag{7}$$

Equation 7 is depicted in Fig. 5, where the original parameters taken from Jost et al. (2017) are c_1 = 618±71 and d_1 = 0.64±0.06 (black dashed line, Fig. 5). From our study, an updated fit is provided with c_2 = 1800±95 and d_2 = 0.58±0.07 (blue solid line, Fig. 5).

Figure 5 shows the variation of retention coefficients with RI. In contrast to Fig. 4, both the riming-retention and freezing-retention measurements fit well with the parameterization given in Eq. 7. This analysis corroborates our experimental results for mm sized raindrops with μm sized cloud droplets. These results can be categorized with timescale analysis and follow a similar relation with both previous experimental (Jost et al., 2017) and theoretical (Stuart and Jacobson, 2003, 2004) studies.

https://doi.org/10.5194/egusphere-2024-3917
Preprint. Discussion started: 19 December 2024

3.6 Physical parameters

Our study shows that retention is dependent on the size of the droplets which needs to be considered when modeling the mass flux of trace substances with numerical models. An aspect of the importance of the physical parameters is surface area to volume ratio. The rain sized drops in this study have a surface area to volume ratio of 3×10^3 m^{-1}. The cloud sized droplets in earlier retention-riming studies have a surface area to volume ratio of about 2×10^7 m^{-1}. Thus, this ratio is approximately 4 orders of magnitude higher for the cloud droplets compared to the rain drops. As such, the dissolved substances in raindrops would have more diffusional volume and smaller surface area. Additionally, low surface area to volume ratio for the case of the rain drops is an indicator of lower overall desorption as well (Jost, 2017).

Another physical parameter influencing retention is the ventilation coefficient. It describes the enhanced heat and mass transfer around hydrometers in an airflow. For the riming-retention studies, substances measured inside a wind tunnel (µm sized droplets) had ventilation coefficients of about 30 to 32 (Jost et al., 2017, Table 4). In contrast, the ventilation coefficient in the acoustic levitator for the 2 mm diameter drops was about 5.6 (Szakáll et al., 2021). As such, a smaller ventilation coefficient would incur less transfer of mass and heat for the 2 mm raindrops as compared to the retention measurements for µm sized droplets. This could be seen as an important physical parameter aiding higher expulsion times and, consequently, higher retention coefficients as seen in the RI analysis. In a real atmospheric scenario, 2 mm drops falling at their terminal velocity have a ventilation coefficient of about 15 (Pruppacher and Klett, 2010). A higher ventilation coefficient would increase the mass transfer and thereby decrease the expulsion timescale. However, the ventilation coefficients of heat and mass transfer is almost the same. Therefore an increase in mass transfer would also imply a faster freezing time.

4 Conclusions

Our results show higher retention coefficients close to 1 for mm sized raindrops for similar substances from previously studied retention coefficients (von Blohn et al., 2011; Jost et al., 2017; Borchers et al., 2024) in µm sized cloud droplets. It is important to note that in addition to the differences in droplet size, the freezing pathways were also different. The previous studies utilized the riming-retention mechanism while in the present work we incorporated a contact-free freezing-retention mechanism.

Substances studied as single components show very little sensitivity (for 2-nitrophenol and acetic acid) with changes in either pH or temperatures. Formic acid as a single component is not sensitive to changes in pH or temperatures. Binary mixtures also do not show any sensitivity for changes in pH and freezing temperature.

We conclude that for rain sized drops (mm and above), most of the chemical species are completely retained during freezing. This can be interpreted as the physical parameters -— such as drop size and ice shell formation -— dominating the chemical properties concerning retention influences. After an ice shell is formed around a drop during the initiation of freezing, it is significantly more difficult for the dissolved species to be expelled from the drop, thus leading to higher mass expulsion timescales.

Our retention indicator analysis shows that the shorter freezing and longer expulsion timescales (a minimum of 5 orders of magnitude higher) lead to higher retention for the investigated species. This indicates that during the freezing of mm sized

https://doi.org/10.5194/egusphere-2024-3917
Preprint. Discussion started: 19 December 2024

raindrops all dissolved trace gases may be removed entirely by precipitation in deep convective clouds or transported within the ice phase into the UT where it can be released upon sublimation.

We derived new parameterizations for the retention indicator to include large mm sized raindrops, and thus, updated the previously obtained ones that only considered $\mu\mathrm{m}$ sized cloud droplets (Jost et al., 2017). This result is beneficial in terms of computational expense for the chemistry coupled atmospheric and earth system modelling as modelling freezing raindrops would not require much additional computational resources.

Our experiments were conducted with single components and binary mixtures but in the real atmosphere, air is mixed with numerous complex trace gases that are in constant turbulent motion. Our current database does not have many substances with H^* values lower than 10^3, and such substances might behave differently during freezing. Future retention experiments that sample for trace gas at the ground level and at different vertical profiles would improve our understanding of the underlying micro-physical and chemical processes within convective systems. Our experiments also indicate that it is critical to further investigate the ice shell formation process during the freezing of raindrops.

Future studies should investigate how these and similar organic compounds behave when they are in the real atmosphere. In Part II we investigate the retention of a complex mixture of organic compounds sampled from Beijing urban aerosols through the same experimental setup with high resolution mass spectrometry analysis.

Data availability. The data supporting this study are available at the repository Gautam and coauthors (2024). Additional data (if required) for this study are available upon request from the corresponding authors.

Appendix A: Characterization of INP

A1 Freezing profile of levitated drops

To characterize the INP (AgI) we levitated drops and recorded their drop surface temperature as they froze, at three pairs of different concentrations and cold room temperatures: 0.2, 0.01, and 0.0003 g/L, and corresponding cold room temperatures of -15, -20, and -28$^\circ\mathrm{C}$. For both combinations of concentration and temperature, the freezing profiles of about 50 drops were recorded. The crucial information derived from these three sets of measurements was obtaining the freezing profiles of the levitated drops during their freezing. Figure A1 shows a typical drop freezing profile as the temporal evolution of the drop surface temperature. The drop when injected to the nodes of the standing wave, had initially a temperature higher than 0$^\circ\mathrm{C}$. The warm drop underwent gradual and uniform cooling and reached a supercooled stage (0 to 20 seconds). The supercooled stage continued until nucleation was initiated, where the rapid crystal growth started (about 25 seconds) and drop surface temperature rose sharply to about 0$^\circ\mathrm{C}$. The rapid crystal growth can be interpreted as adiabatic freezing and the corresponding temperature was taken as the freezing temperature of the drop. At this temperature, the supercooled drop entered an ice-water equilibrium, visible as the flattened section in Fig. A1 (30 to 80 seconds). During this stage, transfer of latent heat took place that can be interpreted as the diabatic freezing of the levitated drop. The supercooled drop then underwent a phase transition

https://doi.org/10.5194/egusphere-2024-3917
Preprint. Discussion started: 19 December 2024

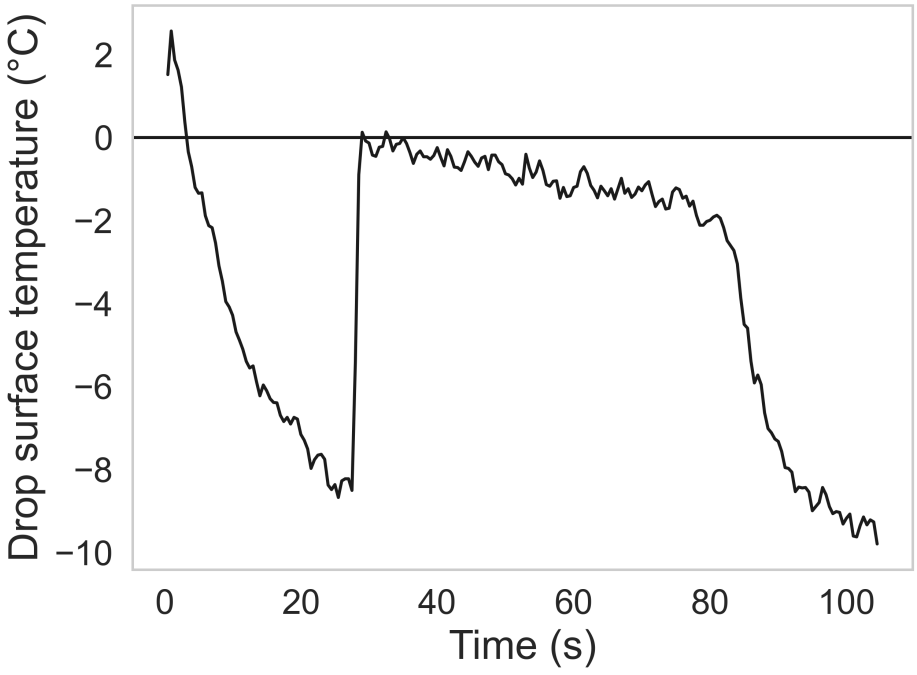

Figure A1. Evolution of drop surface temperature during its freezing as measured by the infrared thermometer.

from liquid to solid state. Finally, the drop surface temperature cooled down to ambient temperature, reaching a steady state (100 seconds) once it was completely frozen.

A2 Frozen fraction

Within the range of the sample size of 50 drops for each set of frozen fraction measurements, the precise drop freezing temperatures varied. We grouped the recorded drop freezing temperatures in bins with a width of 0.5 °C. Corresponding to each bin, the number of frozen drops at each interval were grouped. A cumulative distribution was formed with the grouped bins. As commonly used in ice nucleation studies, frozen fraction or f_{ice} was determined, which is calculated as the fraction of total drops that were frozen at a particular temperature (more details in Szakáll et al., 2021). The temperature at which f_{ice} was 50% was taken as the 'average drop freezing temperature' for each set of concentration and cold room temperature pair.

The frozen fractions for each set of measurements are shown in Fig. A2. The average drop freezing temperature was -3.9°C for AgI concentration of 0.2 g/L and cold room temperature of -15°C. For the combination of 0.01 g/L and -20 °C, the average drop freezing temperature was -6.7 °C and -8.9 °C for the combination of 0.0003 g/L and -28°C. We conducted our retention measurements at a cold room temperature of -23°C. To obtain the freezing profile at this temperature, we refitted the freezing profile obtained for -20°C using the following equation:

https://doi.org/10.5194/egusphere-2024-3917
Preprint. Discussion started: 19 December 2024

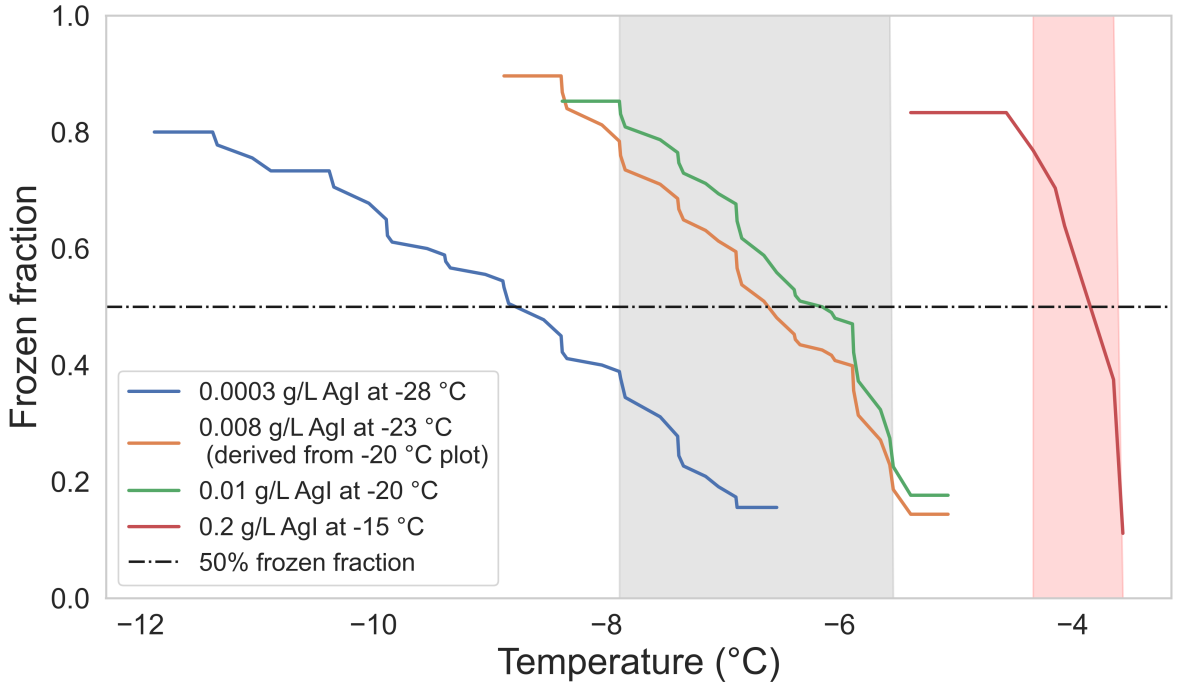

Figure A2. Frozen fraction at different ambient temperatures and concentrations of AgI. Shaded regions mark the two selected temperature ranges for retention measurements. The shaded regions lie within the interval where the frozen fraction is in between 0.8 and 0.2.

$$f_{ice\_23} = 1 - \exp \frac{c_{23} * \ln(1 - f_{ice\_20})}{c_{20}} \tag{A1}$$

where f_{ice_23} is the desired frozen fraction distribution at -23°C. c_{20} and c_{23} are the INP concentrations at the two different temperatures of -20°C and -23°C, respectively. f_{ice_20} is the experimentally derived frozen fraction at -20°C. The cooling rate of the drop surface temperature was practically identical at these two cold room temperatures. Equation A1 is adopted from the relation between ice nucleation active sites (n_s) and f_{ice} and at a particular INP concentration and temperature (see Szakáll et al., 2021, Eq 5).

We selected the interval where frozen fraction lies between 20% to 80% as the temperature deviation during our retention experiments. Shaded regions in Fig. A2 show this temperature deviation for experiments done at -15°C and -23°C cold room temperatures. The average drop freezing temperatures (frozen fraction at 50%) in these two cases were $-3.9 \pm 0.3°C$ (red-shaded region) and $-6.9 \pm 1.1°C$ (gray shaded region).

https://doi.org/10.5194/egusphere-2024-3917
Preprint. Discussion started: 19 December 2024

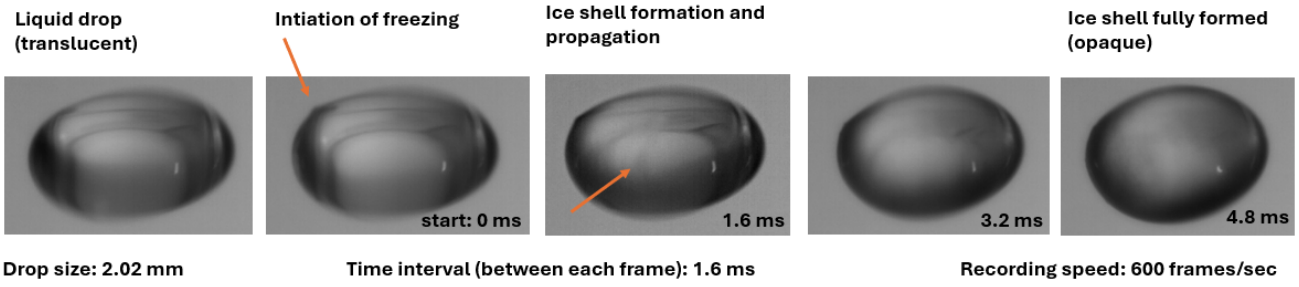

Figure B1. Consecutive frames showing the formation of ice-shell, recorded with a high speed camera at 600 frames per second, and at a cold room temperature of -15 °C. In the liquid phase (leftmost image), the drop is seen as translucent, which gradually turns opaque as the ice shell is formed (rightmost image).

Appendix B: Ice shell formation during freezing

The investigation of the drop freezing mechanism in the acoustic levitator led to the realization of the ice shell formation. During the rapid crystal growth stage within the first 25 s, as discussed in Appendix A1, Fig. A1, an ice shell formed around the supercooled drop within milliseconds (Fig. B1). After the formation of the shell, freezing inside the drop proceeded gradually until it was completely frozen. The shell formation process was recorded with a high speed camera setup at 600 frames per second, and at a cold room temperature of -15 °C.

This observation validates the higher retention coefficients of the substances measured during our freezing-retention experiments, as compared to the previously measured substances involving riming-retention. The ice shell inhibited the expulsion of the dissolved chemical substances from the drop. The expulsion timescale as discussed and calculated in Section 3.5 was several orders of magnitude higher than the freezing time scale of 4.8 milliseconds (Fig. B1). This led to a higher value of the retention indicator, even for more volatile substances such as 2-nitrophenol, which had the lowest effective Henry's law constant among the investigated substances (Figure 5 and Table 3).

Author contributions. MG, MZ, AT, JS, SM participated in designing the experiments; MG, MH performed the experiments; MG, MH, JS conducted analytical measurements, MG analysed the data and wrote the manuscript draft; AT, JS, MH, SB, KD, MZ reviewed and edited the manuscript

Competing interests. The authors declare no competing interests.

https://doi.org/10.5194/egusphere-2024-3917
Preprint. Discussion started: 19 December 2024

Acknowledgements. This work was funded by the Deutsche Forschungsgemeinschaft (DFG, German Research Foundation) – TRR 301 – Project-ID 428312742.

https://doi.org/10.5194/egusphere-2024-3917
Preprint. Discussion started: 19 December 2024

References

Andreae, M. O.: Emission of trace gases and aerosols from biomass burning–an updated assessment, Atmospheric Chemistry and Physics, 19, 8523–8546, 2019.

Barth, M., Stuart, A. L., and Skamarock, W.: Numerical simulations of the July 10, 1996, stratospheric-tropospheric experiment: Radiation, Aerosols, and Ozone (STERAO)-deep convection experiment storm: Redistribution of soluble tracers, Journal of Geophysical Research: Atmospheres, 106, 12 381–12 400, 2001.

Barth, M., Kim, S.-W., Wang, C., Pickering, K., Ott, L., Stenchikov, G., Leriche, M., Cautenet, S., Pinty, J.-P., Barthe, C., et al.: Cloud-scale model intercomparison of chemical constituent transport in deep convection, Atmospheric Chemistry and Physics, 7, 4709–4731, 2007.

Bela, M. M., Barth, M. C., Toon, O. B., Fried, A., Homeyer, C. R., Morrison, H., Cummings, K. A., Li, Y., Pickering, K. E., Allen, D. J., et al.: Wet scavenging of soluble gases in DC3 deep convective storms using WRF-Chem simulations and aircraft observations, Journal of Geophysical Research: Atmospheres, 121, 4233–4257, 2016.

Borchers, C., Seymore, J., Gautam, M., Dörholt, K., Müller, Y., Arndt, A., Gömmer, L., Ungeheuer, F., Szakáll, M., Borrmann, S., et al.: Retention of α-pinene oxidation products and nitro-aromatic compounds during riming, EGUsphere, 2024, 1–25, 2024.

Brand, A.: Experimentelle Untersuchungen des Retentionskoeffizienten organischer Säuren in Wassertropfen, Diploma thesis, University of Mainz, Germany, 2014.

Carlton, A., Wiedinmyer, C., and Kroll, J.: A review of Secondary Organic Aerosol (SOA) formation from isoprene, Atmospheric Chemistry and Physics, 9, 4987–5005, 2009.

Corti, T., Luo, B., De Reus, M., Brunner, D., Cairo, F., Mahoney, M., Martucci, G., Matthey, R., Mitev, V., Dos Santos, F., et al.: Unprecedented evidence for deep convection hydrating the tropical stratosphere, Geophysical Research Letters, 35, 2008.

Cuchiara, G., Fried, A., Barth, M., Bela, M., Homeyer, C., Gaubert, B., Walega, J., Weibring, P., Richter, D., Wennberg, P., et al.: Vertical transport, entrainment, and scavenging processes affecting trace gases in a modeled and observed SEAC4RS case study, Journal of Geophysical Research: Atmospheres, 125, e2019JD031 957, 2020.

Cuchiara, G., Fried, A., Barth, M., Bela, M., Homeyer, C., Walega, J., Weibring, P., Richter, D., Woods, S., Beyersdorf, A., et al.: Effect of Marine and Land Convection on Wet Scavenging of Ozone Precursors Observed During a Seac4rs Case Study, Journal of Geophysical Research: Atmospheres, 128, e2022JD037 107, 2023.

Davidovits, P., Kolb, C. E., Williams, L. R., Jayne, J. T., and Worsnop, D. R.: Mass accommodation and chemical reactions at gas- liquid interfaces, Chemical reviews, 106, 1323–1354, 2006.

Diehl, K., Debertshäuser, M., Eppers, O., Schmithüsen, H., Mitra, S., and Borrmann, S.: Particle surface area dependence of mineral dust in immersion freezing mode: investigations with freely suspended drops in an acoustic levitator and a vertical wind tunnel, Atmospheric Chemistry and Physics, 14, 12 343–12 355, 2014.

Ervens, B.: Modeling the processing of aerosol and trace gases in clouds and fogs, Chemical reviews, 115, 4157–4198, 2015.

Ervens, B., George, C., Williams, J., Buxton, G., Salmon, G., Bydder, M., Wilkinson, F., Dentener, F., Mirabel, P., Wolke, R., et al.: CAPRAM 2.4 (MODAC mechanism): An extended and condensed tropospheric aqueous phase mechanism and its application, Journal of Geophysical Research: Atmospheres, 108, 2003.

Gautam, M. and coauthors: Retention During Freezing of Raindrops, Part I: Investigation of Single and Binary Mixtures, https://doi.org/10.5281/zenodo.14319648, 2024.

Haynes, W. M.: CRC handbook of chemistry and physics, CRC press, 2016.

https://doi.org/10.5194/egusphere-2024-3917
Preprint. Discussion started: 19 December 2024

Hodzic, A., Campuzano-Jost, P., Bian, H., Chin, M., Colarco, P. R., Day, D. A., Froyd, K. D., Heinold, B., Jo, D. S., Katich, J. M., et al.: Characterization of organic aerosol across the global remote troposphere: a comparison of ATom measurements and global chemistry models, Atmospheric Chemistry and Physics, 20, 4607–4635, 2020.

Iribarne, J., Barrie, L., and Iribarne, A.: Effect of freezing on sulfur dioxide dissolved in supercooled droplets, Atmospheric Environment (1967), 17, 1047–1050, 1983.

Iribarne, J., Pyshnov, T., and Naik, B.: The effect of freezing on the composition of supercooled droplets—II. Retention of S (IV), Atmospheric Environment. Part A. General Topics, 24, 389–398, 1990.

Johnson, B. J., Betterton, E. A., and Craig, D.: Henry's law coefficients of formic and acetic acids, Journal of Atmospheric Chemistry, 24, 113–119, 1996.

Jost, A.: A Wind Tunnel Investigation on the Effects of Accretional Growth of Ice Hydrometeors: Implications on Microphysics and Organic Chemistry, Phd thesis, University of Mainz, Germany, 2017.

Jost, A., Szakáll, M., Diehl, K., Mitra, S. K., and Borrmann, S.: Chemistry of riming: the retention of organic and inorganic atmospheric trace constituents, Atmospheric Chemistry and Physics, 17, 9717–9732, 2017.

Kolb, C., Cox, R. A., Abbatt, J., Ammann, M., Davis, E., Donaldson, D., Garrett, B. C., George, C., Griffiths, P., Hanson, D., et al.: An overview of current issues in the uptake of atmospheric trace gases by aerosols and clouds, Atmospheric Chemistry and Physics, 10, 10 561–10 605, 2010.

Lamb, D. and Blumenstein, R.: Measurement of the entrapment of sulfur dioxide by rime ice, Atmospheric Environment (1967), 21, 1765–1772, 1987.

Lohmann, U. and Feichter, J.: Global indirect aerosol effects: a review, Atmospheric Chemistry and Physics, 5, 715–737, 2005.

Long, Y., Chaumerliac, N., Deguillaume, L., Leriche, M., and Champeau, F.: Effect of mixed-phase cloud on the chemical budget of trace gases: A modeling approach, Atmospheric Research, 97, 540–554, 2010.

Mari, C., Jacob, D. J., and Bechtold, P.: Transport and scavenging of soluble gases in a deep convective cloud, Journal of Geophysical Research: Atmospheres, 105, 22 255–22 267, 2000.

Martini, M., Allen, D. J., Pickering, K. E., Stenchikov, G. L., Richter, A., Hyer, E. J., and Loughner, C. P.: The impact of North American anthropogenic emissions and lightning on long-range transport of trace gases and their export from the continent during summers 2002 and 2004, Journal of Geophysical Research: Atmospheres, 116, 2011.

Mitra, S. and Hannemann, A.: On the scavenging of SO 2 by large and small rain drops: V. A wind tunnel and theoretical study of the desorption of SO 2 from water drops containing S (IV), Journal of atmospheric chemistry, 16, 201–218, 1993.

Pruppacher, H. R. and Klett, J. D.: Microstructure of atmospheric clouds and precipitation, Microphysics of clouds and precipitation, pp. 10–73, 2010.

Ryu, Y.-H. and Min, S.-K.: Improving Wet and Dry Deposition of Aerosols in WRF-Chem: Updates to Below-Cloud Scavenging and Coarse-Particle Dry Deposition, Journal of Advances in Modeling Earth Systems, 14, e2021MS002 792, 2022.

Schwartz, S. E.: Mass-transport considerations pertinent to aqueous phase reactions of gases in liquid-water clouds, in: Chemistry of multiphase atmospheric systems, pp. 415–471, Springer, 1986.

Scott, T. A.: Solid and liquid nitrogen, Physics Reports, 27, 89–157, 1976.

Seinfeld, J. H. and Pandis, S. N.: Atmospheric chemistry and physics: from air pollution to climate change, John Wiley & Sons, 2016.

https://doi.org/10.5194/egusphere-2024-3917
Preprint. Discussion started: 19 December 2024

Shrivastava, M., Cappa, C. D., Fan, J., Goldstein, A. H., Guenther, A. B., Jimenez, J. L., Kuang, C., Laskin, A., Martin, S. T., Ng, N. L., et al.: Recent advances in understanding secondary organic aerosol: Implications for global climate forcing, Reviews of Geophysics, 55, 509–559, 2017.

Snider, J. R. and Huang, J.: Factors influencing the retention of hydrogen peroxide and molecular oxygen in rime ice, Journal of Geophysical Research: Atmospheres, 103, 1405–1415, 1998.

Snider, J. R., Montague, D. C., and Vali, G.: Hydrogen peroxide retention in rime ice, Journal of Geophysical Research: Atmospheres, 97, 7569–7578, 1992.

Sporre, M. K., Blichner, S. M., Schrödner, R., Karset, I. H., Berntsen, T. K., Van Noije, T., Bergman, T., O'donnell, D., and Makkonen, R.: Large difference in aerosol radiative effects from BVOC-SOA treatment in three Earth system models, Atmospheric Chemistry and Physics, 20, 8953–8973, 2020.

Stuart, A. L. and Jacobson, M.: A timescale investigation of volatile chemical retention during hydrometeor freezing: Nonrime freezing and dry growth riming without spreading, Journal of Geophysical Research: Atmospheres, 108, 2003.

Stuart, A. L. and Jacobson, M.: Chemical retention during dry growth riming, Journal of Geophysical Research: Atmospheres, 109, 2004.

Szakáll, M., Debertshäuser, M., Lackner, C. P., Mayer, A., Eppers, O., Diehl, K., Theis, A., Mitra, S. K., and Borrmann, S.: Comparative study on immersion freezing utilizing single-droplet levitation methods, Atmospheric Chemistry and Physics, 21, 3289–3316, 2021.

Thibodeaux, L. J. and Mackay, D.: Handbook of chemical mass transport in the environment, CRC Press, 2010.

Tost, H., Lawrence, M. G., Brühl, C., Jöckel, P., Team, G., et al.: Uncertainties in atmospheric chemistry modelling due to convection parameterisations and subsequent scavenging, Atmospheric Chemistry and Physics, 10, 1931–1951, 2010.

Tremp, J., Mattrel, P., Fingler, S., and Giger, W.: Phenols and nitrophenols as tropospheric pollutants: emissions from automobile exhausts and phase transfer in the atmosphere, Water, Air, and Soil Pollution, 68, 113–123, 1993.

Tsigaridis, K., Daskalakis, N., Kanakidou, M., Adams, P., Artaxo, P., Bahadur, R., Balkanski, Y., Bauer, S., Bellouin, N., Benedetti, A., et al.: The AeroCom evaluation and intercomparison of organic aerosol in global models, Atmospheric Chemistry and Physics, 14, 10 845–10 895, 2014.

von Blohn, N., Diehl, K., Mitra, S., and Borrmann, S.: Wind tunnel experiments on the retention of trace gases during riming: nitric acid, hydrochloric acid, and hydrogen peroxide, Atmospheric Chemistry and Physics, 11, 11 569–11 579, 2011.

von Blohn, N., Diehl, K., Nölscher, A., Jost, A., Mitra, S. K., and Borrmann, S.: The retention of ammonia and sulfur dioxide during riming of ice particles and dendritic snow flakes: laboratory experiments in the Mainz vertical wind tunnel, Journal of Atmospheric Chemistry, 70, 131–150, 2013.

Wang, J., Krejci, R., Giangrande, S., Kuang, C., Barbosa, H. M., Brito, J., Carbone, S., Chi, X., Comstock, J., Ditas, F., et al.: Amazon boundary layer aerosol concentration sustained by vertical transport during rainfall, Nature, 539, 416–419, 2016.

Warneck, P.: Chemistry of the natural atmosphere, vol. 71, Elsevier, 1999.

Warneck, P. and Williams, J.: The atmospheric chemist's companion: Numerical data for use in the atmospheric sciences, Springer, 2012.

Williamson, C. J., Kupc, A., Axisa, D., Bilsback, K. R., Bui, T., Campuzano-Jost, P., Dollner, M., Froyd, K. D., Hodshire, A. L., Jimenez, J. L., et al.: A large source of cloud condensation nuclei from new particle formation in the tropics, Nature, 574, 399–403, 2019.

4.4 *Retention of α-pinene oxidation products and nitro-aromatic compounds during riming*

The following publication addresses the underrepresented topic of chemical retention during rime freezing processes. Riming is an important growth process of graupel and hailstones in mixed-phase zones of clouds, during which supercooled liquid droplets freeze on the surface of ice particles by contact. Compounds dissolved in the supercooled cloud droplets can remain in the ice or be released to the gas phase during freezing, which might play an important role in the vertical redistribution of these compounds in the atmosphere by convective cloud processes. This is important for estimating the availability of these compounds in the upper troposphere, where organic matter can promote new particle formation and growth. The amount of a chemical species remaining in the ice phase can be described by the retention coefficient. Up to now, only inorganic, and small organic molecules have been investigated regarding their retention during the freezing process. We performed experiments in the Mainz vertical wind tunnel under dry and wet growth conditions as well as different pH values to obtain the retention coefficients of cis-pinic acid, cis-pinonic acid and (-)-pinanediol, 4-nitrophenol, 4-nitrocatechol, 2-nitrobenzoic acid and 2-nitrophenol. Our results are in accordance with previous studies which showed a dependence between the dimensionless effective Henry's law constant H^* and the retention coefficient for inorganic and small organic molecules. Our results reveal that this correlation can also be applied to more complex organic molecules.

I was a significant contributor to this publication. Specifically, I along with CB, MG, KD, YM, AA, LG, AT, AV, and TH designed and performed the wind tunnel experiments; I along with MG, MS, AT, AV, and TH reviewed and edited the paper.

Supplementary material supporting this manuscript can be found in Section 8

Atmos. Chem. Phys., 24, 13961–13974, 2024
https://doi.org/10.5194/acp-24-13961-2024

Atmospheric Chemistry and Physics
Open Access
EGU

Retention of α-pinene oxidation products and nitro-aromatic compounds during riming

Christine Borchers[1], Jackson Seymore[2], Martanda Gautam[2], Konstantin Dörholt[3], Yannik Müller[1], Andreas Arndt[2], Laura Gömmer[2], Florian Ungeheuer[3], Miklós Szakáll[2], Stephan Borrmann[2,4], Alexander Theis[4], Alexander L. Vogel[3], and Thorsten Hoffmann[1]

[1]Department of Chemistry, Johannes Gutenberg University, Mainz, Germany
[2]Institute for Atmospheric Physics, Johannes Gutenberg University, Mainz, Germany
[3]Institute for Atmospheric and Environmental Sciences, Goethe University Frankfurt, Frankfurt am Main, Germany
[4]Particle Chemistry Department, Max Planck Institute for Chemistry, Mainz, Germany

Correspondence: Thorsten Hoffmann (t.hoffmann@uni-mainz.de)

Received: 15 May 2024 – Discussion started: 14 June 2024
Revised: 10 October 2024 – Accepted: 26 October 2024 – Published: 17 December 2024

Abstract. Riming is an important growth process of graupel and hailstones in the mixed-phase zones of clouds, during which supercooled liquid droplets freeze on the surface of ice particles by contact. Compounds dissolved in the supercooled cloud droplets can remain in the ice or be released to the gas phase during freezing, which might play an important role in the vertical redistribution of these compounds in the atmosphere by convective cloud processes. This is important for estimating the availability of these compounds in the upper troposphere, where organic matter can promote new particle formation and growth. The amount of organic material remaining in the ice phase can be described by the retention coefficient. Experiments were performed in the Mainz vertical wind tunnel under dry and wet growth conditions (temperature from −12 to −3 °C and a liquid water content (LWC) of $0.9 \pm 0.2\,\mathrm{g\,m^{-3}}$ and $2.2 \pm 0.2\,\mathrm{g\,m^{-3}}$) as well as with different pH values (4 and 5.6) to obtain the retention coefficients of α-pinene oxidation products and nitro-aromatic compounds. For *cis*-pinic acid, *cis*-pinonic acid, and (−)-pinanediol, mean retention coefficients of 0.96 ± 0.07, 0.92 ± 0.11, and 0.98 ± 0.08 were obtained. 4-Nitrophenol, 4-nitrocatechol, 2-nitrobenzoic acid, and 2-nitrophenol showed mean retention coefficients of 1.01 ± 0.07, 1.01 ± 0.14, 0.99 ± 0.04, and 0.21 ± 0.12. Only the retention coefficient of 2-nitrophenol showed a dependence on temperature, growth regime, and pH. This is in accordance with previous studies, which showed a dependence between the dimensionless effective Henry's law constant H^* and the retention coefficient for inorganic and small organic molecules. Our results reveal that this correlation can also be applied to more complex organic molecules and that retention under these conditions is not a significant factor for molecules with H^* below 10^3, while retention close to 1 can be expected for compounds with H^* above 10^8.

1 Introduction

The observation of a large number of small particles at high altitudes, which has already been made several times, is attributed to the formation of new particles (new particle formation, NPF) through the process of homogeneous nucleation and early growth. The rate of NPF is strongly dependent on the concentration of low-volatility vapors, the temperature, and the number of particles that are present. Low-volatility vapors are for example sulfuric acid, which is formed from the reaction of sulfur dioxide and hydroxyl radicals or via oxidation of dimethyl sulfide, as well as highly oxidized organic compounds (Xiao et al., 2023; Williamson et al., 2019; Andreae et al., 2018; Kerminen et al., 2018; Twohy et al., 2002). A common explanation for the presence of this high number of small particles at high altitudes is the uplift

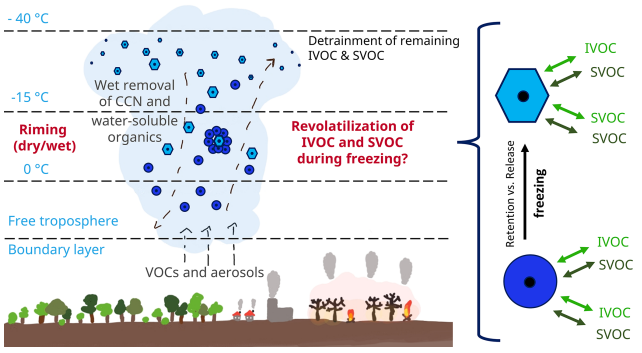

Figure 1. Water-soluble intermediate-volatile and semi-volatile organic compounds (IVOCs and SVOCs) can be dissolved in water droplets (dark blue circles), which can be transported upwards by deep convection. In the mixed-phase zone of the clouds, the water droplets can collide with ice particles (light blue hexagons), resulting in riming.

of condensable vapors with simultaneous removal of existing aerosol particles in deep convective clouds. This removal of larger particles reduces the sinks for small particles and condensable vapors, supporting NPF (Clarke et al., 1998). However, Williamson et al. (2019) showed that tropical convection does not lead to uniquely low particle numbers for larger particles. They then argue that there must be a stronger source of condensable vapors at high altitudes in the marine tropics than in other regions and that most of the models used underestimated available organic matter at high altitudes and predict less NPF in these regions. It is therefore important to investigate the possible transport mechanism of organic precursor components that could lead to NPF at high altitudes (Bardakov et al., 2022).

Among other mechanisms, deep convection plays an important role in the transport of trace substances and aerosols into the upper troposphere. In this region, these substances have a longer atmospheric lifetime, thereby increasing the likelihood of long-range transport. Additionally, they can contribute to NPF (Bardakov et al., 2022; Barth et al., 2007a, b). The fraction that arrives in the upper troposphere is influenced by the liquid-phase and mixed-phase scavenging of the substances. Aircraft measurements from the USA in thunderstorm inflow and outflow regions demonstrate that water-soluble trace gases, such as H_2O_2, are removed with efficiencies between 79 % and 97 %, which are also influenced by the process of retention (Bela et al., 2018; Barth et al., 2016).

Figure 1 shows vertical transport mechanisms of intermediate-volatile and semi-volatile organic compounds (IVOCs and SVOCs).

Organic compounds in the atmosphere can be categorized into different groups depending on their source, such as biogenic, anthropogenic, or compounds originating from the combustion of biomass (de Gouw and Jimenez, 2009). Nitro-aromatic compounds can be formed directly from the combustion of coal or wood but can also be formed as secondary products from the reaction of phenols or cresols with NO_x (Wang et al., 2020; Harrison et al., 2005). Terrestrial vegetation emits large quantities of volatile organic compounds (VOCs) such as isoprene and various monoterpenes (MTs), with the most important MT, α-pinene, contributing around one-third of global MT emissions (Sindelarova et al., 2014). In the atmosphere, oxidation by OH radicals, ozone, or NO_3 radicals results in various products spanning orders of magnitude in volatility. Products such as 2-methyl tetrols, pinanediol, terpenylic acid, pinonic acid, and pinic acid have been described as major oxidation products (Kołodziejczyk et al., 2020; Bianchi et al., 2019; Nozière et al., 2015; Müller et al., 2012; Kroll and Seinfeld, 2008; Claeys et al., 2004; Hoffmann et al., 1997). At standard conditions, the saturation vapor pressure of these oxidation products is too large to be relevant for new particle formation. Highly oxygenated organic molecules (HOMs) exhibit a sufficient low vapor pressure for NPF (Bianchi et al., 2019); however, their formation via autoxidation, a rapid OH-radical-induced oxidation process in the atmosphere, is suppressed at low temperatures (Stolzenburg et al., 2018). Hence, the higher-volatility major oxidation products of isoprene and monoterpenes might be relevant for NPF in the upper troposphere, where HOM formation is suppressed and the colder temperatures cause saturation of the major oxidation products, which are classified as SVOCs at standard conditions. Both classes of compounds focused on in this study, i.e., pinene oxidation products and nitro-aromatic compounds, are IVOCs (saturation mass concentration C^*, $300 < C^* < 3\times10^6\,\mu g\,m^{-3}$) or SVOCs ($0.3 < C^* < 300\,\mu g\,m^{-3}$) (Simon et al., 2020; Andreae et al., 2018).

Water-soluble IVOCs and SVOCs can be dissolved in water droplets (dark blue circles in Fig. 1), which can be transported upwards via deep convection. In the mixed-phase zone of clouds, retention or release of IVOCs and SVOCs during riming can occur. Riming describes the collision and freezing of supercooled water droplets on the surface of hydrometeors such as a graupel or snowflakes (light blue hexagon in Fig. 1), which leads to their growth. The organic compounds can be trapped in the ice phase and then washed out by precipitation, or they can return to the gas phase by volatilization during freezing. This revolatilization leads to a vertical redistribution in the atmosphere and could explain the occurrence of semi-volatile organic compounds at high altitudes in regions with deep convection. However, if the organic substances remain in the ice phase during freezing, they could also be transported further upwards and released into the gas phase by sublimation of the ice particles there (Pruppacher and Klett, 2010; Snider and Huang, 1998).

The proportion of the compound that remains in the ice can be described by the retention coefficient R, which indicates the relative fraction of the trapped compound with a value between 0 and 1 (Bela et al., 2018; Stuart and Jacobson, 2003; Snider et al., 1992; Iribarne and Pyshnov, 1990).

The retention of a compound is influenced by its chemical properties, such as the dimensionless effective Henry's law solubility constant H^*, as well as physical parameters such as temperature, droplet size, liquid water content in the cloud, ventilation, and potentially the pH of the droplet, which also influences H^*. Compounds with a small H^* are more likely to return to the gas phase during riming, which results in a lower retention coefficient. In addition, external conditions have a greater influence on retention for these kind of compounds, which is in contrast to compounds with high H^* (Cuchiara et al., 2023; Jost et al., 2017; Stuart and Jacobson, 2004, 2003).

Previous measurements of inorganic and small organic species in the wind tunnel in Mainz confirm the correlation between H^* and R as well as the stronger dependence of retention on external factors such as temperature for lower H^*. Hydrochloric acid, nitric acid, malonic acid, and oxalic acid are characterized by a high H^* value and remain completely in the ice phase during freezing. Compounds with more moderate H^* values such as ammonia, hydrogen peroxide, formic acid, and acetic acid have retention factors of 0.92 ± 0.21, 0.64 ± 0.11, 0.68 ± 0.09, and 0.72 ± 0.16. Retention of the organic compounds shows a dependence on temperature and ventilation. Additionally, sulfur dioxide shows both the lowest H^* value and retention coefficient (0.46 ± 0.16) of the compounds discussed, with a dependence on external conditions as well (Jost et al., 2017; v. Blohn et al., 2013; von Blohn et al., 2011).

Up to now, only inorganic and small organic molecules have been investigated with regard to their retention during the freezing process. Measurements of rain, hail, and cloud water have already shown that they contain α-pinene oxidation products and nitrophenols (Spolnik et al., 2020; Desyaterik et al., 2013; Ganranoo et al., 2010). It is therefore likely that these compounds are also present in the supercooled droplets within the mixed-phase zones of clouds. In contrast to the smaller organic molecules and inorganic compounds, the retention coefficients for α-pinene oxidation products and nitrophenols are unknown. In this study, therefore, the retention coefficients of three α-pinene oxidation products (pinonic acid, pinic acid, and pinanediol) and four nitro-aromatic compounds (2-nitrobenzoic acid, 4-nitrocatechol, 4-nitrophenol, and 2-nitrophenol) are investigated in a series of wind tunnel experiments under simulated atmospheric conditions.

2 Experimental procedures

2.1 Mainz vertical wind tunnel

The experiments were carried out in the vertical wind tunnel of Johannes Gutenberg University of Mainz, shown schematically in Fig. 2. Here, hydrometeors ranging from a few tens of micrometers to centimeters can float freely in a vertical airstream at their terminal fall velocity. The prevailing conditions such as ventilation, mass, and heat transfer are very similar to those in the atmosphere (Pruppacher and Klett, 2010). A vacuum pump continuously sucked dried ambient air through the system to produce an airflow in the wind tunnel. For riming experiments the tunnel was cooled down to $-18\,^{\circ}\mathrm{C}$, and water droplets were produced using up to four spray nozzles. These droplets were transported via the airflow to the experimental region (red circle, zoomed-in red rectangle in Fig. 2). In the experimental region the supercooled droplets collided with three different surfaces – a simulated graupel, a liquid nitrogen finger, and Teflon-coated bars – and froze on the substrate. A detailed description of the experiments is provided in Sect. 2.3, "Retention measurements". Further details on the wind tunnel can be found in two reviews by Diehl et al. (2011) and Szakáll et al. (2010).

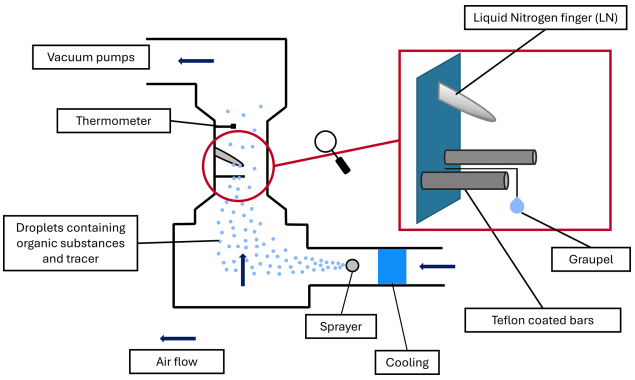

Figure 2. Schematic of the wind tunnel. Cooled air transported the generated water droplets containing the compounds into the experimental region (red circle). Red rectangle – the enlarged experimental area shows the three surfaces on which the riming took place: graupel, the liquid nitrogen finger, and Teflon-coated bars.

2.2 Growth regimes

For riming, a distinction is made between dry and wet growth conditions, which are determined by the combination of temperature, liquid water content, and ventilation. During freezing latent heat is released, which warms the surface of the rime collectors. Under dry growth conditions the surface temperature of the rime collector remains well below $0\,^{\circ}\mathrm{C}$, and all the accreted cloud water freezes within some milliseconds on the rime collector, preserving a close-to-spherical shape. The surface temperature increases with increasing liquid water content, droplet size, and collision frequency of the droplets with the hydrometeor. If the temperature rises to a maximum value of $0\,^{\circ}\mathrm{C}$, wet growth conditions are reached. At this point, not all the water that has collided with the rime collector freezes immediately. During wet growth, the freezing rate of an element of liquid input is rather low in comparison to dry growth conditions, resulting in a dense ice structure (Pruppacher and Klett, 2010; Macklin, 1961; List, 1960).

The earlier wind tunnel measurements on retention coefficients (Jost et al., 2017; v. Blohn et al., 2013; von Blohn et al., 2011) focused solely on retention during dry growth conditions. Thus, the question of to what extent wet growth conditions affect retention remained. For example, Michael and Stuart (2009) found in their theoretical study that during wet growth conditions, H^* is an important but not a dominant factor. They observed that retention increased with increasing H^* (from 300 to 3×10^6) and then leveled off with further increasing H^*, resulting in low retention values for compounds with high H^* such as HCl. Here other factors like the ice–liquid interface supercooling and the liquid water content are major determiners of the extent of retention. In the present study, the measurements were carried out under dry and wet growth conditions. However, unlike the study of Michael and Stuart (2009), we did not observe the droplets shedding off during these experiments. Calculations of the surface temperature during the growth of graupel reveals that under our wet growth conditions, the surface temperature varied between -0.8 and -2.2 °C for -3 and -5 °C ambient temperature, respectively, and had a measured LWC of $2.2\,\mathrm{g\,m^{-3}}$ (Theis et al., 2022; v. Blohn et al., 2009; Pflaum and Pruppacher, 1979). For temperatures higher than -3 °C, no freezing was observed on the Teflon-coated bars and little freezing could be observed on the graupel. During wet growth experiments, small cloud droplets coalesced and formed larger millimeter-sized drops before freezing. A photo of an example ice sample is provided in the Supplement (Fig. S1 in the Supplement). This coalescence of droplets during our experiments is representative of the wet growth of graupel rather than the wet growth of hail – where the accreted liquid water is shed off from the surface due to the faster fall speeds.

2.3 Retention measurements

Dilute aqueous solutions with different compositions were used for the experiments. Single-component measurements were carried out for the α-pinene oxidation products and 2-nitrophenol. The aqueous solution to be analyzed contained one of the compounds of interest (pinonic acid, pinic acid, pinanediol, or 2-nitrophenol) and sodium bromide (NaBr; Sigma-Aldrich, $\geq 99\,\%$). For the other nitroaromatic compounds (2-nitrobenzoic acid, 4-nitrocatechol, and 4-nitrophenol), a mixture of all organics and NaBr was used, an experimental setup that comes closer to the complex conditions in the atmosphere. All samples contained NaBr as an internal standard (IS) to account for dilution and evaporation effects. The retention of NaBr is assumed to be 1; i.e., NaBr remains completely in the droplets during freezing. HCl (30 %) was added if the measurements were carried out at a pH value of 4. The concentrations of the chemicals used are shown in Table 1.

To generate the supercooled droplets, the solution containing the analyte and the IS was nebulized with a gas stream of nitrogen ($> 99.8\,\%$) and either two or four spray nozzles, depending on the experiment. Two spray nozzles and a nitrogen flow of $20\,\mathrm{L\,min^{-1}}$ were used for dry growth and four spray nozzles and a flow of $24\,\mathrm{L\,min^{-1}}$ for wet growth conditions. The number of spray nozzles influences the liquid water content (LWC) and thus the growth regime.

For dry growth conditions a lower LWC is required; therefore only two spray nozzles were used. The resulting droplet size distribution in the wind tunnel was measured using a custom in-line digital holographic instrument, similar to the holographic imaging and velocimetry instrument for small cloud ice (HIVIS) described by Weitzel et al. (2020). The measurements were not taken simultaneously to each retention experiment but measured independently under the same conditions during the retention experiments. After the cloud of droplets was produced, a camera (Basler acA2040) captured the holograms containing the images of the droplets at 90 fps (frames per second). Typical measurement time was 1 minute. Approximately 5400 holograms were reconstructed and analyzed for each measurement with two and four nozzles. Using a telecentric lens with a 0.5 magnification, the pixel size of the holograms was $2.72\,\mu\mathrm{m} \times 2.72\,\mu\mathrm{m}$, which yielded a sample area and volume of $5.57 \times 5.57\,\mathrm{mm^2}$ and $2.48\,\mathrm{cm^3}$, respectively. For the reconstruction of the holograms, a depth of 8 cm was chosen as this represents the central part of the measurement section where the collectors were exposed to the cloud of supercooled droplets during the experiments. The holograms were reconstructed at each $\Delta z = 100\,\mu\mathrm{m}$ distance along the optical axis using the method of Fugal et al. (2004). This produced an in-focus image of the droplets independent of their location within the sample volume. The particle sizes were obtained from the particle detection algorithm of Fugal et al. (2009), which determined the normalized number and volume distributions. Figure 3a shows the number distribution of the supercooled droplets in the measurement section of the tunnel when two spray nozzles were used. Figure 3b shows the volume distribution of the droplets, which represents the normalized cloud liquid water content (LWC) per size interval. We observed no difference in the distribution when using four nozzles (see Fig. S2). The LWC was measured using a dew-point meter (DP3-D/SH, MBW Calibration Ltd., Wettingen, Switzerland) in conjunction with a 5 m long heated pipe. Wind tunnel air was sampled isokinetically through the heated pipe to evaporate the droplets. The absolute humidity was then obtained from the dew point measurement. In a second step, a droplet separator was installed at the inlet to the heated tube to measure the dew point of the wind tunnel air without droplets. The difference between the two absolute humidities gives an LWC of $0.9 \pm 0.2\,\mathrm{g\,m^{-3}}$ for dry growth and $2.2 \pm 0.2\,\mathrm{g\,m^{-3}}$ for wet growth conditions.

During retention measurements, the droplets were transported downstream of the sprayer into the experimental section. The distance between the sprayer and the experimental region is approx. 3 m (Jost, 2012). In the experimental sec-

Table 1. Concentrations of the investigated solutions.

Compound	Concentration (μmol L^{-1})	Label, purity	IS concentration NaBr (μmol L^{-1})
cis-Pinonic acid	10	Sigma Aldrich, 98 %	10
cis-Pinic acid	10	Synthesized, N/A	10
(1R,2R,3S,5R)-(−)-Pinanediol	15	Merck, 99 %	10
2-Nitrophenol	30	Thermo Scientific, 99 %	10
2-Nitrobenzoic acid	10	Thermo Scientific, 95 %	10
4-Nitrocatechol	10	Thermo Scientific, ≥ 98 %	10
4-Nitrophenol	10	Alfa Aesar, 99 %	10

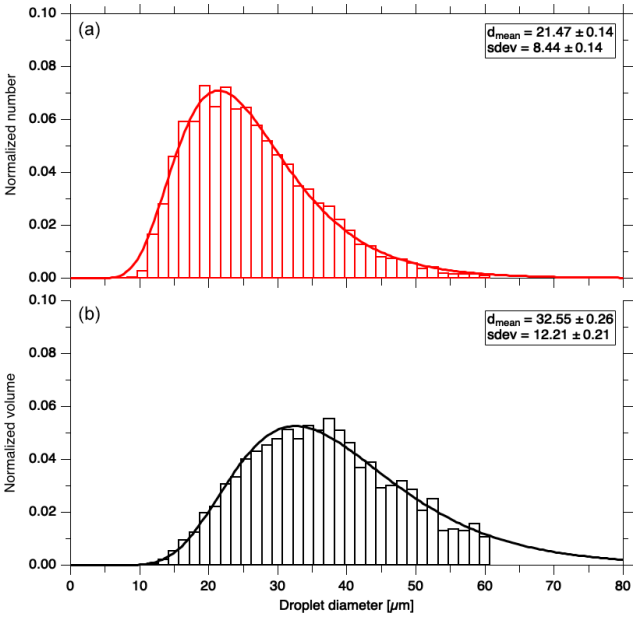

Figure 3. Normalized droplet number **(a)** and volume distribution **(b)** of the supercooled droplets generated using two spraying nozzles. The lines represent log-normal fit functions.

tion, the supercooled droplets collided with three different surfaces that were used as rime ice collectors and froze on them. The first surface was a Teflon-coated bar (FEP; outer diameter 6 mm) and the second was an ice sphere (graupel) with a diameter of 7 mm, which comes closer to real atmospheric sizes for graupel. According to the American Meteorological Society glossary of meteorology, graupel is defined as rimed particles with diameters less than 5 mm; larger ones are called hailstones. However, we refer to the particle investigated as graupel according to the flow conditions present rather than the particle size. The larger diameter was necessary to obtain a sufficient sample volume for analysis. The last surface was a cold tube made of Teflon (PFA) that was constantly filled with liquid nitrogen (LN finger tube). This sample determined the liquid-phase concentration of the droplets immediately before riming occurs. At the surface of the LN finger tube, freezing is so fast that the retention can be assumed to be 1, and the concentration of the droplets can be determined before riming.

To produce the simulated graupel, a silicon mold was filled with ultra-pure water and frozen. The graupel were "captively floated" to avoid the loss of graupel and any contamination on contact with the wind tunnel walls. For this purpose, they were attached to a nylon fiber with a diameter of 80 µm. Under these conditions, the rime collectors were exposed to the airflow containing the supercooled droplets at 3 m s^{-1}, which corresponds to a typical fall velocity of graupel. (Wang and Kubicek, 2013; Pruppacher and Klett, 2010). The ice samples were collected after each experimental run and stored at −25 °C until they were melted for the chemical analysis.

2.4 UHPLC-HRMS analysis

For analysis, the ice samples were melted and filtered through polyamide (PA) membranes (pore size – 0.20 µm; Altmann Analytik) to remove potential particles without affecting the concentration of the analytes. Analysis was performed in triplicate using a Dionex UltiMate 3000 ultra-high-performance liquid chromatography (UHPLC) system coupled to a heated electrospray ionization source (HESI) or atmospheric pressure chemical ionization (APCI) and with a high-resolution Q-Exactive Orbitrap mass spectrometer (HRMS) (all Thermo Fisher Scientific). A Hypersil GOLD C18, 50 × 2.0 mm column with 1.9 µm particle size (Thermo Fisher Scientific) was used for the chromatography. Eluent A consisted of 98 % liguid chromatography–mass spectrometry (LC-MS) grade water (Thermo Fisher Scientific) with 0.04 % formic acid and acetonitrile (VWR Chemicals); eluent B consisted of 98 % acetonitrile (ACN) and water, and the injection volume was 5 µL. Different H_2O/ACN gradients were used for the different compounds. For pinonic acid, pinic acid, pinanediol, 2-nitrobenzoic acid, 4-nitrocatechol, and 4-nitrophenol, a flow rate of 0.5 mL min^{-1} and a gradient as described in the following were used: starting with 2 % eluent B isocratically for 1 min, increasing to 20 % B over 2.5 min, then further increasing to 90 % over 1.5 min, after which B was held at 90 % for 4 min, decreased to 2 % over 0.5 min, and held again for 1.5 min. For pinanediol, a

post-column flow of 50 mmol L^{-1} NH_4OH in MeOH was added after 1 min at a flow rate of 0.1 mL min^{-1} to enhance ionization. The HESI source was used in negative mode, resulting in the formation of deprotonated molecular ions. Sheath gas and auxiliary gas flow were 40 and 20 a.u. (arbitrary unit), respectively. The temperature of the auxiliary gas heater was 150 °C, and the capillary temperature was 350 °C. The sprayer voltage was set to −4.00 kV.

A different gradient with a flow rate of 0.3 mL min^{-1} was used for 2-nitrophenol. Starting with 2 % eluent B isocratically for 1 min, increasing to 20 % B over 2.5 min, then further increasing to 90 % over 1.5 min, after which B was again held at 90 % for 0.3 min, decreased to 2 % over 0.2 min, and held again for 0.5 min. To further enhance ionization, a post-column flow of 50 mmol L^{-1} NH_4OH in MeOH was added after 1 min at a flow rate of 0.1 mL min^{-1}. The APCI source was used in negative mode, resulting in the formation of deprotonated molecular ions. Sheath gas and auxiliary gas flow were 23 and 5 a.u., respectively. The vaporizer temperature was 375 °C, and the capillary temperature was 350 °C.

2.5 Calculation of the retention coefficient

Equation (1) was used for compounds with a retention coefficient R close to 1:

$$R = \frac{c^{\text{sample}}_{\text{compound}} / c^{\text{LN}}_{\text{compound}}}{c^{\text{sample}}_{\text{IS}} / c^{\text{LN}}_{\text{IS}}}. \quad (1)$$

The numerator describes the ratio between the concentration of the compound of interest in the ice sample ($c^{\text{sample}}_{\text{compound}}$) (Teflon coated bars or graupel) and in the LN finger sample ($c^{\text{LN}}_{\text{compound}}$). The denominator describes the same ratio but for the IS ($c^{\text{sample}}_{\text{IS}}/c^{\text{LN}}_{\text{IS}}$). Thus, it is not necessary to consider a dilution, evaporation, and desorption correction as these effects change both the compound and IS concentrations in the nitrogen finger sample accordingly. Therefore, a change in this ratio is solely an effect of the retention of the compound during the riming process.

The calculation is different for compounds with a lower effective Henry's law constant (below 10^4), which leads to higher desorption. These compounds are transferred to the gas phase in larger amounts before and during the freezing process, resulting in a higher gas-phase concentration in the tunnel. Therefore, it cannot be ruled out that the measured concentrations of the LN finger tube samples could be influenced by additional adsorption out of gas-phase components. This would no longer provide a suitable correction for determining the retention coefficient.

As the LN finger sample is not available, the sprayer sample (the solution from which the droplets are produced) is used instead. As the distance between the two sampling points (sprayer and graupel/bar) is large, it is necessary to determine the amount of compound that is transferred to the gas phase before freezing. The desorption correction coefficient D (see Eq. S3 in the Supplement) will be utilized. A detailed description of the desorption correction coefficient can be found in the Supplement.

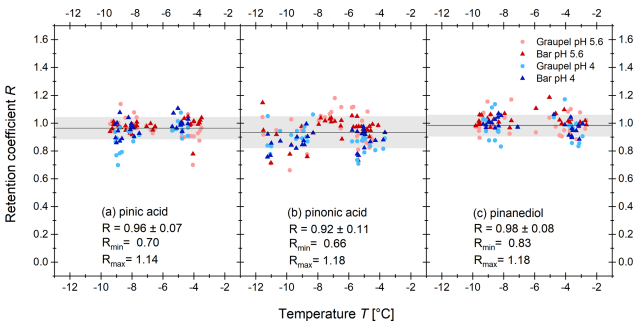

Figure 4. Experimentally determined retention coefficients of **(a)** pinic acid, **(b)** pinonic acid, and **(c)** pinanediol as a function of the temperature during the experiment for different rime collectors. The circles represent the graupel samples and the triangles the Teflon-coated bars. For the blue symbols, the pH was adjusted to 4 by adding HCl (30 %), the red symbols are without adding HCl. The solid black line represents the mean of all measurements, and the gray area represents 1 standard deviation.

To calculate the retention coefficient R for compounds with a lower retention coefficient, Eq. (1) was extended to include the desorption correction coefficient using the sprayer solution sample instead of the LN finger (see Eq. 2):

$$R = \frac{c^{\text{sample}}_{\text{compound}} / c^{\text{sprayer}}_{\text{compound}}}{c^{\text{sample}}_{\text{IS}} / c^{\text{sprayer}}_{\text{IS}} \cdot D}. \quad (2)$$

Equations (1) and (2) yield identical results for compounds with a desorption correction coefficient of approximately 1. This is illustrated using pinic acid as a representative example in the Supplement (Fig. S3).

3 Results and discussion

3.1 Retention measurements

The results of the retention measurements for the α-pinene oxidation products are shown in Fig. 4; those for 4-nitrocatechol, nitrobenzoic acid, and 4-nitrophenol are shown in Fig. 5; and the desorption-corrected R for 2-nitrophenol in Fig. 6.

3.1.1 Pinic acid and pinonic acid

Figure 4 shows the results for (panel a) pinic and (panel b) pinonic acids. Pinic acid and pinonic acid both show no pH dependence, temperature dependence, or influence from the rime regime. This agrees with the earlier findings for compounds with high H^*. The retention coefficients for pinic acid vary between 0.70 and 1.14 with a mean value of

0.96 ± 0.07. For pinonic acid, a mean retention coefficient of 0.92 ± 0.11 was determined. The variation in the measured values of R is greater than that for pinic acid and lies between 0.66 and 1.18. This is probably due to the lower H^*, which makes pinonic acid more sensitive to slight changes in the experimental conditions. The scatter of the values is comparable to that observed in other studies on retention. Theoretical and experimental studies have demonstrated that the retention of compounds with a low H^* is dependent on the freezing conditions (Jost et al., 2017; v. Blohn et al., 2013; von Blohn et al., 2011; Stuart and Jacobson, 2004, 2003). The results shown here indicate that slight differences in freezing conditions across the experiments may exert an influence on the retention of compounds despite their high H^* values.

3.1.2 Pinanediol

The results for pinanediol are depicted in Fig. 4c. No effect on the investigated parameters could be found for this diol. The mean retention coefficient was 0.98 ± 0.08 with a minimum value of 0.83 and a maximum value of 1.18, which is an exception to previous findings (Jost et al., 2017). In comparison to pinic and pinonic acid, pinanediol showed a lower H^* (see Table 3). A lower retention coefficient is expected for compounds in this range, as well as a dependence on temperature. However, no temperature, pH, or growth regime dependence was seen. This deviation from the expected behavior could be because the Henry's law constant for pinanediol is estimated using the bond method implemented in the HENRYWIN™ software as part of EPI Suite™. The bond method breaks down the molecule into a sum of the individual bonds that make up the compound. The exact structure and spatial orientation of the molecule is not considered. Due to the large deviations of the polyols in the original method by Hine and Mookerjee (1975), further correction factors were included in the method. However, the predictions are less accurate for molecules with a more complex structure (Meylan and Howard, 1991; Hine and Mookerjee, 1975). Pinanediol is a cyclic diol. Due to its capped ring form, it is sterically hindered, and thus the potential interactions between the OH groups are not considered by the model. Since there are no experimental data for the Henry's law constant, there is no current alternative to the estimation.

3.1.3 4-Nitrocatechol and 4-nitrophenol

The results for 4-nitrocatechol and 4-nitrophenol are shown in Fig. 5a and b. Overall, no pH or temperature dependence is recognizable. Furthermore, no difference between wet and dry growth conditions can be observed. This agrees with the current literature. As Stuart and Jacobson (2004, 2003) have shown, a temperature or pH dependence is not expected for compounds with high effective Henry's law constants, such as 4-nitrocatechol or 4-nitrophenol. Mean retention coefficients of 1.01 ± 0.14 and 1.01 ± 0.07 were determined for 4-nitrocatechol and 4-nitrophenol, respectively. For 4-nitrocatechol, the derived retention coefficients showed a large scatter that has no current explanation. A minimum value of 0.63 and a maximum value of 1.41 was obtained. 4-Nitrophenol showed a smaller scatter with values between 0.79 and 1.28.

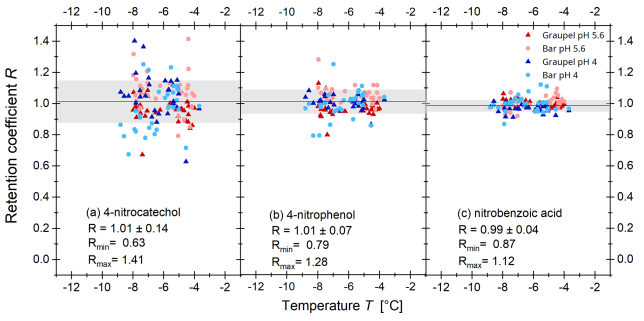

Figure 5. Experimentally determined retention coefficients of **(a)** 4-nitrocatechol, **(b)** 4-nitrophenol, and **(c)** nitrobenzoic acid as a function of the temperature during the experiment for different riming collectors. The circles represent the graupel samples and the triangles the bars. For the blue symbols, the pH was adjusted to 4 by adding HCl (30 %), the red symbols are without adding HCl. The black line represents the mean of all measurements, and the gray area represents 1 standard deviation.

3.1.4 2-Nitrobenzoic acid

For 2-nitrobenzoic acid in Fig. 5c, no dependence on the investigated parameters was found. The average retention coefficient is 0.99 ± 0.04, with the lowest scatter among the measured compounds. The smallest value measured was 0.87 and the largest 1.12. This is probably because 2-nitrobenzoic acid has the lowest pK_a value of all the compounds studied. In the pH range investigated, most of the 2-nitrobenzoic acid molecules are deprotonated, unlike the other components studied. This makes a transition into the gas phase less likely, and therefore small differences in the measurement conditions have less influence on the results.

3.1.5 2-Nitrophenol

2-Nitrophenol (Fig. 6) showed significantly lower retention coefficients than the other compounds presented above. The retention coefficients shown here are desorption corrected according to Eq. (2). At pH 4, the different rime collectors (Teflon-coated bar, graupel) showed a statistically significant (significance level $\alpha = 0.05$) negative temperature dependence (lines and equations in Fig. 6; Table 2). The bar samples show a slightly stronger temperature dependence than the graupel samples. This is probably due to the metal rod inside the Teflon-coated bar and the resulting faster heat transfer. It is also noticeable in these measurements that the graupel samples (light red and light blue circles in Fig. 6b)

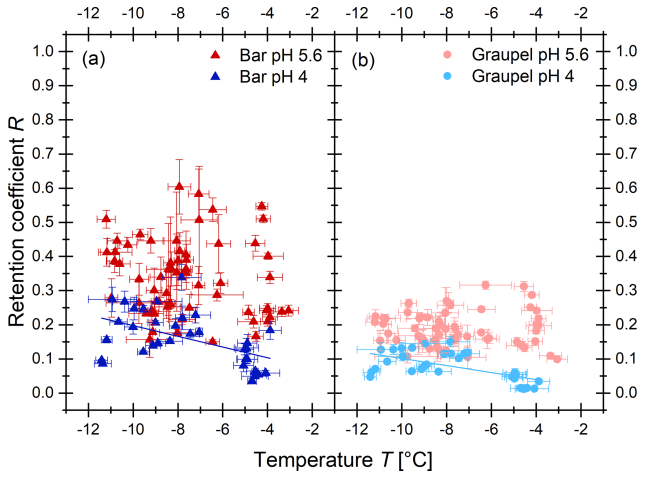

Figure 6. Experimentally determined desorption-corrected retention coefficients of 2-nitrophenol as a function of the temperature during the experiment for different rime collectors. The triangles represent the Teflon-coated bar samples **(a)** and the circles the graupel **(b)**. For the blue symbols, the pH was adjusted to 4 by adding HCl (30 %); the red symbols are without adding HCl. The line represents a linear fit.

have an overall lower retention coefficient than the bar samples (red and blue triangles in Fig. 6a). This might also be explained by the metal rod inside the Teflon-coated bar. The faster heat transfer leads to a shorter freezing time and thus to a higher retention coefficient. At a pH value of 5.6, no statistically significant negative temperature trend could be determined. This could be attributed to the greater scattering of the values, which is presumably caused by fluctuations in the conditions in the wind tunnel and slight variations in the pH value of the solution utilized. The fluctuation in the values could conceal an existing temperature trend.

The data points (Fig. 6) below −6 °C were obtained from dry growth conditions, while the ones higher than that represent wet growth conditions. A closer inspection of the data reveals that the temperature dependency might also be a result of the riming regimes. When separating the data between the two regimes, the temperature dependency vanishes. Therefore, the difference in retention values between wet and dry growth conditions might be due to the longer freezing times of the accreted and coalesced droplets. The droplets accreted during the wet growth regime remained liquid for some time and formed a larger, millimeter-sized drop before they froze. This means that dissolved 2-nitrophenol was able to further desorb from the drops before ice shell formation occurred, which reduces further expulsion from the freezing droplet. This resulted in slightly lower retention values for the rime collectors grown during wet growth. Considering the absolute retention values for wet growth, it becomes apparent that 2-nitrophenol will not be retained in atmospherically significant amounts during wet growth conditions. However, as the values between dry and wet growth

Table 2. Measured retention coefficients of 2-nitrophenol and their temperature dependencies.

Conditions	Mean retention coefficient R	Temperature dependency of R
Bar pH 5.6	0.34 ± 0.11	–
Graupel pH 5.6	0.19 ± 0.05	–
Bar pH 4	0.16 ± 0.07	$R_{B_4} = (-0.016 \pm 0.005)$ $T + (0.041 \pm 0.037)$
Graupel pH 4	0.08 ± 0.04	$R_{G_4} = (-0.010 \pm 0.002)$ $T + (-0.002 \pm 0.019)$

overlap within the experimental uncertainty, a temperature dependency is provided here, which is applicable within the investigated temperature and growth condition range simulated in the present study. As the temperature dependence in the analyzed range has only a minor influence on the retention compared to the data scattering, the mean values were determined for all sets of measurements. The mean retention coefficients for the various riming conditions are shown in Table 2. The overall mean retention coefficient was determined to be 0.21 ± 0.12. The measured values of R were between a minimum of 0.01 and a maximum of 0.60.

In addition to the dependence on temperature, growth regime, and the riming collectors already discussed, the pH dependence was also analyzed, as retention is also strongly dependent on the dissociation of the molecules. As the retention for the rime collectors is different, the comparisons are only carried out within the same collectors. The mean retention coefficients for the graupel samples at pH 5.6 and pH 4 were 0.19 ± 0.05 and 0.08 ± 0.04, respectively. At pH 5.6 it is more likely that 2-nitrophenol is dissociated in comparison to at pH 4. A dissociated molecule needs to be neutralized by a proton before leaving the droplet during riming. At pH 5.6, more molecules are available that do not evaporate without recombination, which might explain the higher retention coefficient.

3.2 Relationship between the Henry's law constant and retention

Jost et al. (2017) have shown a correlation between the retention coefficient R and the dimensionless effective Henry's law constant H^* ($H^* = K_H \cdot \overline{R}T$, with K_H – effective Henry's law constant; $\overline{R}$ – gas constant; and T – temperature) for inorganic and small organic molecules, which can be described by Eq. (3).

$$R(H^*) = \left(1 + \left(a/H^*\right)^b\right)^{-1}, \quad (3)$$

where R is the retention coefficient, H^* is the dimensionless effective Henry's law constant, and a and b are constants that are determined by a fit. To test whether this relation-

ship is also applicable to the larger organic molecules investigated here, the mean values of retention coefficients of the compounds were plotted against their dimensionless effective Henry's law constants (Fig. 7). H^* was determined for the investigated pH values and at 298 K. Since most of the compounds analyzed in this study did not show any pH dependence within the pH range of 4–5.6, a pH value of 4 was used for the calculation of H^* for these compounds. This is a typical value found in cloud water samples (Pye et al., 2020; Löflund et al., 2002). For 2-nitrophenol, the mean retention coefficient for each of the pH values (pH 4 and 5.6) was calculated and plotted (Fig. 7). The fact that a pH dependence was only found for 2-nitrophenol is consistent with the literature. A pH dependence is only to be expected for compounds with low H^*. Additionally, a dependence is expected primarily in a pH range near the pK_a value, as the impact on the ratio between dissociated and non-dissociated molecules is most pronounced in this range (Reijenga et al., 2013; Stuart and Jacobson, 2003). The pK_a values of pinic acid and pinonic acid are the most similar to the investigated pH values. However, the H^* values seem to be too high to detect an influence of pH on the measurements. The calculated values of H^* are listed in Table 3. Since there are no measured Henry's law constants nor reaction enthalpies for some of the more complex organic compounds, these were predicted using the bond method of the HENRYWIN™ software, which provides the values for 298 K.

The compounds measured in this study are the colored, filled symbols in Fig. 7; the ones measured by Jost et al.(2017), v. Blohn et al. (2013), von Blohn et al. (2011), and in earlier investigations in the wind tunnel are the gray, half-filled symbols. The dashed gray line represents the fit for the gray, half-filled symbols, i.e., previous measurements. Since the retention of formaldehyde, as shown in Jost et al. (2017), depends on not only H^* but also the hydration to the diol, the value is not taken into account when determining the fit. The resulting parameters are $a_{grey} = (2.41 \pm 1.06) \times 10^4$ and $b_{grey} = 0.27 \pm 0.04$. The solid red line is the new fit function in which all compounds are considered. Here again formaldehyde was not included into the fit. Pinanediol was also excluded from the fit as it appears to be an outlier (see Sect. 3.1.2). The values $a_{red} = (3.34 \pm 1.61) \times 10^4$ and $b_{red} = 0.36 \pm 0.06$ result for the fit function.

As Fig. 7 shows, the retention coefficients of larger organic molecules do also scale with H^*, which agrees with the previous measurements. Only pinanediol and formaldehyde do not fit at first glance. A comparison of the new fit function (solid red line) with the values already known from the literature (dashed gray line) shows that the inflection in the fit function is steeper than was previously assumed. Our results show that the retention of compounds with an H^* below 10^3 is close to 0; i.e., most of the compound dissolved in water is released into the gas phase during riming. This is also evident from the equilibrium distribution of species between the liquid and gas phase in a confined system, which is a function of

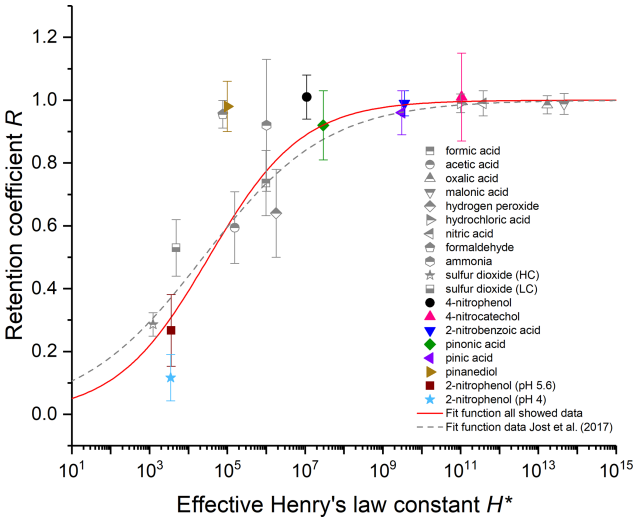

Figure 7. Measured retention coefficients as a function of H^*. Colorful filled symbols – compounds investigated in the present study. Gray symbols – wind tunnel data from earlier studies (Jost et al., 2017; v. Blohn et al., 2013; von Blohn et al., 2011) Solid red line – new fit to wind tunnel data. Dashed gray line – fit of the gray data points only.

the LWC (see Fig. S9 in the Supplement). For species with $H^* < 10^4$ just a maximum of 10 % is present in the liquid droplets, even for LWCs of up to 10 g m^{-3}, which are only reached within severe storms (Lohmann et al., 2020). For $H^* > 10^3$, the compounds are present in significant amounts. For compounds with an H^* value above 10^8, a retention of 1 is expected, with most of the compound remaining in the ice phase during freezing. This finding is in accordance with the literature. Stuart and Jacobson (2004) suggest a threshold value between 10^6 and 10^{10} M atm^{-1} for dry growth riming, which is on the same order of magnitude as the values presented here. For the compounds in-between 10^3 and 10^8, the retention coefficient is highly dependent on H^*. However, the retention estimation is still afflicted by some degree of uncertainty, especially in this H^* range. A close inspection of the data shows that it is not obvious that pinanediol and formaldehyde are outliers. It might also be that the transition from low to high retention values occurs in a smaller range of H^*, and retention is 1 already for $H^* > 10^5$. We cannot ultimately clarify the steepness of the curve, and the limiting regimes might be closer than assumed here. Jost et al. (2017) argued that formaldehyde cannot be explained solely by H^*, and aqueous-phase kinetics must be considered. However, such explanations are lacking for pinanediol. This might indicate that the transition from low to high retention values occurs at lower H^*. Support for that is given from the fit when taking all measurements into account, i.e., also formaldehyde and pinanediol (see Fig. S10). To finally answer the question about the transition behavior of the function, further retention measurements in the range $10^4 < H^* < 10^6$ are needed.

Table 3. Retention coefficient of the measured compounds and their pK_a values, Henry's law constants, and dimensionless effective Henry's law constants at 298 K and pH 4 for all compounds except 2-nitrophenol (pH 4 and 5.6).

Compound	Mean retention coefficient R	Acid dissociation constant pK_a	Henry's law constant[a] $M\,atm^{-1}$	Dimensionless effective Henry's law constant
4-Nitrocatechol	1.01 ± 0.14	7.23[b]	4.35×10^9	1.06×10^{11}
2-Nitrobenzoic acid	0.99 ± 0.04	2.17[c]	2.08×10^6	3.49×10^9
cis-Pinic acid	0.96 ± 0.07	4.64[b]	1.02×10^8	3.06×10^9
cis-Pinonic acid	0.92 ± 0.11	5.19[d]	1.12×10^6	2.93×10^7
4-Nitrophenol	1.01 ± 0.07	7.15[c]	4.52×10^5	1.11×10^7
(−)-Pinanediol	0.98 ± 0.08	14.68[b]	4.08×10^3	9.97×10^4
2-Nitrophenol (pH 5.6)	0.27 ± 0.11	7.23[c]	1.43×10^2	3.50×10^3
2-Nitrophenol (pH 4)	0.12 ± 0.07	7.23[c]	1.43×10^2	3.58×10^3

[a] Calculated using US EPA (2012) Estimation Programs Interface Suite™ for Microsoft® Windows, v 4.11. United States Environmental Protection Agency, Washington, DC, USA. [b] Calculated using Advanced Chemistry Development (ACD/Labs) Software V11.02 (©1994–2024 ACD/Labs). [c] Haynes (2014). [d] Kołodziejczyk et al. (2019).

However, to our current knowledge, and particularly because of the lack of reliable measurements of H^* for pinanediol, we believe that the parameterization given above (Eq. 3), with $a_{red} = (3.34 \pm 1.61) \cdot 10^4$ and $b_{red} = 0.36 \pm 0.06$ is most trustworthy to calculate retention in the transition regime.

4 Conclusions

Wind tunnel experiments were carried out in the vertical wind tunnel of Johannes Gutenberg University, Mainz, to determine the retention coefficients R of three α-pinene oxidation products and four nitro-aromatic compounds. The experiments were performed in the temperature range from −12 to −3 °C with a liquid water content of $0.9 \pm 0.2\,g\,m^{-3}$ and $2.2 \pm 0.2 g\,m^{-3}$ to represent dry and wet growth conditions and to simulate mixed-phase cloud conditions. The wind speed ($3\,m\,s^{-1}$) was chosen to match the typical fall velocity of graupel. The temperature and pH dependences (pH 4 and 5.6) of the compounds were studied, as well as the dependence on the growth regimes. Two different rime collectors were also considered: a Teflon-coated metal bar and graupel. Stuart and Jacobson (2004, 2003) hypothesized a dependence on external influences such as temperature and pH for compounds with a low dimensionless effective Henry's law constant H^*. Of the compounds investigated, 2-nitrophenol has the lowest H^*. In agreement with the current literature, the retention coefficients of 2-nitrophenol determined show a significant dependence on pH and on the type of rime collector. The mean retention coefficients for the graupel samples are $R_{G5.6} = 0.19 \pm 0.05$ (pH 5.6) and $R_{G4} = 0.08 \pm 0.04$ (pH 4). This indicates that changes in the pH value can influence retention and must be taken into account. At pH 4, 2-nitrophenol also showed a dependence between dry and wet growth conditions. The temperature dependence and the dependence on growth conditions seem to overlap, as the growth conditions differ in not only liquid water content but also temperature. Since the measured values between dry and wet growth overlap within the experimental uncertainty, a temperature dependence is reported in this study. The higher scattering of the values obtained from the measurements with pH 5.6 could be the reason why the temperature trend and the difference between the growth regimes found at pH 4 are not visible at pH 5.6.

2-Nitrobenzoic acid, 4-nitrophenol, and 4-nitrocatechol showed retention coefficients of 0.99 ± 0.04, 1.01 ± 0.07, and 1.01 ± 0.14, respectively, with no significant dependence on temperature, pH, type of rime collector, or growth regime. For *cis*-pinic acid and *cis*-pinonic acid, retention coefficients of 0.96 ± 0.07 and 0.92 ± 0.11 were obtained, which also showed no dependence on the parameters investigated. This study shows that there appears to be no difference between dry and wet growth conditions for compounds with a high effective Henry's law constant and that H^* can also be used to estimate retention coefficients for wet growth conditions, at least for graupel and the ambient conditions used in this study (wet growth conditions – ambient temperature of −3 and −5 °C, LWC of $2.2\,g\,m^{-3}$, surface temperature of −0.8 and −2.2 °C, and no shedding of water). This is in contrast to a modeling study by Michael and Stuart (2009), which indicates a lower influence of H^* and low retention coefficients even for compounds with high H^* under wet growth conditions for hailstones. However, it should be noted that in this study, hail was investigated at a surface temperature of 0 °C and with shedding of water. It is therefore possible that the differences in the experimental conditions are responsible for the discrepancies in the observed outcomes. The retention coefficient for pinanediol was determined to be 0.98 ± 0.08, with no significant temperature dependence. This was not expected due to the comparably low H^*. However, the Henry's law constant is only predicted and may be subject to errors due to the specific structure of the molecule. For this reason, it is important to determine Henry's law constants of more and different molecules to aid in the understanding and modeling of processes in the atmosphere.

The retention coefficients for 4-nitrophenol and 2-nitrophenol differ considerably. Since they are structural isomers, it is obvious that they have the same molecular formula and the same functional groups, although they are arranged differently. The different arrangement allows for the formation of an intramolecular hydrogen bond between the OH and the nitro group in 2-nitrophenol. This can result in the non-dissociated form being stabilized, which may explain why 4-nitrophenol exhibits greater solubility than 2-nitrophenol. This could be due to the fact that 4-nitrophenol undergoes easier solvation and displays the capacity to form intermolecular hydrogen bonds. This property may also be responsible for the observed differences in Henry's law constants and retention (Achard et al., 1996; Schwarzenbach et al., 1988). In contrast to the bond method used in this study, the group method of the HENRYWIN™ software predicts the same Henry's law constant for both isomers. This clearly shows the importance of reliable prediction or measurement of H^* and the importance of chemical structure.

We demonstrated here that the retention coefficients of more complex organic molecules depend mainly on the dimensionless effective Henry's law constant. These experiments have improved the parameterization of retention coefficients using the dimensionless effective Henry's law constant. The results show that the retention of compounds with an H^* below 10^3 is not a significant factor, and thus most of the compound dissolved in the supercooled drops is released into the gas phase during freezing. For compounds with an H^* value above 10^8, retention close to 1 is expected, and the compound remains completely in the ice phase during freezing. These compounds can be effectively washed out by precipitation or transported further upwards and released by sublimation of the ice particles. At high altitudes and low temperatures, the volatility of these compounds is even lower, and it is possible that particulate residuals form after sublimation. This probably has an impact on the chemistry of the upper troposphere and ultimately on the Earth's radiative budget. In the intermediate range of H^*, the improved fit of R vs. H^* (Eq. 4, with $a_{\mathrm{red}} = (3.34 \pm 1.61) \times 10^4$ and $b_{\mathrm{red}} = 0.36 \pm 0.06$) can be used to estimate the retention coefficient and thus further improve cloud models that account for transport of organic trace components. However, the present results show that more retention measurements are needed for compounds with $10^4 < H^* < 10^6$ to clarify the sharpness of the transition between the two boundaries of zero retention and full retention.

Data availability. Data are available upon request from the corresponding author, Thorsten Hoffmann (t.hoffmann@uni-mainz.de).

Supplement. The supplement related to this article is available online at: https://doi.org/10.5194/acp-24-13961-2024-supplement.

Author contributions. CB, JS, MG, KD, YM, AA, LG, AT, AV, and TH designed and performed the wind tunnel experiments; FU synthesized pinic acid; CB performed the analytical measurement, analyzed the data, and wrote the manuscript draft; and JS, MG, MS, AT, AV, and TH reviewed and edited the paper.

Competing interests. The contact author has declared that none of the authors has any competing interests.

Disclaimer. Publisher's note: Copernicus Publications remains neutral with regard to jurisdictional claims made in the text, published maps, institutional affiliations, or any other geographical representation in this paper. While Copernicus Publications makes every effort to include appropriate place names, the final responsibility lies with the authors.

Financial support. This research has been supported by the Deutsche Forschungsgemeinschaft (grant no. TRR 301 – project ID 428312742).

This open-access publication was funded by Johannes Gutenberg University Mainz.

Review statement. This paper was edited by Anne Perring and reviewed by Jefferson Snider and Amy L. Stuart.

References

Achard, C., Jaoui, M., Schwing, M., and Rogalski, M.: Aqueous Solubilities of Phenol Derivatives by Conductivity Measurements, J. Chem. Eng. Data, 41, 504–507, https://doi.org/10.1021/je950202o, 1996.

Andreae, M. O., Afchine, A., Albrecht, R., Holanda, B. A., Artaxo, P., Barbosa, H. M. J., Borrmann, S., Cecchini, M. A., Costa, A., Dollner, M., Fütterer, D., Järvinen, E., Jurkat, T., Klimach, T., Konemann, T., Knote, C., Krämer, M., Krisna, T., Machado, L. A. T., Mertes, S., Minikin, A., Pöhlker, C., Pöhlker, M. L., Pöschl, U., Rosenfeld, D., Sauer, D., Schlager, H., Schnaiter, M., Schneider, J., Schulz, C., Spanu, A., Sperling, V. B., Voigt, C., Walser, A., Wang, J., Weinzierl, B., Wendisch, M., and Ziereis, H.: Aerosol characteristics and particle production in the upper troposphere over the Amazon Basin, Atmos. Chem. Phys., 18, 921–961, https://doi.org/10.5194/acp-18-921-2018, 2018.

Bardakov, R., Thornton, J. A., Riipinen, I., Krejci, R., and Ekman, A. M. L.: Transport and chemistry of isoprene and its oxidation products in deep convective clouds, Tellus B, 73, 1979856, https://doi.org/10.1080/16000889.2021.1979856, 2022.

Barth, M. C., Bela, M. M., Fried, A., Wennberg, P. O., Crounse, J. D., St. Clair, J. M., Blake, N. J., Blake, D. R., Homeyer, C. R., Brune, W. H., Zhang, L., Mao, J., Ren, X., Ryerson, T. B., Pollack, I. B., Peischl, J., Cohen, R. C., Nault, B. A., Huey, L. G., Liu, X., and Cantrell, C. A.: Convective transport and scavenging of peroxides by thunderstorms observed over the cen-

tral U.S. during DC3, J. Geophys. Res.-Atmos., 121, 4272–4295, https://doi.org/10.1002/2015JD024570, 2016.

Barth, M. C., Kim, S.-W., Wang, C., Pickering, K. E., Ott, L. E., Stenchikov, G., Leriche, M., Cautenet, S., Pinty, J.-P., Barthe, Ch., Mari, C., Helsdon, J. H., Farley, R. D., Fridlind, A. M., Ackerman, A. S., Spiridonov, V., and Telenta, B.: Cloud-scale model intercomparison of chemical constituent transport in deep convection, Atmos. Chem. Phys., 7, 4709–4731, https://doi.org/10.5194/acp-7-4709-2007, 2007a.

Barth, M. C., Kim, S.-W., Skamarock, W. C., Stuart, A. L., Pickering, K. E., and Ott, L. E.: Simulations of the redistribution of formaldehyde, formic acid, and peroxides in the 10 July 1996 Stratospheric-Tropospheric Experiment: Radiation, Aerosols, and Ozone deep convection storm, J. Geophys. Res., 112, D13310, https://doi.org/10.1029/2006JD008046, 2007b.

Bela, M. M., Barth, M. C., Toon, O. B., Fried, A., Ziegler, C., Cummings, K. A., Li, Y., Pickering, K. E., Homeyer, C. R., Morrison, H., Yang, Q., Mecikalski, R. M., Carey, L., Biggerstaff, M. I., Betten, D. P., and Alford, A. A.: Effects of Scavenging, Entrainment, and Aqueous Chemistry on Peroxides and Formaldehyde in Deep Convective Outflow Over the Central and Southeast United States, J. Geophys. Res.-Atmos., 123, 7594–7614, https://doi.org/10.1029/2018jd028271, 2018.

Bianchi, F., Kurtén, T., Riva, M., Mohr, C., Rissanen, M. P., Roldin, P., Berndt, T., Crounse, J. D., Wennberg, P. O., Mentel, T. F., Wildt, J., Junninen, H., Jokinen, T., Kulmala, M., Worsnop, D. R., Thornton, J. A., Donahue, N., Kjaergaard, H. G., and Ehn, M.: Highly Oxygenated Organic Molecules (HOM) from Gas-Phase Autoxidation Involving Peroxy Radicals: A Key Contributor to Atmospheric Aerosol, Chem. Rev., 119, 3472–3509, https://doi.org/10.1021/acs.chemrev.8b00395, 2019.

Claeys, M., Graham, B., Vas, G., Wang, W., Vermeylen, R., Pashynska, V., Cafmeyer, J., Guyon, P., Andreae, M. O., Artaxo, P., and Maenhaut, W.: Formation of secondary organic aerosols through photooxidation of isoprene, Science (New York, N.Y.), 303, 1173–1176, https://doi.org/10.1126/science.1092805, 2004.

Clarke, A. D., Varner, J. L., Eisele, F., Mauldin R. L., Tanner, D., and Litchy, M.: Particle production in the remote marine atmosphere: Cloud outflow and subsidence during ACE 1, J. Geophys. Res., 103, 16397–16409, 1998.

Cuchiara, G. C., Fried, A., Barth, M. C., Bela, M. M., Homeyer, C. R., Walega, J., Weibring, P., Richter, D., Woods, S., Beyersdorf, A., Bui, T. V., and Dean-Day, J.: Effect of Marine and Land Convection on Wet Scavenging of Ozone Precursors Observed During a SEAC 4 RS Case Study, J. Geophys. Res. Atmos., 128, e2022JD037107, https://doi.org/10.1029/2022JD037107, 2023.

de Gouw, J. and Jimenez, J. L.: Organic aerosols in the Earth's atmosphere, Environ. Sci. Technol., 43, 7614–7618, https://doi.org/10.1021/es9006004, 2009.

Desyaterik, Y., Sun, Y., Shen, X., Lee, T., Wang, X., Wang, T., and Collett, J. L.: Speciation of "brown" carbon in cloud water impacted by agricultural biomass burning in eastern China, J. Geophys. Res.-Atmos., 118, 7389–7399, https://doi.org/10.1002/jgrd.50561, 2013.

Diehl, K., Mitra, S. K., Szakáll, M., Blohn, N. von, Borrmann, S., and Pruppacher, H. R.: The Mainz vertical wind tunnel facility: a review of 25 years of laboratory experiments on cloud physics and chemistry: Aerodynamics, models, and experiments, Wind Tunnels: Aerodynamics, Models, and Experiments, Nova Science Publisher's, New York, 69–92, ISBN 978-1-61209-204-1, 2011.

Fugal, J. P., Shaw, R. A., Saw, E. W., and Sergeyev, A. V.: Airborne digital holographic system for cloud particle measurements, Appl. Opt., 43, 5987–5995, https://doi.org/10.1364/ao.43.005987, 2004.

Fugal, J. P., Schulz, T. J., and Shaw, R. A.: Practical methods for automated reconstruction and characterization of particles in digital in-line holograms, Meas. Sci. Technol., 20, 75501, https://doi.org/10.1088/0957-0233/20/7/075501, 2009.

Ganranoo, L., Mishra, S. K., Azad, A. K., Shigihara, A., Dasgupta, P. K., Breitbach, Z. S., Armstrong, D. W., Grudpan, K., and Rappenglueck, B.: Measurement of nitrophenols in rain and air by two-dimensional liquid chromatography-chemically active liquid core waveguide spectrometry, Anal. Chem., 82, 5838–5843, https://doi.org/10.1021/ac101015y, 2010.

Harrison, M. A., Barra, S., Borghesi, D., Vione, D., Arsene, C., and Iulian Olariu, R.: Nitrated phenols in the atmosphere: a review, Atmos. Environ., 39, 231–248, https://doi.org/10.1016/j.atmosenv.2004.09.044, 2005.

Haynes, W. M.: CRC Handbook of Chemistry and Physics, CRC Press, 2704 pp., https://doi.org/10.1201/b17118, 2014.

Hine, J. and Mookerjee, P. K.: Structural effects on rates and equilibriums. XIX. Intrinsic hydrophilic character of organic compounds. Correlations in terms of structural contributions, The J. Organ. Chem., 3, 292–298, https://doi.org/10.1021/jo00891a006, 1975.

Hoffmann, T., Odum, J. R., Bowman, F., Collins, D., Klockow, D., Flagan, R. C., and Seinfeld, J. H.: Formation of Organic Aerosols from the Oxidation of Biogenic Hydrocarbons, J. Atmos. Chem., 26, 189–222, https://doi.org/10.1023/A:1005734301837, 1997.

Iribarne, J. V. and Pyshnov, T.: The effect of freezing on the composition of supercooled droplets – I. Retention of HCl, HNO_3, NH_3 and H_2O_2, Atmos. Environ. A, 24, 383–387, https://doi.org/10.1016/0960-1686(90)90118-7, 1990.

Jost, A.: Bereifungsexperimente zur Bestimmung des SO_2 – Retentionskoeffizienten; durchgeführt am vertikalen Windkanal der Johannes Gutenberg Universität Mainz, Diplomarbeit, Institut für Physik der Atmosphäre, Johannes Gutenberg Universität Mainz, Mainz, 189 pp., 2012.

Jost, A., Szakáll, M., Diehl, K., Mitra, S. K., and Borrmann, S.: Chemistry of riming: the retention of organic and inorganic atmospheric trace constituents, Atmos. Chem. Phys., 17, 9717–9732, https://doi.org/10.5194/acp-17-9717-2017, 2017.

Kerminen, V.-M., Chen, X., Vakkari, V., Petäjä, T., Kulmala, M., and Bianchi, F.: Atmospheric new particle formation and growth: review of field observations, Environ. Res. Lett., 13, 103003, https://doi.org/10.1088/1748-9326/aadf3c, 2018.

Kołodziejczyk, A., Pyrcz, P., Pobudkowska, A., Błaziak, K., and Szmigielski, R.: Physicochemical Properties of Pinic, Pinonic, Norpinic, and Norpinonic Acids as Relevant α-Pinene Oxidation Products, The J. Phys. Chem. B, 123, 8261–8267, https://doi.org/10.1021/acs.jpcb.9b05211, 2019.

Kołodziejczyk, A., Pyrcz, P., Błaziak, K., Pobudkowska, A., Sarang, K., and Szmigielski, R.: Physicochemical Properties of Terebic Acid, MBTCA, Diaterpenylic Acid Acetate, and Pinanediol as Relevant α-Pinene Oxidation Products, ACS omega, 5, 7919–7927, https://doi.org/10.1021/acsomega.9b04231, 2020.

Kroll, J. H. and Seinfeld, J. H.: Chemistry of secondary organic aerosol: Formation and evolution of low-volatility organics in the atmosphere, Atmos. Environ., 42, 3593–3624, https://doi.org/10.1016/j.atmosenv.2008.01.003, 2008.

List, R.: Zur Thermodynamik teilweise wässriger Hagelkörner, J. Appl. Mathe. Phys. (ZAMP), 11, 273–306, https://doi.org/10.1007/BF01602676, 1960.

Löflund, M., Kasper-Giebl, A., Schuster, B., Giebl, H., Hitzenberger, R., and Puxbaum, H.: Formic, acetic, oxalic, malonic and succinic acid concentrations and their contribution to organic carbon in cloud water, Atmos. Environ., 36, 1553–1558, https://doi.org/10.1016/S1352-2310(01)00573-8, 2002.

Lohmann, U., Lüönd, F., and Mahrt, F.: An introduction to clouds: From the microscale to climate, First published 2016, Reprinted 2020, Cambridge University Press, Cambridge, XXVI, 391 stron, [16] stron tablic, ISBN 9781107018228, 399 pp., 2020.

Macklin, W. C.: Accretion in mixed clouds, Q. J. Roy. Meteorol. Soc., 87, 413–424, https://doi.org/10.1002/qj.49708737312, 1961.

Meylan, W. M. and Howard, P. H.: Bond contribution method for estimating henry's law constants, Environ. Toxicol. Chem., 10, 1283–1293, https://doi.org/10.1002/etc.5620101007, 1991.

Michael, R. and Stuart, A. L.: The fate of volatile chemicals during wet growth of a hailstone, Environ. Res. Lett., 4, 15001, https://doi.org/10.1088/1748-9326/4/1/015001, 2009.

Müller, L., Reinnig, M.-C., Naumann, K. H., Saathoff, H., Mentel, T. F., Donahue, N. M., and Hoffmann, T.: Formation of 3-methyl-1,2,3-butanetricarboxylic acid via gas phase oxidation of pinonic acid – a mass spectrometric study of SOA aging, Atmos. Chem. Phys., 12, 1483–1496, https://doi.org/10.5194/acp-12-1483-2012, 2012.

Nozière, B., Kalberer, M., Claeys, M., Allan, J., D'Anna, B., Decesari, S., Finessi, E., Glasius, M., Grgić, I., Hamilton, J. F., Hoffmann, T., Iinuma, Y., Jaoui, M., Kahnt, A., Kampf, C. J., Kourtchev, I., Maenhaut, W., Marsden, N., Saarikoski, S., Schnelle-Kreis, J., Surratt, J. D., Szidat, S., Szmigielski, R., and Wisthaler, A.: The molecular identification of organic compounds in the atmosphere: state of the art and challenges, Chem. Rev., 115, 3919–3983, https://doi.org/10.1021/cr5003485, 2015.

Pflaum, J. C. and Pruppacher, H. R.: A Wind Tunnel Investigation of the Growth of Graupel Initiated from Frozen Drops, J. Atmos. Sci., 36, 680–689, https://doi.org/10.1175/1520-0469(1979)036<0680:AWTIOT>2.0.CO;2, 1979.

Pruppacher, H. R. and Klett, J. D.: Microphysics of Clouds and Precipitation, 18, Springer Netherlands, Dordrecht, 975 pp., https://doi.org/10.1007/978-0-306-48100-0, 2010.

Pye, H. O. T., Nenes, A., Alexander, B., Ault, A. P., Barth, M. C., Clegg, S. L., Collett Jr., J. L., Fahey, K. M., Hennigan, C. J., Herrmann, H., Kanakidou, M., Kelly, J. T., Ku, I.-T., McNeill, V. F., Riemer, N., Schaefer, T., Shi, G., Tilgner, A., Walker, J. T., Wang, T., Weber, R., Xing, J., Zaveri, R. A., and Zuend, A.: The acidity of atmospheric particles and clouds, Atmos. Chem. Phys., 20, 4809–4888, https://doi.org/10.5194/acp-20-4809-2020, 2020.

Reijenga, J., van Hoof, A., van Loon, A., and Teunissen, B.: Development of Methods for the Determination of pKa Values, Anal. Chem. insights, 8, 53–71, https://doi.org/10.4137/ACI.S12304, 2013.

Schwarzenbach, R. P., Stierli, R., Folsom, B. R., and Zeyer, J.: Compound properties relevant for assessing the environmental partitioning of nitrophenols, Environ. Sci. Technol., 22, 83–92, https://doi.org/10.1021/es00166a009, 1988.

Simon, M., Dada, L., Heinritzi, M., Scholz, W., Stolzenburg, D., Fischer, L., Wagner, A. C., Kürten, A., Rörup, B., He, X.-C., Almeida, J., Baalbaki, R., Baccarini, A., Bauer, P. S., Beck, L., Bergen, A., Bianchi, F., Bräkling, S., Brilke, S., Caudillo, L., Chen, D., Chu, B., Dias, A., Draper, D. C., Duplissy, J., El-Haddad, I., Finkenzeller, H., Frege, C., Gonzalez-Carracedo, L., Gordon, H., Granzin, M., Hakala, J., Hofbauer, V., Hoyle, C. R., Kim, C., Kong, W., Lamkaddam, H., Lee, C. P., Lehtipalo, K., Leiminger, M., Mai, H., Manninen, H. E., Marie, G., Marten, R., Mentler, B., Molteni, U., Nichman, L., Nie, W., Ojdanic, A., Onnela, A., Partoll, E., Petäjä, T., Pfeifer, J., Philippov, M., Quéléver, L. L. J., Ranjithkumar, A., Rissanen, M. P., Schallhart, S., Schobesberger, S., Schuchmann, S., Shen, J., Sipilä, M., Steiner, G., Stozhkov, Y., Tauber, C., Tham, Y. J., Tomé, A. R., Vazquez-Pufleau, M., Vogel, A. L., Wagner, R., Wang, M., Wang, D. S., Wang, Y., Weber, S. K., Wu, Y., Xiao, M., Yan, C., Ye, P., Ye, Q., Zauner-Wieczorek, M., Zhou, X., Baltensperger, U., Dommen, J., Flagan, R. C., Hansel, A., Kulmala, M., Volkamer, R., Winkler, P. M., Worsnop, D. R., Donahue, N. M., Kirkby, J., and Curtius, J.: Molecular understanding of new-particle formation from α-pinene between -50 and $+25$ °C, Atmos. Chem. Phys., 20, 9183–9207, https://doi.org/10.5194/acp-20-9183-2020, 2020.

Sindelarova, K., Granier, C., Bouarar, I., Guenther, A., Tilmes, S., Stavrakou, T., Müller, J.-F., Kuhn, U., Stefani, P., and Knorr, W.: Global data set of biogenic VOC emissions calculated by the MEGAN model over the last 30 years, Atmos. Chem. Phys., 14, 9317–9341, https://doi.org/10.5194/acp-14-9317-2014, 2014.

Snider, J. R. and Huang, J.: Factors influencing the retention of hydrogen peroxide and molecular oxygen in rime ice, J. Geophys. Res., 103, 1405–1415, https://doi.org/10.1029/97JD02847, 1998.

Snider, J. R., Montague, D. C., and Vali, G.: Hydrogen peroxide retention in rime ice, J. Geophys. Res., 97, 7569–7578, https://doi.org/10.1029/92JD00237, 1992.

Spolnik, G., Wach, P., Rudziński, K. J., Szmigielski, R., and Danikiewicz, W.: Tracing the biogenic secondary organic aerosol markers in rain, snow and hail, Chemosphere, 251, 126439, https://doi.org/10.1016/j.chemosphere.2020.126439, 2020.

Stolzenburg, D., Fischer, L., Vogel, A. L., Heinritzi, M., Schervish, M., Simon, M., Wagner, A. C., Dada, L., Ahonen, L. R., Amorim, A., Baccarini, A., Bauer, P. S., Baumgartner, B., Bergen, A., Bianchi, F., Breitenlechner, M., Brilke, S., Buenrostro Mazon, S., Chen, D., Dias, A., Draper, D. C., Duplissy, J., El Haddad, I., Finkenzeller, H., Frege, C., Fuchs, C., Garmash, O., Gordon, H., He, X., Helm, J., Hofbauer, V., Hoyle, C. R., Kim, C., Kirkby, J., Kontkanen, J., Kürten, A., Lampilahti, J., Lawler, M., Lehtipalo, K., Leiminger, M., Mai, H., Mathot, S., Mentler, B., Molteni, U., Nie, W., Nieminen, T., Nowak, J. B., Ojdanic, A., Onnela, A., Passananti, M., Petäjä, T., Quéléver, L. L. J., Rissanen, M. P., Sarnela, N., Schallhart, S., Tauber, C., Tomé, A., Wagner, R., Wang, M., Weitz, L., Wimmer, D., Xiao, M., Yan, C., Ye, P., Zha, Q., Baltensperger, U., Curtius, J., Dommen, J., Flagan, R. C., Kulmala, M., Smith, J. N., Worsnop, D. R., Hansel, A., Donahue, N. M., and Winkler, P. M.: Rapid growth of organic aerosol nanoparticles over a wide tropospheric

temperature range, P. Natl. Acad. Sci. USA, 115, 9122–9127, https://doi.org/10.1073/pnas.1807604115, 2018.

Stuart, A. L. and Jacobson, M. Z.: A timescale investigation of volatile chemical retention during hydrometeor freezing: Non-rime freezing and dry growth riming without spreading, J. Geophys. Res., 108, 4178, https://doi.org/10.1029/2001JD001408, 2003.

Stuart, A. L. and Jacobson, M. Z.: Chemical retention during dry growth riming, J. Geophys. Res., 109, D07305, https://doi.org/10.1029/2003JD004197, 2004.

Szakáll, M., Mitra, S. K., Diehl, K., and Borrmann, S.: Shapes and oscillations of falling raindrops – A review, Atmos. Res., 97, 416–425, https://doi.org/10.1016/j.atmosres.2010.03.024, 2010.

Theis, A., Szakáll, M., Diehl, K., Mitra, S. K., Zanger, F., Heymsfield, A., and Borrmann, S.: Vertical Wind Tunnel Experiments and a Theoretical Study on the Microphysics of Melting Low-Density Graupel, J. Atmos. Sci., 79, 1069–1087, https://doi.org/10.1175/JAS-D-21-0162.1, 2022.

Twohy, C. H., Clement, C. F., Gandrud, B. W., Weinheimer, A. J., Campos, T. L., Baumgardner, D., Brune, W. H., Faloona, I., Sachse, G. W., Vay, S. A., and Tan, D.: Deep convection as a source of new particles in the midlatitude upper troposphere, J. Geophys. Res., 107, AAC6-1–AAC6-10, https://doi.org/10.1029/2001JD000323, 2002.

US EPA.: Estimation Programs Interface Suite™ for Microsoft® Windows, v 4.1, United States Environmental Protection Agency, Washington, DC, USA, 2012.

v. Blohn, N., Diehl, K., Mitra, S. K., and Borrmann, S.: Riming of Graupel: Wind Tunnel Investigations of Collection Kernels and Growth Regimes, J. Atmos. Sci., 66, 2359–2366, https://doi.org/10.1175/2009JAS2969.1, 2009.

v. Blohn, N., Diehl, K., Nölscher, A., Jost, A., Mitra, S. K., and Borrmann, S.: The retention of ammonia and sulfur dioxide during riming of ice particles and dendritic snow flakes: laboratory experiments in the Mainz vertical wind tunnel, J. Atmos. Chem., 70, 131–150, https://doi.org/10.1007/s10874-013-9261-x, 2013.

von Blohn, N., Diehl, K., Mitra, S. K., and Borrmann, S.: Wind tunnel experiments on the retention of trace gases during riming: nitric acid, hydrochloric acid, and hydrogen peroxide, Atmos. Chem. Phys., 11, 11569–11579, https://doi.org/10.5194/acp-11-11569-2011, 2011.

Wang, H., Gao, Y., Wang, S., Wu, X., Liu, Y., Li, X., Huang, D., Lou, S., Wu, Z., Guo, S., Jing, S., Li, Y., Huang, C., Tyndall, G. S., Orlando, J. J., and Zhang, X.: Atmospheric Processing of Nitrophenols and Nitrocresols From Biomass Burning Emissions, J. Geophys. Res.-Atmos., 125, e2020JD033401, https://doi.org/10.1029/2020JD033401, 2020.

Wang, P. K. and Kubicek, A.: Flow fields of graupel falling in air, Atmos. Res., 124, 158–169, https://doi.org/10.1016/j.atmosres.2013.01.003, 2013.

Weitzel, M., Mitra, S. K., Szakáll, M., Fugal, J. P., and Borrmann, S.: Application of holography and automated image processing for laboratory experiments on mass and fall speed of small cloud ice crystals, Atmos. Chem. Phys., 20, 14889–14901, https://doi.org/10.5194/acp-20-14889-2020, 2020.

Williamson, C. J., Kupc, A., Axisa, D., Bilsback, K. R., Bui, T., Campuzano-Jost, P., Dollner, M., Froyd, K. D., Hodshire, A. L., Jimenez, J. L., Kodros, J. K., Luo, G., Murphy, D. M., Nault, B. A., Ray, E. A., Weinzierl, B., Wilson, J. C., Yu, F., Yu, P., Pierce, J. R., and Brock, C. A.: A large source of cloud condensation nuclei from new particle formation in the tropics, Nature, 574, 399–403, https://doi.org/10.1038/s41586-019-1638-9, 2019.

Xiao, Q., Zhang, J., Wang, Y., Ziemba, L. D., Crosbie, E., Winstead, E. L., Robinson, C. E., DiGangi, J. P., Diskin, G. S., Reid, J. S., Schmidt, K. S., Sorooshian, A., Hilario, M. R. A., Woods, S., Lawson, P., Stamnes, S. A., and Wang, J.: New particle formation in the tropical free troposphere during CAMP2Ex: statistics and impact of emission sources, convective activity, and synoptic conditions, Atmos. Chem. Phys., 23, 9853–9871, https://doi.org/10.5194/acp-23-9853-2023, 2023.

5. Conclusion

Atmospheric organic matter has a vital role in many processes that moderate climate systems as well as influence air quality and thereby public health. These organic compounds are a critical yet understudied constituent of the chemical composition of Earth's atmosphere. Its transport from the lower troposphere where its primary emissions sources are to the UTLS is one of the most important and yet unresolved issues in cloud chemistry and global models. While there are limitations on what is currently known about ice phase processing in tropical deep convective clouds and in extratropical WCB and their contribution to the redistribution of atmospheric trace organic substances, new publications continue to address these knowledge gaps. Investigating these areas of interest is especially important to furthering the understanding of the formation and the atmospheric life cycle of organic aerosols and in particular secondary organic aerosols.

In finding answers to the questions that surround organic transport, the underlying microphysical, multiphase chemical aspects, and macrophysical transport processes are explored. The processes of chemical retention during drop freezing and rime freezing could potentially explain underestimated new particle formation in the upper atmosphere. Diffusional ice uptake represents a process by which organics are removed from the stratosphere by cirrus clouds. These experiments presented in these publications demonstrate the measurement of retention coefficients through the use of the Mainz Wind Tunnel or an acoustic levitation apparatus; the measurement of gas-ice partitioning coefficients through the use of a self-designed Flowtube apparatus; and the significance of these measurements for atmospheric processing and the associated transport of the implicated organic species.

Specifically, the wind tunnel riming retention studies using pinene oxidation products and nitrophenols demonstrate that they behave according to the known relationship with effective Henry's Law solubilities. However, the acoustic levitator experiments demonstrate that raindrop freezing retention does not have a sigmoidal relation with effective Henry's Law solubilities. These studies begins to challenge the existing understanding of retention's relationship with Henry's Law solubilities, or at minimum highlight the physical factors that influence retention.

The experiments using the flowtube apparatus to measure ice-gas partitioning coefficients demonstrate an inverse relationship between partitioning coefficients and

temperature for carbonyls. This was observed for all species except methyl vinyl ketone. This experiment showed a linear correlation between ΔS and ΔH which was statistically validated and determined with 99% confidence to not be a statistical artifact. This compensation behavior could be an indication of a surface liquid layer or quasi-liquid layer behavior involved in the uptake process and could also indicate a single dominant influence on a compound's uptake. The most significant physicochemical properties that correlated with uptake were identified to be vapor pressure and molar mass, which indicated that smaller compounds with higher vapor pressures are more readily taken into the ice phase.

Altogether, these publications display how the microphysical and multiphase chemistry of hydrometeor freezing inform the macrophysical transport of atmospheric transport. Each of these papers continue to demonstrate that the properties and behaviors of organics in the atmosphere are diverse and not always comparable to those of inorganics. Most importantly, they show the critical need for experimental data to inform the theoretical and modeling aspects of atmospheric research.

6. Outlook

The limitations of these studies should not be understated as these limitations guide the proceeding of future investigations. The most apparent limitations on these experiments are the ways in which the conditions of the upper atmosphere fail to be properly replicated. For the acoustic levitator experiments, this is most apparent in the drop size ranges, artifacts from the sonic field, reduced ventilation. For the single and binary mixture experiment along with the wind tunnel studies on select single components, one of the most chemically relevant aspects is the measurement of species in ideal solutions, i.e. single component solutions with limited matrix effects. As opposed to the acoustic levitator experiment using a complex solution of aerosols, these single component studies may be neglecting possible matrix effects that could be present in natural hydrometeors.

The investigation of the potential matrix effects with the complex solution in the acoustic levitator is still a first demonstration of retention within a complex mixture. Considering the matrix effects, the applicability of the conclusions there to other locations or samplings with different aerosol compositions—thereby potentially different matrix effects—could be challenged. There is not enough evidence to assume matrix effects are either negligible or the same elsewhere as in this experiment, but the assumption is not unreasonable. Rainwater tends to show negligible matrix effects for other properties and analyses (Pang et al., 2017; Sauret-Szczepanski et al., 2006). Average rainwater DOC is on the order of μM which could be assumed to be dilute enough for matrix effects to be negligible compared to pure water solutions. However, these are still unsupported assumptions that are required for broad application of those conclusions.

Future studies into chemical retention require the measurement of riming retention for complex solutions in conditions that best reproduce the conditions of the upper atmosphere. This requires aerosol extract experiments in the wind tunnel. Additionally, more studies in the wind tunnel that investigate substance with low Henry's law solubility are required to better understand the relationship between retention and Henry's law solubility. While the acoustic levitator experiments challenge some aspects of the current understanding of this relationship, more experimental data is needed for the lower end of the curve. Further, measurement of retention in complex mixtures would benefit greatly from higher accuracy chemical structure information and assignment. The biggest limitation on the direct and accurate comparison of

the Henry's law solubilities and the retentions measured for the hundreds of compounds in the complex mixture is the inability to estimate the Henry's law solubility due to lack of high confidence structural assignment. With these adjustments, future studies could potentially present high accuracy predictions of the chemical retentions for a wide variety of organic compounds.

As for the Flowtube experiments, these measurements are exclusively a description of the gas-to-ice solid solution equilibrium and neglect investigation of gas-to-liquid or liquid-to-ice equilibrium. The partitioning coefficients measured do not directly describe whether a compound is actually incorporated into the ice crystal lattice or if it phase separates into crystal grain boundaries, but only its uptake into the bulk phase. However, since molecular size has a negative correlation with uptake, it may suggest incorporation into the ice crystal lattice or void space. It is also difficult to say if this data describes uptake into a liquid solution phase that coexists with ice, but the observed compensation effect may insinuate its presence. While the measurements here are for multicomponent mixtures of compounds, single component uptake is likely the same, which is also supported by Huffman and Snider (2004).

Further investigation of ice-gas partitioning coefficients should seek to determine the contribution of liquid layer influence and should focus on measuring on ice-specific surface area and the volume of solution associated with the liquid layer. Additionally, similar experiments with other families of compounds are required to better understand the root of the compensation effect seen here. Crystallographic analysis of this data may also yield more information about the ice uptake process. With more investigation to reveal the main contributors of additivity, it seems possible that the entropy-enthalpy compensation seen here could be used to help model the uptake process with a significant degree of accuracy. However, this requires the investigation of more organics and in particular to review the behavior of methyl-vinyl ketone to understand its deviations from the expected exothermic behavior.

7. References

Albrecht, B. A.: Aerosols, Cloud Microphysics, and Fractional Cloudiness, Science (1979), 245, 1227–1230, https://doi.org/10.1126/SCIENCE.245.4923.1227, 1989.

Altieri, K. E., Turpin, B. J., and Seitzinger, S. P.: Oligomers, organosulfates, and nitrooxy organosulfates in rainwater identified by ultra-high resolution electrospray ionization FT-ICR mass spectrometry, Atmos Chem Phys, 9, 2533–2542, https://doi.org/10.5194/acp-9-2533-2009, 2009.

Altieri, K. E., Hastings, M. G., Peters, A. J., and Sigman, D. M.: Molecular characterization of water soluble organic nitrogen in marine rainwater by ultra-high resolution electrospray ionization mass spectrometry, Atmos Chem Phys, 12, 3557–3571, https://doi.org/10.5194/acp-12-3557-2012, 2012.

Andreae, M. O. and Gelencsér, A.: Black carbon or brown carbon? The nature of light-absorbing carbonaceous aerosols, Atmos Chem Phys, 6, 3131–3148, https://doi.org/10.5194/acp-6-3131-2006, 2006.

Andreae, M. O., Afchine, A., Albrecht, R., Holanda, B. A., Artaxo, P., Barbosa, H. M. J., Borrmann, S., Cecchini, M. A., Costa, A., Dollner, M., Fütterer, D., Järvinen, E., Jurkat, T., Klimach, T., Konemann, T., Knote, C., Krämer, M., Krisna, T., Machado, L. A. T., Mertes, S., Minikin, A., Pöhlker, C., Pöhlker, M. L., Pöschl, U., Rosenfeld, D., Sauer, D., Schlager, H., Schnaiter, M., Schneider, J., Schulz, C., Spanu, A., Sperling, V. B., Voigt, C., Walser, A., Wang, J., Weinzierl, B., Wendisch, M., and Ziereis, H.: Aerosol characteristics and particle production in the upper troposphere over the Amazon Basin, Atmos. Chem. Phys, 18, 921–961, https://doi.org/10.5194/acp-18-921-2018, 2018.

Andrés Casquero-Vera, J., Lyamani, H., Dada, L., Hakala, S., Paasonen, P., Román, R., Fraile, R., Petäjä, T., Olmo-Reyes, F. J., Alados-Arboledas, L., Andrés, J., and Vera, C.: New particle formation at urban and high-altitude remote sites in the south-eastern Iberian Peninsula, Atmos. Chem. Phys, 20, 14253–14271, https://doi.org/10.5194/acp-20-14253-2020, 2020.

Anon: ENVIRONMENTAL PROTECTION AGENCY 40 CFR Part 50 Technical Correction to the National Ambient Air Quality Standards for Particulate Matter, n.d.

Arashiro, M., Lin, Y.-H., Sexton, K. G., Zhang, Z., Jaspers, I., Fry, R. C., Vizuete, W. G., Gold, A., and Surratt, J. D.: In vitro exposure to isoprene-derived secondary organic aerosol by direct deposition and its effects on COX-2 and IL-8 gene expression, Atmos Chem Phys, 16, 14079–14090, https://doi.org/10.5194/acp-16-14079-2016, 2016.

Audiffren, N., Cautenet, S., and Chaumerliac, N.: A Modeling Study of the Influence of Ice Scavenging on the Chemical Composition of Liquid-Phase Precipitation of a Cumulonimbus Cloud, J Appl Meteorol Climatol, 38, 1148–1160, https://doi.org/10.1175/1520-0450(1999)038<1148:AMSOTI>2.0.CO;2, 1999.

Baker, B., Baker, M. B., Jayaratne, E. R., Latham, J., and Saunders, C. P. R.: The Influence of Diffusional Growth Rates On the Charge Transfer Accompanying Rebounding Collisions Between Ice Crystals and Soft Hailstones, Quarterly Journal of the Royal Meteorological Society, 113, 1193–1215, https://doi.org/10.1002/QJ.49711347807;PAGE:STRING:ARTICLE/CHAPTER, 1987.

Bardakov, R., Thornton, J. A., Riipinen, I., Krejci, R., and Ekman, A. M. L.: Transport and chemistry of isoprene and its oxidation products in deep convective clouds, Tellus B Chem Phys Meteorol, 73, 1–21, https://doi.org/10.1080/16000889.2021.1979856, 2021.

Barrefors, G. and Petersson, G.: Volatile hydrocarbons from domestic wood burning, Chemosphere, 30, 1551–1556, https://doi.org/10.1016/0045-6535(95)00048-D, 1995.

Behr, P., Terziyski, A., and Zellner, R.: Acetone adsorption on ice surfaces in the temperature range T = 190-220 K: Evidence for aging effects due to crystallographic changes of the adsorption sites, Journal of Physical Chemistry A, 110, 8098–8107, https://doi.org/10.1021/JP0563742/ASSET/IMAGES/LARGE/JP0563742F00011.JPEG, 2006.

Bela, M. M., Barth, M. C., Toon, O. B., Fried, A., Ziegler, C., Cummings, K. A., Li, Y., Pickering, K. E., Homeyer, C. R., Morrison, H., Yang, Q., Mecikalski, R. M., Carey, L., Biggerstaff, M. I., Betten, D. P., and Alford, A. A.: Effects of Scavenging, Entrainment, and Aqueous Chemistry on Peroxides and Formaldehyde in Deep Convective Outflow Over the Central and Southeast United States, Journal of Geophysical Research: Atmospheres, 123, 7594–7614, https://doi.org/10.1029/2018JD028271, 2018.

Bilde, M. and Pandis, S. N.: Evaporation rates and vapor pressures of individual aerosol species formed in the atmospheric oxidation of α- and β- pinene, Environ Sci Technol, 35, 3344–3349, https://doi.org/10.1021/es001946b, 2001.

Von Blohn, N., Diehl, K., Mitra, S. K., and Borrmann, S.: The retention of nitric acid, hydrochloric acid, and hydrogen peroxide Wind tunnel experiments on the retention of trace gases during riming: nitric acid, hydrochloric acid, and hydrogen peroxide The retention of nitric acid, hydrochloric acid, and hydrogen peroxide, Atmos. Chem. Phys. Discuss, 11, 17447–17472, https://doi.org/10.5194/acpd-11-17447-2011, 2011a.

Von Blohn, N., Diehl, K., Mitra, S. K., and Borrmann, S.: Wind tunnel experiments on the retention of trace gases during riming: Nitric acid, hydrochloric acid, and hydrogen peroxide, Atmos Chem Phys, 11, 11569–11579, https://doi.org/10.5194/ACP-11-11569-2011, 2011b.

Borchers, C., Seymore, J., Gautam, M., Dörholt, K., Müller, Y., Arndt, A., Gömmer, L., Ungeheuer, F., Szakáll, M., Borrmann, S., Theis, A., Vogel, A. L., and Hoffmann, T.: Retention of α -pinene oxidation products and nitro-aromatic compounds during riming, Atmos Chem Phys, 24, 13961–13974, https://doi.org/10.5194/ACP-24-13961-2024, 2024a.

Borchers, C., Seymore, J., Gautam, M., Dörholt, K., Müller, Y., Arndt, A., Gömmer, L., Ungeheuer, F., Szakáll, M., Borrmann, S., Theis, A., Vogel, A. L., and Hoffmann, T.:

Retention of α-pinene oxidation products and nitro-aromatic compounds during riming, https://doi.org/10.5194/egusphere-2024-1443, 2024b.

Brownscombe, J. L. and Hallett, J.: Experimental and field studies of precipitation particles formed by the freezing of supercooled water, Quarterly Journal of the Royal Meteorological Society, 93, 455–473, https://doi.org/10.1002/QJ.49709339805;CTYPE:STRING:JOURNAL, 1967.

de Bruijne, K., Ebersviller, S., Sexton, K. G., Lake, S., Leith, D., Goodman, R., Jetters, J., Walters, G. W., Doyle-Eisele, M., Woodside, R., Jeffries, H. E., and Jaspers, I.: Design and Testing of Electrostatic Aerosol *In Vitro* Exposure System (EAVES): An Alternative Exposure System for Particles, Inhal Toxicol, 21, 91–101, https://doi.org/10.1080/08958370802166035, 2009.

Carter, W. P. and L Carter, W. P.: Development of Ozone Reactivity Scales for Volatile Organic Compounds, J. Air & Waste Manage. Assoc, 44, 881–899, https://doi.org/10.1080/1073161X.1994.10467290, 1994.

Cerully, K. M., Bougiatioti, A., Hite, J. R., Guo, H., Xu, L., Ng, N. L., Weber, R., and Nenes, A.: On the link between hygroscopicity, volatility, and oxidation state of ambient and water-soluble aerosols in the southeastern United States, Atmos Chem Phys, 15, 8679–8694, https://doi.org/10.5194/acp-15-8679-2015, 2015.

Chan, M. N., Choi, M. Y., Ng, N. L., and Chan, C. K.: Hygroscopicity of water-soluble organic compounds in atmospheric aerosols: Amino acids and biomass burning derived organic species, Environ Sci Technol, 39, 1555–1562, https://doi.org/10.1021/es049584l, 2005.

Chang, D., Wang, Z., Guo, J., Li, T., Liang, Y., Kang, L., Xia, M., Wang, Y., Yu, C., Yun, H., Yue, D., and Wang, T.: Characterization of organic aerosols and their precursors in southern China during a severe haze episode in January 2017, Science of the Total Environment, 691, 101–111, https://doi.org/10.1016/j.scitotenv.2019.07.123, 2019.

Chylek, P., Lee, J. E., Romonosky, D. E., Gallo, F., Lou, S., Shrivastava, M., Carrico, C. M., Aiken, A. C., and Dubey, M. K.: Mie Scattering Captures Observed Optical Properties of Ambient Biomass Burning Plumes Assuming Uniform Black, Brown, and Organic Carbon Mixtures, Journal of Geophysical Research: Atmospheres, 124, 11406–11427, https://doi.org/10.1029/2019JD031224;PAGE:STRING:ARTICLE/CHAPTER, 2019.

Clarke, A. D., Varner, J. L., Eisele, F., Mauldin, R. L., Tanner, D., and Litchy, M.: Particle production in the remote marine atmosphere: Cloud outflow and subsidence during ACE 1, Journal of Geophysical Research Atmospheres, 103, 16397–16409, https://doi.org/10.1029/97JD02987, 1998.

Clarke, A. D., Eisele, F., Kapustin, V. N., Moore, K., Tanner, D., Mauldin, L., Litchy, M., Lienert, B., Carroll, M. A., and Albercook, G.: Nucleation in the equatorial free troposphere: Favorable environments during PEM-Tropics, Journal of Geophysical Research Atmospheres, 104, 5735–5744, https://doi.org/10.1029/98JD02303, 1999.

Cohen, A. J., Brauer, M., Burnett, R., Anderson, H. R., Frostad, J., Estep, K., Balakrishnan, K., Brunekreef, B., Dandona, L., Dandona, R., Feigin, V., Freedman, G., Hubbell, B., Jobling, A., Kan, H., Knibbs, L., Liu, Y., Martin, R., Morawska, L., Pope, C. A., Shin, H., Straif, K., Shaddick, G., Thomas, M., van Dingenen, R., van Donkelaar, A., Vos, T., Murray, C. J. L., and Forouzanfar, M. H.: Estimates and 25-year trends of the global burden of disease attributable to ambient air pollution: an analysis of data from the Global Burden of Diseases Study 2015, The Lancet, 389, 1907–1918, https://doi.org/10.1016/S0140-6736(17)30505-6, 2017.

Dekoutsidis, G., Groß, S., Wirth, M., Krämer, M., and Rolf, C.: Characteristics of supersaturation in midlatitude cirrus clouds and their adjacent cloud-free air, Atmos Chem Phys, 23, 3103–3117, https://doi.org/10.5194/ACP-23-3103-2023, 2023.

Dominé, F. and Thibert, E.: Mechanism of incorporation of trace gases in ice grown from the gas phase, Geophys Res Lett, 23, 3627–3630, https://doi.org/10.1029/96GL03290, 1996.

Eliuk, S. and Makarov, A.: Evolution of Orbitrap Mass Spectrometry Instrumentation, Annual Review of Analytical Chemistry, 8, 61–80, https://doi.org/10.1146/annurev-anchem-071114-040325, 2015.

Franz, T. P. and Eisenreich, S. J.: Accumulation of polychlorinated biphenyls and polycyclic aromatic hydrocarbons in the snowpack of Minnesota and Lake Superior, J Great Lakes Res, 26, 220–234, https://doi.org/10.1016/S0380-1330(00)70688-5, 2000.

Fries, E., Haunold, W., Jaeschke, W., Hoog, I., Mitra, S. K., and Borrmann, S.: Uptake of gaseous aromatic hydrocarbons by non-growing ice crystals, Atmos Environ, 40, 5476–5485, https://doi.org/10.1016/J.ATMOSENV.2006.03.055, 2006.

Fries, E., Starokozhev, E., Haunold, W., Jaeschke, W., Mitra, S. K., Borrmann, S., and Schmidt, M. U.: Laboratory studies on the uptake of aromatic hydrocarbons by ice crystals during vapor depositional crystal growth, Atmos Environ, 41, 6156–6166, https://doi.org/10.1016/j.atmosenv.2007.04.028, 2007.

Gordon, S. B., Bruce, N. G., Grigg, J., Hibberd, P. L., Kurmi, O. P., Lam, K. H., Mortimer, K., Asante, K. P., Balakrishnan, K., Balmes, J., Bar-Zeev, N., Bates, M. N., Breysse, P. N., Buist, S., Chen, Z., Havens, D., Jack, D., Jindal, S., Kan, H., Mehta, S., Moschovis, P., Naeher, L., Patel, A., Perez-Padilla, R., Pope, D., Rylance, J., Semple, S., and Martin, W. J.: Respiratory risks from household air pollution in low and middle income countries, Lancet Respir Med, 2, 823–860, https://doi.org/10.1016/S2213-2600(14)70168-7, 2014.

Heft-Neal, S., Burney, J., Bendavid, E., and Burke, M.: Robust relationship between air quality and infant mortality in Africa, Nature, 559, 254–258, https://doi.org/10.1038/s41586-018-0263-3, 2018a.

Heft-Neal, S., Burney, J., Bendavid, E., and Burke, M.: Robust relationship between air quality and infant mortality in Africa, Nature, 559, 254–258, https://doi.org/10.1038/s41586-018-0263-3, 2018b.

Heitto, A., Wu, C., Aliaga, D., Blacutt, L., Chen, X., Gramlich, Y., Heikkinen, L., Huang, W., Krejci, R., Laj, P., Moreno, I., Sellegri, K., Velarde, F., Weinhold, K., Wiedensohler, A., Zha, Q., Bianchi, F., Andrade, M., Lehtinen, K. E. J., Mohr, C., and Yli-Juuti, T.: Analysis of atmospheric particle growth based on vapor concentrations measured at the high-altitude GAW station Chacaltaya in the Bolivian Andes, Atmos. Chem. Phys, 24, 1315–1328, https://doi.org/10.5194/acp-24-1315-2024, 2024.

Von Hessberg, P., Pouvesle, N., Winkler, A. K., Schuster, G., and Crowley, J. N.: Interaction of formic and acetic acid with ice surfaces between 187 and 227 K. Investigation of single species- and competitive adsorption, Physical Chemistry Chemical Physics, 10, 2345–2355, https://doi.org/10.1039/B800831K, 2008.

Heymsfield, A. J., Schmitt, C., Chen, C. C. J., Bansemer, A., Gettelman, A., Field, P. R., and Liu, C.: Contributions of the Liquid and Ice Phases to Global Surface Precipitation: Observations and Global Climate Modeling, J Atmos Sci, 77, 2629–2648, https://doi.org/10.1175/JAS-D-19-0352.1, 2020.

Huffman, W. A. and Snider, J. R.: Ice-oxyhydrocarbon interactions in the troposphere, Journal of Geophysical Research: Atmospheres, 109, https://doi.org/10.1029/2003jd003778, 2004.

Iribarne, J. V. and Pyshnov, T.: The effect of freezing on the composition of supercooled droplets—I. Retention of HCl, HNO3, NH3 and H2O2, Atmospheric Environment. Part A. General Topics, 24, 383–387, https://doi.org/10.1016/0960-1686(90)90118-7, 1990.

John H. Seinfeld and Spyros N. Pandis: Atmospheric Chemistry and Physics: From Air Pollution to Climate Change, 3rd Edition, 1–1152 pp., 2019.

Jost, A., Szakáll, M., DIehl, K., Mitra, S. K., and Borrmann, S.: Chemistry of riming: The retention of organic and inorganic atmospheric trace constituents, Atmos Chem Phys, 17, 9717–9732, https://doi.org/10.5194/ACP-17-9717-2017, 2017a.

Jost, A., Szakáll, M., DIehl, K., Mitra, S. K., and Borrmann, S.: Chemistry of riming: The retention of organic and inorganic atmospheric trace constituents, Atmos Chem Phys, 17, 9717–9732, https://doi.org/10.5194/ACP-17-9717-2017, 2017b.

Kanakidou, M., Seinfeld, J. H., Pandis, S. N., Barnes, I., Dentener, F. J., Facchini, M. C., Van Dingenen, R., Ervens, B., Nenes, A., Nielsen, C. J., Swietlicki, E., Putaud, J. P., Balkanski, Y., Fuzzi, S., Horth, J., Moortgat, G. K., Winterhalter, R., Myhre, C. E. L., Tsigaridis, K., Vignati, E., Stephanou, E. G., and Wilson, J.: Organic aerosol and global climate modelling: a review, Atmos Chem Phys, 5, 1053–1123, https://doi.org/10.5194/acp-5-1053-2005, 2005.

Kumar, M., Burrell, E., Hansen, J. C., and Francisco, J. S.: Molecular insights into organic particulate formation, Commun Chem, 2, https://doi.org/10.1038/s42004-019-0183-7, 2019.

Kurtén, T., Hyttinen, N., Louise D'Ambro, E., Thornton, J., and Prisle, N. L.: Estimating the saturation vapor pressures of isoprene oxidation products C5H12O6 and C5H10O6 using

COSMO-RS, Atmos Chem Phys, 18, 17589–17600, https://doi.org/10.5194/acp-18-17589-2018, 2018.

Lamb, D. and Verlinde, J.: Physics and Chemistry of Clouds, Cambridge University Press, 275–414 pp., https://doi.org/10.1017/CBO9780511976377, 2011.

Landrigan, P. J., Fuller, R., Acosta, N. J. R., Adeyi, O., Arnold, R., Basu, N. (Nil), Baldé, A. B., Bertollini, R., Bose-O'Reilly, S., Boufford, J. I., Breysse, P. N., Chiles, T., Mahidol, C., Coll-Seck, A. M., Cropper, M. L., Fobil, J., Fuster, V., Greenstone, M., Haines, A., Hanrahan, D., Hunter, D., Khare, M., Krupnick, A., Lanphear, B., Lohani, B., Martin, K., Mathiasen, K. V, McTeer, M. A., Murray, C. J. L., Ndahimananjara, J. D., Perera, F., Potočnik, J., Preker, A. S., Ramesh, J., Rockström, J., Salinas, C., Samson, L. D., Sandilya, K., Sly, P. D., Smith, K. R., Steiner, A., Stewart, R. B., Suk, W. A., van Schayck, O. C. P., Yadama, G. N., Yumkella, K., and Zhong, M.: The Lancet Commission on pollution and health, The Lancet, 391, 462–512, https://doi.org/10.1016/S0140-6736(17)32345-0, 2018.

Laskin, A., Smith, J. S., and Laskin, J.: Molecular characterization of nitrogen-containing organic compounds in biomass burning aerosols using high-resolution mass spectrometry, Environ Sci Technol, 43, 3764–3771, https://doi.org/10.1021/es803456n, 2009.

Lelieveld, J., Haines, A., and Pozzer, A.: Age-dependent health risk from ambient air pollution: a modelling and data analysis of childhood mortality in middle-income and low-income countries., Lancet Planet Health, 2, e292–e300, https://doi.org/10.1016/S2542-5196(18)30147-5, 2018.

Lesins, G., Chylek, P., and Lohmann, U.: A study of internal and external mixing scenarios and its effect on aerosol optical properties and direct radiative forcing, Journal of Geophysical Research: Atmospheres, 107, AAC 5-1, https://doi.org/10.1029/2001JD000973;REQUESTEDJOURNAL:JOURNAL:21562202D;PAGE:STRING:ARTICLE/CHAPTER, 2002.

Li, L., Fang, Z., He, C., and Shi, Q.: Separation and characterization of marine dissolved organic matter (DOM) by combination of Fe(OH) 3 co-precipitation and solid phase extraction followed by ESI FT-ICR MS, Anal Bioanal Chem, 411, 2201–2208, https://doi.org/10.1007/S00216-019-01663-Y/FIGURES/7, 2019.

Lichtveld, K. M., Ebersviller, S. M., Sexton, K. G., Vizuete, W., Jaspers, I., and Jeffries, H. E.: In vitro exposures in diesel exhaust atmospheres: Resuspension of PM from filters versus direct deposition of PM from air, Environ Sci Technol, 46, 9062–9070, https://doi.org/10.1021/es301431s, 2012a.

Lichtveld, K. M., Ebersviller, S. M., Sexton, K. G., Vizuete, W., Jaspers, I., and Jeffries, H. E.: In Vitro Exposures in Diesel Exhaust Atmospheres: Resuspension of PM from Filters versus Direct Deposition of PM from Air, Environ Sci Technol, 46, 9062–9070, https://doi.org/10.1021/es301431s, 2012b.

Lindsey, D. T. and Fromm, M.: Evidence of the cloud lifetime effect from wildfire-induced thunderstorms, Geophys Res Lett, 35, https://doi.org/10.1029/2008GL035680;SUBPAGE:STRING:FULL, 2008.

Liu, Z., Yim, S. H. L., Wang, C., and Lau, N. C.: The Impact of the Aerosol Direct Radiative Forcing on Deep Convection and Air Quality in the Pearl River Delta Region, Geophys Res Lett, 45, 4410–4418, https://doi.org/10.1029/2018GL077517, 2018.

Mace, G. G., Benson, S., Humphries, R., Gombert, P. M., and Sterner, E.: Natural marine cloud brightening in the Southern Ocean, Atmos Chem Phys, 23, 1677–1685, https://doi.org/10.5194/ACP-23-1677-2023, 2023.

Mahowald, N.: Supporting Online Material Aerosol Indirect Effect on Biogeochemical Cycles and Climate Downloaded from, Phys. Earth Planet. Inter, 57, 63, https://doi.org/10.1126/science.1208265, 1952.

Mahowald, N.: Aerosol Indirect Effect on Biogeochemical Cycles and Climate, Science (1979), 334, 794–796, https://doi.org/10.1126/science.1207374, 2011.

Mari, C., Jacob, D. J., and Bechtold, P.: Transport and scavenging of soluble gases in a deep convective cloud, Journal of Geophysical Research Atmospheres, 105, 22255–22267, https://doi.org/10.1029/2000JD900211;WGROUP:STRING:PUBLICATION, 2000.

Martins, C. P. B., Bromirski, M., Prieto Conaway, M. C., and Makarov, A. A.: Orbitrap Mass Spectrometry: Evolution and Applicability, Comprehensive Analytical Chemistry, 71, 3–18, https://doi.org/10.1016/bs.coac.2016.01.001, 2016.

McNeill, V. F.: Aqueous organic chemistry in the atmosphere: Sources and chemical processing of organic aerosols, Environ Sci Technol, 49, 1237–1244, https://doi.org/10.1021/es5043707, 2015.

Mead, R. N., Mullaugh, K. M., Brooks Avery, G., Kieber, R. J., Willey, J. D., and Podgorski, D. C.: Insights into dissolved organic matter complexity in rainwater from continental and coastal storms by ultrahigh resolution Fourier transform ion cyclotron resonance mass spectrometry, Atmos Chem Phys, 13, 4829–4838, https://doi.org/10.5194/acp-13-4829-2013, 2013.

Mead, R. N., Felix, J. D., Avery, G. B., Kieber, R. J., Willey, J. D., and Podgorski, D. C.: Characterization of CHOS compounds in rainwater from continental and coastal storms by ultrahigh resolution mass spectrometry, Atmos Environ, 105, 162–168, https://doi.org/10.1016/j.atmosenv.2015.01.057, 2015.

Mülmenstädt, J., Sourdeval, O., Delanoë, J., and Quaas, J.: Frequency of occurrence of rain from liquid-, mixed-, and ice-phase clouds derived from A-Train satellite retrievals, Geophys Res Lett, 42, 6502–6509, https://doi.org/10.1002/2015GL064604, 2015.

Nguyen, T. B., Laskin, J., Laskin, A., and Nizkorodov, S. A.: Nitrogen-containing organic compounds and oligomers in secondary organic aerosol formed by photooxidation of isoprene, Environ Sci Technol, 45, 6908–6918, https://doi.org/10.1021/es201611n, 2011.

Orem, M. W. and Adamson, A. W.: Physical adsorption of vapor on ice: II. n-alkanes, J Colloid Interface Sci, 31, 278–286, https://doi.org/10.1016/0021-9797(69)90337-3, 1969.

Petters, M. D., Kreidenweis, S. M., and Ziemann, P. J.: Prediction of cloud condensation nuclei activity for organic compounds using functional group contribution methods, Geosci Model Dev, 9, 111–124, https://doi.org/10.5194/GMD-9-111-2016, 2016.

Rager, J. E., Lichtveld, K., Ebersviller, S., Smeester, L., Jaspers, I., Sexton, K. G., and Fry, R. C.: A Toxicogenomic Comparison of Primary and Photochemically Altered Air Pollutant Mixtures, Environ Health Perspect, 119, 1583–1589, https://doi.org/10.1289/ehp.1003323, 2011.

Reemtsma, T., These, A., Linscheid, M., Leenheer, J., and Spitzy, A.: Molecular and Structural Characterization of Dissolved Organic Matter from the Deep Ocean by FTICR-MS, Including Hydrophilic Nitrogenous Organic Molecules, Environ Sci Technol, 42, 1430–1437, https://doi.org/10.1021/es7021413, 2008.

Reiss, R., Anderson, E. L., Cross, C. E., Hidy, G., Hoel, D., McClellan, R., and Moolgavkar, S.: Evidence of Health Impacts of Sulfate-and Nitrate-Containing Particles in Ambient Air, Inhal Toxicol, 19, 419–449, https://doi.org/10.1080/08958370601174941, 2007.

Remucal, C. K., Cory, R. M., Sander, M., and McNeill, K.: Low molecular weight components in an aquatic humic substance as characterized by membrane dialysis and Orbitrap mass spectrometry, Environ Sci Technol, 46, 9350–9359, https://doi.org/10.1021/es302468q, 2012.

Reynolds, J. C., Last, D. J., McGillen, M., Nijs, A., Horn, A. B., Percival, C., Carpenter, L. J., and Lewis, A. C.: Structural analysis of oligomeric molecules formed from the reaction products of oleic acid ozonolysis, Environ Sci Technol, 40, 6674–6681, https://doi.org/10.1021/ES060942P, 2006.

Rudich, Y., Donahue, N. M., and Mentel, T. F.: Aging of organic aerosol: Bridging the gap between laboratory and field studies, Annu Rev Phys Chem, 58, 321–352, https://doi.org/10.1146/annurev.physchem.58.032806.104432, 2007.

Sander, R.: Compilation of Henry's law constants (version 5.0.0) for water as solvent, Atmos Chem Phys, 23, 10901–12440, https://doi.org/10.5194/ACP-23-10901-2023, 2023.

Schwartz, S. E.: Mass-Transport Considerations Pertinent to Aqueous Phase Reactions of Gases in Liquid-Water Clouds, in: Chemistry of Multiphase Atmospheric Systems, Springer Berlin Heidelberg, Berlin, Heidelberg, 415–471, https://doi.org/10.1007/978-3-642-70627-1_16, 1986.

Seymore, J., Felix, J. D., Abdulla, H., Bergmann, D., Campos, M. L. A. M., and Florêncio, J.: Pandemic-Related Anthropogenic Influences on the Dissolved Organic Matter Chemical Character in São Paulo State Wet Deposition by Ultrahigh-Resolution Mass Spectrometry, ACS Earth Space Chem, 7, 1929–1946, https://doi.org/10.1021/acsearthspacechem.3c00076, 2023.

Shi, J., Fulford, M., Li, H., Marzook, M., Reisjalali, M., Salvalaglio, M., and Molteni, C.: Investigating the quasi-liquid layer on ice surfaces: a comparison of order parameters, Physical Chemistry Chemical Physics, 24, 12476–12487, https://doi.org/10.1039/D2CP00752E, 2022.

Sleighter, R. L. and Hatcher, P. G.: Molecular characterization of dissolved organic matter (DOM) along a river to ocean transect of the lower Chesapeake Bay by ultrahigh resolution electrospray ionization Fourier transform ion cyclotron resonance mass spectrometry, Mar Chem, 110, 140–152, https://doi.org/10.1016/J.MARCHEM.2008.04.008, 2008.

Snider, J. R. and Huang, J.: Factors influencing the retention of hydrogen peroxide and molecular oxygen in rime ice, Journal of Geophysical Research: Atmospheres, 103, 1405–1415, https://doi.org/10.1029/97JD02847, 1998.

Snider, J. R., Montague, D. C., and Vali, G.: Hydrogen peroxide retention in rime ice, Journal of Geophysical Research: Atmospheres, 97, 7569–7578, https://doi.org/10.1029/92JD00237, 1992.

Sokolov, O. and Abbatt, J. P. D.: Adsorption to ice of n-alcohols (ethanol to 1-hexanol), acetic acid, and hexanal, Journal of Physical Chemistry A, 106, 775–782, https://doi.org/10.1021/JP013291M/ASSET/IMAGES/MEDIUM/JP013291ME00004.GIF, 2002.

Sonntag, D.: Fortschritte in der Hygrometrie, Meteorologische Zeitschrift, 3, 51–66, https://doi.org/10.1127/metz/3/1994/51, 1994.

Sotty, J., Garçon, G., Denayer, F.-O., Alleman, L.-Y., Saleh, Y., Perdrix, E., Riffault, V., Dubot, P., Lo-Guidice, J.-M., and Canivet, L.: Toxicological effects of ambient fine (PM2.5-0.18) and ultrafine (PM0.18) particles in healthy and diseased 3D organo-typic mucocilary-phenotype models, Environ Res, 176, 108538, https://doi.org/10.1016/j.envres.2019.108538, 2019.

Steenhof, M., Gosens, I., Strak, M., Godri, K. J., Hoek, G., Cassee, F. R., Mudway, I. S., Kelly, F. J., Harrison, R. M., Lebret, E., Brunekreef, B., Janssen, N. A., and Pieters, R. H.: In vitro toxicity of particulate matter (PM) collected at different sites in the Netherlands is associated with PM composition, size fraction and oxidative potential - the RAPTES project, Part Fibre Toxicol, 8, 26, https://doi.org/10.1186/1743-8977-8-26, 2011.

Stuart, A. L. and Jacobson, M. Z.: A timescale investigation of volatile chemical retention during hydrometeor freezing: Nonrime freezing and dry growth riming without spreading, Journal of Geophysical Research: Atmospheres, 108, https://doi.org/10.1029/2001JD001408, 2003.

Stuart, A. L. and Jacobson, M. Z.: Chemical retention during dry growth riming, Journal of Geophysical Research: Atmospheres, 109, https://doi.org/10.1029/2003JD004197, 2004.

Sun, J. and Ariya, P. A.: Atmospheric organic and bio-aerosols as cloud condensation nuclei (CCN): A review, https://doi.org/10.1016/j.atmosenv.2005.05.052, February 2006.

Twigg, M. V. and Phillips, P. R.: Cleaning the Air We Breathe - Controlling diesel Particulate Emissions from Passenger Cars, https://doi.org/10.1595/147106709X390977, n.d.

Valberg, P. A.: Is PM More Toxic Than the Sum of Its Parts? Risk-Assessment Toxicity Factors vs. PM-Mortality "Effect Functions," Inhal Toxicol, 16, 19–29, https://doi.org/10.1080/08958370490442935, 2004.

Vizuete, W., Sexton, K. G., Nguyen, H., Smeester, L., Aagaard, K. M., Shope, C., Lefer, B., Flynn, J. H., Alvarez, S., Erickson, M. H., and Fry, R. C.: From the Field to the Laboratory: Air Pollutant-Induced Genomic Effects in Lung Cells, Environ Health Insights, 9s4, EHI.S15656, https://doi.org/10.4137/EHI.S15656, 2015.

Wang, P., Yang, Y., Xue, D., Ren, L., Tang, J., Leung, L. R., and Liao, H.: Aerosols overtake greenhouse gases causing a warmer climate and more weather extremes toward carbon neutrality, Nat Commun, 14, 1–11, https://doi.org/10.1038/S41467-023-42891-2;SUBJMETA=106,1108,35,674,694,704,824;KWRD=ATMOSPHERIC+CHEMISTRY,ATTRIBUTION,CLIMATE+AND+EARTH+SYSTEM+MODELLING, 2023.

Weigel, R., Borrmann, S., Kazil, J., Minikin, A., Stohl, A., Wilson, J. C., Reeves, J. M., Kunkel, D., De Reus, M., Frey, W., Lovejoy, E. R., Volk, C. M., Viciani, S., D'amato, F., Schiller, C., Peter, T., Schlager, H., Cairo, F., Law, K. S., Shur, G. N., Belyaev, G. V, and Curtius, J.: Atmospheric Chemistry and Physics In situ observations of new particle formation in the tropical upper troposphere: the role of clouds and the nucleation mechanism, Atmos. Chem. Phys, 11, 9983–10010, https://doi.org/10.5194/acp-11-9983-2011, 2011.

Willey, J. D., Kieber, R. J., Eyman, M. S., Avery, G. B., Willey, D., Kieber, R. J., Eyman, M. S., Brooks, G., and Jr, A.: Rainwater dissolved organic carbon: Concentrations and global flux, Global Biogeochem Cycles, 14, 139–148, https://doi.org/10.1029/1999GB900036, 2000.

Williamson, C. J., Kupc, A., Axisa, D., Bilsback, K. R., Bui, T. P., Campuzano-Jost, P., Dollner, M., Froyd, K. D., Hodshire, A. L., Jimenez, J. L., Kodros, J. K., Luo, G., Murphy, D. M., Nault, B. A., Ray, E. A., Weinzierl, B., Wilson, J. C., Yu, F., Yu, P., Pierce, J. R., and Brock, C. A.: A large source of cloud condensation nuclei from new particle formation in the tropics, Nature 2019 574:7778, 574, 399–403, https://doi.org/10.1038/s41586-019-1638-9, 2019.

Willoughby, A. S., Wozniak, A. S., and Hatcher, P. G.: Detailed source-specific molecular composition of ambient aerosol organic matter using ultrahigh resolution mass spectrometry and 1H NMR, Atmosphere (Basel), 7, 1–7, https://doi.org/10.3390/atmos7060079, 2016.

(WMO), W. M. O.: Technical Regulations - Basic Documents No. 2: Volume IV – Quality Management, WMO-No. 49, IV, 15, 2011.

Wu, R., Vereecken, L., Tsiligiannis, E., Kang, S., Albrecht, S. R., Hantschke, L., Zhao, D., Novelli, A., Fuchs, H., Tillmann, R., Hohaus, T., Carlsson, P. T. M., Shenolikar, J., Bernard, F., Crowley, J. N., Fry, J. L., Brownwood, B., Thornton, J. A., Brown, S. S., Kiendler-Scharr, A., Wahner, A., Hallquist, M., and Mentel, T. F.: Molecular composition and volatility of

multi-generation products formed from isoprene oxidation by nitrate radical, Atmos Chem Phys, 21, 10799–10824, https://doi.org/10.5194/acp-21-10799-2021, 2021.

8. Supplementary Material

8.1 Supplementary for Gas-Ice Partitioning Coefficients

Gas-Ice Partitioning Coefficients of Carbonyls during Diffusional Ice Crystal Growth

Jackson Seymore*[1], Miklós Szakáll[1], Alexander Theis[3], Subir Mitra[3], Christine Borchers[2], Thorsten Hoffmann[2]

[1] Institute for Atmospheric Physics, Johannes Gutenberg University, Mainz, Germany
[2] Department of Chemistry, Johannes Gutenberg–University, Mainz, Germany
[3] Particle Chemistry Department, Max Planck Institute for Chemistry, Mainz, Germany

*Corresponding author: seymorej@uni-mainz.de

Table S1. Bubbler Concentrations and Henry Solubilities

	H^{cp}		$H_s^{cp}T$	Target Flowtube Gas Concentration	Molar Mass	Target Bubbler Liquid concentration (uM)		
	mol/(m^3 Pa)	M/atm	K	ppbv	g/mol	-40 ºC (d =165)	-30 ºC (d = 55)	-20 ºC (d = 18)
Benzaldehyde	0.4	40.53	5200	10	106.12	109	36	12
MVK	0.26	26.34	7800	10	70.09	91	30	10
Methacrolein	0.045	4.56	4600	10	70.09	12	4	1
Acetaldehyde	0.13	13.17	5900	10	44.05	38	13	4
Formaldehyde	32	3242.4	7100	10	30.03	10447	3482	1159
Acetone	0.27	27.36	5500	10	58.08	76	25	8
Nopinone	14	1418.55		10	138.21	2341	780	260
Norcamphor	0.43	43.57	5100	10	110.15	116	39	13
Camphor	0.54	54.72	4800	10	152.23	142	47	16
Diacetyl	0.73	73.97	5700	10	86.09	209	70	23
Glyoxal	4100	415433	7500	10	58.04	1389975	463325	154161
Hydroxyacetone	77	7802.03		10	74.08	12873	4291	1428
Methylglyoxal	35	3546.38	7500	10	72.06	11866	3955	1316
Propionaldehyde	0.099	10.03	4300	10	58.08	25	8	3

Table S2. Target m/z for MS analysis (Compounds given in elution order)

Species	Elemental Formula	Monoisotopic Mass (Da)	MS Analyte	Analyte Elemental Formula	Target m/z used $[M-H]^-$	Expected RT (min)
Hydroxyacetone	C3H6O2	74.0368	Hydroxyacetone-DNPH	C9H10N4O5	253.0573	1.3

Formaldehyde	CH2O	30.0106	Formaldehyde-DNPH	C7H6N4O4	209.0311	1.9
Acetaldehyde	C2H4O	44.0262	Acetaldehyde-DNPH	C8H8N4O4	223.0467	2.7
Acetone	C3H6O	58.0419	Acetone-DNPH	C9H10N4O4	237.0624	3.5
Propionaldehyde	C3H6O	58.0419	Propionaldehyde-DNPH	C9H10N4O4	237.0624	3.9
Methacrolein	C4H6O	70.0419	Methacrolein-DNPH	C10H10N4O4	249.0624	4.5
MVK	C4H6O	70.0419	MVK-DNPH	C10H10N4O4	249.0624	4.8
Benzaldehyde	C7H6O	106.0419	Benzaldehyde-DNPH	C13H10N4O4	285.0624	5.4
Glyoxal	C2H2O2	58.0055	Glyoxal-bis-DNPH	C14H10N8O8	417.0534	5.7
Norcamphor	C7H10O	110.0732	Norcamphor-DNPH	C13H14N4O4	289.0937	5.7
Methylglyoxal	C3H4O2	72.0211	Methylglyoxal-bis-DNPH	C15H12N8O8	431.0700	6.5
Diacetyl	C4H6O2	86.0368	Diacetyl-bis-DNPH	C16H14N8O8	445.0856	7.2
Nopinone	C9H14O	138.1045	Nopinone-DNPH	C15H18N4O4	317.1250	7.8
Camphor	C10H16O	152.1201	Camphor-DNPH	C16H20N4O4	331.1412	8.2

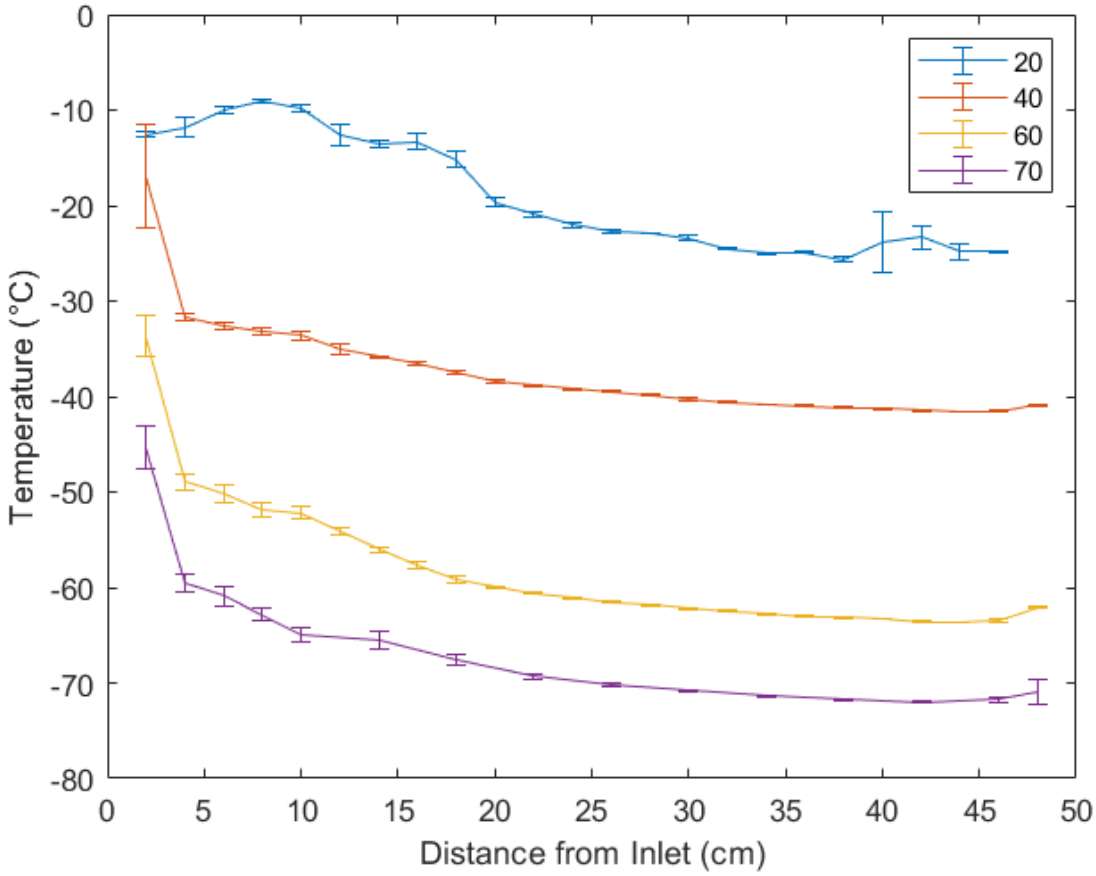

Figure S1. Temperature Profile along z-axis of Flowtube

Section S1. Discussion on Entropy-Enthalpy Compensation

Reviewing this data in accordance with the definitions laid out by Liu and Guo, (2001) and Pan et al. (2015), it appears unlikely that the Entropy-Enthalpy Compensation (EEC) effect seen here is a spurious finding. The linearity from the regressions in Table 3 are strong and thus there is relatively low standard error in ΔH and ΔS, especially comparing to the significant range of ΔH and ΔS values (–145 to 21 kJ mol^{-1}, –621 to 44 J mol^{-1} K^{-1} respectively). The lack of strong convergence to an isoequilibrium when extrapolating from Figure 2 (also more clearly demonstrated in Figure S2) shows that this system however does not readily appear to meet the definitions to be an isokinetic relation (IKR).

This correlation between ΔS and ΔH can further be explored under the constraints that Sharp (2001) places on EEC for 95% confidence. The range of ΔG in this experiment is from

–9 to 24.4 kJ mol^{-1} while the range of temperatures experiments were run was between –20 and –40 °C, (the harmonic mean being –30.3 °C or 242.9 K). While $|\Delta G| < |\Delta H|$ for most cases here, there is a significant range of $|\Delta G|$ and in the same magnitude as $|\Delta H|$ such that ΔG cannot be considered constant. The compensation temperature (235.5 K) however does fall within the 2σ range of the experimental temperature (242.9 K) and so this analysis alone does not meet the 95% confidence interval for nontrivial correlation. But, if the data from Fries et al. (2007) is included in this analysis, Tc and r^2 are instead 225.9 K and 0.9788 respectively with the harmonic mean experimental temperature as 244.9 K; this places Tc outside of the 2σ range of the experimental temperature and thus meets Sharp's criteria for a nontrivial correlation.

In regards to IKR as viewed through the Griessen et al. (2020) and Griessen and Dam (2021) EEC analysis, the Compensation Quality Factor (CQF) values are rather low, both below 0.25. This supports the observation of the absence of strong coalescence to an isoequilbrium and no noticeable IKR. The increase in CQF when including the data from Fries et al. (2007) also indicates that with the inclusion of more data, coalescence could be statistically inferred.

It should be noted that the explanation of EEC from solvation effects is not specific to aqueous systems. Computational work has identified instead two causes for EEC in solvent-solute interactions: solvent reorganization and molar shift (Grunwald and Steel, 1995). Regardless of aqueous nonspecificity, the EEC's implication of a surface liquid layer can still be made. There are other less likely potential explanations currently in literature such as the influence of hidden Carnot cycles from microphase transitions (Starikov and Nordén, 2007) or the loss of translational and rotational entropy during gas phase association (Ryde, 2014). However, these seem unlikely to be the dominant mechanism for the EEC seen here and are outside the scope of discussion here.

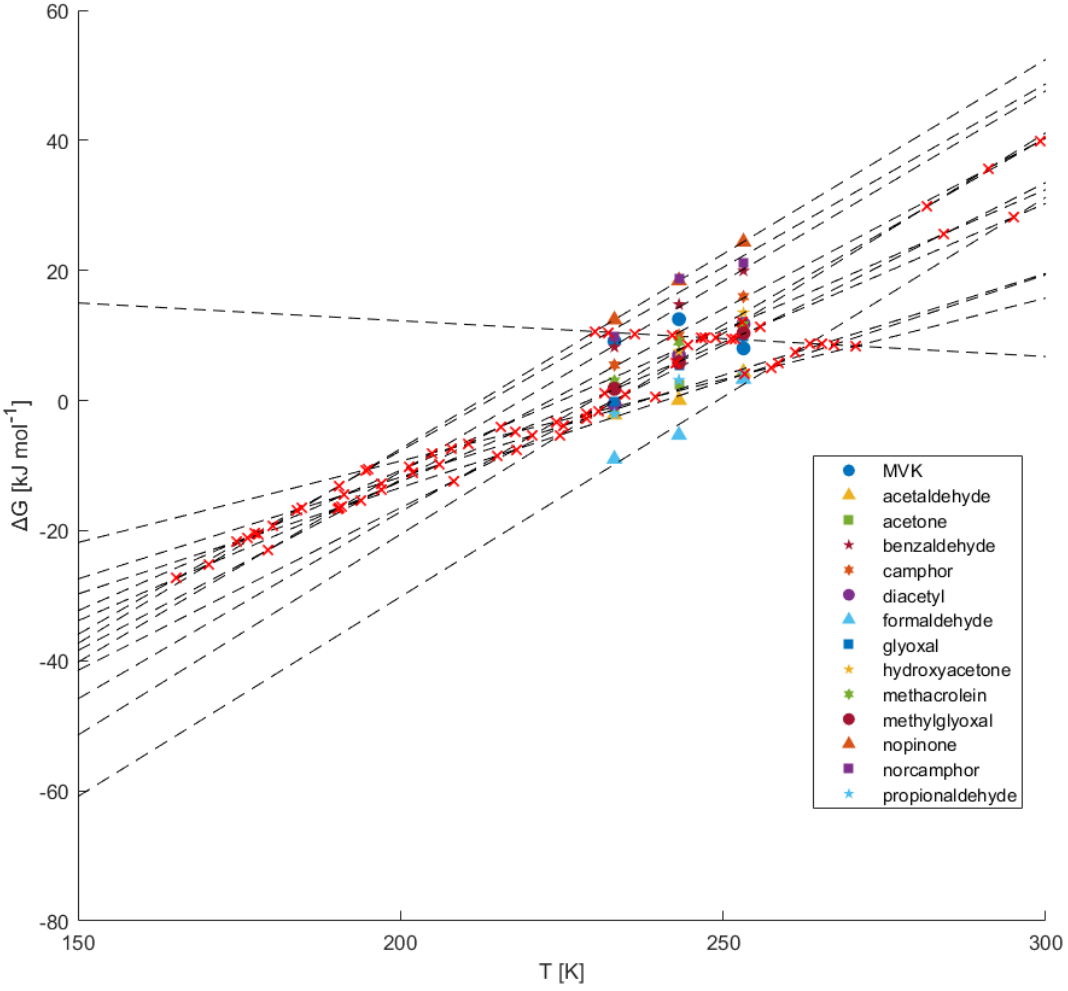

Figure S2. Plot of Temperature versus ΔG. Red x's indicate intersections of the extrapolated linear regressions.

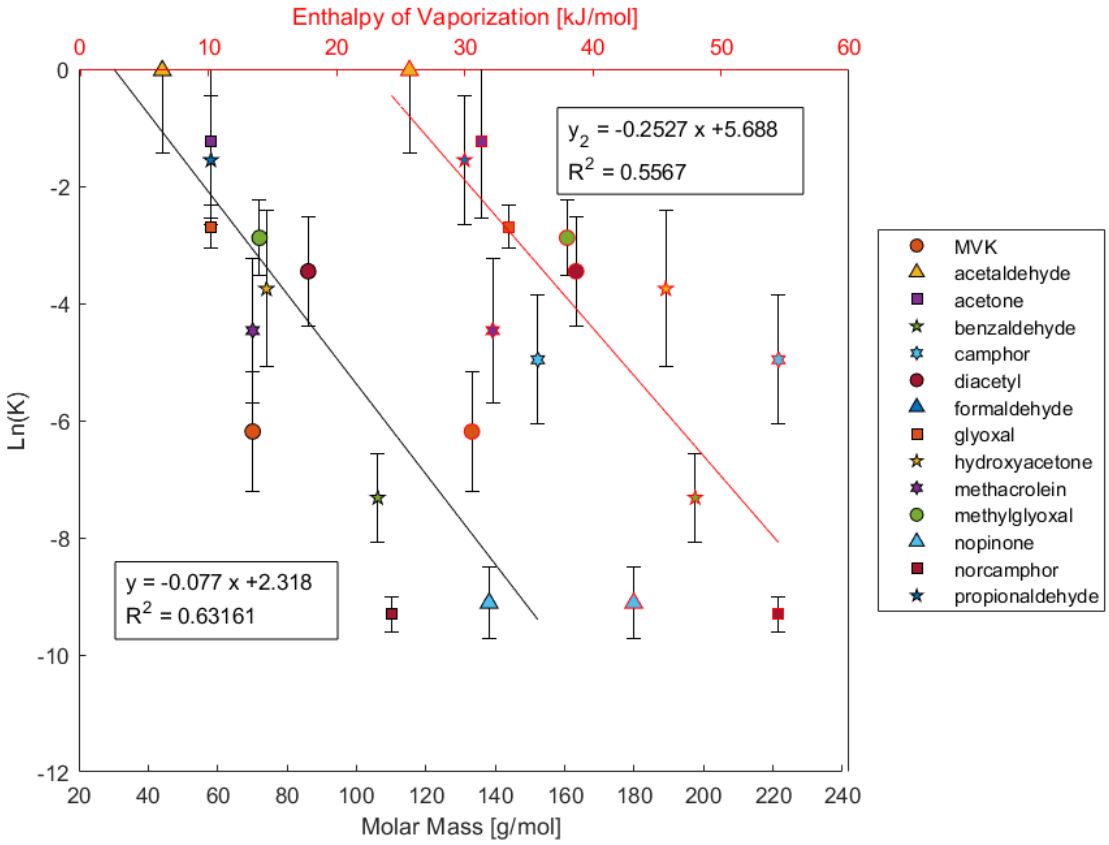

Figure S3. Scatterplot of ln(K) at –30 ºC versus the heat of vaporization (red line) and molar mass (black line).

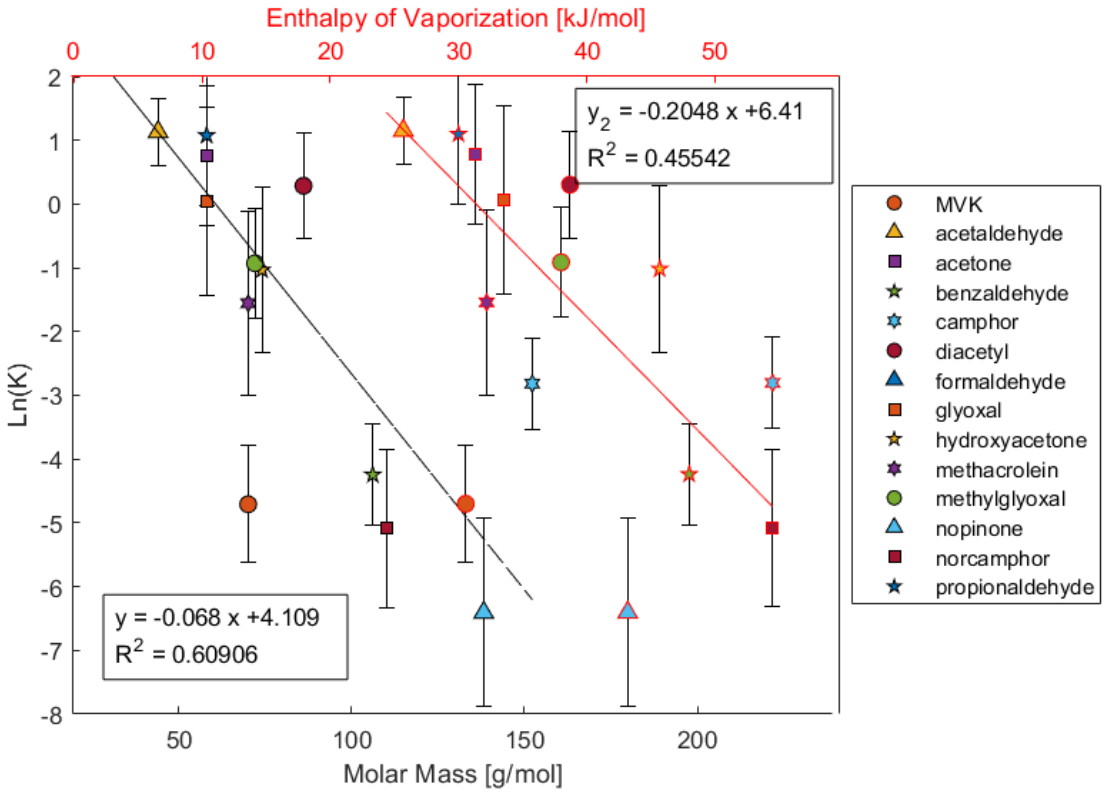

Figure S4. Scatterplot of ln(K) at –40 ºC versus the heat of vaporization (red line) and molar mass (black line).

References

Fries, E., Starokozhev, E., Haunold, W., Jaeschke, W., Mitra, S. K., Borrmann, S., and Schmidt, M. U.: Laboratory studies on the uptake of aromatic hydrocarbons by ice crystals during vapor depositional crystal growth, Atmos Environ, 41, 6156–6166, https://doi.org/10.1016/j.atmosenv.2007.04.028, 2007.

Griessen, R. and Dam, B.: Simple Accurate Verification of Enthalpy-Entropy Compensation and Isoequilibrium Relationship, ChemPhysChem, 22, 1774–1784, https://doi.org/10.1002/CPHC.202100431, 2021.

Griessen, R., Boelsma, C., Schreuders, H., Broedersz, C. P., Gremaud, R., and Dam, B.: Single Quality Factor for Enthalpy-Entropy Compensation, Isoequilibrium and Isokinetic Relationships, ChemPhysChem, 21, 1632–1643, https://doi.org/10.1002/CPHC.202000390, 2020.

Grunwald, E. and Steel, C.: Solvent Reorganization and Thermodynamic Enthalpy-Entropy Compensation, J. Am. Chem. Soc, 5687–5692 pp., 1995.

Liu, L. and Guo, Q. X.: Isokinetic relationship, isoequilibrium relationship, and enthalpy-entropy compensation, https://doi.org/10.1021/cr990416z, March 2001.

Pan, A., Biswas, T., Rakshit, A. K., and Moulik, S. P.: Enthalpy-Entropy Compensation (EEC) Effect: A Revisit, Journal of Physical Chemistry B, 119, 15876–15884, https://doi.org/10.1021/acs.jpcb.5b09925, 2015.

Ryde, U.: A fundamental view of enthalpy-entropy compensation, Medchemcomm, 5, 1324–1336, https://doi.org/10.1039/c4md00057a, 2014.

Sharp, K.: Entropy—enthalpy compensation: Fact or artifact?, Protein Science, 10, 661–667, https://doi.org/10.1110/ps.37801, 2001.

Starikov, E. B. and Nordén, B.: Enthalpy-entropy compensation: A phantom or something useful?, Journal of Physical Chemistry B, 111, 14431–14435, https://doi.org/10.1021/JP075784I/ASSET/IMAGES/LARGE/JP075784IF00001.JPEG, 2007.

8.2 Supplementary for Part II Freezing of Raindrops

Supplemental Information: Retention measurements of Complex WSOC from Beijing PM Samples through Acoustic Levitation

Jackson Seymore*[1,2], Martanda Gautam[2], Miklós Szakáll[2], Alexander Theis[2], Jialiang Ma[3], Alexander L. Vogel[3], Lingli Zhou[4]

[1] Max Planck Graduate Center, Max Planck Institute for Chemistry, Mainz, Germany
[2] Institute for Atmospheric Physics, Johannes Gutenberg University, Mainz, Germany
[3] Institute for Atmospheric and Environmental Sciences, Goethe-University Frankfurt, Germany
[4] South China Institute of Environmental Sciences, Ministry of Ecology and Environment, Guangzhou, P.R. China
*Corresponding author: seymorej@uni-mainz.de

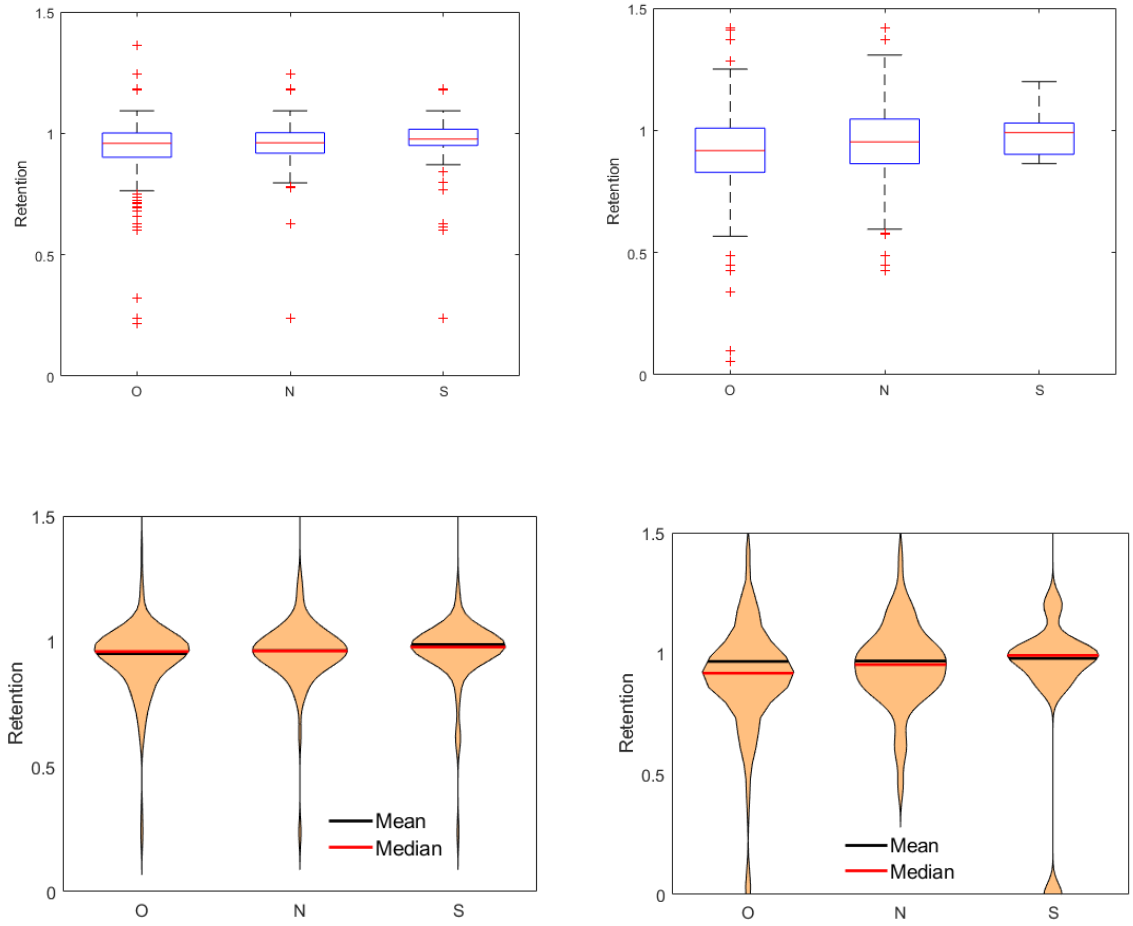

Figure S1. Boxplots and Violin plots of the Retention Coefficients of species observed grouped by heteroatom; Left (-)HESI, Right (+)HESI

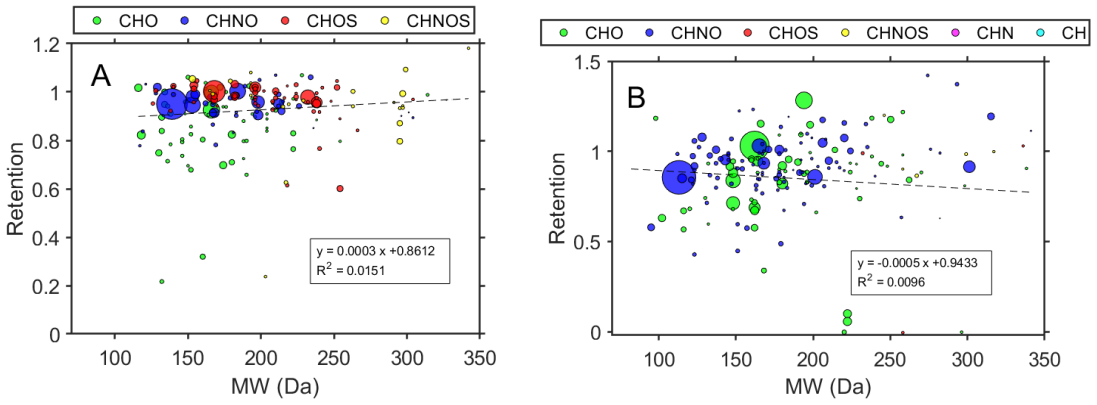

Figure S2. Retention Coefficient as a function of Molecular Weight (MW); (A) (−)HESI, (B) (+)HESI; Color denotes compositional class of the assigned compound as used in Fig. 1: Green for CHO, blue for CHNO, red for CHOS, yellow for CHNOS, magenta for CHN, cyan for CH. Dashed line shows linear fit.

Table S1. Parameters for Stable Distribution Fit presented in Figure 3

Mean	0.8894	
Log Likelihood	224.657	
Parameter	**Value**	**Std. Error**
Alpha (α)	1.38642	0.06988
Beta (β)	-0.61652	0.10241
Gamma (γ)	0.07289	0.00383
Delta (δ)	0.95409	0.00608

Table S2. Parameters for t Location-Scale Distribution Fit presented in Figure 3

Mean	0.9442	
Log Likelihood	210.775	
Parameter	**Value**	**Std. Error**
Mu (μ)	0.94415	0.00566
Sigma (σ)	0.08665	0.00630
Nu (ν)	2.02867	0.26969

Two separate csv files are provided as summaries of the MS data with the calculated retention coefficient; one for (-)HESI and (+)HESI are published through Zenodo at the following DOI: https://doi.org/10.5281/zenodo.15166745

Supplement of Atmos. Chem. Phys., 24, 13961–13974, 2024
https://doi.org/10.5194/acp-24-13961-2024-supplement

Atmospheric Chemistry and Physics Open Access

Supplement of

Retention of α-pinene oxidation products and nitro-aromatic compounds during riming

Christine Borchers et al.

Correspondence to: Thorsten Hoffmann (t.hoffmann@uni-mainz.de)

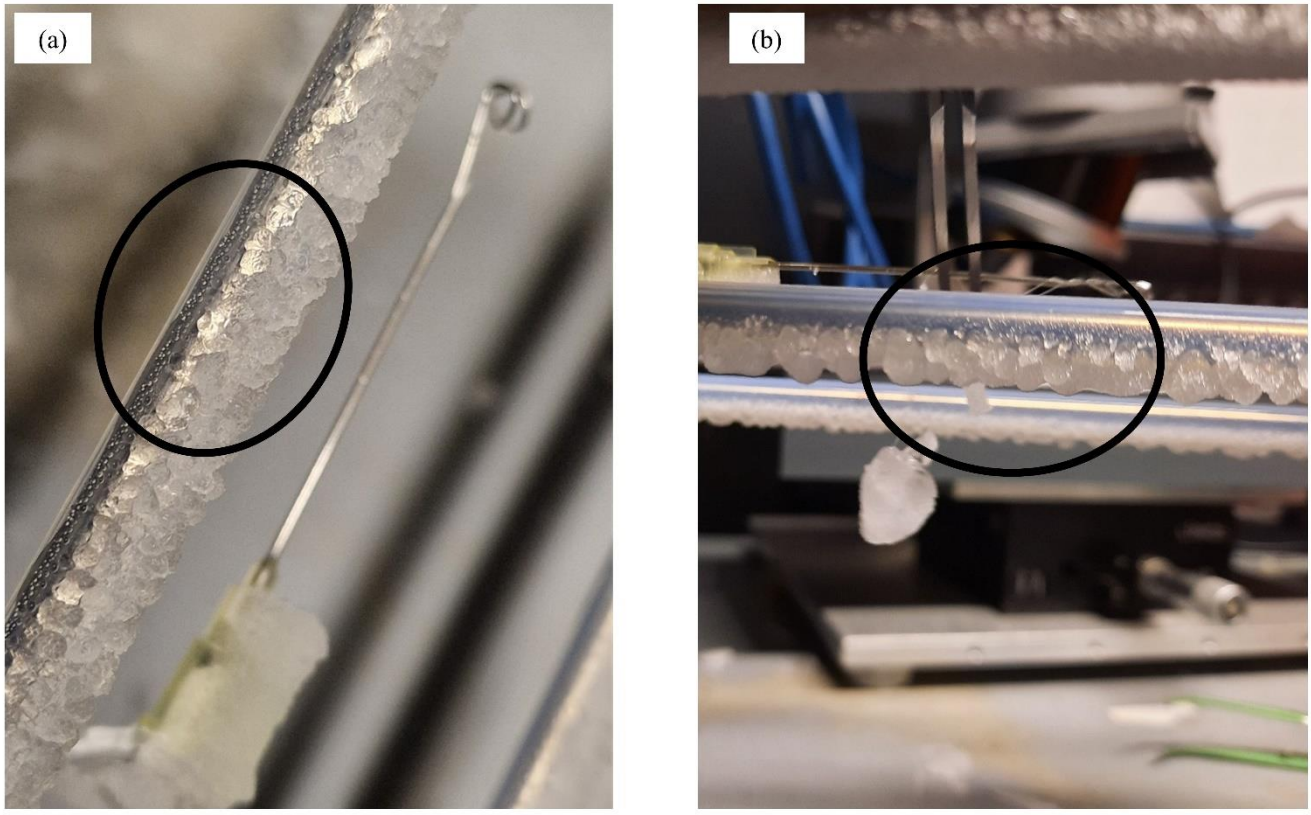

Figure S1: Photo of ice grown under dry (a)) and wet (b)) growth conditions.

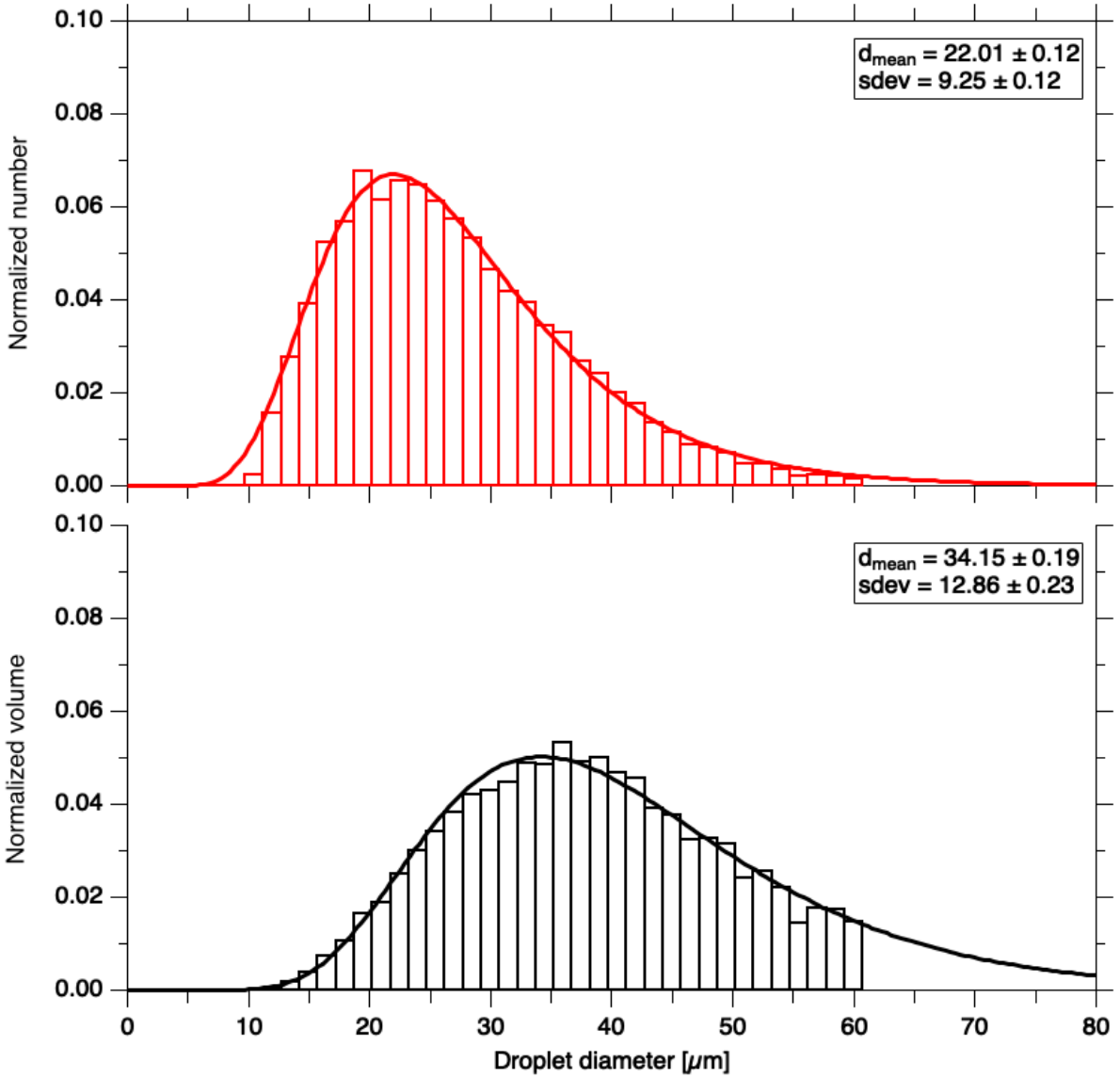

20 **Figure S2: Normalized droplet number (a) and volume distribution (b) of the supercooled droplets generated using four spraying nozzles. The lines represent the log-normal fit functions.**

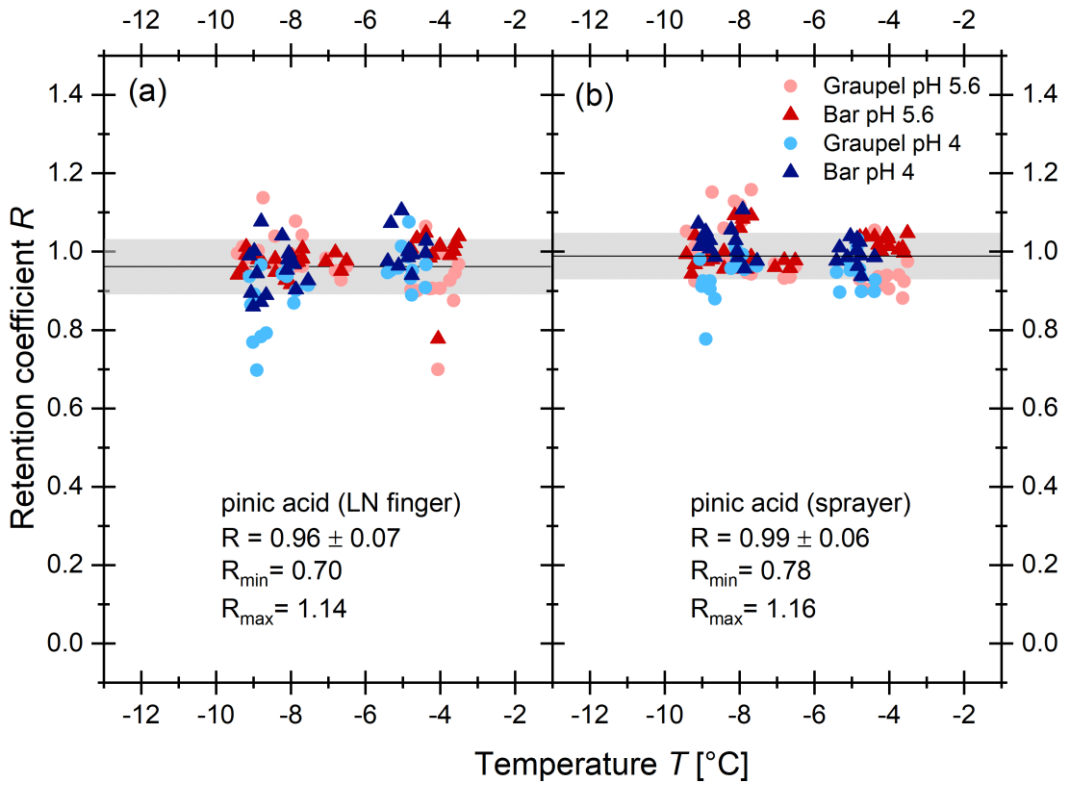

Figure S3: Experimentally determined retention coefficients of pinic acid using (a) the LN finger and (b) the sprayer solution as a function of the temperature during the experiment for different rime collectors. The circles represent the graupel samples and the triangles those of the Teflon-coated bars. For the blue symbols, the pH was adjusted to 4 by adding HCl (30 %), the red symbols are without adding HCl. The solid black line represents the mean of all measurements, and the grey area represents one standard deviation.

Desorption correction procedure

2-nitrophenol has the lowest effective Henry's law constant and therefore possesses the highest probability of transition from the droplet phase to the gas phase, resulting in a high gas phase concentration in the wind tunnel. For such a substance the measurement technique using the liquid nitrogen finger collection is not reliable since the gas molecules might adsorb on the liquid nitrogen cooled ice and thereby bias the retention value. Also, there is currently no other reliable measurement technique for measuring the desorption of a highly volatile substance right at the point where the retention measurements were carried out. Therefore, the desorption coefficient valid for the retention measurement was estimated based on a two step temperature and exposure time correction outlined in detail in the following.

First step: desorption measurements

The same solution (see Table 1) used for the retention measurements, containing 2-nitrophenol and NaBr as internal standard (IS), was nebulized and the droplets were transported downstream in the wind tunnel. The droplets were sampled in a vial in the lower horizontal part of the tunnel after a residence time of approximately 1 s (point A in figure S4). The solution was then collected and measured by UHPLC-HRMS. Desorption measurements were carried out at different temperatures (between 0 °C and 19 °C) to obtain a temperature dependency.

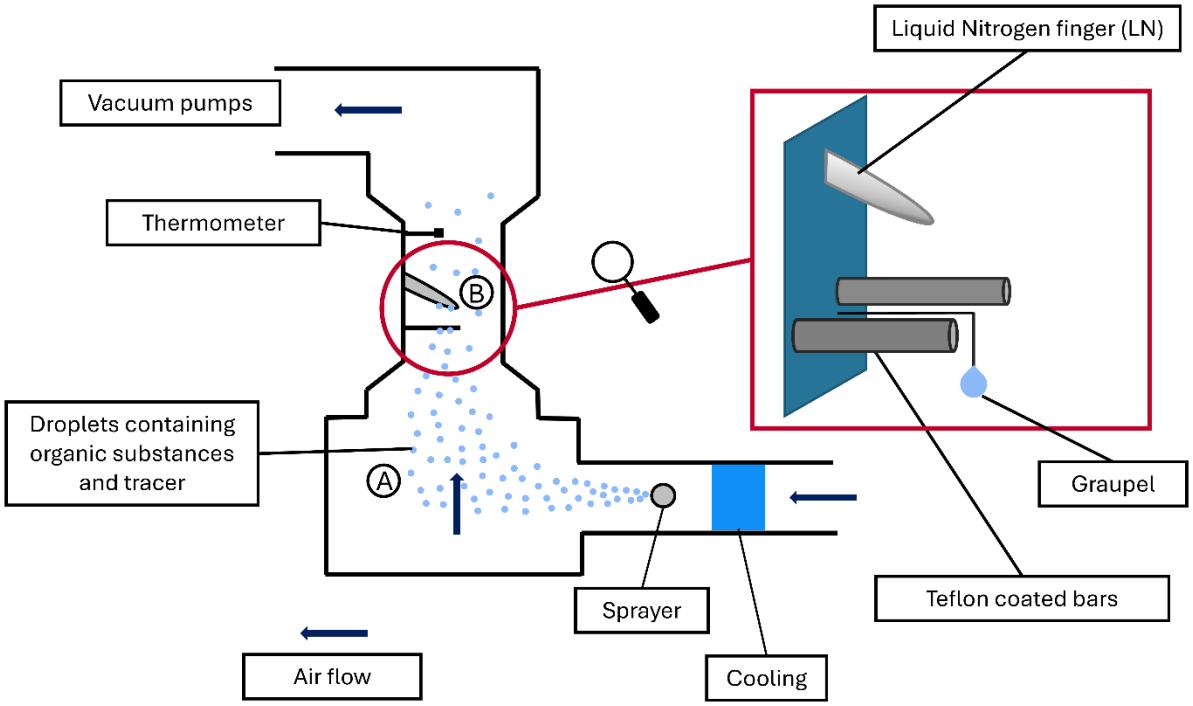

Figure S4: Schematic of the wind tunnel. Cooled air transported the generated water droplets containing the compounds into the experimental region (red circle). Red rectangle: The enlarged experimental area shows the three surfaces on which the riming took place: Graupel, liquid nitrogen finger and Teflon-coated bars. Desorption measurements were performed at point A and retention measurements were performed at point B.

The definition of the desorption coefficient is shown in Eq. (S1). The numerator describes the ratio of the compound remaining in the sample (droplets sampled in a vial) to a reference sample, which is in this case the sprayer solution, which is the solution immediately before droplet formation, takes place ($c_{\mathrm{compound}}^{\mathrm{vial}}/c_{\mathrm{compound}}^{\mathrm{sprayer}}$). The denominator describes the same ratio but for the IS ($c_{\mathrm{IS}}^{\mathrm{vial}}/c_{\mathrm{IS}}^{\mathrm{sprayer}}$):

$$D_{\mathrm{compound}} = \frac{c_{\mathrm{compound}}^{\mathrm{vial}}/c_{\mathrm{compound}}^{\mathrm{sprayer}}}{c_{\mathrm{IS}}^{\mathrm{vial}}/c_{\mathrm{IS}}^{\mathrm{sprayer}}} \quad \text{(S1)}$$

Figure S5 shows the desorption coefficient as a function of the temperature as measured in the lower part of the wind tunnel. Obvious from Fig. S5 is a strong dependence of the desorption coefficient of 2-nitrophenol on temperature, indicating less

desorption at lower temperatures. This is expected since the mass transfer rate of a dissolved compound to the environment decreases for decreasing temperatures. The reason for this is that the mass transfer depends, among others on the temperature-dependent parameters like gas- and aqueous-phase diffusivities and the effective Henry's law constant. The observed variations in the values are greater than those expected due to analytical measurement error. These variations are likely attributable to fluctuations in the conditions within the wind tunnel, which were expected to be also present during the retention measurements.

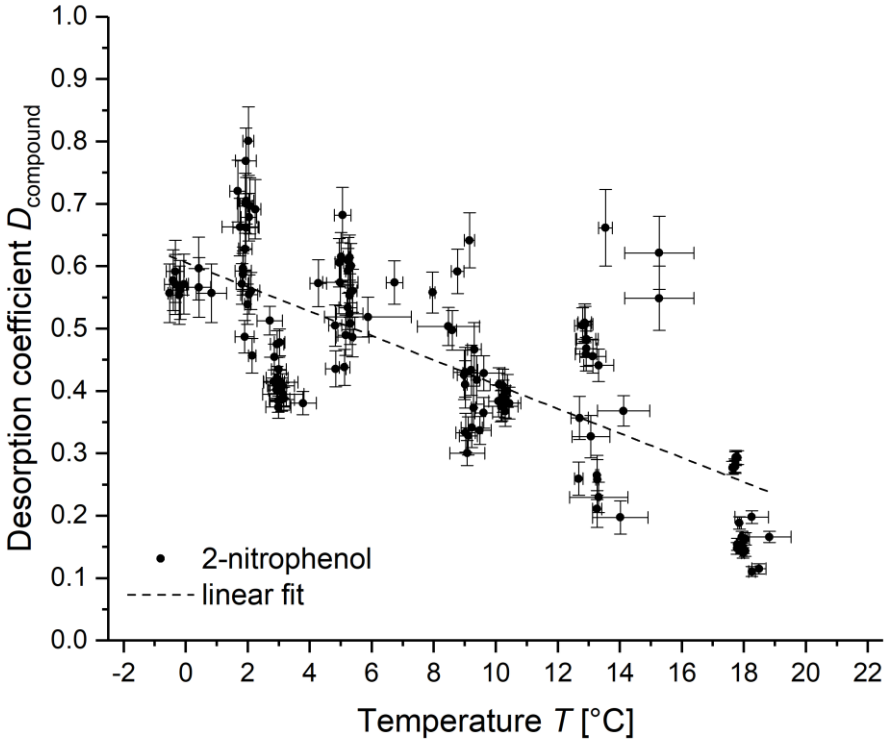

Figure S5: Desorption coefficient for 2-nitrophenol. The errors correspond to the error of the analytical measurement (y-axis) or the standard deviation of the temperature measurement during the collection time of each sample (x-axis). The dashed line represents a linear regression.

A statistically significant linear trend is visible in the measurement series. A linear regression with the equation $D_{\mathrm{compound}} = a_{\mathrm{D}} \cdot x \cdot [°C]^{-1} + b_{\mathrm{D}}$ was performed to extrapolate the desorption to the temperatures present during the experiments. This leads to the following equation, S2, for the fit function.

$$D_{\mathrm{compound}} = (-0.020 \pm 0.002) \cdot x \cdot [°C]^{-1} + (0.606 \pm 0.015) \quad \text{(S2)}$$

Extrapolating the results to the experimental conditions (e.g. -10 °C and -4 °C) yields $D_{\mathrm{compound}} = 0.81$ and $D_{\mathrm{compound}} = 0.67$ for typical dry and wet growth conditions respectively.

Second step: semi-empirical exposure time correction

The exposure time in the tunnel from the point of the desorption (point A in figure S4) to the retention measurements (point B in figure S4) is another 3 s (overall 4 s) which introduced another source of uncertainty. Thus, the measured *D* after one second of exposure had to be corrected for this time effect. This was done by a semi-empirical approach using theory and the results of the first step introduced above. From the convective diffusion equation assuming a well-mixed droplet, Pruppacher and Klett (2010, p. 775, Eq. 17-144) showed that the desorption of a dissociating gas with the initial condition of zero gas phase concentration follows a $1/t$ law. This functional relationship was used to fit the data from the first step to get a time dependence correction of the desorption coefficient. More specifically the following fit function was utilized:

$$D(T, L, t) = c(T, L) + \left(\frac{a(T,L)}{1+a(T,L)b(T,L)t}\right) \qquad \text{Eq (S3)}$$

Here $D(T, L, t)$ is the temperature (T), liquid water content (L), and time (t) dependent desorption correction coefficient which asymptotically approaches the equilibrium value at a given temperature and liquid water content $c(T, L)$. That is, when t tends towards infinity Eq. (S3) approaches $c(T, L)$. This coefficient describes the fraction of 2-nitrophenol in the liquid phase in equilibrium with its gas phase. It was derived from the assumption of the equilibrium gas/liquid partitioning in a confined system consisting of a single gas (2-nitrophenol) and a given amount of liquid water (1 and 2 g/m^3) (Seinfeld and Pandis 2006, p.290, Eq. 7.9). In the referenced Eq. 7.9 from Seinfeld and Pandis (2006) the temperature dependent Henry's law constant was calculated according to Guo and Brimblecombe (2007) for the temperatures used during the retention measurements. The results are shown in Fig. (S6).

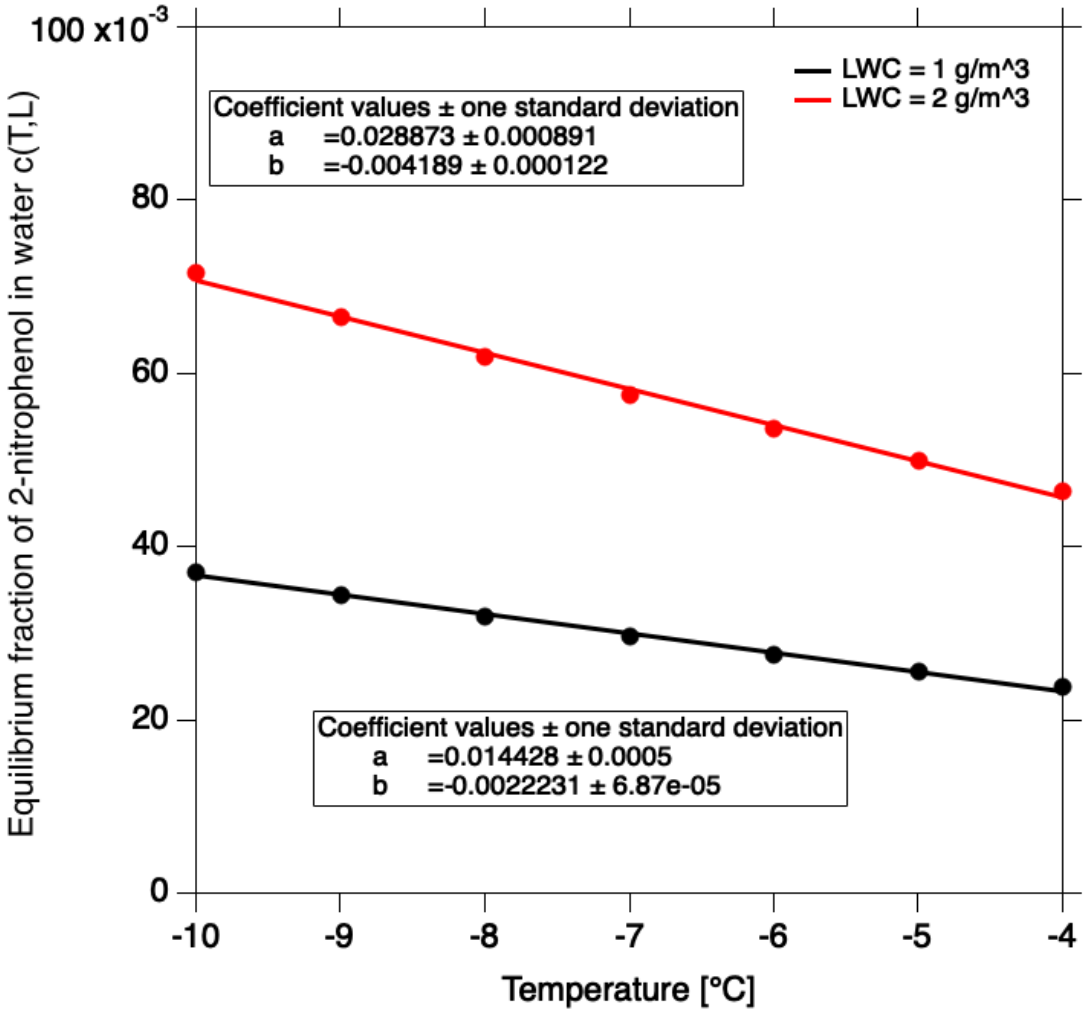

Figure S6: Equilibrium fraction of 2-nitrophenol in water as a function of temperature and liquid water content. Coefficients a and b represent the fit values of the intercept and slope of the linear regressions. Black: LWC = 1 g/m^3. Red: LWC = 2 g/m^3.

When t approaches zero Eq. (S3) yields $c(T,L) + a(T,L) = 1$, which yields $a(T,L) = 1 - c(T,L)$. Hence, the only unknown in Eq. (S3) is coefficient $b(T,L)$ which was used as a fit parameter and thereby parameterized as a function of T and L. Accordingly Eq. (S3) was used along with the extrapolated desorption values to the temperatures prevailed during the retention and the equilibrium fractions (Fig. S6) to derive a parameterization of D which depends on temperature, liquid water content and time.

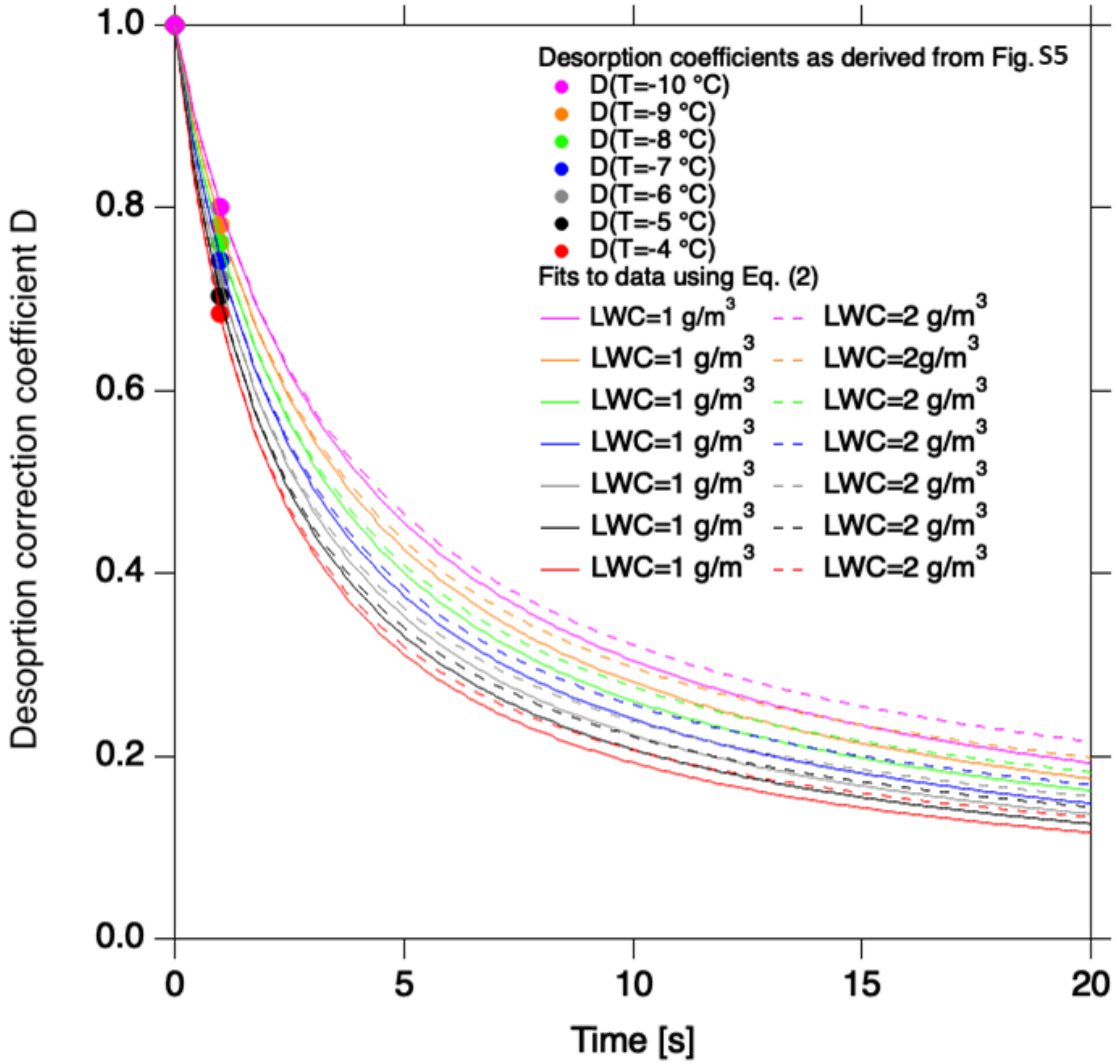

Figure S7: Desorption correction coefficient as a function of time for different temperatures and liquid water contents obtained from Eq. (S3). Solid lines: LWC = 1 g/m^3. Dashed lines LWC = 2 g/m^3. The data points were calculated from Eq. (S2).

From the results shown in Fig. S7 it is obvious that a significant part (37 %) of 2-nitrophenol desorb from the droplets from the point between the desorption and retention measurements (Point A and B in Figure S4). For example at -10 °C the desorption between Point A and B decreases from 0.81 to 0.51. For each curve in Fig. S7 a fit coefficient *b(T, L)* was obtained corresponding to a certain temperature and liquid water content. By plotting these as a function of temperature (Fig. S8) a linear relationship of *b(T, L)* on the temperature and liquid water content was derived.

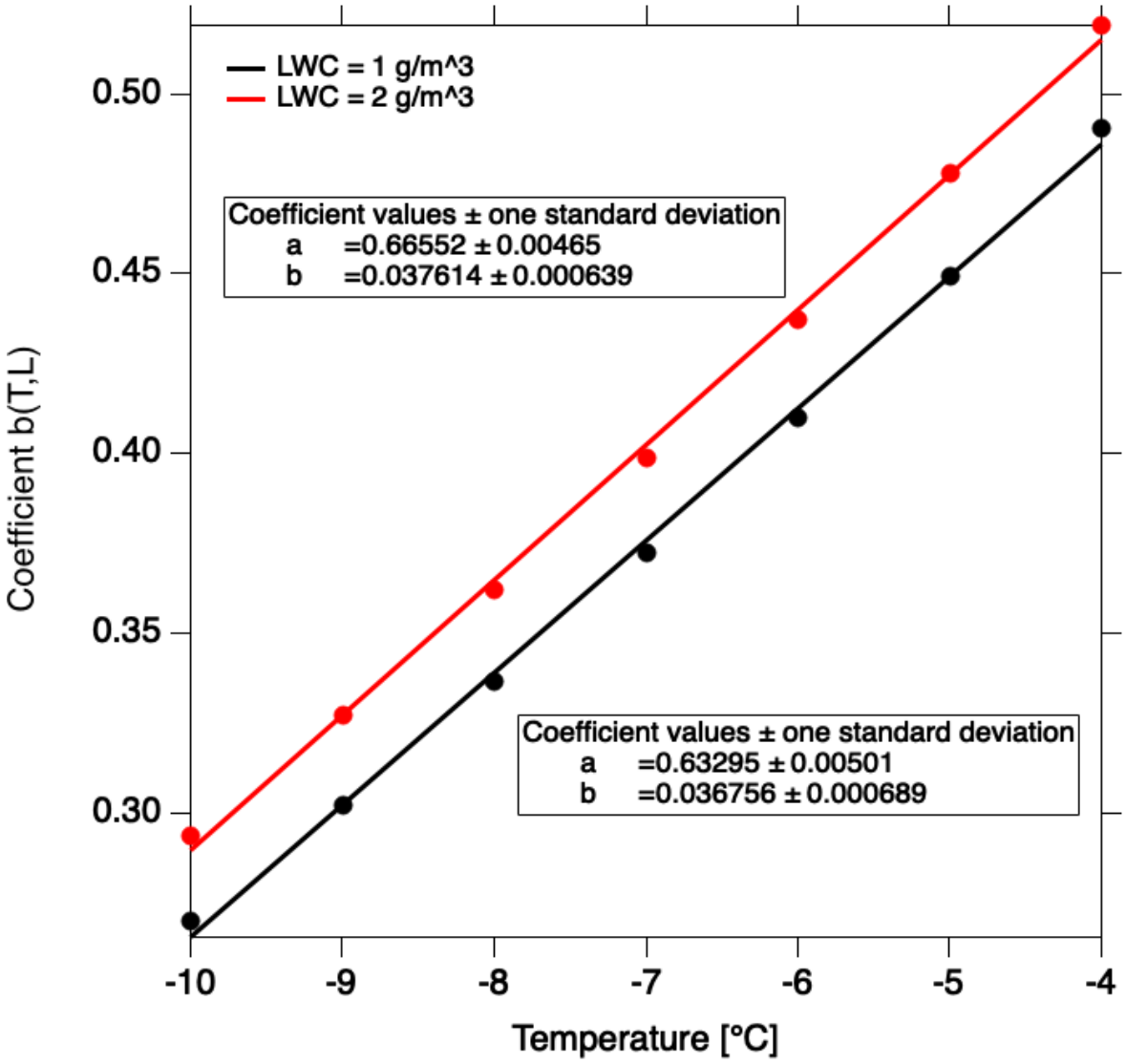

Figure S8: Dependency of the fit parameter *b(T,L)* on the temperature and liquid water content as derived from Fig. S7. Red and black points: values for LWC's of 1 and 2. Red and black lines: fit to the data. Coefficients a and b represent the intercepts and the slopes of the linear regressions.

A close glance at Fig. S7 reveals that the difference between 1 and 2 g/m3 is below 1 %. Thus, the final desorption correction function that was used to correct the retention values for 2-nitrophenol at a given temperature and at the location of the retention measurements is given by Eq. (S3) which was evaluated at t = 4 s and LWC=L= 1 g/m^3. The used parameters were:

$$c(T, L = 1) = 0.0144 - 0.0022\,T\ [°C]$$

$$a(T, L = 1) = 1 - c(T, L)$$

$$b(T, L = 1) = 0.6330 + 0.0368\,T\ [°C]$$

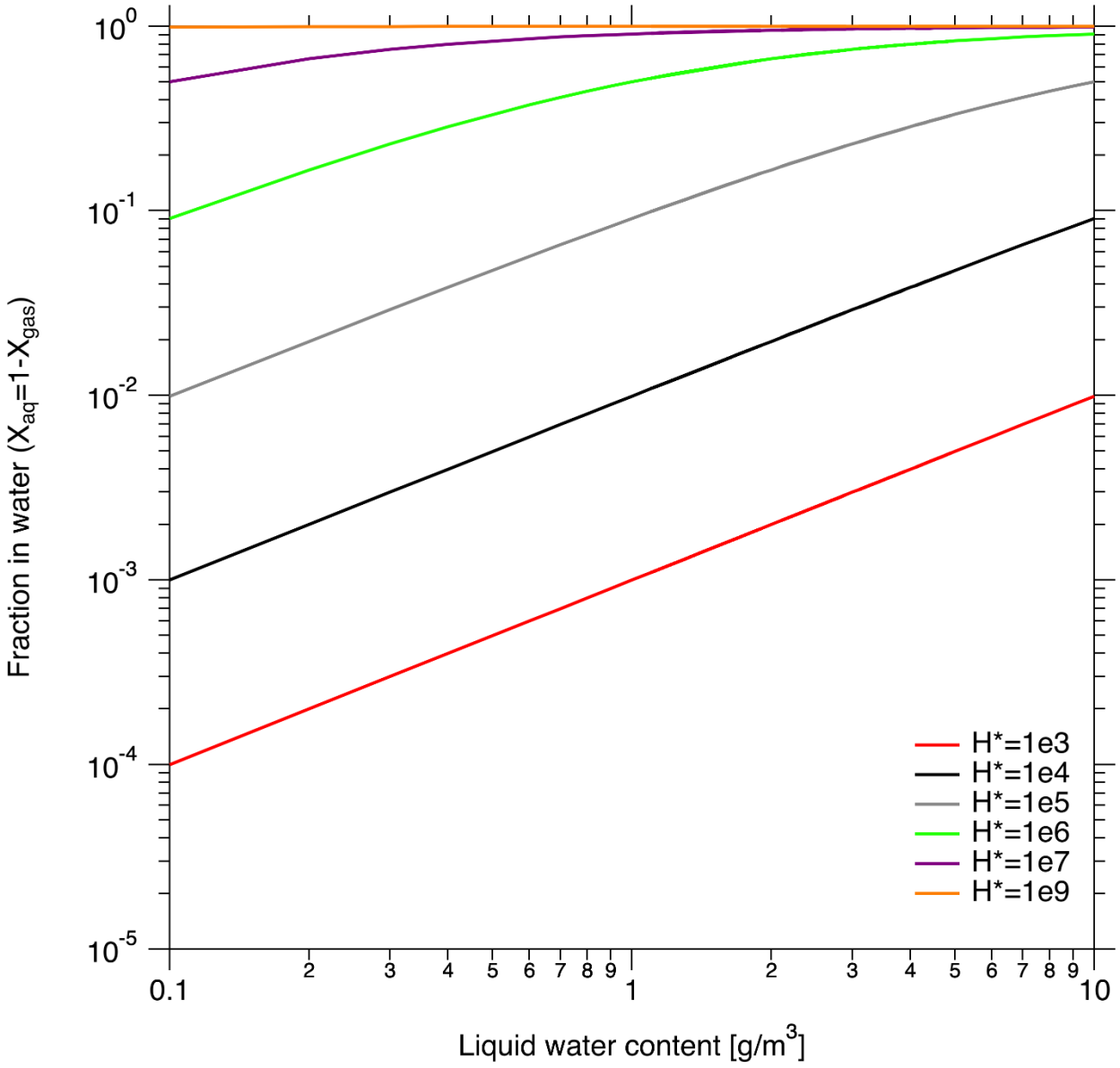

Figure S9: Equilibrium distribution of species between the liquid and gas phase in a confined system as function of the LWC. Figure according to Seinfeld and Pandis (2006).

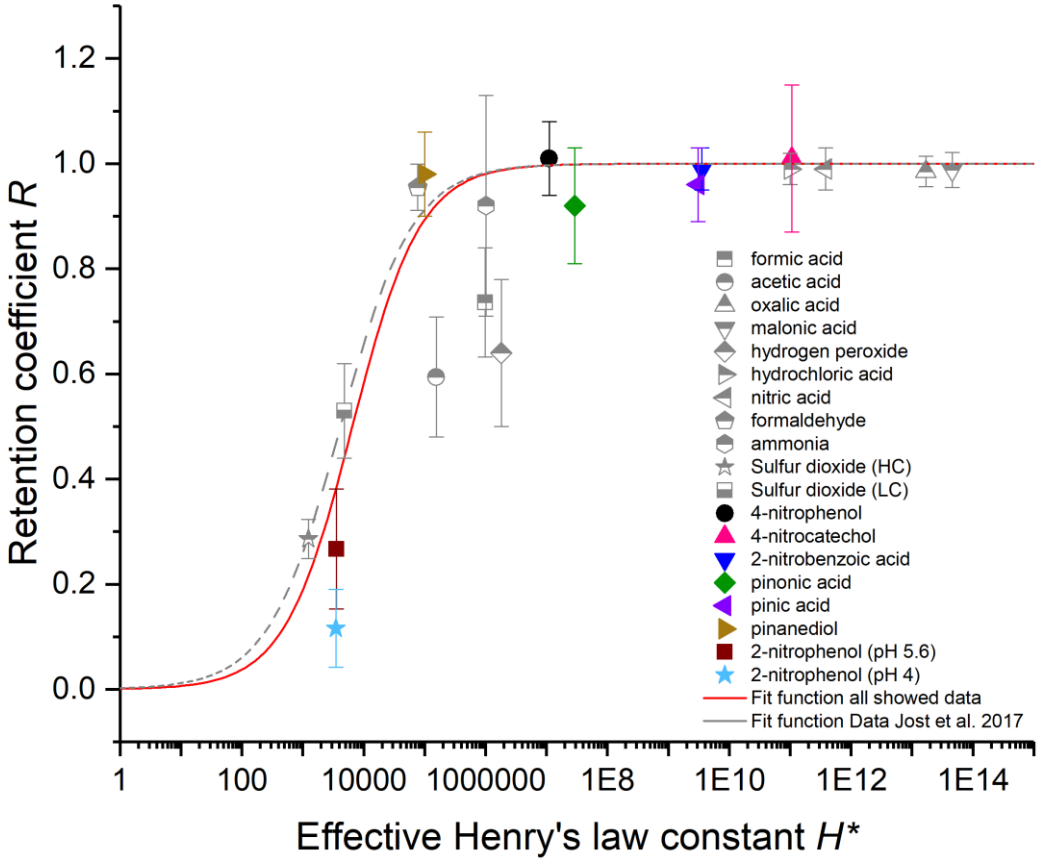

120

Figure S10: Retention coefficient as a function of H^*. Colorful filled symbols: substances investigated in the present study. Grey symbols: wind tunnel data from earlier studies (Jost et al., 2017; v. Blohn et al., 2013; 2011). Fit function: $R_{H^*} = \left(1 + (a\,/\,H^*)^b\right)^{-1}$. Red solid line: new fit to wind tunnel data with all substances ($a_{\mathrm{red}} = (6.51 \pm 2.01) \cdot 10^3$ and $b_{\mathrm{red}} = 0.78 \pm 0.16$). Grey dashed line: fit of only the grey data points $a_{\mathrm{grey}} = (4.15 \pm 1.47) \cdot 10^3$ and $b_{\mathrm{grey}} = 0.74 \pm 0.18$.

125

References

Guo, X. X. and Brimblecombe, P.: Henry's law constants of phenol and mononitrophenols in water and aqueous sulfuric acid, Chemosphere, 68, 436–444, https://doi.org/10.1016/j.chemosphere.2007.01.011, available at: https://www.sciencedirect.com/science/article/pii/S0045653507000069, 2007.

Jost, A., Szakáll, M., Diehl, K., Mitra, S. K., and Borrmann, S.: Chemistry of riming: the retention of organic and inorganic atmospheric trace constituents, Atmos. Chem. Phys., 17, 9717–9732, https://doi.org/10.5194/acp-17-9717-2017, 2017.

Pruppacher, H. R. and Klett, J. D.: Microphysics of Clouds and Precipitation, 18, Springer Netherlands, Dordrecht, 975 pp., 2010.

Seinfeld, J. H. and Pandis, S. N.: Atmospheric chemistry and physics of air pollution, 2nd ed., Wiley, New York, 203 pp., 2006.

v. Blohn, N., Diehl, K., Nölscher, A., Jost, A., Mitra, S. K., and Borrmann, S.: The retention of ammonia and sulfur dioxide during riming of ice particles and dendritic snow flakes: laboratory experiments in the Mainz vertical wind tunnel, J Atmos Chem, 70, 131–150, https://doi.org/10.1007/s10874-013-9261-x, 2013.

v. Blohn, N., Diehl, K., Mitra, S. K., and Borrmann, S.: Wind tunnel experiments on the retention of trace gases during riming: nitric acid, hydrochloric acid, and hydrogen peroxide, Atmos. Chem. Phys., 11, 11569–11579, https://doi.org/10.5194/acpd-11-17447-2011, 2011.